

Investigation of TDLAS for its Application as Primary Standard for Partial Pressure Measurements

vorgelegt von
M.Sc.-Physiker
Gerardo José Padilla Víquez
San José, Costa Rica

von der Fakultät II – Mathematik and Naturwissenschaften
der Technischen Universität Berlin
zur Erlangung des akademischen Grades
Doktor der Naturwissenschaften
- Dr.rer.nat. -

genehmigte Dissertation

Promotionsausschuss:

Vorsitzender: Prof. Dr. rer. nat. Erwin Sedlmayr
Berichter: Prof. Dr.-Ing. Hans Joachim Eichler
Berichter Priv. Doz. Dr.-Ing. Heinz-Detlef Kronfeldt
Berichter Dr. Karl Jousten
Berichter Priv. Doz. Dr. Joachim Seidel

Tag der wissenschaftliche Aussprache: 30. November 2005

Berlin 2005

- Para mi Osita, por supuesto. -

Table of Contents

List of Abbreviations and Mathematical Symbols	7
Summary	13
Zusammenfassung.....	14
1. Introduction.....	15
2. Theoretical Aspects	18
2.1. Vibrational-Rotational Infrared Spectra of Gases	18
2.2. Tunable Diode Laser Absorption Spectroscopy	24
2.2.1. Beer-Lambert Law	24
2.2.2. Deconvolution of Spectra Affected by the “Apparatus-Function”	26
2.3. Herriott-Cell.....	29
2.4. Uncertainty Analysis	35
2.5. Some Considerations about Traceability	36
2.6. Functional-Structural Linear Analysis.....	37
3. Experimental Setup and Methods of Measurement	47
3.1. General Description of the Spectrometer	47
3.1.1. General Description of Our Line Intensity and Partial Pressure Measurement Method....	49
3.2. Laser-Sources	51
3.3. Herriott-Cell.....	52
3.3.1. Herriott Cell Characterization	54
3.3.2. Absorption Path Length Measurements	60
3.4. Gas Density Measurements	61
3.4.1. Gas Density Measurements of Pure Gas	61
3.4.2. Gas Density Measurements of a Gas in a Mixture	62
3.5. Pressure Measurements	64
3.5.1. Pressure Measurements with the 10 Torr Capacitance Diaphragm Gage	65
3.5.2. Pressure Measurements with the 1000 Torr Capacitance Diaphragm Gage	66
3.5.3. Pressure Measurements with the Spinning Rotor Gage	67
3.6. Temperature Measurements	71
3.7. Absorbance Measurements.....	74
3.8. Wave-Number Measurements	80
3.8.1. Free Spectral Range Measurements	89
3.9. Integrated Absorbance Measurements.....	92
3.10. Line Intensity Measurements.....	111
3.11. Partial Pressure Measurements	112
4. Experimental Results and Analysis	114
4.1. Length Measurements.....	114

4.2.	Pressure Measurements	115
4.3.	Temperature Measurements	116
4.4.	Gas Density Measurements	121
4.5.	Transmission Measurements for Linearization of the Absorbance Scale	121
4.6.	Line Intensity Measurements of CO ₂	129
4.7.	Partial Pressure Measurements of CO ₂	132
4.8.	Line Intensity Measurements of CO.....	140
5.	Discussion of TDLAS for Application as Primary Standard for Partial Pressure Measurements..	146
6.	Conclusions	150
7.	Appendix	153
7.1.	Description of Data Manipulation for Line Intensity and Partial Pressure Measurements ..	153
7.2.	Certificates of Calibration (mini-copies).....	157
7.3.	IPSIAM-Results-File names.....	167
7.4.	Glossary.....	170
8.	References	184

List of Abbreviations and Mathematical Symbols

Abbreviations¹

BAM	Bundesanstalt für Materialforschung und –prüfung (Bureau for Materials Research and Testing)
BIPM	Bureau international des poids et mesures (International Bureau of Weights and Measures)
CDG	Capacitance Diaphragm Gage(s)
FSR	Free Spectral Range
GUM	Guide to the Expression of Uncertainty in Measurement
HWHM	Half width at half maximum
IEC	International Electrotechnical Commission
IEEE	Institute of Electrical and Electronics Engineers
IEEE-488	IEEE Standard Digital Interface for Programmable Instrumentation
IFCC	International Federation of Clinical Chemistry
IG	Ionization Gage
IPSIAM	Integrated Processing System for Integrated Absorbance Measurements
ISO	International Organization for Standardization
IUPAC	International Union of Pure and Applied Chemistry
IUPAP	International Union of Pure and Applied Physics
LIA	Lock-In Amplifier(s)
NMI	National Metrology Institute(s)
OAP	Off Axis Parabolic (mirror)
OCE	Open Confocal Etalon
OIML	International Organization of Legal Metrology
PBS	Pellicle-Beam-Splitter
PMD	Pressure Measurement Device(s)
PTB	Physikalisch-Technische Bundesanstalt (Physical-Technical Bureau)
SRG	Spinning Rotor Gage(s)
TDLAS	Tunable Diode Laser Absorption Spectroscopy
TMD	Temperature Measurement Device(s)

¹ For the sake of clarity and readability, we will repeat the description of the abbreviations or mathematical symbols whenever they are used for the first time through this work, or when the given context requires explanation to avoid confusion.

VCMHC	Vacuum Chamber with a Movable Herriott Cell
VIM	International Vocabulary of basic and general terms in metrology

Mathematical Symbols (Latin Symbols) ²

A	Element (scalar or 2x2 matrix) of a Gaussian-Matrix in ray -optics.
A_{abs}	Area of the absorbance vs. wave-number curve (integrated absorbance).
A_p	Area of the segment p of the absorbance vs. wave-number curve.
$A_{u \rightarrow l}$	Einstein coefficient for spontaneous emission.
B	Element (scalar or 2x2 matrix) of a Gaussian-Matrix in ray -optics.
B	Molecular rotational constant.
$B_{l \rightarrow u}$	Einstein coefficient for induced absorption.
$B_{u \rightarrow l}$	Einstein coefficient for induced emission.
b	Intercept of a linear fit.
C	Element (scalar or 2x2 matrix) of a Gaussian-Matrix in ray -optics.
c	Velocity of light in vacuum (299792458 m/s).
D	Element (scalar or 2x2 matrix) of a Gaussian-Matrix in ray -optics.
D	Diameter of the SRG-ball; Molecular centrifugal constant.
E	Energy of some molecular state.
ex_i	Measurement error of x_i .
ey_i	Measurement error of y_i .
$F(J)$	Molecular rotational term.
ΔF	Frequency marker (Etalon) free spectral range.
$F_f(\nu - \nu_c)$	Form-function with maximum value in ν_c . Its value depends on ν , ν_c , and on other parameters not shown.
$G(\nu)$	Molecular vibrational term.
g	Acceleration of gravity; or statistical weight.
h	Height difference between a PMD and the VCMCH.
$I(\nu)$	Transmitted intensity of the radiation at the frequency ν directed after the absorbing media to the detector.
$I_o(\nu)$	Input intensity of the radiation at the frequency ν directed toward the absorbing media (and afterward to the detector) i.e. radiation intensity before being affected by the absorbing media.

² The symbols used throughout this work, which represent a physical quantity, denote either the “true” value (unknown) of the physical quantity or the average of its traceable measurement.

I_B	Molecular moment of inertia about an axis perpendicular to the inter-nuclear axes and going through the molecule's center of mass.
I_c	Total electrical current injected to the diode-laser by its controller.
I_{cB}	Constant base electrical current injected to the diode-laser by its controller.
$I_{c\Delta}$	Modulated electrical current injected to the diode-laser by its controller.
I_{D0}	Optical intensity arriving at Detector 1 (in the Detection channel) when the absorption cell was empty.
I_{FM}	Optical intensity arriving at Detector 3 (in the Frequency Marker channel) after being transmitted by the Etalon.
I_{Dk}	Optical intensity arriving at Detector 1 (in the Detection channel) when the absorption cell contained some absorbing media which absorbed with an absorption coefficient $k(\nu_j - \nu_c)$.
$I_{D\Theta k}$	Optical intensity arriving at the entrance window of the recipient containing the absorbing media, which after traveling the absorbing path length and being affected by the absorbing media, originates the output optical intensity I_{Dk} at the output window of the recipient.
I_{R0}	Optical intensity arriving at Detector 2 (in the Reference channel) which is simultaneous to I_{D0} .
I_{Rk}	Optical intensity arriving at Detector 2 (in the Reference channel) which is simultaneous to I_{Dk} .
J	Rotational quantum number.
K	Family-number for a Herriott Cell close-path configuration.
k	Coverage factor to calculate an expanded uncertainty.
$k(\nu - \nu_c)$	Absorption coefficient of the absorbing media for the specific radiation frequency ν and line center ν_c .
k	Boltzmann constant: $(1.38066 \cdot 10^{-23} \pm 1 \cdot 10^{-28})$ J/K.
L	Path-Length of the radiation through the absorbing media.
L_{HC}	Path-Length of the radiation inside the Herriott Cell.
L_0	Path-Length of the radiation in VCMHC, but outside the Herriott Cell.
ℓ	Separation distance between the mirrors of the Herriott Cell.
M	Molecular weight.
M	Matrix size 2x2 or 4x4 used in the Gauss-matrices formalism of ray -optics.
m	Slope of a linear fit.
m_f	Slope of the deceleration rate vs. rotation frequency linear fit of the SRG offset characterization.
m_{ST}	Linear coefficient of the temperature dependency of the line intensity.
m_{uma}	Atomic mass unit.
m_{Vt}	Time to voltage linear transformation coefficient of a triangular ramp.

m_{YV}	Voltage to current linear transformation coefficient of a diode -laser controller.
m_{vY}	Current to wave-number linear transformation coefficient of a diode -laser.
N	Number of round-trips for a Herriott Cell close-path configuration.
n	Molecular density of the absorbing media (number of absorbing molecules per volume).
n_i	Molecular density of the gas number “ i ” of some gas mixture containing N different gas- “species”, and “ i ” being a natural number between 1 and N . Note that the differentiation among several gases does not include the isotopic difference, i.e. all the isotopes of the “same” chemical component are treated as belonging to the same gas with label “ i ”.
P	Total pressure of some gas or gas mixture.
$P(b, m)$	Vector of parameters (b, m).
P_e	“Evaluated” pressure i.e. the result of evaluating the calibrating function of a PMD with the device reading. P_e equals the traceable pressure at the measuring pressure port of the PMD.
P_i	Partial pressure of the gas number “ i ” of some gas mixture containing N different gas- “species”, and “ i ” being a natural number between 1 and N . Note that the differentiation among several gases does not include the isotopic difference, i.e. all the isotopes of the “same” chemical component are treated as belonging to the same gas with label “ i ”.
Q_p	Sum of absorbances α_j for the segment p , used in the calculation of the integrated absorbance and its uncertainty.
R	Ideal gas constant: $(8.31451 \pm 7 \cdot 10^{-5})$ J/(K mol).
R	Pearson correlation coefficient.
R_v^0 / π	Steradiancy: radiancy per unit of solid angle measured with respect to the projected area.
r_0	Distance from the Herriott Cell front-mirror’s center to input/output hole.
S	Line intensity of the absorption line.
S'	Integrated absorption, (integrated absorbance per unit length) of the absorption line.
T	Thermodynamic temperature.
t_{rk}	Optical transmission of the absorbing media that presents an absorption coefficient k .
$uPP(i, j)$	Covariance matrix for the elements of the vector P .
$uWW(i, j)$	Covariance matrix for the elements of the vector W .
$uXX(i, j)$	Covariance matrix for the elements of the vector X .
$uZZ(i, j)$	Covariance matrix for the elements of the vector Z .

V_{FM}	Signal (Voltage) recorded in channel3 of the digitizing oscilloscope which corresponds to the measurement of the optical intensity I_{FM} in Detector-3.
V_{D0}	Signal (Voltage) recorded in channel1 of the digitizing oscilloscope which corresponds to the measurement of the optical intensity I_{D0} in Detector-1.
V_{R0}	Signal (Voltage) recorded in channel2 of the digitizing oscilloscope which corresponds to the measurement of the optical intensity I_{R0} in Detector2.
V_{Dk}	Signal (Voltage) recorded in channel1 of the digitizing oscilloscope which corresponds to the measurement of the optical intensity I_{Dk} in Detector-1.
V_{Rk}	Signal (Voltage) recorded in channel2 of the digitizing oscilloscope which corresponds to the measurement of the optical intensity I_{Rk} in Detector-2.
V_{TR}	Voltage of the triangular ramp of the function generator.
v_i	Vector characterizing the position and angle of a ray at the point i .
$W(i)$	Accessory vector used in the calculation of the integrated absorbance for a segment p , and its uncertainty.
$X(i)$	Accessory vector used in the calculation of the total integrated absorbance and its uncertainty.
$x(K, N)$	Function used in the characterization of the Herriott Cell.
x_i	Average measurement number “ i ”, of the quantity assigned to the abscissa.
x'_i	True value of the average measurement number “ i ” of the quantity assigned to the abscissa.
y_i	Average measurement number “ i ” of the quantity assigned to the ordinate scale.
Z	Signed distance from the VCMHC base point to the Herriott Cell back mirror (this distance is positive between when the back mirror is located between the base point and the confocal position).
Z_p	Sum of products $\alpha_j \cdot (t_j + t_{j+1})$ for the segment p , used in the calculation of the integrated absorbance and its uncertainty.
$Z(x, y)$	Vector sample.

Mathematical Symbols (Greek Symbols)

β	Angle of a ray to the normal vector of the intersecting surface.
δ	Intercept of the deceleration rate vs. rotation frequency linear fit of the SRG offset characterization.
$\delta(i, j)$	Dirac’s delta for the indexes i and j .
θ	Argument of a trigonometric function (angle).
φ	Argument of a trigonometric function (angle).

ν	Frequency (expressed in Hz or its decimal multiples or submultiples) or Wave-number (expressed in cm^{-1}) of radiation. The context will make clear which of this two is being used.
Ξ_p	Function of Ψ_p used in the calculation of the integrated absorbance and its uncertainty.
ξ	Offset-correcting term equal to the average of the plateau signal at 100% absorption.
$\mu_{x'}$	Expected value of x' for the distribution of true values x'_i .
Π_p	Function of Ψ_p used in the calculation of the integrated absorbance and its uncertainty.
ρ	Mass-density of the SRG-ball; or effective radius of curvature of the spherical mirrors of the Herriott Cell.
ρ_ν	Radiation spectral energy density.
σ_o	Accommodation coefficient of the SRG.
σ_{exex}	Variance of the distribution of errors of measurement of the x_i .
σ_{eyey}	Variance of the distribution of errors of measurement of the y_i .
$\sigma_{x'x'}$	Variance of the distribution of true values x'_i .
ν	Vibrational quantum number.
Ψ_p	Temporal position of the frequency marker signal maxima p .
Ω_p	Function of Ψ_p used in the calculation of the integrated absorbance and its uncertainty.
ω	Rotation frequency of the SRG-ball.
ω_e	Vibrational frequency of the harmonic oscillator.

Summary

The goal of this work was to investigate the viability of Tunable Diode Laser Absorption Spectroscopy (TDLAS) for its use as a primary standard for partial pressure measurements.

To undertake this investigation, we constructed a 3-channel spectrometer and developed a new controlling and processing software IPSIAM (Integrated Processing System for Integrated Absorbance Measurements) to implement a measurement procedure based on the direct numerical integration of the absorbance vs. wave-number curve (implied by the Beer-Lambert law).

In order to improve the accuracy of the input quantities of our measurement procedure, we developed three novel measuring systems, which in spite of being simple, delivered good improvements to their respective tasks. The first permits the simultaneous indirect measuring of the input intensity (entering the chamber) and transmitted intensity (leaving the chamber), with such accuracy that the ratio of them gives us the transmission figure with a relative uncertainty of 0.1%. The second was the application of a linear model to the characterization of our Herriott Cell, which permitted us the indirect measurement of the Herriott Cell parameters, i.e. the effective curvature radius and mirrors' distance, with reduced uncertainty (0.01%) using an external IR-laser interferometer and without having to remove the Herriott Cell out of the chamber. The third was the direct measuring of the gas temperature inside the chamber using two internal PT-100 sensors. Each sensor was welded to 4 small rods (4-wire resistance measurement) from the feed-trough connector to avoid contact with the chamber walls. With our method we dropped the gas' temperature uncertainty from 0.2% to 0.002%.

We developed two new algorithms in order to improve the accuracy of our measurements. After observing that some of our measurements were affected by a non-negligible apparatus-function, we developed a new algorithm to deconvolutionate the spectra and get rid off the error introduced by the apparatus-function to the integrated absorbance measurement. Our deconvolution algorithm, as far as we know, is the first one capable of correcting such measurements. We implemented our algorithm in one of our IPSIAM programs, and made several simulations, which agreed with the measured data. Another new algorithm developed by us permitted the measurement of the integrated absorbance and the calculation of its uncertainty according to GUM (by the first time, as far as we know).

To improve the accuracy of the measurements' output quantities (line intensities and partial pressures) we made repeated measurements and analyzed them in the framework of functional-structural linear analysis. Our system measured several line intensities of CO₂ with a relative expanded uncertainty of 1.0% ($k = 2$, about 95% level of confidence) which signifies an improvement in the level of accuracy by a factor of 4 (probably a factor of 10) in terms of the uncertainty figures given in HITRAN (nevertheless our results are in agreement with the values given in HITRAN). We measured partial pressures of CO₂ with a relative expanded uncertainty of 1.5% ($k = 2$, about 95% level of confidence); our results are in agreement with the corresponding gravimetric values reported by the PTB-Braunschweig (for a 5% CO₂ in N₂ mixture) and by the BAM (for a 0.1% CO₂ in N₂ mixture). As far as we know these are the first TDLAS traceable measurements of the corresponding line intensities and of partial pressures of CO₂.

The metrological level reached by our measuring installation permits to consider it as a primary standard for partial pressure measurements of CO₂.

Zusammenfassung

Ziel der vorliegenden Arbeit war die Untersuchung der Verwendbarkeit der durchstimmbaren Diodenlaser-Absorptionsspektroskopie (TDLAS) als Primärmethode für Partialdruck-Messung.

Um diese Untersuchung durchführen zu können, konstruierten wir ein 3-Kanal-Spektrometer, das eine Vakuumkammer mit beweglicher Herriott-Zelle umfasst. Weiterhin haben wir eine neue Steuerungs- und Verarbeitungssoftware IPSIAM (Integrated Processing System for Integrated Absorbance Measurements) entwickelt. Es wurde ein Messverfahren auf Basis der direkten numerischen Integration des Absorptionsvermögens (nach dem Beer-Lambert-Gesetz) eingesetzt.

Um die Genauigkeit der Eingangsgrößen unseres Messverfahrens zu verbessern, entwickelten wir drei neuartige Messsysteme, die trotz ihrer Einfachheit Verbesserungen bei der Lösung ihrer jeweiligen Aufgaben lieferten. Das erste Messsystem erlaubte die gleichzeitige indirekte Messung der Ein- und Ausgangsintensität. Die so erreichte relative Unsicherheit der optischen Transmission beträgt nur 0.1 % ($k = 1$). Das zweite Messsystem beruht auf der Anwendung eines Linearmodells zur Charakterisierung der Herriott-Zelle ohne diese aus der Kammer entfernen zu müssen. Eine indirekte Messung der Herriott-Zellenparameter (wirksamer Krümmungsradius und Distanz der Spiegel) wurde so ermöglicht. Es wurde eine relative Unsicherheit von 0.01 % ($k = 1$) erreicht. Das dritte System ermöglichte die direkte Messung der Gastemperatur unter Verwendung von zwei PT-100-Sensoren im Inneren der Vakuumkammer. Mit dieser Methode ließ sich die Unsicherheit der Gastemperatur um einen Faktor 100 auf 0.002 % verringern.

Nachdem eine nicht vernachlässigbare Apparatefunktion des Spektrometers beobachtet wurde, entwickelten wir einen neuen Algorithmus zur Entfaltung von Spektren. Damit konnte der durch die Apparatefunktion auftretende Integrationsfehler beseitigt werden. Nach unserem Wissensstand ist dies der erste Entfaltungs-Algorithmus, der in der Lage ist, Messungen des vorliegenden Typs zu korrigieren. Ein weiterer neu entwickelter Algorithmus erlaubt die Messung des Gesamt-Absorptionsvermögens und erstmals die Berechnung der zugehörigen Unsicherheit gemäß GUM.

Um die Genauigkeit der Ergebnisse der Messungen (Linienintensitäten und Partialdruck) zu verbessern, haben wir wiederholt gemessen und analysierten die Ergebnisse mit Hilfe der Funktional-Struktural-Linearanalyse. Mit unserem System konnten wir mehrere Linienintensitäten von CO_2 mit einer relativen Unsicherheit von 1.0 % ($k = 2$, Vertrauensniveau von ungefähr 95 %) messen. Das ergab eine Verbesserung der Genauigkeit um wenigstens den Faktor 4 (wahrscheinlich sogar den Faktor 10) im Vergleich zu den Unsicherheiten in HITRAN. Dennoch stimmen unsere Ergebnisse mit den in HITRAN gegebenen Werten überein. Wir haben den Partialdruck von CO_2 mit einer relativen Unsicherheit von 1.5 % ($k = 2$, Vertrauensniveau von ungefähr 95 %) gemessen. Unsere Ergebnisse stehen in Übereinstimmung mit den entsprechenden gravimetrischen Werten der PTB-Braunschweig (für eine Mischung von 5 % CO_2 in N_2) und der BAM (für eine Mischung von 0.1 % CO_2 in N_2). Unsere Messungen sind die ersten rückführbaren TDLAS-Messungen der entsprechenden Linienintensitäten und des Partialdrucks von CO_2 (so weit wir wissen).

Die an unserem Messplatz erreichten geringen Messunsicherheiten zeigen, dass TDLAS als Primärmethode zur Partialdruckbestimmung zumindest von CO_2 geeignet ist.

1. Introduction

The accurate measurement of gas partial pressures and gas concentrations are important tasks needed in many different fields like environmental control [1, 2], semiconductor and others industrial processing [3, 4] and medical diagnostics [5, 6], among others. In order to calibrate the instruments applied to make such measurements it is necessary to rely on some standard of measurement. Up to now mixtures of gases of “known” concentrations are the standards used to calibrate a wide range of instruments which are used to measure partial pressure or concentration of gas. The principle of operation of such instruments varies widely, including mass – spectroscopy, FTIR – spectroscopy, etc. The “known” mixtures also represent a wide range of quality from user-prepared mixtures to Reference Materials prepared by some National Metrology Institute (NMI) to commercial mixtures available from gas manufacturers. These mixtures may be traceable and are usually prepared using gravimetric techniques like those recommended by international standards [7]. Although being traceable, the gravimetric techniques impose an inherent level of uncertainty on the results which is usually bigger than the resolution that can be achieved with other (instrumental) techniques [1]. Furthermore, through gravimetric procedures it is not possible to prepare gas mixtures of very low concentrations.

At first sight it may seem that mass-spectrometers are candidates to be used as partial pressure secondary standards, but in practice it has been found that the signal of the mass-spectrometers depends heavily on the composition of the specific mixture being measured. For instance two different mixtures A and B may have the same partial pressure of some specific gas X, but the reading of a mass-spectrometer for the gas X in the mixture A will be different from its reading in the mixture B if the other gases present in the mixtures are not the same, or they are present in different proportions. That means, it is practically impossible to calibrate a mass-spectrometer to detect a given species in a general fashion, and therefore it is not suitable for being used as a reliable partial-pressure measurement instrument, and of course it is even further away of being used as a secondary standard.

The initial goal of this work was to investigate the viability of Tunable Diode Laser Absorption Spectroscopy (TDLAS) for its use as a primary standard for partial pressure measurements. To this end we had to find out:

- if TDLAS can be a reliable partial pressure measurement technique (PPMT),
- if the TDLAS-PPMT can be set up as an absolute method with traceability for all its input quantities, and
- if the TDLAS-PPMT can reach a metrological level high enough to be considered as a primary standard (see the definition of primary standard in section 7.4)

It is worth to point out here that gravimetric procedures permit to make gas mixtures of known partial pressures, but not to measure directly the partial pressure of some gas in a given (unknown)

sample. This last measurement is done by some instrument which has to be calibrated using reference materials. As we will show in this work, we have been able to demonstrate that TDLAS can be set up as a reliable absolute measurement technique for partial pressure measurements. In our approach we use the linear relation between the integrated absorbance and the product of the absorbing molecules density (i.e. number of molecules per cubic meter) times the absorbing length. This linear relation is implied by the Beer Lambert law. The corresponding proportionality factor is defined as the Line Intensity of the absorption line. We also found that when TDLAS is set up under several conditions, to be detailed later, it fulfills the metrological requirements to be used as a primary standard for partial pressures measurements. One of those prerequisites is to know the value of the line intensity of the absorption lines used to take the measurements. These values must be known with at least the same accuracy level as that of the sought partial pressure measurements accuracy. Given that the line intensity uncertainty values found in the literature lie between 2% and 40% and that the other input quantities of the Beer-Lambert law may be determined with uncertainty values of 0.5% or better, it is desirable to improve the accuracy of the line intensities to this same level in order to construct a Partial Pressure Measurement System which could be used as a Primary Standard.

In order to measure the line intensities for several gases and absorption lines, we have constructed a three-channel spectrometer, which incorporates the Vacuum Chamber with a Movable Herriott Cell (VCMHC) developed by E. Lanzinger and K. Jousten as part of an earlier doctoral research work at the PTB-Berlin [8], as well as other electronic and optic equipments used with the one-channel spectrometer at that time, like a Phase Sensitive Detector (PSD or Lock-in Amplifier), and a Fourier Transformed Infrared Spectrometer (FTIR-Spectrometer). New equipment was added in order to improve the experiment from a one-channel to a three-channel system, including another Phase Sensitive Detector, two ray-splitters and other equipment to be described in chapter 3. Using this system we were able to make traceable measurements of line intensities of several CO₂ absorption lines (R10 to R16) of the band centered at 4977.8 cm⁻¹. Furthermore, the uncertainties of our measurements are significantly smaller than those found up to now in the literature. For instance a typical value of our line intensity measurements has a relative uncertainty of 1.2% with about 95% of confidence ($k = 2$, traceable measurement). In addition our uncertainties are expressed according to the GUM. As far as we know our results are the first traceable measurements of line intensities for the absorption lines measured. The applicability of this technique for the absolute measurements of partial pressures was confirmed through measurements; that we carried out on samples sent by PTB – Braunschweig and on certified gas mixtures prepared by the German Federal Agency for Materials Science and Testing - BAM (Bundesanstalt für Materialforschung und –prüfung); as well as through measurements carried out by the Inorganic Analytic Group of PTB - Braunschweig [9, 10], using gas mixtures prepared by them.

The improvement in accuracy of the line intensity measurements was possible not only through the improvement from one to three channels of our spectrometer, but also through the improvements made to the methods for collecting and analyzing the measured data. We have

developed and used a completely new set of programs which permitted the automatic measurement of data, as well as its modular and documented processing. Our approach avoided the assumption of some particular absorption form-function, as is the case for analysis programs which perform a fit against an a priori selected form-function like Gaussian, Voigt, etc. So instead of calculating such a fit, we choose to perform a direct numerical integration of the absorbance vs. wave-number curve. The procedures of measurement are described in chapter 3.

The theoretical frame of this work is described in chapter 2, which along the necessary general theoretical basis also include in the section 2.6 a summary of an earlier work of the author [11] that had found wide application on this research. Being traceability one of the most important characteristics of the measurements that we have carried out, it is appropriate to include a copy of the certificates of calibration of all the calibrated equipment used in this work. Such copies can be found in appendix 7.2. This work is intended to be useful mainly for scientists working in metrology (especially partial pressure metrology) but it could be of interest also for researchers working in several fields, like applied spectroscopy, molecular physics, gas analysis, etc. Given that some of these scientists may not necessarily belong to National Metrology Institutes or otherwise be familiar with the modern metrological concepts, we have included as appendix 7.4 a reproduction of some of the definitions of terms found on the International Vocabulary of Metrology [12], and from the Guide to the Expression of Uncertainty in Measurement. In section 2.5 we discuss also some aspects of traceability, which is a modern metrological concept and it is very important for this work.

In Chapter 4 we present the experimental results and the corresponding analysis about the Line Intensity Measurements of some absorption lines of CO and CO₂ and its application to the measurement of partial pressure of CO₂.

In chapter 5 we discuss the applicability of TDLAS as a Primary Standard for Partial Pressure Measurements, including its advantages and limitations.

In chapter 6 we make the general conclusions and of this work, as well as the list of some of the tasks that lie ahead to continue this line of research.

All the appendices are collected together in chapter 7.

2. Theoretical Aspects

In this chapter we will try to summarize the theoretical background needed for the development of this work. In more detail the material can be found in many good text books [13, 14], and specialized books [15, 16] from which we just give a few references as example.

One subsection of this chapter contains new material developed by the author: the Section 2.2.2, which presents our algorithm to correct spectra affected by the apparatus-function.

The section 2.6 presents a summary of some functional-structural methods for linear analysis. These methods were developed since many years ago (mainly by statisticians) but have not found general application among the other branches of science. As we will see, the application of these Functional-Structural methods for linear analysis to our research has been very useful and permitted a physically consistent interpretation of several statistical parameters evaluated with our measurements.

2.1. Vibrational-Rotational Infrared Spectra of Gases

The molecular spectroscopy studies the interaction of electromagnetic radiation with molecules, especially when the energy states of the molecules are changed as a consequence of such interaction.

A photon of energy ΔE will be absorbed by a molecule if through that absorption the molecule can change its original molecular state of energy E_1 to a new molecular state of energy E_2 , where

$$\Delta E = h\nu = E_2 - E_1 . \quad (1)$$

The total number of energy levels of any molecule is enormous and some simplifications are necessary. The approximation in treating the molecule as if it possessed several distinct reservoirs of energy is in the majority of cases good enough to describe the observed molecular phenomena. In this case the total energy may be viewed as additively composed from the different reservoirs, which can be described by an equation such as:

$$E_{total} = E_{translational} + E_{nuclear\ orientational} + E_{rotational} + E_{vibrational} + E_{electronical} . \quad (2)$$

The photons of the electromagnetic radiation in the infrared have energies that are similar to the vibrational-rotational energy differences of most molecules. Therefore the structure of the IR-

spectra will be determined by the quantum-mechanical laws that govern the vibrations and rotations of molecules.

Rotation

The quantum-mechanical solution for a molecule having some rotational energy can be described with help of the rotational quantum number J as

$$\frac{E_r}{hc} = F(J) = B \cdot J \cdot (J+1) - D \cdot J^2 \cdot (J+1)^2 + \dots \quad (3)$$

where:

- E_r is the rotational energy,
- $F(J)$ is the rotational term value,
- B is the rotational constant, and
- D is the centrifugal constant.

For the rotational constant B we have

$$B = \frac{h}{8 \cdot \pi^2 \cdot c \cdot I_B} \quad (4)$$

where:

- I_B is the moment of inertia about an axis perpendicular to the inter-nuclear axis, and going through the molecule's center of mass,
- h is the Planck constant, and
- c is the velocity of light in vacuum.

The term $D \cdot J^2 \cdot (J+1)^2$ has its origin in the non-rigidity of the molecule and is very small compared with the $B \cdot J \cdot (J+1)$ term.

A transition purely rotational (i.e. the molecular energy changes from a rotational state to another without changing the vibrational state of the molecule) can take place only on molecules which have a permanent electrical dipole moment.

The selection rule $\Delta J = \pm 1$ applies to any transition affecting the rotational energy levels (i.e. rotational transitions or vibrational-rotational transitions).

Vibration

The vibration of a diatomic molecule can be described in the simplest case by a harmonic oscillator. Finer details of the observed infrared and Raman spectra may require considering the diatomic molecule as an anharmonic oscillator.

In general for a polyatomic molecule, it holds that, according to classical electrodynamics, any motion of the molecule which produces a variation of its electric or magnetic moments leads to the emission or absorption of radiation. From the variation of the different moments, the variation of the electric dipole moment is the one which produces (or absorbs) the strongest intensities of radiation.

In the harmonic oscillator approximation, any vibrational motion of the (polyatomic) molecule may be resolved into a sum of normal vibrations which frequencies correspond also to the frequencies of the photons that can be absorbed or emitted by the molecule.

The eigenvalues of the vibrational energy E_v , taking into account the anharmonic corrections, (for small anharmonicity) are discretized and characterized by the quantum vibration number v as follows.

$$\frac{E_v}{h \cdot c} = G(v) = \omega_e \cdot \left(v + \frac{1}{2}\right) - \omega_e \cdot x_e \cdot \left(v + \frac{1}{2}\right)^2 + \omega_e \cdot y_e \cdot \left(v + \frac{1}{2}\right)^3 + \dots \quad (5)$$

where

- E_v is the vibrational energy,
- $G(v)$ is the vibrational term value,
- ω_e is the vibrational frequency of the harmonic oscillator,
- $\omega_e \cdot x_e$ is the anharmonic quadratic term coefficient,
- $\omega_e \cdot y_e$ is the anharmonic cubic term coefficient.

Furthermore it holds that $\omega_e \cdot y_e \ll \omega_e \cdot x_e \ll \omega_e$.

The classical solution of the anharmonic oscillator (based on Fourier series) may be represented as a superposition of fundamental and overtone vibrations as follows:

$$x = \left(x_{01} \cdot \sin\{2 \cdot \pi \cdot \nu_{osc.} \cdot t\} + x_{02} \cdot (3 + \cos\{2 \cdot \pi \cdot 2 \cdot \nu_{osc.} \cdot t\}) + \right. \\ \left. + x_{03} \cdot (3 + \cos\{2 \cdot \pi \cdot 3 \cdot \nu_{osc.} \cdot t\}) + \dots \right), \quad (6)$$

where x_{01} , x_{02} , x_{03} , are the amplitudes of the fundamental, the first, and the second overtone, respectively.

Turning back to the quantum mechanical description, the selection rules for the harmonic oscillator are $\Delta v = \pm 1$, but for the anharmonic oscillator other transitions are also permitted with $\Delta v = \pm 2, \pm 3, \dots$. The observed transitions which take place between the ground state ($v = 0$) and these other superior states ($v = 2, 3, \dots$ etc.) do not present frequencies which are exactly two, three, etc. times the frequency of the transition from $v = 1$ to $v = 0$ (as it should be if the classical solution were the correct one), but are explained correctly with the quantum mechanical equations. In spite of that the bands 1-0, 2-0, 3-0, etc. are still frequently named to as fundamental, first overtone (second harmonic), second overtone (third harmonic) and so on.

Vibrational-rotational energy levels

By taking into consideration the interaction of vibration and rotation we obtain the term values on the molecule, for the approximation of the vibrating rotator, as

$$E_{vib-rot} = G(v) + F_v(J) = \left(\omega_e \cdot \left(v + \frac{1}{2} \right) - \omega_e \cdot x_e \cdot \left(v + \frac{1}{2} \right)^2 + \dots \right. \\ \left. + B_v \cdot J \cdot (J+1) - D_v \cdot J^2 \cdot (J+1)^2 + \dots \right). \quad (7)$$

A molecule may undergo pure rotational transitions (in which the vibrational state do not change, i.e. $\Delta J = \pm 1$, $\Delta v = 0$) but usually a transition in which the vibrational state changes implies also a change in the rotational state ($\Delta v = \pm 1, \pm 2, \pm 3, \dots$; $\Delta J = \pm 1$). Only in the special case when the molecule's angular momentum \vec{J} is in the molecular axis, it is possible to have “pure vibrational” transitions ($\Delta v = \pm 1$, $\Delta J = 0$).

Thermal distribution of quantum states and line intensities

The intensity of a spectral line depends on the probability that a molecule undergoes a transition and on the number of molecules which populates the states affected by that transition.

If the gas is in thermal equilibrium, the population of molecules in a given state is governed by the Boltzmann distribution, with the corresponding statistical weights g , which depends on the degeneracy of each state. The relation of the number of molecules per unit volume n_l with energy E_l to the number of molecules per unit volume n_u with energy E_u is given by

$$\frac{n_l}{n_u} = \frac{g_l}{g_u} \cdot \exp \left\{ -\frac{E_l - E_u}{kT} \right\} \quad (8)$$

where the label l denotes the lower quantum state and the label u denotes the upper quantum state, g is the statistical weight (which is equal to the degeneracy of the state) and k is the Boltzmann constant.

According to Einstein, the stochastic process of a molecule changing from one state to another under the influence of electromagnetic radiation can be described statistically under thermodynamic equilibrium with the help of some coefficients (Einstein coefficients), which are:

- $B_{l \rightarrow u}$ Einstein coefficient for induced absorption,
- $B_{u \rightarrow l}$ Einstein coefficient for induced emission, and
- $A_{u \rightarrow l}$ Einstein coefficient for spontaneous emission.

The coefficient $A_{u \rightarrow l}$ gives directly the probability of a molecule to undergo a transition from the upper to the lower state by spontaneous emission.

The coefficient $B_{l \rightarrow u}$ ($B_{u \rightarrow l}$) is defined in such a way that the probability of a molecule to undergo a transition from the lower to the upper state (upper to lower state) by induced absorption (induced emission) is equal to the product of this coefficient with the radiation spectral energy density $\rho_{\nu(lu)}$.

The radiation spectral energy density is described by the Planck blackbody distribution:

$$\rho_{\nu(lu)} = \frac{8 \cdot \pi \cdot h \cdot \nu^3(lu)}{c^3} \cdot \left(\exp \left\{ \frac{h \cdot \nu(lu)}{k \cdot T} \right\} - 1 \right)^{-1} . \quad (9)$$

At equilibrium, the number of molecules per unit volume per unit time that undergo a transition from the lower to the upper state must be equal to the number of molecules that undergo a transition the other way around (from the upper to the lower state), because only under this condition the distribution of states populations can be a stable (time independent) Boltzmann distribution. Therefore at equilibrium, it holds that

$$n_l \cdot B_{l \rightarrow u} \cdot \rho_{\nu(lu)} = n_u \cdot (A_{u \rightarrow l} + B_{u \rightarrow l} \cdot \rho_{\nu(lu)}) , \quad (10)$$

which rearranged implies for the relation of populations that

$$\frac{n_l}{n_u} = \frac{A_{u \rightarrow l} + B_{u \rightarrow l} \cdot \rho_{\nu(lu)}}{B_{l \rightarrow u} \cdot \rho_{\nu(lu)}} . \quad (11)$$

Substituting n_l/n_u from equation (8) in equation (11) we find for $\rho_{\nu(lu)}$ that

$$\rho_{\nu(lu)} = \frac{A_{u \rightarrow l}}{B_{l \rightarrow u}} \cdot \left(\frac{g_l \cdot B_{l \rightarrow u}}{g_u \cdot B_{u \rightarrow l}} \cdot \exp \left\{ -\frac{E_l - E_u}{k \cdot T} \right\} - 1 \right)^{-1} . \quad (12)$$

Comparing equation (9) with equation (12), and using the Bohr's condition for the absorbed or emitted radiation ($E_u - E_l = h \cdot \nu(lu)$), we find that the Einstein coefficients must fulfill the following relations:

$$A_{u \rightarrow l} = \frac{8 \cdot \pi \cdot h \cdot \nu^3(lu)}{c^3} \cdot B_{u \rightarrow l} , \quad (13)$$

$$g_l \cdot B_{l \rightarrow u} = g_u \cdot B_{u \rightarrow l} . \quad (14)$$

Now, assuming that the gas is uniformly distributed, in thermal equilibrium at temperature T , and presents isotropic optical properties, we may define the steradiancy, i.e. radiancy per unit of solid

angle measured with respect to the projected area, as R_v^0/π . Choosing the steradiancy to correspond to a blackbody at temperature T , we have that

$$\frac{R_v^0}{\pi} = \frac{c \cdot \rho_v}{4 \cdot \pi} . \quad (15)$$

With help of the steradiancy we can define a spectral absorption coefficient per unit length at the frequency ν , which, after integrating over the complete solid angle, fulfills the following equation:

$$-4 \cdot \frac{dR_v^0}{dL} d\nu = c \cdot \rho_v \cdot k_{L,\nu} d\nu , \quad (16)$$

which represents the rate of absorption of radiant energy per unit volume per unit time of photons of energy $h \cdot \nu$, in the frequency interval between ν and $\nu + d\nu$. Therefore the number of induced transitions n_{tr} from the state with energy E_l to the state with energy E_u , which is equal to the number of absorbed photons, (both per unit volume per unit time) is

$$n_{tr} = c \cdot \int_{-\infty}^{+\infty} \frac{\rho_v}{h \cdot \nu} \cdot k_{L,\nu} d\nu . \quad (17)$$

If the absorption coefficient is non-zero only for a narrow frequency range $\Delta\nu$ centered at $\nu(l, u)$ the last equation may be approximated by

$$n_{tr} = \frac{c \cdot \rho_{\nu(lu)}}{h \cdot \nu(lu)} \cdot \int_{-\infty}^{+\infty} k_{L,\nu} d\nu . \quad (18)$$

On the other hand, the net number of induced transitions n_{tr} can be calculated with help of the Einstein coefficients for induced absorption and induced emission as

$$n_{tr} = (n_l \cdot B_{l \rightarrow u} - n_u \cdot B_{u \rightarrow l}) \cdot \rho_{\nu(lu)} . \quad (19)$$

Substituting n_{tr} from equation (19) in equation (18) and rearranging we find the theoretical expression that links the integrated absorption S'_{lu} with the Einstein coefficients and the thermal distributions of the molecules as follows:

$$\begin{aligned} S'_{lu} &\equiv \int_{-\infty}^{+\infty} k_{L,\nu} d\nu = (n_l \cdot B_{l \rightarrow u} - n_u \cdot B_{u \rightarrow l}) \cdot \frac{h \cdot \nu(lu)}{c} \\ &= n_l \cdot B_{l \rightarrow u} \cdot \left(1 - \frac{n_u \cdot g_l}{n_l \cdot g_u}\right) \cdot \frac{h \cdot \nu(lu)}{c} \\ &= \frac{c^2}{8 \cdot \pi \cdot \nu^2(lu)} \cdot n_l \cdot A_{u \rightarrow l} \cdot \frac{g_u}{g_l} \cdot \left(1 - \frac{n_u \cdot g_l}{n_l \cdot g_u}\right) \end{aligned} \quad (20)$$

Substituting the products of densities and statistical weights from the Boltzmann distribution (equation (8)) in equation (20) we find, for thermal equilibrium:

$$\begin{aligned} S'_{lu} &= n_l \cdot B_{l \rightarrow u} \cdot \left(1 - \exp \left\{ \frac{-h \cdot \nu(lu)}{k \cdot T} \right\} \right) \cdot \frac{h \cdot \nu(lu)}{c} \\ &= \frac{c^2}{8 \cdot \pi \cdot \nu^2(lu)} \cdot n_l \cdot A_{u \rightarrow l} \cdot \frac{g_u}{g_l} \cdot \left(1 - \exp \left\{ \frac{-h \cdot \nu(lu)}{k \cdot T} \right\} \right) \end{aligned} \quad (21)$$

Finally for this subsection we will relate the integrated absorption S' with the integrated absorbance A_{abs} and the line intensity S as they are usually defined in the literature and as we will use them in this work (an operational definition of A_{abs} and S will be given in section 2.2.1), for the case in which the molecular density in the lower state n_l may be approximated as the total molecular density n of the absorbing gas, and for an absorption path-length L , then it holds that

$$\frac{A_{abs}}{L} = S \cdot n = S' . \quad (22)$$

2.2. Tunable Diode Laser Absorption Spectroscopy

2.2.1. Beer-Lambert Law

The line intensity gives a measure of the strength of the absorption (or emission) of radiation by some molecule when two specific energy levels of this molecule are affected by this radiation (either going from the lower energy level to the upper one during absorption of radiation, or the other way around during emission). It seems justified to use here the word “strength” in connection with our every-day experience: if we observe some light-emitting source through some material, we usually distinguish between the highly transparent materials (those which absorption of the light was “weak”) and opaque materials (those which absorption of light was “strong”). Nevertheless we know that the physical process behind absorption or emission of light is the change of energy state of some molecule (or atom) under interaction with some photon with the right energy to fit in to the energy difference of those molecular (or atomic) states. Such interactions between photons and molecules during absorption or emission are described correctly by means of the Einstein coefficients which give a measure of the probability of the transitions involved under some temperature and in the presence of some photon density. It is possible to demonstrate that the line intensity is proportional to the probability of absorption (or emission) of radiation by the transition between the two energetic states associated with that line intensity. Furthermore we can visualize this “probability measure” as the probability of interaction between a photon (of some specific frequency) and a molecule (in some

specific energy state), so the line intensity is a “transversal cross section” for this interaction, as evidenced when we look at the corresponding SI units for the line intensity: $\text{m}^2/(\text{molecule} \cdot \text{s})$ (area per molecule and per second - available for the photon to undergo a “collision”). Given that the molecule can stay in each energetic level or state only a finite period of time, the amount of energy associated with each state is not exact, but varies in connection with the life time of the state as dictated by the uncertainty principle. Therefore there is not only one exact energy-match (frequency-match) for the photon being emitted or absorbed during the transition, but a window of values best described by a bell-shaped distribution (either symmetric or not) which dictates the specific probability that a photon with a particular frequency may be absorbed or emitted by the transition. The sum of all this probability factors for all the possible frequencies of the photons being absorbed or emitted by this transition, gives the overall line intensity mentioned above. As a consequence, if one wants to measure the line intensity for some specific transition, a possible way is to observe the amount of absorption of tunable monochromatic radiation for all the possible photon frequencies involved, and to perform the corresponding sum of coefficients. This sum can be done as the integration over the absorption line in an absorbance vs. wave-number graph. In this case the graph itself contains all the physical information collected during the experiment and, if the experiment is performed correctly, this experimental data can be easily understood by means of the Lambert-Beer law,

$$I(\nu) = I_0(\nu) \exp\{-k(\nu - \nu_c) \cdot n \cdot L\}, \quad (23)$$

where:

- $I(\nu)$ is the transmitted (i.e. not absorbed) intensity of the radiation at the frequency ν directed after the absorbing media to the detector,
- $I_0(\nu)$ is the input intensity of the radiation at the frequency ν directed toward the absorbing media i.e. radiation intensity before being affected by the absorbing media,
- n is the molecular density of the absorbing media (number of absorbing molecules per volume),
- L is the length path of the radiation through the absorbing media, and
- $k(\nu - \nu_c)$ is the absorption coefficient of the absorbing media for the specific radiation frequency ν and line center ν_c .

If the measurement was not made with a “monochromatic” source, the mathematical model needed to understand the experimental data still uses the Lambert-Beer law but only as part of a more complicated equation, as we will see in section 2.2.2.

As mentioned above, the overall sum of the $k(\nu - \nu_c)$ absorption coefficients over all the possible wave-numbers is what forms the quantity defined as line intensity (denoted here as S)

$$S = \int_{-\infty}^{+\infty} k(\nu - \nu_c) \cdot d\nu. \quad (24)$$

It is important to remind that although the Lambert-Beer law does not present an explicit dependency with temperature, the spectral absorption coefficients $k(\nu - \nu_c)$ do depend on temperature and therefore the Line Intensity S also does depend on temperature. It is customary to report the S value at some conventional temperature, like 296 K.

In some cases the distribution of absorption coefficients (vs. wave-number) is well described by some known mathematical distribution, like those of Gauss, Lorentz or Voigt, and denoted here in general as “form functions” - $F_f(\nu - \nu_c)$. Therefore it is customary to write down the relation between the spectral absorption coefficient - $k(\nu - \nu_c)$ - and the Line Intensity - S - as

$$k(\nu - \nu_c) = S \cdot F_f(\nu - \nu_c) , \quad (25)$$

where the $F_f(\nu - \nu_c)$ is always normalized such that

$$\int_{-\infty}^{\infty} F_f(\nu - \nu_c) d\nu = 1 . \quad (26)$$

In this case it is possible to extract the S value from the experimental data by mean of a “fit procedure” which optimizes the parameters needed to bring some form function as close as possible to the experimental data. Although this may be very efficient from a numerical calculation point of view, care must be taken to assure that the experimental conditions were such that the data can be really explained by means of one of this form functions, for instance that the pressure was low enough to have a domination of Doppler broadening (which can be modeled by a Gaussian distribution). Furthermore it has been observed by many authors that the experimental apparatus itself can affect the form of the spectrum (the so called apparatus form function) in a way that is not easy to model, and the experimental determination of this apparatus form function can be very time and effort consuming. Based on these considerations and aimed to reach accuracy as high as possible, we have developed some procedures as part of our analysis programs, to numerically integrate directly the area of the “ $k(\nu - \nu_c)$ vs. ν ” curve (A_{abs}). In this way we have not to worry about the validity of assumptions regarding form functions. Nevertheless each procedure has advantages and disadvantages and in our case we have to be sure that we cover a spectral window wide enough around the absorption peak to be certain that we are integrating as much as necessary and that the discretization step in frequency space is small enough to achieve the needed accuracy. We have developed some tests to verify that our measurements meet both requirements.

2.2.2. Deconvolution of Spectra Affected by the “Apparatus-Function”

The Lambert-Beer law, described by the equation (23), permits to understand the absorption of radiation by an absorbing media under the assumption that the excited states of the transition

involved are poorly populated (i.e. in that forms it does not take account for stimulated emission). Therefore, if the stimulated emission can be neglected, equation (23) describes accurately the absorption of radiation process. To apply this equation as measurement model there must be monochromatic irradiation. The Laser is our best approximation for a monochromatic radiation and yet each laser beam has some type of emission profile, which in frequency (or wave number) domain looks sort of bell-like. For diode lasers, the half width at half maximum (HWHM) in wave-number domain is usually in the order of 10^{-3} cm^{-1} for pulsed-lasers and 10^{-4} cm^{-1} for lasers driven in continuous wave (cw) mode [17], so that they are usually narrower than the majority of the vibration-rotation absorption lines under Doppler-broadening. Actually the laser beam profile is usually narrow enough to consider equation (23) as a good approximation for the measurement model of several TDLAS techniques.

More rigorously treated, the transmitted intensity measurements of a spectroscopic experiment (in which the absorption peak of some transition is registered in dependency of the “irradiated wave-number” $\bar{\nu}$) are well described by a modified version of equation (23) which takes into account the apparatus function. In case of TDLAS the apparatus function $A(\nu - \bar{\nu})$ is basically the finite emission profile of the laser, which explicitly written in the equation (23) transforms it to

$$I(\bar{\nu} - \nu_c) = \bar{I}_0(\bar{\nu}) \int_{-\infty}^{+\infty} A(\nu - \bar{\nu}) \cdot \exp\{-n \cdot L \cdot S(T) \cdot F_f(\nu - \nu_c)\} d\nu , \quad (27)$$

where

- $\bar{\nu}$ is the center of the laser emission profile and equal to the measured wave-number,
- $I(\bar{\nu} - \nu_c)$ is the measured intensity for to the measured wave-number $\bar{\nu}$,
- $\bar{I}_0(\bar{\nu})$ is the total (integrated) intensity emitted by the laser for all the wave-numbers simultaneously at a given time point t and which, without absorbing media, is detected at that point t as the intensity for the measured wave-number $\bar{\nu}$, and
- $A(\nu - \bar{\nu})$ is the emission profile of the laser, which is also a bell-like normalized form function, such that

$$\int_{-\infty}^{+\infty} A(\nu - \bar{\nu}) d\nu = 1 . \quad (28)$$

From (27) and (28) we see that, when the absorption is very small, and the exponential can be approximated by its linear term, the convolution of the two normalized form-functions leaves another normalized form function. This is the origins of the implicit believe of many authors, that the apparatus form function produces broadening of the observed absorption peak, while the

integrated absorbance is kept constant under that deformation. This is true only to the extent that the linear approximation to the exponential term of the absorption is accurate enough for the purposes of the measurement application. In other cases it is necessary to deconvolute the equation (27) in order to get rid off the apparatus-function and to recover the “real” extinction function, from which the line intensity can be determined.

The deconvolution algorithms for spectroscopic analysis found by us in the literature, including books [18, 19] and articles [20, 21, 22, 23] assumed (explicitly or implicitly) the conservation of the area under the absorbance vs. wave-number curve³, and therefore those algorithms are not suitable to correct the measured spectra which was affected by the apparatus function in order to obtain the line intensity from the integrated absorbance. Other articles [24, 25] and books [26, 27] describe correctly the error introduced by the apparatus function in the integrated absorbance measurement, but they do not offer a solution to correct the affected measured data (at least not to obtain the correct area under the curve).

Given that some of our measurements gave evidence of being affected by a not negligible apparatus-function and that we did not find in the literature an algorithm appropriate to deconvolute the equation (27), we developed our own algorithm, which we will explain next.

Our solution is based on the measurement of two spectra of the same absorption line: one with strong absorption (to have a big area to integrate) and other with weak absorption. The idea is to take advantage that our facility is capable of produce and control very high levels of vacuum, so that we can measure gas absorptions at very low pressures, where the Doppler broadening is completely dominant. Furthermore we can take measurements also with short absorption path-length, so that the exponential absorption term can be approximated by the linear term of its Taylor expansion. From this measurement (Doppler-broadened weak absorption) we can found a preliminary apparatus-function by the deconvolution with a theoretical Gaussian extinction function, which HWHM is the theoretical one for the respective molecule and temperature, and a preliminary value for the line intensity. Then, we use the preliminary apparatus-function to deconvolute the strong-absorption spectra, and from it we measure an improved value for the line intensity. With the new line intensity we run the whole process again, finding iteratively improved versions of the apparatus function and of the line intensity until they converge to stationary values.

We implemented the deconvolutions with the discrete Fourier-transform and the inverse discrete Fourier-transform. The equation to calculate the apparatus-function is:

³ Some examples to can be taken from the following citations: From [18], page 93: “deconvolution seems to preserve the (line) intensity quite well when the response function is reasonably completely removed”. From [19], page 44: “Measurements of the total integral absorption S may be made by using the methods of equivalent widths. Such measurements are independent of instrumental broadening...”. From [20], page 62: “The total area of the component bands are not effected by self-deconvolution”. From [21], page 250: “Since the deconvolution procedure conserves the area under the original spectral line ...”. From [22] page 1833: “Since the apparatus function $A(\nu)$ can be determined experimentally for a given instrument, one can use the method of deconvolution first devised by Van Cittert in 1931 to invert the convolution integral by an iterative calculation.” (This iterative method from Van Cittert uses the constancy of the area under the curve as part of the algorithm).

$$A(\nu - \bar{\nu}) = FT^{-1} \left\{ \frac{FT\{(I_{01}(\bar{\nu}) - I_1(\bar{\nu} - \nu_c))/I_{01}(\bar{\nu})\}}{FT\{n_1 \cdot L_1 \cdot S \cdot \Phi(\nu - \nu_c)\}} \right\}, \quad (29)$$

where

- I_1 is the transmitted intensity for the weak absorption measurement,
- I_{01} is the original (predicted) intensity for the weak absorption measurement,
- $\Phi(\nu - \nu_c)$ is the ideal Gauss form-function with theoretical HWHM for the weak absorption measurement.

As we mentioned, with the apparatus-function we deconvolutionate the strong absorption measurement and obtained the improved corresponding extinction function, as follows:

$$\exp\{-k(\nu - \nu_c) \cdot n_2 \cdot L_2\} = FT^{-1} \left\{ \frac{FT\{I_2(\bar{\nu} - \nu_c)/I_{02}(\bar{\nu})\}}{FT\{A(\nu - \bar{\nu})\}} \right\}, \quad (30)$$

where

- I_2 is the transmitted intensity for the strong absorption measurement, and
- I_{02} is the original (predicted) intensity for the strong absorption measurement.

When the iterative process has reached a certain limit of accuracy, we integrate numerically the negative logarithm of the final corrected extinction function (i.e. we integrate the corrected absorbance vs. wave-number function) to obtain the corrected line intensity at the measured temperature $S(T)$:

$$S(T) = \frac{\int_{-\infty}^{+\infty} \{k(\nu - \nu_c) \cdot n_2 \cdot L_2\} d\nu}{n_2 \cdot L_2} = \frac{A_{abs}(T)}{n_2 \cdot L_2}. \quad (31)$$

2.3. Herriott-Cell

The Herriott Cell was originally proposed by Herriott as a laser resonator [28]. Since the proposal of Altmann et al. [29], it has been widely used for gaseous absorption measurements with weak line intensities. Other applications are: optical delay line [30], high reflectivity measurements [31], to separate a sequence of pulses [32] and as improving part of a high resolution interferometer [33].

The Herriott Cell consist of two concave spherical mirrors facing each other axially, so that they form a cavity, and one of them having a small hole near its edge. If the distance between the mirrors is conveniently chosen and a ray is injected in the cavity through the hole at some convenient angle, the ray will travel several times through the cavity and, after some number of reflections, it will leave the cavity through the same hole. There are many distances between the mirrors that fulfill

the close-path output condition, so if we call front mirror the mirror having the hole, and back mirror the other one, it is possible to vary the total length traveled by the ray through the repositioning of the back mirror. An important property of the “classical” arrangement of the Herriott Cell is that the direction of the output ray is independent of the number of reflections that the ray has undergone, so it is possible to adjust and fix the input and output optics of the experiment without having to re-adjust when another path-length is selected. The Figure 1 shows a schematic illustration of the Herriott Cell with the mirrors at “confocal” distance, in which the ray makes four passes through the cell. The Figure 2 shows a picture of our apparatus where two spherical mirrors identical to the ones used in the VCMHC are positioned so that the ray makes six passes through the cell.

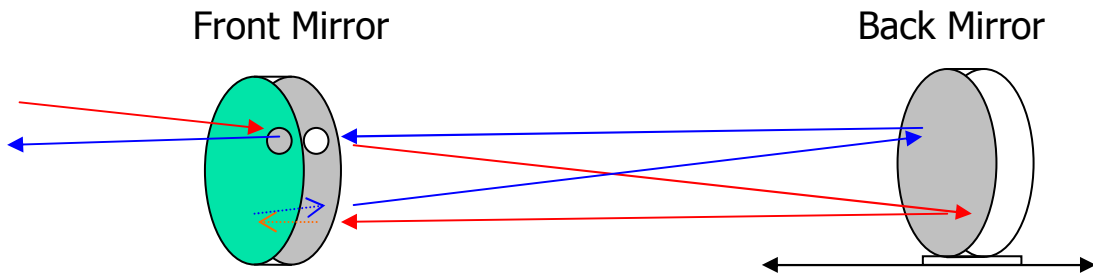


Figure 1. Herriott Cell: the path-length of the ray is (stepwise) selectable by re-positioning the back mirror.

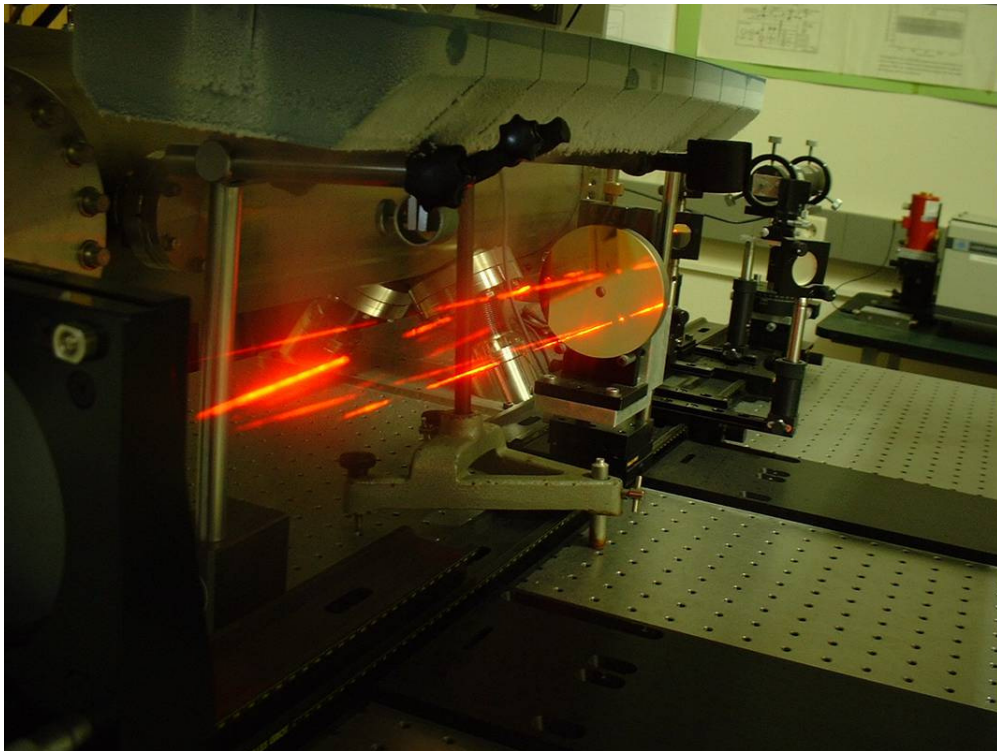


Figure 2. Picture of a Herriott Cell in our system illuminated by a He-Ne laser.

As it is customary in most Herriott Cell applications, we will calculate the total path length traveled by the ray inside the Herriott Cell (Herriott Cell path length, for short) using ray optics, i.e.

we will neglect the possible wave optic effects and we will keep our experimental arrangement in such way that this simplification may be always valid. For instance we will not increase the number of reflections in the Herriott Cell beyond 65 (i.e. 66 passes), as then the reflecting points come to close to each other and interference among the rays at these points could not be neglected any longer.

We will discuss rays in the paraxial approach [34], i.e. the angle of incidence β of the ray to any interacting surface (measured from the normal vector to the surface, as usually), is smaller than about 15° ($\beta \leq 0.25$ radians), so that $\sin(\beta) \approx \tan(\beta) \approx \beta$. We also use the Gauss-Matrices formalism [35], so that a ray starting in the point P_1 is characterized by its distance and its angle to the z -axis (see Figure 3), and these parameters are combined to the ray vector v_1 .

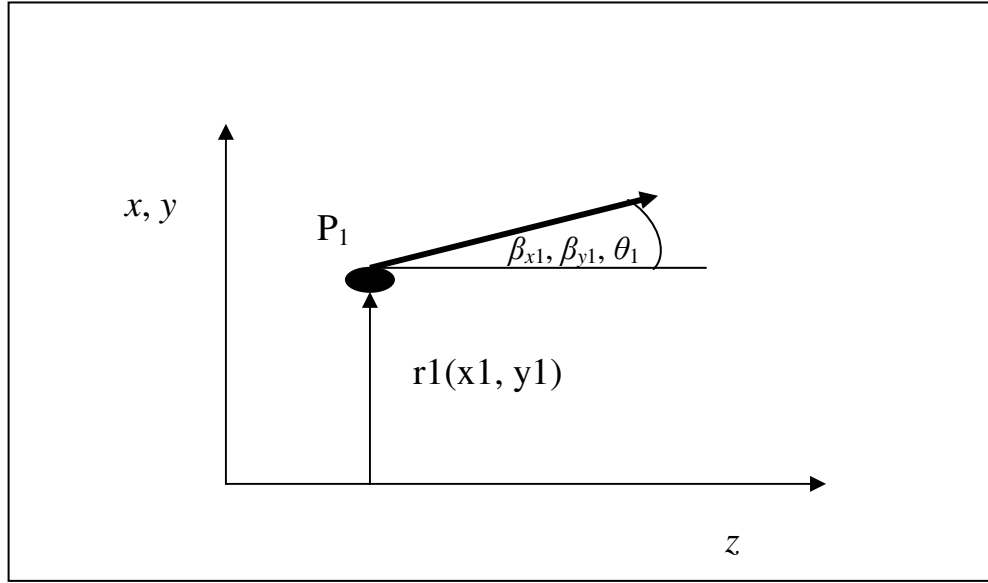


Figure 3. Illustration for the ray optics with Gauss-Matrices formalism.

Some examples of the vector v_1 are:

For circular symmetry,

$$v_1 = \begin{pmatrix} r_1 \\ \theta_1 \end{pmatrix}, \quad (32)$$

and for one-dimensional systems (separable rays),

$$v_{1X} = \begin{pmatrix} x_1 \\ \beta_{x1} \end{pmatrix}, \quad v_{1Y} = \begin{pmatrix} y_1 \\ \beta_{y1} \end{pmatrix}. \quad (33)$$

Now the optical transformations can be easily expressed in terms of appropriate matrices. For example the propagation from P_1 to P_2 at distance ℓ along the z -axis is described by (for a one dimensional system)

$$\mathbf{v}_2 = \begin{pmatrix} x_2 \\ \beta_{x2} \end{pmatrix} = \begin{pmatrix} 1 & \ell \\ 0 & 1 \end{pmatrix} \cdot \begin{pmatrix} x_1 \\ \beta_{x1} \end{pmatrix}. \quad (34)$$

In the paraxial approach we can write in general the propagation of ray vectors through first order optical systems as

$$\mathbf{v}_2 = \mathbf{M} \cdot \mathbf{v}_1, \quad (35)$$

where \mathbf{M} is a matrix of the form

$$\mathbf{M} = \begin{pmatrix} A & B \\ C & D \end{pmatrix} \quad (36)$$

and A , B , C and D are scalars for one-dimensional systems or 2x2 matrices for two-dimensional systems. If the ray goes through several surfaces (transmissions, and/or refractions, and/or reflections) the vector of the final \mathbf{v}_2 ray can be calculated using the equation (35). In that case, the matrix \mathbf{M} is the product of all the matrices \mathbf{M}_j , where \mathbf{M}_j is the matrix corresponding to the j^{th} surface:

$$\mathbf{M} = \prod_{j=1}^n \mathbf{M}_j. \quad (37)$$

It is useful to recall the Sylvester's formula [34], which states that given a 2x2 matrix

$$\mathbf{M} = \begin{pmatrix} A & B \\ C & D \end{pmatrix}, \quad (36)$$

its N^{th} power is given by

$$\mathbf{M}^N = \frac{1}{\sin\{\varphi\}} \cdot \begin{pmatrix} A \cdot \sin\{N \cdot \varphi\} - \sin\{(N-1) \cdot \varphi\} & B \cdot \sin\{N \cdot \varphi\} \\ C \cdot \sin\{N \cdot \varphi\} & D \cdot \sin\{N \cdot \varphi\} - \sin\{(N-1) \cdot \varphi\} \end{pmatrix}, \quad (38)$$

where

$$\cos\{\varphi\} = \frac{A+D}{2}. \quad (39)$$

If we now consider an optical resonator formed by two spherical mirrors with radius of curvature ρ_1 and ρ_2 , it follows that, after one round trip (i.e. two reflections), the original ray vector \mathbf{v}_0 is transformed into the ray vector $\mathbf{v}_1 = \mathbf{M} \cdot \mathbf{v}_0$, where \mathbf{M} is the resonator's round trip matrix,

$$\mathbf{M} = \begin{pmatrix} A & B \\ C & D \end{pmatrix} = \begin{pmatrix} 2 \cdot g_2 - 1 & 2 \cdot \ell \cdot g_1 \\ \frac{2}{\ell} \cdot (2 \cdot g_1 \cdot g_2 - g_1 - g_2) & 4 \cdot g_1 \cdot g_2 - 2 \cdot g_2 - 1 \end{pmatrix}, \quad (40)$$

where ℓ is the distance between the two spherical mirrors and $g_i = 1 - \ell/\rho_i$.

If the ray is reproduced after N round trips (close-path condition) then $\mathbf{v}_N = \mathbf{M}^N \cdot \mathbf{v}_0$ and \mathbf{M}^N must be the unity matrix. For the Herriott cell, the first (input) ray would be reproduced after the last

reflection (reflection number $2 \cdot N$). That last reflection would take place in the surface where the hole is located (if there were not hole). When the close-path condition is reached in the Herriott Cell, the output ray leaves the cavity through the hole (i.e. after $2 \cdot N - 1$ reflections). Nevertheless we can still use the round trip matrix M , and the condition that M^N must be the unity matrix, because once the ray comes back to the input (output) point, it is not important for the description of the (already traveled) path if the ray is reflected once more (reproducing the first ray) or it escapes through the hole. Using the Sylvester's formula we have

$$M^N = \begin{pmatrix} 1 & 0 \\ 0 & 1 \end{pmatrix} = \frac{1}{\sin\{\varphi\}} \cdot \begin{pmatrix} A \cdot \sin\{N \cdot \varphi\} - \sin\{(N-1) \cdot \varphi\} & B \cdot \sin\{N \cdot \varphi\} \\ C \cdot \sin\{N \cdot \varphi\} & D \cdot \sin\{N \cdot \varphi\} - \sin\{(N-1) \cdot \varphi\} \end{pmatrix} \quad (41)$$

with

$$\cos\{\varphi\} = \frac{A + D}{2} = 2 \cdot g_1 \cdot g_2 - 1 . \quad (42)$$

From equation (41) we see that, for the off-diagonal terms, we have

$$\begin{aligned} \sin\{N \cdot \varphi\} = 0 &\Rightarrow N \cdot \varphi = p \cdot 2 \cdot \pi \quad \forall \quad p \in \mathbb{Z} \\ \sin\{\varphi\} \neq 0 &\Rightarrow \varphi = \frac{p \cdot 2 \cdot \pi}{N} \quad \forall \quad \frac{p}{N} \notin \mathbb{Z} \end{aligned} \quad (43)$$

and, for the terms in the diagonal, we have

$$\frac{\sin\{(N-1) \cdot \varphi\}}{\sin\{\varphi\}} = -1 . \quad (44)$$

Substituting φ from equation (43) in equation (42), we have

$$\cos\left\{\frac{p \cdot 2 \cdot \pi}{N}\right\} = 2 \cdot g_1 \cdot g_2 - 1 , \quad (45)$$

which we can transform in

$$\frac{\cos\{\varphi\} + 1}{2} = \cos^2\left\{\frac{\varphi}{2}\right\} = \cos^2\left\{\frac{p \cdot \pi}{N}\right\} = g_1 \cdot g_2 . \quad (46)$$

Now let's define the effective radius of curvature of both mirrors ρ as $\rho = (\rho_1 \cdot \rho_2)^{1/2}$ and the factor g as $g = 1 - L/\rho$. From equation (46) we find that

$$g_1 \cdot g_2 = g^2 = \left(1 - \frac{\ell}{\rho}\right)^2 = \cos^2\left\{\frac{p \cdot \pi}{N}\right\} , \quad (47)$$

and only when the distance between the mirrors ℓ fulfills the equation (47) for some integral number p and some (natural) number of round-trips N , the resonator condition leads to a close-path trajectory and the output ray escapes through the hole (after $2 \cdot N$ passes and $2 \cdot N - 1$ reflections).

In our setup, the mirror's separation can be adjusted from semi-confocal ($\ell = f/2 = \rho/4$) to confocal ($\ell = f = \rho/2$), so that in taking the square root of equation (47) we need to choose the roots of equal sign at each side of the equation which leads to the following expression for ℓ :

$$\ell = \rho \cdot \left(1 - \cos \left\{ \frac{p \cdot \pi}{N} \right\} \right). \quad (48)$$

It is interesting to note that p can be physically interpreted as the number of turns that the ray undergoes along the ellipsoid of reflecting points, until it returns to the initial (entrance and exit) point. It has been shown [36] that the number of round trips N can be related with the number of turns p and an integral number K , which was called the Family-number, through the following equation:

$$N = 2 \cdot p + K. \quad (49)$$

Substituting p from equation (49) in equation (48) we obtain:

$$\ell = \rho \cdot \left(1 - \cos \left\{ \frac{\pi}{2} \cdot \left(1 - \frac{K}{N} \right) \right\} \right). \quad (50)$$

The whole path-length L_{HC} traveled by the ray inside the Herriott cell, after N round-trips, is given with a very good approximation by [32]

$$L_{HC} = 2 \cdot N \cdot \left(\ell + \frac{r_0^2}{2 \cdot \rho - \ell} \right), \quad (51)$$

where r_0 is the radial distance between the entrance hole and the mirror's axis. After substituting the mirror's separation ℓ from equation (50) in equation (51) and re-arranging the result, we get the equation for L_{HC} as

$$L_{HC} = 2 \cdot N \cdot \rho \cdot \left(1 - \sin \left\{ \frac{K \cdot \pi}{2 \cdot N} \right\} + \frac{r_0^2}{\rho^2 \cdot \left(1 + \sin \left\{ \frac{K \cdot \pi}{2 \cdot N} \right\} \right)} \right). \quad (52)$$

2.4. Uncertainty Analysis

The uncertainty determinations made in this work were done according to the prescriptions of the Guide to the Expression of Uncertainty in Measurement (GUM) [37]. Several concepts and explanations of the GUM have been incorporated in appendix 7.4 (glossary), in order to facilitate its lecture as complementary material for this work.

The following is the “Summary of procedure for evaluating and expressing uncertainty” as given in GUM (clause 8):

“1 Express mathematically the relationship between the measurand Y and the input quantities X_i on which Y depends: $Y = f(X_1, X_2, \dots, X_N)$. The function f should contain every quantity, including all corrections and correction factors, that can contribute a significant component of uncertainty to the result of the measurement (see 4.1.1 and 4.1.2).

2 Determine x_i , the estimated value of input quantity X_i either on the basis of the statistical analysis of series of observations or by other means (see 4.1.3).

3 Evaluate the standard uncertainty $u(x_i)$ of each input estimate x_i . For an input estimate obtained from the statistical analysis of series of observations, the standard uncertainty is evaluated as described in 4.2 (Type A evaluation of standard uncertainty). For an input estimate obtained by other means, the standard uncertainty $u(x_i)$ is evaluated as described in 4.3 (Type B evaluation of standard uncertainty).

4 Evaluate the covariances associated with any input estimates that are correlated (see 5.2).

5 Calculate the result of the measurement, that is, the estimate y of the measurand Y , from the functional relationship f using for the input quantities X_i the estimates x_i obtained in step 2 (see 4.1.4).

6 Determine the combined standard uncertainty $u_c(y)$ of the measurement result y from the standard uncertainties and covariances associated with the input estimates, as described in clause 5. If the measurement determines simultaneously more than one output quantity, calculate their covariances (see 7.2.5, H.2, H.3, and H.4).

7 If it is necessary to give an expanded uncertainty U , whose purpose is to provide an interval $y - U$ to $y + U$ that may be expected to encompass a large fraction of the distribution of values that could reasonably be attributed to the measurand Y , multiply the combined standard uncertainty $u_c(y)$ by a coverage factor k , typically in the range 2 to 3, to obtain $U = k u_c(y)$. Select k on the basis of the level of confidence required of the interval (see 6.2, 6.3, and especially annex G, which discusses the selection of a value of k that produces an interval having a level of confidence close to a specified value).

8 Report the result of the measurement y together with its combined standard uncertainty $u_c(y)$ or expanded uncertainty U as discussed in 7.2.1 and 7.2.3; use one of the formats recommended in 7.2.2 and 7.2.4. Describe, as outlined also in clause 7, how y and $u_c(y)$ or U were obtained.”

The combined uncertainty $u_c(y)$ mentioned in the paragraph 6 above is calculated according to the following formula (GUM equation 13):

$$u_c^2(y) = \sum_{i=1}^N \sum_{j=1}^N \frac{\partial f}{\partial x_i} \cdot \frac{\partial f}{\partial x_j} \cdot u(x_i, x_j) \quad (53)$$

where $u(x_i, x_j)$ is the estimated covariance associated with x_i and x_j .

But if several output quantities are measured simultaneously, not only the variances of each one of the output quantities must be calculated, but also their covariances. In other words, all the elements of the output covariance matrix must be calculated and the equation (53) is replaced by a more general expression as follows (GUM equation H.9)

$$u(y_l, y_m) = \sum_{i=1}^N \sum_{j=1}^N \frac{\partial y_l}{\partial x_i} \cdot \frac{\partial y_m}{\partial x_j} u(x_i, x_j) \quad (54)$$

The equation (54) permits to calculate the elements of the output covariance matrix $u(y_l, y_m)$ (in our notation $u_{YY}[l,m]$) in terms of the input covariance matrix $u(x_i, x_j)$ (in our notation $u_{XX}[i,j]$) and can be regarded as the more general form of the law of propagation of uncertainty. The elements of the diagonal of the covariance matrices are the variances of the corresponding quantities (e.g. $u(x_i, x_i) = u^2(x_i)$).

2.5. Some Considerations about Traceability

Traceability is a concept on modern metrology developed to help assuring the credibility of the stated accuracy of a (traceable) measurement. It does not imply that a traceable measurement has a high level of accuracy, but that the level of accuracy stated by the measurement result (whether enough accurate or not for some particular purpose), characterized by the stated uncertainty of the measurement result can be considered as a reasonable and credible in the sense that the reported uncertainty really covers a window of results, each of them being a reasonable value of the measurand at the level of confidence stated. The definition of traceability is found in the International Vocabulary of Basic and General Terms in Metrology (VIM). A copy of such definition is included in the glossary of this work, appendix 7.4.

The importance of traceability as a mean to bring confidence in the result of a measurement has been recognized in several fields including commerce and industrial production. To illustrate the implications of this concept we will cite from the web-site of the International Bureau of Weights and Measures (BIPM):

“Metrology is of fundamental importance in industry and trade – not only from the point of view of the consumer but also for those involved in manufacturing. Both groups must have confidence in the accuracy and reliability of the measurements upon which they depend. Within the manufacturing process, to ensure the accuracy of measuring instruments, it is essential that they should be periodically calibrated against more accurate standards, which in turn should have their calibration traceable to even more accurate national measurement standards at the national level and, eventually, the international level. When these various levels of calibration have been documented, a chain of traceable calibrations is created.

Traceability means that the result of a measurement, no matter where it is made, can be related to a national or international measurement standard, and that this relationship is documented. In addition, the measuring instrument must be calibrated by a measurement standard that is itself traceable. Traceability is thus defined as the property of the result of a measurement or the value of a standard whereby it can be related to stated references, usually national or international, through an unbroken chain of comparisons all having stated uncertainties. The concept of traceability is important because it makes possible the comparison of the accuracy of measurements worldwide according to a standardized procedure for estimating measurement uncertainty.”

It is clear from the citation that the property of traceability is very desirable for any measurement which result should be credible and accepted by many different parties. The results of experimental research must be as credible as possible. The measurement results of the scientific experiments must be stated in such a way that their comparability to the results of other experiments could be established as clear and as sound as possible. Traceability is the best way to provide confidence and comparability to any measurement result. Establishing traceability to the result of a measurement imply necessarily some effort and investment (both, in time and money), and it may seem for some people as something belonging to the quality control labs in the industry or governmental agencies. Nevertheless, the research labs may benefit enormously if they incorporate some elements of the “metrological culture” (especially traceability) for the assurance of their results. On this regard it would be ideal, if some day all the published experimental results in the different scientific journals could have the property of being traceable.

2.6. Functional-Structural Linear Analysis

This subsection corresponds basically to an earlier publication of the author [11]

The linear relationship, $Y = m \cdot X + b$, is widely used in all the different fields of Science as a useful tool in the analysis of data (X, Y) that seems to be linearly related. In the most part of the

published works, the Ordinary Least Squares technique is used to find out the values of the parameters m and b of the best fit line.

To answer the question; which is the best fit line of this collection of (X,Y) pairs, the statistician needs some extra information. The reason for this is that given a collection of pairs, several lines could be drawn, all of them being reasonable estimators of the "best fit line". Even if X and Y are assumed to be measured without error, only in the case when all the X_i and Y_i are exactly located in some line, the parameters of that line can be determined without ambiguity. If the points (X_i, Y_i) are not exactly located in some line, but rather spread in a line-shaped cloud, then the information of the collection of points itself is not enough to determine a unique best line fit. For example if we use the Ordinary Least Squares technique for that collection of points, we will get one set of parameters if we calculate the regression of Y on X , and a different one if we calculate the regression of X on Y . Which of those is the "correct" best fit line? The answer to that question may arise considering which the purpose of the relation sought is. If you are willing to predict some Y value given an X value, probably you will choose the regression of Y on X as your best fit line; but if you are going to use a Y value to predict an X value, you better use the regression of X on Y as your best fit line. And what if we are not trying to predict anything, but to observe some scientific law, or to corroborate some hypothesis about the m and b value? And what if one or both variables are subject to error?

Two types of information are essential to look for the "correct" best fit line [38]:

- a) Information about the purpose of the best fit line. In other words, how do you plan to use the parameters of the best fit line?
- b) Technical information about the nature and structure of the data. For example: Do you know the variance of errors associated with the data? Are there replicate measurements among the points? Were the observations random pairs? Were all points taken under the same conditions? Is there any information about a third variable associated with X and Y ?

Depending on the answers to the above questions, the statistician would recommend, at least, one of three general frameworks to address the situation, each of one with several techniques available: Regression, Functional or Structural analysis [39].

Three frameworks for linear analysis

Regression analysis

"Regression" is a statement forged by Galton in a work done between 1866 and 1868. His 1877 synonym for "regression" was "reversion" ([39] page 308). He used it to indicate "regression to mediocrity" in a situation where he found that the average stature of adult offspring increased with parent's stature, but not by as much. The term stuck firmly and was further used in association with studies of variables for predicting purposes.

Least Squares theory roots origins to Gauss, who brought its fundamental results [40].

Though the Least Squares method was developed considering an error-free independent variable, it is well suited to predict Y values even if X is subject to error, provided that the population parameters from which the new X is drawn are identical to those of the data set to which the regression was fitted [41]. For the situation in which the parameters of the estimation population differ from those of the prediction population, the prediction equation is no longer given by the Least Squares method and a structural relation is required to address this situation [42]. As usual, we call Ordinary Least Squares the technique that minimizes only the Y deviations from the line, but the Least Squares method include other techniques, like minimizing the X deviations from the line, which is equivalent to interchange the X and Y data and to apply then an Ordinary Least Squares. Since Ordinary Least Squares is not symmetric respect to the interchange of variables, the Ordinary Least Squares parameters should not be algebraically manipulated to calculate X for a given Y . Instead it is necessary to calculate the new parameters m' b' from the regression of X on Y (Ordinary Least Squares with the Y data in the abscissa axis).

When dealing with predicting values, we usually try to establish some "estimation" in the statistical sense. In general there will exist more than one consistent estimator of a parameter (one that tends to the "true value" as the sample tends to the population), even if we confine ourselves only to unbiased estimators (those that are close to the true value even for finite samples). We need further criteria to choose between estimators, all of them with the common property of consistency. Such criteria arise naturally if we consider the sampling variances of the estimators. An unbiased consistent estimator with a smaller variance will deviate less from the true value than one with a larger variance. Hence we may regard it as better.

Least Squares method gives the minimum variance unbiased linear estimators of any set of linear functions of the parameters m and b . Therefore Least Squares is usually considered the best method for regression analysis. Least Squares method is conceptually distinct from Maximum Likelihood (ML) method, but coincides with the ML method in the normally distributed observations case [43].

The results obtained by the Least Squares method assume nothing concerning the distribution of the errors (ϵ_{xi} , ϵ_{yi}) except the conditions concerning their first- and second-order moments. We make unbiased estimators of the parameters, and of the sampling variances and covariances of these estimators, without distributional assumptions. However, if we wish to test hypotheses concerning the parameters (constraints derived from physical laws or similar information), we need distributional information or distributional assumptions. In those cases there are other methods with better performance for that task than the Least Squares method, because now the minimum variance is not enough criteria any longer.

Those other methods arise in the frameworks of Functional Analysis and Structural Analysis as we will see next.

Functional analysis

There is a field of interest concerning relationships of a strictly functional kind between variables, such as those of classical physics; this subject is of statistical interest because the functionally related variables are subject to observational or instrumental errors. Kendall & Stuart call this the problem of functional relationship. This point of view is very useful in several situations in Metrology, as any device of measurement is working based on the applications of known physical laws which are combined to bring a general mathematical model or function that relates the readings of the equipment with the external stimulus applied to it. Some of these functions are quite simple like the mathematical model of the pressure balance. For these simple models it is desirable to test the hypothesis about the values of the parameters assigned to the mathematical model, as they work in some stable equipment of measurement. This practice is especially useful if several laboratories undergo such a study, so that their findings need to be compared in order to establish the equivalence of their metrological systems.

Structural analysis

In some cases, the function relating reading to external signals may be too complicated to handle, like the model relating the external pressure and the response in frequency of some kinds of frequency-based pressure transducers. In those cases, a practical approach is just trying to find the structural relation among the variables observed, in the sense that we understand that there exist some physical laws behind the relationship among the variables, but since we do not have a workable model for that function, we do not apply the functional relationship, but instead, we try to observe the underlying structure that the variables show and we try to find out the best estimates of the parameters that impose that structure.

Mathematical models

Regression relationships

The regression of y on x is defined to be the line that gives the relation between x and the expected value of y , given x . In this situation, y is called the dependent and x the independent variable. The regression relationship between x and y is written as

$$y = b + m \cdot x + e \quad (55)$$

Where $b + m \cdot x$ is the population regression line and e represents the "error", or deviation, of Y from the straight line. The following basic statistics for calculating m and b are used with the Ordinary Least Squares and several other methods:

The variance of the x data:

$$S_x^2 = \frac{\sum_{i=1}^N (x_i - \bar{x})^2}{N} \quad (56)$$

The variance of the y data:

$$S_y^2 = \frac{\sum_{i=1}^N (y_i - \bar{y})^2}{N} \quad (57)$$

The covariance between the y and x data:

$$S_{xy} = \frac{\sum_{i=1}^N (x_i - \bar{x}) \cdot (y_i - \bar{y})}{N} \quad (58)$$

And the Pearson correlation coefficient:

$$r = \frac{S_{xy}}{S_x \cdot S_y} \quad (59)$$

The different methods that use the statistics (56) to (59) deliver a best fit line which passes through the centroid of the data (\bar{x}, \bar{y}) , so once m is obtained, b can be solved from (55) (since $\bar{e} = 0$) to obtain

$$b = \bar{y} - m \cdot \bar{x} . \quad (60)$$

The Ordinary Least Squares solution for the regression of y on x (y is the dependent variable) gives for m :

$$m = \frac{S_{xy}}{S_x^2} . \quad (61)$$

For the regression of x on y (x is the dependent variable) the value of m given by Least Squares is:

$$m = \frac{S_{xy}}{S_y^2} . \quad (62)$$

The Ordinary Least Squares estimation of the overall uncertainty of the fit is given by the variance S (basic variance of the system):

$$S^2 = \frac{\sum_{i=1}^N (y_i - [b + m \cdot x_i])^2}{N - 2} \quad (63)$$

The experimental variances for the parameters m and b , $S^2(m)$ and $S^2(b)$, are (for Ordinary Least Squares):

$$S^2(m) = \frac{S^2}{N \cdot S_x^2} \quad (64)$$

$$S^2(b) = \frac{S^2(m) \cdot \sum_{i=1}^N x_i^2}{N} \quad (65)$$

And the correlation $r(m, b)$ between the parameters m and b is:

$$r(m, b) = - \frac{\sum_{i=1}^N x_i}{\sqrt{N \cdot \sum_{i=1}^N x_i^2}} \quad (66)$$

Functional- Structural relationships

When we consider that x and y are both subject to error then we may write:

$$x_i = x'_i + ex_i \quad (67)$$

$$y_i = y'_i + ey_i$$

Where x' and y' are the error-free counterpart of x and y . x' and y' are not observable, all we have are the “erroneous” measurements x and y . We assume that x' and y' are perfectly linearly related:

$$y'_i = b + m \cdot x'_i \quad (68)$$

For the derivation of the functional-structural relationships, it is assumed that the expectation values of the errors of x and y are zero, that the errors of x and y are not correlated to each other, and that the distribution of the errors ex is independent of x' and characterized by the variance σ_x^2 . Further it is assumed that the distribution of the errors ey is independent of y' and characterized by the variance σ_y^2 .

If we regard the x' as given numbers, this model is known as the functional relation. If we assume rather that the x' are drawn independently from a $N(\mu, \sigma^2)$ distribution, i.e., x' is normally distributed with mean μ and variance σ^2 , then the model is known as the structural relation.

Regardless of the consideration of x' as a random variable or not (i.e. if the relation is structural or functional) the maximal likelihood estimation of the parameters of these models are the same, provided that we have enough information to calculate them. We need some extra information to avoid the unidentifiability problem. This extra information is the error variances. Madansky [38] found three maximal likelihood relations for the estimation of the slope, depending upon the information available among σ_x^2 , σ_y^2 , or $\lambda = \sigma_y^2 / \sigma_x^2$.

If σ_y^2 is known, then it holds that

$$m = \frac{S_y^2 - \sigma_y^2}{S_{xy}} . \quad (69)$$

If σ_x^2 is known, then it holds that

$$m = \frac{S_{xy}}{S_x^2 - \sigma_x^2} . \quad (70)$$

If $\lambda = \sigma_y^2 / \sigma_x^2$ is known, then it holds that

$$m = \left(\frac{1}{2 \cdot S_{xy}} \right) \cdot \left((S_y^2 - \lambda \cdot S_x^2) \pm \left((S_y^2 - \lambda S_x^2)^2 + 4 \cdot \lambda \cdot S_{xy}^2 \right)^{\frac{1}{2}} \right) , \quad (71)$$

where the sign must be identical to the sign of S_{xy} .

The basic variance of the system is estimated by

$$S^2 = \frac{S_{xy}}{m} \quad (72)$$

From the three possibilities to calculate the parameters of the best fit line in the functional-structural framework, we will treat in more detail the case in which σ_x^2 is known, because this case was applied in our research.

Functional-structural analysis for abscissa-data variance known [44]

The functional-structural model in this case is

$$\begin{aligned}
y_i &= b + m \cdot x'_i + ey_i \\
x_i &= x'_i + ex_i \\
\text{expected}\{x'_i, ey_i, ex_i\} &= (\mu_x, 0, 0) \\
\text{covariance}\{x'_i, ey_i, ex_i\} &= \begin{pmatrix} \sigma_{x'x'} & 0 & 0 \\ 0 & \sigma_{eyey} & 0 \\ 0 & 0 & \sigma_{exex} \end{pmatrix}
\end{aligned} \tag{73}$$

where:

- y_i is the average measurement number “ i ” of the quantity assigned to the ordinate scale,
- ey_i is the measurement error of y_i ,
- x'_i is the true value of the average measurement number “ i ” of the quantity assigned to the abscissa,
- x_i is the average measurement number “ i ”, of the quantity assigned to the abscissa,
- ex_i is the measurement error of x_i ,
- $\mu_{x'}$ is the expected value of x' for the distribution of true values x'_i ,
- $\sigma_{x'x'}$ is the variance of the distribution of true values x'_i ,
- σ_{eyey} is the variance of the distribution of errors of measurement of the y_i ,
- σ_{exex} is the variance of the distribution of errors of measurement of the x_i and
- i goes from 1 to N , for N pair of average measurements (x_i, y_i) .

In this model, the variance σ_{exex} is assumed to be known, and all the other parameters of the model are derived using the σ_{exex} value and the first and second moments of the vector sample; i.e. the vector sample mean $\bar{Z} = (\bar{x}, \bar{y})$, and the vector sample covariance matrix uZZ , which has the components covariances ($uZZ[x, x]$, $uZZ[x, y]$, $uZZ[y, y]$), corrected for the degrees of freedom, such that:

$$uZZ[x, y] = (N-1)^{-1} \cdot \sum_{i=1}^N (x_i - \bar{x}) \cdot (y_i - \bar{y}) \tag{74}$$

The maximal likelihood estimators of the parameters for this model are:

$$\begin{aligned}
\hat{m} &= \frac{uZZ[x, y]}{uZZ[x, x] - \sigma_{exex}} , \quad \hat{b} = \bar{y} - m \cdot \bar{x} , \\
\hat{\mu}_{x'} &= \bar{x} , \quad \hat{\sigma}_{x'x'} = uZZ[x, x] - \sigma_{exex} , \\
\hat{\sigma}_{eyey} &= uZZ[y, y] - m \cdot uZZ[x, y] .
\end{aligned} \tag{75}$$

For the quantities defined in the equation set (75) to be proper estimators of the parameters, $\hat{\sigma}_{x'x'}$ and $\hat{\sigma}_{eyey}$ must be non-negative. The hat in all the estimators' symbols is used to distinguish between the (unknown) parameter and its (calculated) estimator.

The (estimator of the) covariance matrix uPP of the (estimators of the) parameters' vector $P = (b, m)$ is given in this model by

$$uPP = \begin{pmatrix} \bar{x}^2 \cdot \hat{\sigma}[\hat{m}] + N^{-1} \cdot S_{vv} & -\bar{x} \cdot \hat{\sigma}[\hat{m}] \\ -\bar{x} \cdot \hat{\sigma}[\hat{m}] & \hat{\sigma}[\hat{m}] \end{pmatrix}, \quad (76)$$

where

$$\hat{\sigma}[\hat{m}] = \frac{uZZ[x, x] \cdot S_{vv} + \hat{m}^2 \cdot \sigma_{exex}^2}{(N-1) \cdot \hat{\sigma}_{x'x'}^2}, \quad S_{vv} = \frac{\sum_{i=1}^N (y_i - \bar{y} - (x_i - \bar{x}) \cdot \hat{m})^2}{N-2}. \quad (77)$$

This model permits also the estimation \hat{x}' of the true values x' , using the following set of equations:

$$\hat{x}'_i = x_i - \hat{\sigma}_{vv}^{-1} \cdot \hat{\sigma}_{exv} \cdot \hat{v}_i, \quad \hat{v}_i = y_i - \hat{b} - \hat{m} \cdot x_i, \quad (78)$$

$$\hat{\sigma}_{vv} = \frac{\sum_{i=1}^N \hat{v}_i^2}{N-1}, \quad \hat{\sigma}_{exv} = -\hat{m} \cdot \sigma_{exex}.$$

The quantities defined in the last equation are very useful in judging the applicability of the model, through the graphical representation of the pairs (\hat{x}'_i, \hat{v}_i) , which is the equivalent of plotting the residuals in ordinary least squares analysis. This plot often will give an indication of nonlinearity in the data, of lack of homogeneity of the error variances, of no normality of the distribution of errors, or of outlier observations. The structural model we are discussing now postulates constant variance for ey_i and ex_i , therefore $v_i = ey_i - m \cdot ex_i$ will also have constant variance. Furthermore, because both ey_i and ex_i are independent of x_i ; the expected value of v_i given x_i is zero. All this indicates that the plot of v_i versus x_i should be a homogeneous scatter of points around the line $v = 0$, if the analyzed data can be really explained with this structural model.

To complement the graphical check, we present now two useful statistical tools (a test and a “rule of thumb”) that can be used to test the suitability of this model, specifically to judge:

- if the equations (76) and (77) give good estimators of the variances and covariances of the parameters b and m , and (in the positive case);
- if the Student's t-distribution with $(N - 2)$ degrees of freedom is a good approximation for their real distribution (i.e. if the Student's t-distribution is suitable to construct an extended confidence level for the estimated parameters).

The first question can be answered evaluating the following statistic:

$$\chi^2 = \frac{\sum_{i=1}^N (x_i - \bar{x})^2}{\sigma_{exex}} \quad (79)$$

The value of χ^2 given by the equation (79) should be large compared to (or at least similar to) the value of the chi-square distribution with n-1 degrees of freedom in order to consider that the quantities given by the set of equations (75) are good estimators of their parameters.

In that case, and answering the second question, we can use the Student's t distribution to construct the extended confidence intervals of the parameters if the following “rule of thumb” is met:

$$\frac{\sigma_{exex}^2}{(N-1) \cdot (uZZ[x, x] - \sigma_{exex})^2} < 0.001 \quad (80)$$

We finalize this subsection with a general recommendation about the application of linear analysis to different problems: If the purpose of the analysis is to use the resulting equation to predict one of the variables based on the measurement of the other one, then use Ordinary Least Squares accordingly (independent variable assigned to abscissa data) as long as the new data in which the prediction is going to be made has similar variances as the data used to calculate the parameters. If this last condition is not met, or if the purpose of the analysis is to obtain the parameters to assign them some interpretation as physical quantities, then use one of the functional-structural methods. The functional-structural method should be chosen so that the available information about the variances of the variables is used as good as possible.

3. Experimental Setup and Methods of Measurement

We start this part with a general description of our spectrometer. In the following sub-sections we describe the individual components of it, and the methods used to take the measurements of all the input quantities needed to measure the line intensities and the partial pressures of the gases investigated (in our case CO and CO₂). This description includes the specific methodology for the calculation of the corresponding uncertainties. It is important to stress here the necessity to keep in mind that the **result** of a traceable measurement is always a given **average** and its **uncertainty**. This is part of the core of the concept of **traceable measurement** as mentioned in the section 2.5. Whenever we refer to some measurement of a given quantity through this work, we mean its traceable measurement (unless the contrary is stated explicitly) and therefore such measurements should not be confused with the direct reading of the measuring devices (for the quantities that can be measured directly) or with the algebraic manipulation of the direct readings of measuring devices (for the quantities that can only be measured indirectly using some equation and its input quantities). For this research, the direct readings of the measurement devices were always processed through some calibration functions given in (or found based on) the traceable certificates of calibration of their instruments. The result of the calibration function is what we regard as the average of the traceable measurement (for the case of direct measurements). The result of the equation given for some indirect measurement, fed with input quantities which are in turn the average of their traceable measurements, is the average of the traceable (indirect) measurement of the quantity. In any case the result of the traceable measurement is only complete when the reported average is accompanied by its uncertainty. That is why we keep here the description of the considerations, formulae and methods used to calculate the uncertainty of our measurements, together with the description of the considerations, formulae and methods used to calculate the average of our measurements. Note that the word average is used here independently of the number of repetitions for a given measurement. Also in the case when a given quantity was measured only once, that result, as traceable measurement, includes the average (the calibrated result) and its uncertainty.

3.1. General Description of the Spectrometer

The Spectrometer with the three channels that we set up to undertake this research is described as follows (see Figure 4 in page 48): The infrared laser is produced in the Laser Source, this being either a cryogenic Diode-Laser Base System, which is controlled by a Diode-Laser Electronic Control Unit (for the measurements on CO) or a DFB Laser tempered with Peltier-elements (for the

measurements on CO₂). After collimating in an Off Axis Parabolic Mirror (OAP) the ray goes through a monochromator with a resolution of about 1 cm⁻¹ (only for CO measurements). The purpose of the monochromator is to block the transmission of secondary emissions at other wavelengths from the cryogenic diode-laser, and therefore it is not needed when the DFB laser is used (the DFB do not produce secondary emissions). After this, the beam is focused by another OAP in the plane of a chopper and re-collimated by a third OAP.

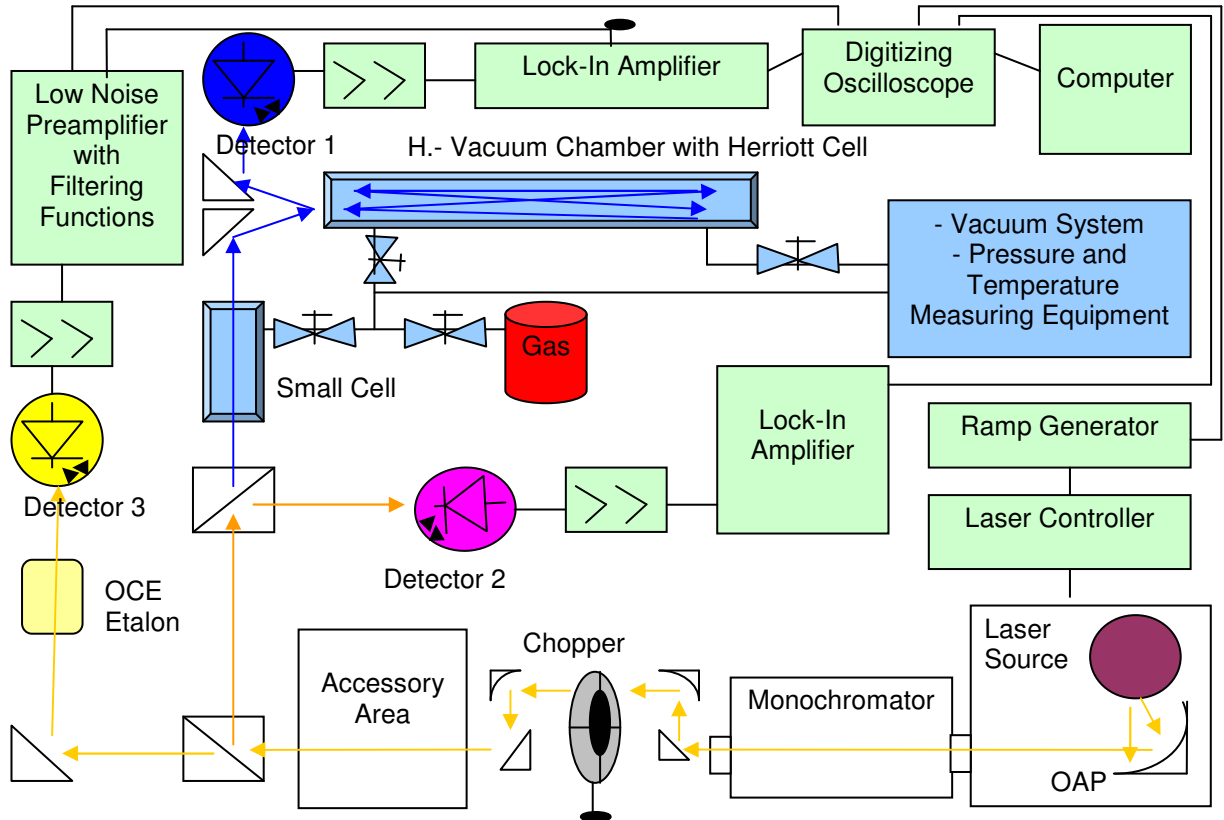


Figure 4: Schematic representation of our spectrometer

The ray goes then to two beam splitters which divide it in three parts: The first part of the ray is focused directly and detected on detector 2, where it is measured as the Reference-Signal. The second part of the ray goes through a Small Cell, then through the VCMHC and finally is focused by a spherical mirror on detector 1, where it is measured as the Detection-Signal. The third part of the ray goes through an Open Confocal Etalon (OCE) (Free Spectral Range – FSR: 0.0103745 cm⁻¹) or through the Ge Etalon (FSR: 0.044396 cm⁻¹ for radiation at 4988 cm⁻¹) and is focused and detected on detector 3, where it is measured as the frequency-marker-signal. The wavelength of the laser is slowly swept around the absorption line under study by means of a triangular ramp. The ramp frequency used is 5 Hz, but we only observe the positive slope part of the signal so that the total observed period has a duration of 0.1 s and is therefore equivalent to a 10 Hz signal with a 50% duty cycle. The ramp voltage is applied directly to the bias temperature connection of the laser controller.

The corresponding three signals detected respectively on the three mentioned detectors are demodulated (From the chopping modulation) by two different systems: the signals from detector 1 and 2 are demodulated using PSD Lock-in Amplifiers (a Perkin Elmer - LIA and a Stanford Research - LIA) and the signal from detector 3 is demodulated by a Band-Pass Filter of a Dual-Channel Filter. The three demodulated and amplified signals are detected simultaneously in channels 1 to 3 of a 500 MHz digitizing oscilloscope, where the ramp voltage signal is also digitized simultaneously in the channel 4. The four digitized signals are transferred to a PC by means of a GPIB card controlled by a LabVIEW program, which also reads other measuring instruments used in the experiment, like the Pressure Measuring Devices (Capacitance Diaphragm Gage – CDG, Spinning Rotor Gage – SRG and Ionization Gage - IG) and the Temperature Measuring Devices (Keithley Scanning System to measure the temperature of the walls of the vacuum chamber and two multimeters to measure the temperature from two PT100 located directly inside the VCMHC).

3.1.1. General Description of Our Line Intensity and Partial Pressure

Measurement Method

Basically we try to measure as accurate as possible all the other input quantities of the Lambert-Beer law. We calculate the corresponding absorption coefficient for each sampled frequency ν_i :

$$k(\nu_i - \nu_c) = \left(\frac{-1}{n \cdot L} \right) \cdot \ln \left(\frac{I(\nu_i - \nu_c)}{I_0(\nu_i - \nu_c)} \right). \quad (81)$$

We record the transmitted intensity $I(\nu_i - \nu_c)$ as we sweep the frequency ν_i through an adequate frequency window around the center of the absorption line ν_c . Both $I(\nu)$ and ν change continually (as do all the other measured quantities for this type of “classical limit” measurement), but we record a discretized sample of all the quantities. Such discretization takes place during the digitization of the signals in the digitizing oscilloscope and in the other digital measuring equipments, like the multimeters.

The oscilloscope samples and records the signals at discrete time points. In order to transform this time scale to a frequency scale we must know how fast the ramp applied to the diode laser is shifting the laser emitted wave-length. For this determination we use the frequency marker: mostly the open confocal etalon OCE and seldom also the Ge etalon. The details of these measurements will be presented in section 3.8.

The number of molecules per volume n can be measured indirectly through measurements of the pressure and temperature of the gas (see section 3.4). The path length of the ray through the

absorbing media L can be measured either directly, like the distance between windows of a one-pass cell, or indirectly using the properties of the Herriott Cell, like in our case (see sections 2.3 and 3.3).

To measure the transmitted intensity $I(v)$ we use the detector 1 as explained below. We also need to know the input intensity $I_0(v)$ that would reach the detector 1 in case that no absorption were taking place. For this reason we measure always a part of the ray directly on detector 2 and we have to include always a “null-scan” in each absorption measurement, in order to learn the transformation function from channel-2- I_0 to channel-1- I_0 .

Finally, in order to calculate the absorbance correctly we need a physical scale to measure the intensities. The scale factor itself is not important as it is eliminated through the division $I(v)/I_0(v)$, (i.e. it is not important to express the intensity with some specific units) but the intensity scale must be physical in the sense that it has no “offset” errors, i.e. the zero of the system must be a real physical zero. In order to find this “physical origin of the system of reference” we have to measure a 100% absorption spectrum so that the portion of the line that was 100% absorbed indicates the position of the “zero” for the physical intensity scale. Furthermore the observed “electrical” intensity scale (as voltage measured with our system) must have a linear relation with the optical intensity that reaches the detector. See section 3.7.

Summarizing, we need at least three measured spectra:

- one without any absorption: the so called null-absorption scan, to prepare the indirect measurement of $I_0(v)$,
- one with full absorption at the center of the line: the so called total-absorption scan, to find the physical origin of the intensity scale, and
- one with partial absorption: the so called partial-absorption scan, to measure the line intensity itself (or the partial pressure later).

These measurements have to be done shifted in time, because they must be carried out by the same detector.

If we had just one optical channel, we would have to measure the frequency mark scan also shifted in time. Another drawback for this case is that $I_0(v)$ could not be indirectly (simultaneously) measured, but estimated only based on null-absorption scans and observations of the not absorbed portions of the spectrograph (the “wings” of the absorption line). These would add bigger uncertainties to the frequency scale and $I_0(v)$ values. In order to avoid these problems we separated the ray in three parts by means of two beam splitters so that we are able to measure simultaneously the absorption signal, the frequency mark signal and the reference signal. This last one is used to measure indirectly $I_0(v)$.

Detailed information about the implementation of this measurement method regarding the data sampling and manipulation can be found in appendix 7.1.

3.2. Laser-Sources

We used two Laser-Sources in this work: A cryogenically cooled lead-salt diode laser and a DFB laser operated at ambient temperature. Their respective equipments are shown in the next table.

Table 1. Equipment dedicated to the production and control of the IR-Laser.

Part	Manufacturer	Moel	Serial Number	Current Working Range	Temperature Working Range	Resolution / Efficiency	Nominal wavelength / wave-number
Diode-Laser-1	Laser Components	IR-2183	322-HV-1-98	(280 - 630) mA	(80 - 130) K	3.4 mW/A at 121 K	2183 cm ⁻¹
Diode-Laser-1 - Thermostat-Head	Laser Photonics	L5736	93-2153	--	--	--	--
Diode-Laser-1 - Base	Laser Photonics	L5120-1	110	--	--	--	--
Diode-Laser-1 - Controller	Laser Photonics	L5830	141	(0 - 1) A	(10 - 300) K	15 µA / 5 mK	--
Diode-Laser-2	Nanoplus	057/4-15	--	(21 - 80) mA	(15 - 30) °C	0.15 W/A at 25 °C	2004 nm
Diode-Laser-2 - Thermostat head	PTB	--	PTB1076920-0000	--	--	--	--
Diode-Laser-2 - Controller	PTB	--	--	(0 - 80) mA	(0 - 30) °C		

3.3. Herriott-Cell

The Herriott Cell is a key component of the spectrometer which permits the realization and measurement of several path lengths which can be step-wise selectable, as we showed in the Herriott Cell theoretical description, section 2.3, page 29.

In order to change the position of the back mirror in the VCMHC, it is mounted on a movable plate which can be axially shifted along a high-precision three-rail system. To shift the plate there are two mechanisms available in our system: a mechanical screw-driven system, which was already used in previous works [8, 47], and an electronically piezo-motor driven system -InchWorm®-.

The VCMHC has a front window located close to the front mirror of the Herriott Cell, which permits the optical coupling of the probe-ray into the Herriott Cell (see Figure 5). A back window at the other end permits the control of the position of the back mirror (see Figure 6). This control is done with an interferometer, by measuring the distance ΔZ traveled by the back mirror from a well determined reference position (base point) to the transmitting position. In order to find the relation between the ΔZ measurements and the ray's configuration inside the Herriott Cell, we used the same He-Ne laser from the IR-laser-source base system which was used to adjust all the optics of our spectrometer. The procedure used on this regard will be explained in the next sub-section.

The equipments mentioned so far that were used for the absorbing path length measurements in our system are listed next (their details can be found in the Table 4, on page 59):

- Herriott Cell in the VCMHC,
- Interferometer,
- He-Ne Laser,
- UHV fed-through Screw-Driver (Drehdurchführung) and
- InchWorm.

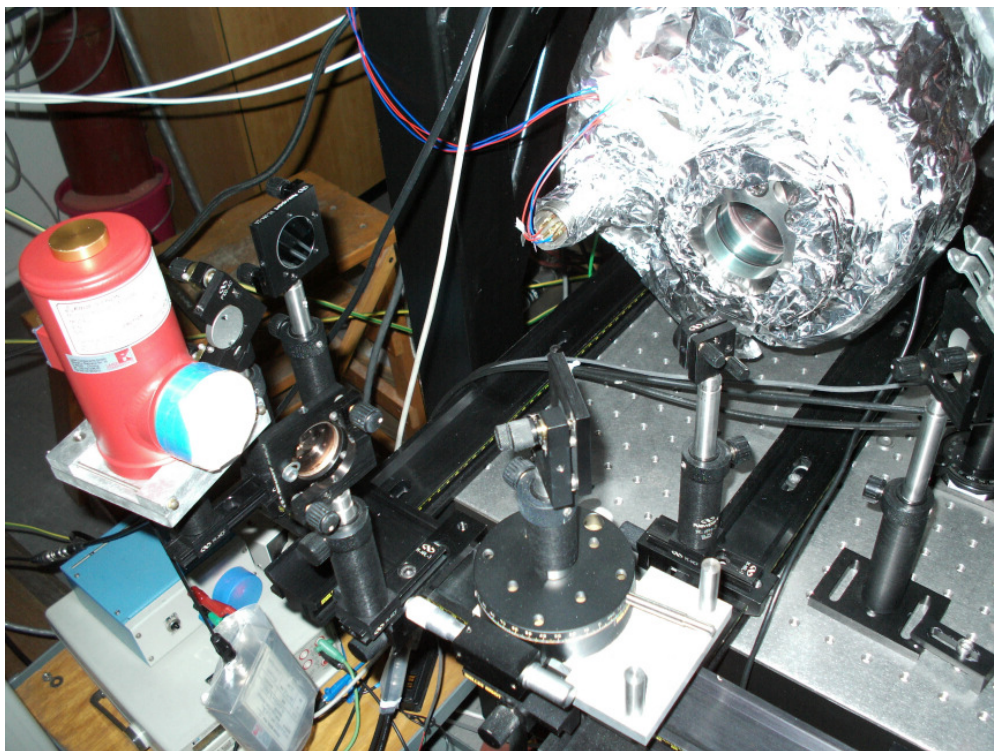


Figure 5. Partial view of the VCMHC, where the front window and the detector-1 can be observed.

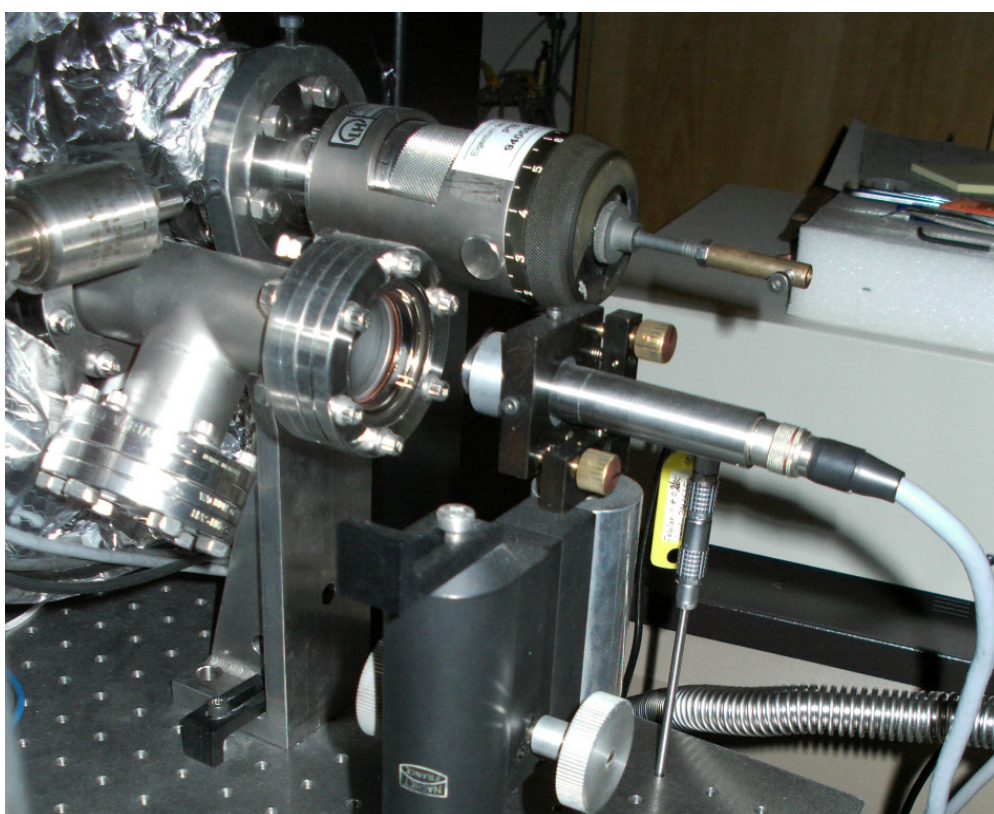


Figure 6. Partial view of the VCMHC, where the back window, the driven-screw and the interferometer sensor can be observed.

3.3.1. Herriott Cell Characterization

We present here how we measured the effective radius of curvature ρ , the family-number K , and the number of round trips N , which permits the measurement of the ray path length inside the Herriott Cell using equation (52).

The mirrors of the VCMHC have a nominal radius of 1 m, but we need a traceable measurement of the radius in order to have a traceable measurement of the absorbing path length L . Earlier researchers have tried to measure this radius through the direct measurement of the mirror's separation ℓ for a known configuration (i.e. K and N known) and using the equation (50), which can be rearranged as follows:

$$\rho = \frac{\ell}{\left(1 - \cos\left\{\frac{\pi}{2} \cdot \left(1 - \frac{K}{N}\right)\right\}\right)} . \quad (82)$$

Since the mirrors of this Herriott Cell are located inside the vacuum chamber, it was inconvenient to use this method [47].

For this reason we developed a novel and simple approach to measure the mirrors' effective radius of curvature ρ and separation ℓ , both indirectly and simultaneously. Our approach is based also on equation (50),

$$\ell = \rho \cdot \left(1 - \cos\left\{\frac{\pi}{2} \cdot \left(1 - \frac{K}{N}\right)\right\}\right) , \quad (50)$$

but we treat it in the frame-work of a linear-analysis:

$$\ell = m \cdot x + b ;$$

with

$$x(K, N) = \left(1 - \cos\left\{\frac{\pi}{2} \cdot \left(1 - \frac{K}{N}\right)\right\}\right) , \quad (83)$$

$$m = \rho ,$$

$$b = 0 ,$$

where ℓ is the mirror's separation, which we interpret now as the measurement of the back-mirror position taking as reference the front mirror's position. We do not know exactly the front's mirror position, but we can measure the back mirror's positions using as reference the mechanical stop point of the screw-driven travel when the piezo-motor is in its "forward-limit" position. This combination places the back mirror at about $0.75 \cdot f$ from the front one and is a very stable and reproducible fixed-point position. This position was called by us the "base-point" position. From the base-point, the back mirror can be shifted toward the confocal position ($0.75 \cdot f \leq \ell < f$) using the screw-driven mechanism; or it can be shifted toward the semi-confocal position ($0.5 \cdot f < \ell \leq 0.75 \cdot f$) using the

InchWorm piezo-system. The key issue is that the base-point is positioned at a fixed distance from the front mirror, so we can use it as a translated system of reference to measure the position of the back mirror. As a result, the linear relation defined by the equations set (83) appears in the new (translated) system with the same slope and with a new intercept. To differentiate both reference systems, we will call Z the position of the back mirror in the new system of reference (i.e. when measured from the base-point), then it holds,

$$\begin{aligned}
Z &= m' \cdot x + b' \\
\text{with} \\
x(K, N) &= \left(1 - \cos \left\{ \frac{\pi}{2} \cdot \left(1 - \frac{K}{N} \right) \right\} \right), \\
m' &= m = \rho, \\
b' &\neq 0.
\end{aligned} \tag{84}$$

We can not directly measure ℓ , but we do can measure the Z positions using the interferometer. Now if $Z_1(K_1, N_1)$ denotes the transmitting position of the back mirror for a given Herriott Cell configuration characterized by the integral numbers K_1, N_1 , when the mirrors are separated by a distance ℓ_1 ; and Z_2 denotes another transmitting position similarly characterized by the integral numbers K_2, N_2 , when the mirrors are separated by a distance ℓ_2 ; it is a fact that

$$\ell_2 - \ell_1 = Z_2 - Z_1, \tag{85}$$

because the distance between two points does not depend on the origin of reference chosen to measured their positions, which gives immediately the well known result that,

$$\frac{\ell_2 - \ell_1}{x_2 - x_1} = \frac{Z_2 - Z_1}{x_2 - x_1} \Rightarrow m = m', \tag{86}$$

i.e. the slope of a regression-line is independent of translations (in x or in y) of the reference system, as we already pointed it out in equation (84), which, compared with equation (83) gives

$$\ell = \rho \cdot x = Z - b'. \tag{87}$$

So, we just need to calculate the two parameters m' and b' with some linear analysis for a group of known pairs (Z, x) and we can then immediately calculate the radius of curvature ρ , and the mirrors separation ℓ . Now the question is: How we know which integral numbers K_i, N_i correspond to a given transmitting position Z_i ? (we need these numbers in order to calculate $x_i(K_i, N_i)$ as given by the equation (83)). The answer is given by the equation (85) thanks to the non-linearity of x with respect to K and N : If the radius ρ is approximately known, then the separation between two

transmitting positions i and j is a distinguishing characteristic which permits to identify the participating number K_i, N_i, K_j, N_j . So we applied the following five-step method:

- Using the nominal radius, the K -values 1 to 9 and their non-zero N -values (from 3 to 33) we generated a table of nominal mirror separation differences ($\ell_i - \ell_j$).
- Using the interferometer, the Screw-Driver, the InchWorm and the He-Ne laser, we measured the distances Z for 21 different transmitting positions. To this end we observed the He-Ne signal transmitted through the Herriott Cell and projected on a screen which was fixed to the Detector-1 window. We repeated the measurement 4 times for each transmitting point, always positioning the He-Ne point in the center of the projected area.
- After calculating the means and standard deviations of the 21 Z s, we calculated a table of differences ($Z_p - Z_q$), which compared with the differences ($\ell_i - \ell_j$) from the first step, allowed us to identify the corresponding integral numbers K and N for each measured Z .
- With the known K s and N s we calculated the x components corresponding to each Z .
- With the 21 pairs (x, Z) we found the parameters m' and b' , and with them, the quantities ρ and $\ell(K, N)$.

According to the theory presented in section 2.6 (page 37), we should use the functional-structural method for this linear analysis, as we are measuring the parameters m and b as physical quantities. Nevertheless, as we explained there, the functional-structural method converges to the “regression of Y on X ”-case when the X -uncertainties are negligible compared with the Y -uncertainties. The present case is one of those, as we know exactly the K and N integral numbers, and the uncertainties of our x -values arise only through the limited computing accuracy of π and the cosine-function (relative uncertainty $\approx 10^{-15}$), while the Z -uncertainties vary from 0.003% to 0.4%. So we use the usual regression formulae of Z on x but conscious of its application as a limiting case for the functional-structural method. Our Z and x measurements are presented in the Table 3, and summarized in the Figure 7. The Z -uncertainties are not observable at this scale.

The result of the linear analysis of the (x, Z) data is presented in the Table 2. From it we have finally found the effective radius of curvature of the mirrors of our Herriott Cell.

- $\rho = 0.99912 \text{ m}$
- $u[\rho] = 0.00011 \text{ m} \quad (0.011\%)$

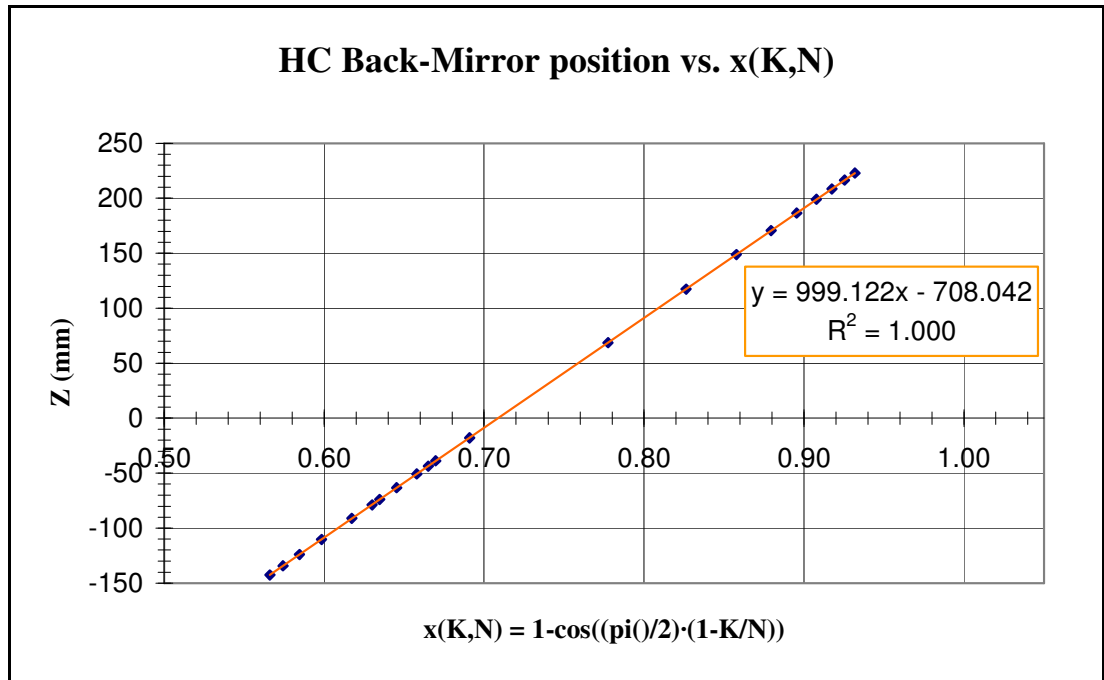


Figure 7. Herriott Cell characterization: Indirect measurement of the mirrors' curvature radius ρ through the Z-vs.-x slope = 999.122 mm.

Table 2. Linear analysis of the Z-vs.-x(K, N) data.

Description	Value	Description	Value
Slope (in mm) m'	999.12208	Intercept (in mm) b'	-708.0421
Slope's standard deviation (in mm) $s[m']$	0.1128	Intercept's standard deviation (in mm) $s[b']$	0.0843
Pearson's correlation coefficient R^2 :	0.99999976	Approximated uncertainty of the predicted Z $u[Z_{\text{predicted}}]$	0.06817
F-statistic F:	78524054.9	Degrees of freedom df:	19
Regression sum of squares SSreg	364891.87	Residual sum of squares SSresid	0.088291

Table 3. Data for the Herriott Cell characterization: Measured Z, their corresponding K and N integral numbers, and their $x(K, N)$ pairs.

K	1	1	1	1	1	1	1
2N	46	42	38	34	30	26	22
Z Average (mm)	222.9258	216.4215	208.5633	198.9460	186.6853	170.7485	148.8565
Z Std. Dev. (mm)	0.0225	0.0346	0.0117	0.0063	0.0214	0.0312	0.0237
$u[Z]$ (%)	0.0101	0.0160	0.0056	0.0032	0.0115	0.0183	0.0159
$x(K,N)$	0.9318	0.9253	0.9174	0.9077	0.8955	0.8795	0.8577
K	1	1	1	6	5	4	3
2N	18	14	10	56	46	36	26
Z Average (mm)	117.4683	68.6623	-17.8043	-38.9288	-43.5485	-50.6265	-63.1848
Z Std. Dev. (mm)	0.0640	0.0450	0.0688	0.0227	0.0249	0.0311	0.0243
$u[Z]$ (%)	0.0545	0.0656	0.3864	0.0582	0.0572	0.0614	0.0384
$x(K,N)$	0.8264	0.7775	0.6910	0.6697	0.6651	0.6580	0.6454
K	5	7	2	5	3	7	4
2N	42	58	16	38	22	50	28
Z Average (mm)	-73.909	-78.781	-91.142	-110.250	-123.883	-134.349	-142.428
Z Std. Dev. (mm)	0.011	0.023	0.012	0.004	0.040	0.024	0.048
$u[Z]$ (%)	0.014	0.029	0.013	0.004	0.032	0.018	0.034
$x(K,N)$	0.635	0.630	0.617	0.598	0.585	0.574	0.566

Table 4. Equipment dedicated to the measurement of the absorption path length.

Part	Manufacturer	Model	Serial Number	Operating Range	Resolution / u[FSR]	Certificate of Calibration Number
Herriott Cell in VCMHC	PTB	--	--	7 m to 63 m Path Length	--	--
IR-Laser Interferometer	Compagnie des Senseurs Optiques		94-14-E / 0108	(0 - 25) cm	0.01 μm	MB/03-5285 /FC
He-Ne Laser	Melles Griot	Part of L5120-1	110	632.8 nm	--	--
Inch-Worm Controller	Burleigh	6100-11-2-3	P6091463	--		--
Inch-worm Motor		UHV L-220	--	(0 - 22) cm	4 nm	--
UHV Fed-through Screw-Driver (Drehdurchführung)	Leybold	88223B1	PTB 94008881	(0 - 30) cm	$\approx 1 \mu\text{m}$	--

3.3.2. Absorption Path Length Measurements

To calculate the total absorbing path length L , we just need to know the input quantities of equation (52) to calculate the distance traveled by the ray inside the Herriott Cell L_{HC} , and the distance traveled by the ray inside the chamber but outside the Herriott Cell, L_0 ; i.e. L_0 is the distance traveled by the incoming ray from chamber's window to the internal surface of the front mirror at hole's point plus the distance traveled by the output ray from the internal surface of the front mirror at hole's point to the chamber's window. Then we can calculate the total absorbing path length L as:

$$L = L_{HC} + L_0 \quad (88)$$

That means that we need to know:

- the ray configuration inside the Herriott Cell (given by the integral numbers K and N),
- the hole-to-mirror center distance r_0 ,
- the Herriott Cell mirrors effective curvature radius ρ and,
- the window-hole-window path-length L_0 .

The r_0 was measured when the VCMHC was constructed and its reported value is [47] $r_0 = (4.25 \pm 0.02)$ cm ($k = 1$).

The mirrors effective curvature radius ρ and the integral numbers K and N corresponding to each transmitting position of the back mirror were found as explained in section 3.3.1.

The L_0 was measured by us through disassembling the front window of the VCMHC, and measuring directly the different segments from the window's internal surface to the mirror's surface at hole's position and taking into account the inclination angles of the ray's trajectory. We determined $L_0 = (26.02 \pm 0.44)$ cm ($k = 1$).

So combining equations (52) and (88) we obtain the final expression for the total absorbing path length L in terms of the mentioned input quantities:

$$L = 2 \cdot N \cdot \rho \cdot \left(1 - \sin \left\{ \frac{K \cdot \pi}{2 \cdot N} \right\} + \frac{r_0^2}{\rho^2 \cdot \left(1 + \sin \left\{ \frac{K \cdot \pi}{2 \cdot N} \right\} \right)} \right) + L_0 \quad (89)$$

For each known configuration the integral numbers K and N are exactly determined (i.e. their uncertainty is zero). The other input quantities are independent from each other, so that the uncertainty of L can be calculated as:

$$u[L] = \left(\left(\frac{\partial L}{\partial \rho} \cdot u[\rho] \right)^2 + \left(\frac{\partial L}{\partial r_0} \cdot u[r_0] \right)^2 + u^2[L_0] \right)^{\frac{1}{2}} \quad (90)$$

After calculating the derivatives, we find finally:

$$u[L] = \left(\begin{aligned} & 4 \cdot N^2 \cdot \left(1 - \sin \left\{ \frac{K \cdot \pi}{2 \cdot N} \right\} - \frac{r_0^2}{\rho^2 \cdot \left(1 + \sin \left\{ \frac{K \cdot \pi}{2 \cdot N} \right\} \right)} \right)^2 \cdot u^2[\rho] + \\ & + \frac{16 \cdot N^2 \cdot r_0^2}{\rho^2 \cdot \left(1 + \sin \left\{ \frac{K \cdot \pi}{2 \cdot N} \right\} \right)^2} \cdot u^2[r_0] + u^2[L_0] \end{aligned} \right)^{\frac{1}{2}} \quad (91)$$

In our measurement-example we had $K = 1$, $N = 14$ and the result was:

- $L = 1115.59$ cm
- $u[L] = 0.51$ cm (0.046%; $k = 1$)

3.4. Gas Density Measurements

We measure the gas density under two different conditions: using pure gas for line intensity measurements and using gas-mixtures for partial-pressure measurements.

3.4.1. Gas Density Measurements of Pure Gas

In this case we measure the gas density indirectly, applying the ideal gas law,

$$n_i = \frac{P_i}{k \cdot T}, \quad (92)$$

where:

- n_i is the gas molecular density of the gas number “ i ” of some gas mixture containing N different gas- “species”, and “ i ” being a natural number between 1 and N . Note that the differentiation among several gases does not include the isotopic difference, i.e. all the isotopes of the “same” chemical component are treated as belonging to the same gas with label “ i ”,

- P_i is its partial pressure,
- k is the Boltzmann constant and
- T is the thermodynamic temperature.

Our pressure measurement devices only can measure the total pressure P ,

$$P = \sum_{i=1}^N P_i , \quad (93)$$

so that, if there is only one component (i.e. using pure gas) the measured total pressure was almost equal to the partial pressure of the gas under study (the “almost” stands for minor purity corrections). In this case we just calculated the corrected pressure P_c based on the total pressure measurement P (see section 3.5), further we measured the gas temperature T , as explained in section 3.6, and finally we applied directly the equation (92) to obtain the gas density n .

The standard uncertainty of the gas density measurement for this case is obtained quite straightforward according to the formulae presented in section 2.4 and the result is:

$$u[n] = n \cdot \left(\sqrt{\left(\frac{u[P]}{P}\right)^2 + \left(\frac{u[T]}{T}\right)^2 + \left(\frac{u[k]}{k}\right)^2} \right) \quad (94)$$

3.4.2. Gas Density Measurements of a Gas in a Mixture

In order to measure indirectly the gas density for this case, when the gas under study was part of a mixture, we applied an equation derived from the Lambert-Beer law, equation (23), and the definition and properties of the Line Intensity, equations (24) to (26), as explained next.

Rearranging the equation (23) and taking natural logarithm results in

$$k(\nu - \nu_c) \cdot n \cdot L = -\ln \left\{ \frac{I(\nu)}{I_0(\nu)} \right\} \quad (95)$$

Substituting k from equation (25) in equation (95), integrating from minus infinite to plus infinite with respect to the wave-number and taking in account equations (24) and (26) results in

$$S \cdot n \cdot L = - \int_{-\infty}^{+\infty} \ln \left\{ \frac{I(\nu)}{I_0(\nu)} \right\} d\nu \quad (96)$$

The right side of equation (96) represents the area under the “absorbance vs. wave-number” curve and is what we call the integrated absorbance A_{abs} :

$$A_{abs} = - \int_{-\infty}^{+\infty} \ln \left\{ \frac{I(\nu)}{I_0(\nu)} \right\} d\nu \quad (97)$$

So that we obtain for the gas density n :

$$n = \frac{A_{abs}}{S \cdot L} \quad (98)$$

Given that the line intensity S depends on the temperature of the absorbing media T , this must be measured also in order to complete the information needed for applying the equation (98) in the measuring of the gas density n . For details about these measurements see the sections 3.9 for A_{abs} ; 3.10 for S ; 3.3 for L ; and 3.6 for T .

The standard uncertainty of the gas density measurement for this case is obtained also according to the formulae presented in section 2.4 but the result is a little more complicated given the correlation between S and A_{abs} :

$$u[n] = n \cdot \left(\sqrt{\left(\frac{u[A_{abs}]}{A_{abs}} \right)^2 + \left(\frac{u[S]}{S} \right)^2 + \left(\frac{u[L]}{L} \right)^2 - 2 \cdot \frac{u[A_{abs}, S]}{A \cdot S}} \right) \quad (99)$$

Where $u(A_{abs}, S)$ is the covariance between the integrated absorbance and the line intensity. Such covariance is given mainly through the temperature dependency of both quantities upon the temperature as explained next. Observe that the path length may or not depend on the temperature according to the particularities of each experimental setup. In our case the dependency of L on T was negligible as explained in section 3.3.2.

Although the line intensity's temperature-dependency has its origin in the temperature dependent distributions of the quantum-mechanical states of the molecules participating in the absorption process, and can therefore be modeled by functions generated through theoretical considerations about the distribution functions of the states involved (rotational, vibrational or rotational-vibrational; upper and lower energy levels, etc.), we preferred the experimental determination of the temperature dependency approach, as in any case the theoretical formula must be tested and its goodness is evaluated by comparing its predictions with the experimental results. Nevertheless, the vacuum chamber used in this work was not designed to permit an active control of the chamber temperature. Although we tried to control the temperature of the chamber walls (using heating bands evenly distributed around the exterior walls of the chamber and an appropriate temperature controller), we had no way to control the temperature of the internal devices installed in the chamber, which had an area of exposure to the gas big enough to influence significantly its temperature. These devices were in thermal contact with the optical table, so that waiting for the equilibrium through the radiation of heat from the interior face of the walls was useless. For this reason we could not perform the study of the temperature dependency of the measured line intensities ourselves. Instead, we took the line intensity values generated by the Java-HAWKS software and the

HITRAN [45] data basis at different temperatures in the range of our temperature measurements and performed a linear regression of the line intensities against the temperature. For convenience we choose $(T - T_0)$ as the abscissa, so that the intercept of the line was the line intensity at the reference temperature T_0 :

$$S(T) = S(T_0) - m_{ST} \cdot (T - T_0) \quad (100)$$

We have written already a minus in front of the slope because the line intensities studied for CO and CO₂ decrease with increasing temperature. More details and reasons for this behavior can be found in section 2.1.

From equation (98) we see that the temperature dependency of the line intensity implies a temperature dependency for the integrated absorbance:

$$A_{abs}(T) = S(T) \cdot n \cdot L \quad (101)$$

Using the last two equations and the prescriptions given in the GUM we find:

$$u[A_{abs}, S] = n \cdot L \cdot \left((T - T_0)^2 \cdot u^2[m_{ST}] + m_{ST}^2 \cdot u^2[T] \right) \quad (102)$$

Finally, we obtain the uncertainty of the density of gas in a mixture, after substituting equation (102) in equation (99):

$$u[n] = n \cdot \left(\sqrt{\left(\frac{u[A_{abs}]}{A_{abs}} \right)^2 + \left(\frac{u[S]}{S} \right)^2 + \left(\frac{u[L]}{L} \right)^2} - 2 \cdot \frac{((T - T_0)^2 \cdot u^2[m_{ST}] + m_{ST}^2 \cdot u^2[T])}{S^2} \right) \quad (103)$$

3.5. Pressure Measurements

The pressure measurement devices used in this work were two capacitance diaphragm gages (CDG), for the measurements made under static conditions (stationary gas in the chamber), two spinning rotor gages (SRG) for the measurements made under dynamic conditions (continuous flow of gas through the chamber) and one ionization gage for the characterization of the residual pressure in the vacuum chamber. The two CDG were read through a digital multimeter, which in turn was controlled by the LabVIEW program through its IEEE-488 port. Each SRG sensor had its own controller. The SRG controllers and the IG were equipped with IEEE-488 ports, which were used to read the SRG or IG output through the LabVIEW program. The details of these equipments are summarized in Table 8, on page 70.

As mentioned in the introduction of this chapter and in section 2.5, we tried to take traceable measurements as much as possible in all the steps along this research. Furthermore we tried to take our measurements with the higher level of accuracy possible. This implies not only using calibrated measuring instruments, but also using accordingly the results of such calibrations in order to convert the instrument reading in a traceable measurement of the measured quantity.

The CDG and SRG used for this research were calibrated directly with the primary standards of the Vacuum Laboratory of the PTB, so that its traceability chain is as short as possible and the accuracy of our pressure measurements is as high as possible. The two CDG were calibrated using the same digital multimeter as read-out interface, as they were used in our experiments.

The principle of operation of any CDG, SRG or IG is described in many textbooks. A very complete explanation including physical concepts as well as constructive details and calibration procedures may be found in the “Wutz Handbuch Vakuumtechnik”⁴⁶. Specifically CDG are described there in the section 12.2.5.5, SRG in the section 12.3, and IG in the section 12.7.

Next we present the calibrating functions of the vacuum gages that we used to perform our traceable pressure measurements. These functions can be found also in the copies of the certificates of calibration, in appendix 7.2. We also describe other corrections applied when it was necessary.

3.5.1. Pressure Measurements with the 10 Torr Capacitance Diaphragm Gage

For the 10 Torr – CDG, the calibrating function is

$$P_e = \frac{1.33322 \cdot P_{10CDG-Torr}}{1 + \frac{e_{10CDG}}{100}} ; \quad (104)$$

where:

- P_e is the evaluated pressure, which equals the traceable pressure at the measuring pressure port of the 10T-CDG. P_e is given here in hPa.
- $P_{10CDG-Torr}$ is the reading of the 10T-CDG in Torr, (i.e. the 10T-CDG is read through an analog output which delivers a 0 V to 10 V signal -which is proportional to the pressure reading in Torr, with a proportionality factor of 1 - this voltage is read with the digital multimeter and send through the IEEE-488 port as the $P_{10CDG-Torr}$).
- e_{10CDG} is the error function (in percentage) of the instrument, as given in its certificate of calibration:

$$e_{10CDG} = \left(a + b \cdot \ln\{P_{mbar}\} + c \cdot (\ln\{P_{mbar}\})^2 + d \cdot (\ln\{P_{mbar}\})^3 + \right. \\ \left. + e \cdot (\ln\{P_{mbar}\})^4 + f \cdot (\ln\{P_{mbar}\})^5 + g \cdot (\ln\{P_{mbar}\})^6 \right) , \quad (105)$$

where $P_{mbar} = 1.33322 \cdot P_{10CDG-Torr}$ and the coefficients a to g are given in the next table.

Table 5: Coefficients of the 10T-CDG calibration.

a	b	c	d	e	f	g
-0.050656106	-0.041595956	0.04615046	-0.03238938	0.00585944	0.00063472	-0.00029885

Finally, taking in account that the height of the 10T-CDG was not the same as the height of the center of the VCMHC, it is possible to perform a “head-column” correction to find the mean gas pressure in the chamber P ,

$$P = P_e \cdot \left(1 - \frac{M \cdot m_{uma} \cdot g \cdot h}{k \cdot T} \right), \quad (106)$$

where

- M is the molecular weight of the gas in g/mol,
- m_{uma} is the atomic mass unit in kg,
- g is the acceleration of gravity in m/s²,
- h is the height difference between the 10TCDG and the VCMCH, in meters,

and as usual, the Boltzmann constant k is given in J/K and the thermodynamic temperature T is given in K. Nevertheless this correction is too small for our measurements (compared with the uncertainty of the evaluated pressure) given the small gas densities in vacuum and the moderate height difference of our setup (40 cm).

The standard uncertainty of the evaluated pressure, in the range of pressures measured with the 10T-CDG for this research, was calculated based on the information given in its certificate of calibration, and found to be 0.3% of the evaluated pressure. Furthermore we took a pressure measurement for each scan, so that when several (N) scans were combined, the final evaluated pressure was the mean of the N measurements and the standard deviation of the N measurements was combined with the standard uncertainty of the evaluated pressure:

$$u[P] = \sqrt{(3 \cdot 10^{-3} \cdot P)^2 + s^2[P_e]} \quad (107)$$

3.5.2. Pressure Measurements with the 1000 Torr Capacitance Diaphragm Gage

For the 1000T – CDG, the calibrating function is:

$$P_e = K_{orr}(P_{1kCDG}) \cdot P_{1kCDG} , \quad (108)$$

where

- P_e is the evaluated pressure, which equals the traceable pressure at the measuring pressure port of the 1000T-CDG (P_e is given here in hPa),
- P_{1kCDG} is the reading of the 1000T-CDG in Torr·10⁻¹, (i.e. the 1000T-CDG is read through an analog output which delivers a 0 V to 100 V signal -which is proportional to the pressure reading in Torr with a proportionality factor of 10⁻¹ - this voltage is read with the digital multimeter and send through the IEEE-488 port as the P_{1kCDG}),
- $K_{orr}(P_{1kCDG})$ is a function of the instrument's reading as given in its certificate of calibration, which is presented next:

$$K_{orr} = \left(a + b \cdot P_{1kCDG} + \frac{c}{P_{1kCDG}} + d \cdot (P_{1kCDG})^2 + \frac{e}{(P_{1kCDG})^2} + f \cdot (P_{1kCDG})^3 + \frac{g}{(P_{1kCDG})^3} \right) \quad (109)$$

where the coefficients a to g are given in the next table.

Table 6: Coefficients of the 1000T-CDG calibration.

a	b	c	d	e	f	g
13.353855	-6.924765·10 ⁻⁴	-1.42844·10 ⁻³	1.212651·10 ⁻⁵	1.247275·10 ⁻³	-8.191386·10 ⁻⁸	-1.097796·10 ⁻⁴

The standard uncertainty of the evaluated pressure, in the range of pressures measured with the 1000T-CDG for this research, was calculated based on the information given in its certificate of calibration, and found to be 0.22% of the evaluated pressure. As with the 10T-CDG, we took a pressure measurement for each scan, so that when several (N) scans were combined, the final evaluated pressure was calculated with the mean of the N measurements and the standard deviation of the N measurements $s[P_e]$ was combined with the standard uncertainty of the evaluated pressure:

$$u[P_e] = \sqrt{(2.2 \cdot 10^{-3} \cdot P_e)^2 + s^2[P_e]} \quad (110)$$

3.5.3. Pressure Measurements with the Spinning Rotor Gage

For the SRG, the calibrating function is:

$$P = \frac{D \cdot \rho \cdot \pi \cdot \left(\frac{\dot{\omega}}{\omega} - (m_f \cdot \omega + \delta) \right) \cdot \sqrt{\frac{8 \cdot R \cdot T}{\pi \cdot M \cdot 10^{-3}}}}{20 \cdot \sigma_o} \quad (111)$$

where

- D is the diameter of the SRG-ball in meters,
- ρ is the mass-density of the SRG-ball in kg/m³,
- $\dot{\omega}/\omega$ is the SRG-ball relative deceleration rate in Hz (or s⁻¹),
- m_f is the slope of the deceleration rate vs. rotation frequency linear fit of the SRG offset characterization,
- ω is the rotation frequency of the SRG-ball in Hz,
- δ is the intercept of the deceleration rate vs. rotation frequency linear fit of the offset characterization in Hz,
- σ_o is the accommodation coefficient of the SRG (dimensionless),
- R is the ideal gas constant: 8.315 J/(K mol)
- T is the thermodynamic temperature of the ball in Kelvin, and
- M is the molecular weight of the gas in g/mol.

The coefficients of the SRG calibrating functions are given in the next table:

Table 7: Coefficients of the SRG1 and SRG2 calibration.

SRG-#	D	ρ	m_f	δ	σ_o
1	$4.762 \cdot 10^{-3}$	$7.715 \cdot 10^3$	0	$3.00 \cdot 10^{-7}$	1.222
2	$4.762 \cdot 10^{-3}$	$7.715 \cdot 10^3$	0	$8.17 \cdot 10^{-7}$	1.274

The coefficients m_f and δ were found through the characterization of the deceleration rate offset in situ on the VCMHC. The other coefficients shown in Table 7 were taken from the calibration certificates of the SRG.

The SRG-controllers monitored continuously the deceleration rate and rotation frequency of the SRG-balls and send the data through the IEEE-488 ports to the controlling computer when the IPSIAM LabVIEW program ordered them to perform a measurement.

The standard uncertainty of the evaluated pressure, as given by the certificate of calibration of the SRG1 and SRG2, is 0.5% of its evaluated pressure, so that for this two PMD we have:

$$u[P] = 5 \cdot 10^{-3} \cdot P \quad (112)$$

When using the SRG we took a pressure measurement for each scan and considered the mean of these measurements and their standard deviation when analyzing several scans together. As we will explain in chapter 4, the scans that we combined had always a dynamic equilibrium, that was stable enough, so that the standard deviation of the measurements was completely negligible compared with the 0.5% of the calibration.

Table 8. Pressure Measurement Devices used in this work.

Part	Manu- Facturer	Model	Serial Number	Measuring Range	Resolution	Certificate of Calibration Number	Short Name
CDG - Sensor	MKS	690A11 TRB	93109 105A	0 – 10 Torr	5 decades	QS8/05	10T-CDG
CDG - controller	MKS	270C-0	15462-2	x1	--		
CDG - Sensor	MKS	931061 02A	931061 02A	(0 - 1000) Torr	5 decades	QS04/05	1000T-CDG
CDG - controller	MKS	270C-5	93103202 A	X1 & x.1	--		
Digital Multimeter	Hewlett Packard	34401A	3146A 31944	(0 - 10) V & (o - 100) V	10 μ V & 0.1 mV	QS8/05 and QS4/05	--
SRG - Sensor	Leybold	VK-201	158 82 D 931100021	(10 ⁻⁷ - 10 ⁻²) mbar	10 ⁻⁷ mbar	QS1/05	SRG-1
SRG - controller	PTB	VISCOVAC VM212	158 83 D 920400019				
SRG - Sensor	PTB	--	1	(10 ⁻⁷ - 10 ⁻²) mbar	10 ⁻⁷ mbar	QS2/05	SRG-2
SRG controller	MKS	--	PTB 0030283				
Ionization Gage	Leybold	IM520 / IE414-170	94008872 / 01025825	(10 ⁻¹² - 10 ⁻³) mbar	10 ⁻² of range per decade	--	IG

3.6. Temperature Measurements

We measured the temperature at two different points inside the VCMHC, located each near an opposite end of the VCMHC cylinder. Furthermore we measure the temperature in seven points distributed evenly over the outside part of the walls of the VCMHC. All the thermometers were of PT100 type.

The two thermometers inside, named here PT100 -1 and PT100 -2 were read with two digital multimeters, which read the resistances of the PT100 in a four wire configuration. These resistances were sent, expressed in ohms, over the IEEE-488 ports of the digital multimeters to the controlling computer when the LabVIEW program ordered them to take the temperature measurements. One temperature measurement per sensor was taken per each absorption scan. The PT100-1 was calibrated by the Thermometry Laboratory at the PTB (together with its digital multimeter as a measuring unit) and was used to record the gas temperature. The PT100-2 was used to monitor possible temperature gradients and relative changes inside the VCMHC and even though it was not calibrated, it played a key role in finding out which of all the “simultaneous” temperature measurements reflected better the gas temperature, as we will see in section 4.3.

The seven external thermometers were read out by a Keithley 7700 Scanner, also in a four wire configuration, but the measurements were sent over the IEEE-488 port of the scanner expressed in degrees Celsius. These 7 thermometers were continuously monitored and recorded by the IPSIAM LabVIEW program every two minutes (or every minute), independently of the oscilloscope scans. The seven external PT -100 together with the Keithley scanner were calibrated internally in the Vacuum Laboratory of the PTB using a temperature working standard, which in turn was calibrated by the thermometry Laboratory of the PTB.

The details of all the Temperature Measurement Devices (TMD) used for this research are presented in the Table 10 on page 73.

The calibrating function of the PT100-1, is:

$$T = m_{R_2} \cdot R_{\Omega}^2 + m_{R_1} \cdot R_{\Omega} + m_{R_0} + 273.15 \quad (113)$$

Where R_{Ω} is the PT100-1 four-wire measured resistance in ohms and the m_{R_i} coefficients were calculated based on the information given in the PT100-1 certificate of calibration and are shown in the next table:

Table 9: Coefficients of the PT100-1 calibration.

PT100-#	m_{r2}	m_{r1}	m_{r0}
1	$-3.1851 \cdot 10^{-4}$	2.6413	-260.9448

The standard uncertainty of the evaluated temperature of one measurement is 6.1 mK, but taking into account that we read and recorded a temperature measurement for each oscilloscope scan, the overall temperature standard uncertainty for a measurement with several scans is

$$u[T] = \sqrt{(2 \cdot m_{r2} \cdot s[R_{\Omega}])^2 + (m_{r1} \cdot s[R_{\Omega}])^2 + (6.1 \cdot 10^{-3})^2}, \quad (114)$$

where $s[R_{\Omega}]$ is the standard deviation of the resistance measurements.

The PT100-1 was calibrated after it was already welded to the rods of the feed-through vacuum-flange. The same multimeter and cables used to read the PT100-1 signals in our spectrometer were used to read the PT100-1 during its calibration. As can be read in its calibration certificate, the calibration was performed by comparison with two PTB working standards. The PT100-1 was introduced in a glass tube and the glass tube were submerged in the calibrating thermal bath (to keep the PT100-1 reading the temperature of a gas, which temperature was controlled trough the thermal bath). The vacuum flange served as a lid to the glass tube in order to prevent convective interchange of the gas in the tube with the atmosphere.

The details of all the Temperature Measurement Devices (TMD) used for this research are presented in the Table 10 on page 73.

Table 10. Temperature Measurement Devices used in this work.

TMD-Part	Manufacturer	Model	Serial Number	Measuring Range	Resolution	Certificate of Calibration Number	Short-name
PT100internal Sensor	--	PT100	--	--	--	165 PTB 03	PT100-1
PT100internal Readout	Hewlett Packard	34401	3146A 31492	(0 - 1) k Ω	1m Ω		
PT100internal Sensor	--	PT100	--	--	--	--	PT100-2
PT100internal Readout	Fluke	8840A	3953007	(0 - 200) Ω	1m Ω		
PT100external Sensors	Keithley	PT100				IC 20050517	T1 to T7
PT100external Readout	Keithley	7700/ 2700	0941028/0 941368	(-200 - 630) °C	0.01°C		Keithley
Working Standard Sensor	ASL	PT100	(A)SV191 5/A V 2572 A	(0 - 50)°C	0.001°C	130 PTB 03	F250
Working Standard Readout	ASL	F250	1249027 214				

3.7. Absorbance Measurements

The absorbance measurements were made based on optical transmission measurements of an infrared laser ray through the absorbing media, as briefly described in the section 3.1. The laser was divided in three rays, two of them being used for the absorbance measurements and therefore we will describe in this section all the equipment and procedures relevant for the detection of these two rays as well as the methods implemented to process that data and obtain the absorbance measurements. The third ray was used to generate a frequency marker signal and that will be covered on the section 3.8.

After being collimated by the OAP in the laser source device, the ray was redirected by a flip-flop mirror toward a second OAP, which focused the ray to a position at 20 cm, where the blade of the chopper was positioned (if the flip-flop mirror was in “flop” state the ray was redirected by a fixed flat mirror positioned behind the flip-flop toward a FTIR, which was used for absolute wave number measurements). After being chopped in this focus point, the ray continues toward a third OAP of the same focal length as the second one, which collimated the ray again and sent it through the “accessory area” and toward the first beam-splitter. The beam-splitters used were of the Pellicle-Beam-Splitter (PBS) type. The ray reflected by the first PBS was focused by a spherical mirror on detector 2, where it was detected as the reference signal. The ray reflected by the second PBS went through a small cell, then through the VCMHC, and was finally focused on to detector 1 as the detection signal.

The signals from detectors 1 and 2 were preamplified by their respective preamplifiers and detected in two Lock-In Amplifiers (LIA) which used the $1/f$ reference signal from the chopper controller to perform the harmonic detection of the chopped signals. The outputs of both LIA were recorded by a four channels digitizing oscilloscope: The detection signal was recorded on the oscilloscope channel 1 and the reference signal on its channel 2. So summarizing we see that the main parts involved in the measurement of the detection signal and the reference signal can be itemized as follows.

a. Equipment shared for the measurement of all signals:

- The chopper unit and its controller
- Two 20 cm focal length OAP
- Two pellicle beam splitters
- The four channel digitizing oscilloscope

b. Equipment dedicated solely to the measurement of the detection signal:

- Detector 1
- Preamplifier 1
- Lock-In Amplifier 1

c. Equipment dedicated solely to the measurement of the reference signal:

- Detector 2
- Preamplifier 2
- Lock-In Amplifier 2

The details of these equipments are presented in two tables: Those of list a. in Table 11, page 78, and those of lists b. and c. in Table 12, page 79.

Now we will explain the main optimization criteria, instrumental set up and operations that we made to measure the absorbance for some specific discretized wave number ν_j . The explanation of the overall data manipulation for all the discretized wave-numbers measured in each scan will be described in appendix 7.1, page 153.

In order to increase the quality of the absorption curve measurements we decided to increase the scan frequency from 0.5 Hz (used in an earlier research in this field and the same Laboratory [47]) to 10Hz reducing the time window where the form of the absorption line could be affected by transient effects. We also increased the number of digitizing points from 500 to 2500 so that we could map more accurately the form of the absorption line and therefore achieve a more exact determination of the area under the absorption curve. That left us a digitizing time per point of only $0.1 \text{ s} / 2500 = 40 \text{ } \mu\text{s}$, making it impossible to read the “R” signal of the LIA [$R = (X^2 + Y^2)^{1/2}$] because this signal is actualized at a 512 Hz rate, i.e. about each 2 ms. So we had to switch to the “fast mode” operation of the LIA, in which the LIA output is given only through “X” while its “Y” output is kept “equal to zero” by the Auto-Phase function of the LIA. In the fast mode the output is actualized each $4 \text{ } \mu\text{s}$ so that the oscilloscope can integrate and average 10 LIA outputs for each discretized point per scan.

To achieve a smooth form of the absorption line, but without over-filtering (which produces an artificial widening of the observed absorption figure), we found an optimizing combination of parameters when operating the chopper at 3140 Hz and setting the LIA’s time constants in $640 \text{ } \mu\text{s}$ for the LIA -1 and $300 \text{ } \mu\text{s}$ for the LIA -2.

Now lets concentrate in the measurements done for a given discretized wave-number ν_j , with j fixed during this explanation (and $1 < j < 2500$). To facilitate the clarity of the exposition we will drop the subscript j from almost all the symbols for the rest of this section, which otherwise would have such label to denote that they belong to the discretized wave-number ν_j .

For the measurement when the VCMHC was empty (what we will call a –null– scan later) we assign the following names:

- I_{D0} is the optical intensity arriving at Detector 1 (in the Detection channel) when the absorption cell was empty,
- V_{D0} is the signal recorded in channel 1 of the digitizing oscilloscope which corresponds to the measurement of the optical intensity I_{D0} in Detector 1,
- I_{R0} is the optical intensity arriving at Detector 2 (in the Reference channel) which is simultaneous to I_{D0} .

- V_{R0} is the signal recorded in channel 2 of the digitizing oscilloscope which corresponds to the measurement of the optical intensity I_{R0} in Detector 2.

Note that V_{D0} is recorded simultaneously with V_{R0} .

For the measurement when VCMHC was filled with some amount of absorbing media (in what we will call a –part– scan) we assign the following names:

- I_{Dk} is the optical intensity arriving at Detector 1 (in the Detection channel) when the absorption cell contained some absorbing media which absorbed with an absorption coefficient $k(v_j - v_c)$,
- V_{Dk} is the signal (Voltage) recorded in channel 1 of the digitizing oscilloscope which corresponds to the measurement of the optical intensity I_{Dk} in Detector 1,
- I_{Rk} is the optical intensity arriving at Detector 2 (in the Reference channel) which is simultaneous to I_{Dk} ,
- V_{Rk} is the signal (Voltage) recorded in channel 2 of the digitizing oscilloscope which corresponds to the measurement of the optical intensity I_{Rk} in Detector 2.

As before, V_{Dk} and V_{Rk} are recorded simultaneously.

Ideally the response of the detection system should be completely linear to the optical intensity, but as we shall see in section 4.5 that is not always the case, or at least not with the level of accuracy required for our research. So we will leave at the moment the relation between recorded detection signal and optical intensity expressed in general as

$$V_{Dk} = f^{-1}(I_{Dk}) , \quad (115)$$

but for simplicity we will continue the talk about the optical intensities as if we were able to find them with the help of the function f : $I_{Dk} = f(V_{Dk})$, We will yet use V as equivalent to I when that helps to the clarity of the concepts.

The absorbance is defined through the following equation:

$$\alpha_k = -\ln \left\{ \frac{I_{Dk}}{I_{D\Theta k}} \right\} ; \quad (116)$$

where

- $I_{D\Theta k}$ is the optical intensity arriving at the entrance window of the recipient containing the absorbing media, which after traveling the absorption path length and being affected by the absorbing media, originates the output optical intensity I_{Dk} at the output window of the recipient.

It is impossible to measure “directly” the original input intensity approaching the absorbing media $I_{D\Theta k}$ as this measurement would destroy the original arrangement ($V_{D\Theta k}$ would denote the signal that we would record if the direct measurement of $I_{D\Theta k}$ was possible). That is why we set up the measurement of the reference channel, as a mean to perform an “indirect” measurement of $I_{D\Theta k}$ as follows:

We find a function $g(V_{R0})$ that transforms the recorded signals from the reference channel (channel 2) in the recorded signals from the detection channel (channel 1) when there was no absorbing media in the chamber:

$$V_{D0} = g(V_{R0}) . \quad (117)$$

Then, assuming that this function does not change during the following minutes separating the null- scan from the part- scan, we apply the same function to find the original input intensity of the detection channel based on the simultaneously recorded signal from the reference channel:

$$I_{D\Theta k} = g(I_{Rk}) . \quad (118)$$

Our function g is actually defined in 18 segments with different mathematical functions, each being a regression for the segment. Each function can be a polynomial from grad 1 to grad 6, but from experience we saw that a linear regression is of sufficient accuracy.

In the next step we make a small offset correction of the Intensity scale after observing the recorded signal of the 100% Absorption scan (called the tot- scan). The level of the signal in the plateau of 100% absorption is always very close to zero, as we perform also an Auto-Offset procedure at the beginning of each scan- measurement, but even if small, the average of that plateau is subtracted from the recorded detection signals and the predicted original signals.

Once we have the offset-corrected and the offset-corrected predicted original input intensity, we can calculate the optical transmission of the absorbing media t_{rk} as

$$t_{rk} = \frac{I_{Dk} - \xi}{I_{D\Theta k} - \xi} , \quad (119)$$

where ξ is the offset-correcting term which is equal to the average of the plateau signal at 100% absorption. We measured these intensities and offset several times, so that the equation (119) is evaluated with the mean value of all those measurements and we calculate the standard uncertainty of the transmission $u[t_r]$ using the means and standard deviations of the repeated measurements as follows:

$$u[t_{rk}] = \sqrt{\frac{s^2[I_{Dk}]}{(I_{D\Theta k} - \xi)^2} + \frac{(I_{Dk} - \xi)^2 \cdot s^2[I_{D\Theta k}]}{(I_{D\Theta k} - \xi)^4} + \left(\frac{I_{Dk} - \xi}{(I_{D\Theta k} - \xi)^2} - \frac{1}{I_{D\Theta k} - \xi} \right)^2 \cdot s^2[\xi]} . \quad (120)$$

Now we can calculate the corresponding absorbance and its standard uncertainty:

$$\alpha_k = -\ln\{t_{rk}\} , \quad (121)$$

$$u[\alpha_k] = \frac{u[t_{rk}]}{t_{rk}} . \quad (122)$$

Table 11. Equipment shared for the measurement of all the optical signals.

Part	Manufacturer	Model	Serial Number	Range	Resolution	Short-name
Chopper	Stanford Research	SR540	7978	(4 - 4000) Hz	1 Hz	Chopper
Digitizing Oscilloscope	Tektronix	TDS 510A	B010441	Ch1: (0 - 10) V Ch2: (0 - 20) V Ch3: (0 - 5) V Ch4: (0 - 2) V	2 mV 4 mV 1 mV 0.4 mV	TDS-510
Second OAP	Kugler GmbH	AS25-200-D-18/90°	Pf12859-3	--	--	OAP2
Third OAP			Pf12859-4	--	--	OAP3
First PBS	Melles griot	03BPL001/05	PTB-200011450	--	--	PBS1
Second PBS		03BPL003/05	PTB-200011452	--	--	PBS2

Table 12. Equipment dedicated to the measurement of the detection signal and of the reference signal.

Part	Manufacturer	Model	Serial Number	Range	Gain or Resolution or Responsivity	Data Sheet Number	Short-name
Detection Signal Detector	EG & G	J10D-M204-R01M-60	5-96-0331	(2 - 5.5) μm	2.6 A/W	400005-1	Detector-1
Detection Signal Preamplifier	Judson	PA-9-44	96-4-9555	DC to 1400 kHz	$2.5 \cdot 10^4$ V/A	PB#218-PA9-44	Preamp-1
Detection Signal Lock In Amplifier	Perkin Elmer	7265 DSP-LIA	492	0.001 Hz to 250 kHz / 2 mV to 1 V	(0 - 90) dB	--	LIA-1
Reference Signal Detector	EG & G	J15D12-M204-S-500U-60	5-04-0698	(2 - 15) μm	$2.1 \cdot 10^4$ V/W	450186-1	Detector-2
Reference Signal Preamplifier	Judson	PA-300	04-03-3180	DC to 1 MHz	10 V/A	490095POD	Preamp-2
Reference Signal Lock In Amplifier	Stanford Research	SR830	21467	1 mHz to 102 kHz / 2 mV to 1 V	(0 - 90) dB	--	LIA 2

3.8. Wave-Number Measurements

The wave-number measurements were made based on optical transmission measurements of an infrared laser through a Germanium Etalon or (mainly) through an Open Confocal Etalon that was developed by Pustogow as part of an earlier doctoral research at the Technical University Berlin [48]. As mentioned in the section 3.1, the laser wave-number was swept using a current-ramp in order to scan the whole absorption line of interest. Here we will present the methods implemented to process the respective data and obtain the relative wave-number measurements.

Continuing the description made in the second paragraph of section 3.7, in page 74, the ray transmitted by the second PBS was redirected by flat mirrors towards the Etalon. The ray transmitted through the Etalon, with intensity I_{FM} , was redirected and focused by a spherical mirror onto the Detector 3. The signal from this detector was preamplified and sent to a second “Low Noise Preamplifier” (LNP) which has also filtering functions. The signal was processed through a Band Pass filter (0.03 – 100) Hz, which filter out the 3kHz modulation from the chopper. The output of the LNP is recorded in the channel 3 of the digitizing oscilloscope as the frequency marker signal V_{FS} . This is done as the signals are swept through different wave-numbers repetitively, with a repetition frequency determined by the effective ramp-frequency of the function generator, 10 Hz. This ramp frequency commands the trigger of the digitizing oscilloscope and also affects the current to wavelength conversion of the tunable diode laser as we will see later.

Summarizing the equipment description for this section, the main parts involved in the measurement of the frequency marker signal, and that were not already mentioned in the list a. in page 74 , can be itemized as follows:

Equipment shared for the measurement of all signals at different wave-numbers:

- The function generator

Equipment dedicated solely to the measurement of the frequency marker signal:

- The Germanium Etalon, or
- The Open Confocal Etalon
- Detector 3
- Preamplifier 3
- The Low Noise Preamplifier with Filter

The details of these equipments are presented in Table 14 in page 91.

The method of measurement is the following: A triangular ramp from the function generator is used to sweep the wavelength of the laser. In order to obtain a sampling as linear as possible in the wave-number axis of the absorbance vs. wave-number curve, the current injected to the diode-laser is modified linearly in time as follows: The laser controller injects the diode-laser with a current I_C composed of a constant base current I_{CB} plus a “delta” current $I_{C\Delta}$:

$$I_C = I_{CB} + I_{C\Delta} . \quad (123)$$

The $I_{C\Delta}$ is obtained from an internal linear voltage-to-current converter in the laser controller, which is fed with the voltage of the triangular ramp from the function generator output V_{TR} :

$$I_{C\Delta} = m_{I_C V} \cdot V_{TR} \quad (124)$$

The voltage-to-current coefficients $m_{I_C V}$ are 20 mA/V for the L5830 controller and 10 mA/V for the DFB controller. The base currents used are typically 390 mA for the L5830 controller and 40 mA for the DFB controller.

For each recorded period τ , the triangular ramp voltage V_{TR} is a linear function of time t ,

$$V_{TR} = m_{Vt} \cdot \left(t - \frac{\tau}{2} \right) . \quad (125)$$

Substituting equations (125) and (124) in equation (123) we obtain

$$I_C = I_{CB} + m_{Vt} \cdot m_{I_C V} \cdot \left(t - \frac{\tau}{2} \right) \quad (126)$$

$$0 \leq t \leq \tau .$$

If the current to wave-number conversion rate dv/dI_C was constant, so would be the timely variation of the wave number as the current is linearly swept:

$$\frac{dv}{dI_C} = \text{constant} = m_{v I_C} \Rightarrow \frac{dv}{dt} = \frac{dv}{dI_C} \cdot \frac{dI_C}{dt} = \text{constant} \quad (127)$$

$$\Rightarrow \frac{dv}{dt} = m_{v I_C} \cdot m_{I_C V} \cdot m_{Vt}$$

In this case the observed Etalon transmission (see Figure 8, page 82) would present its maxima (the Airy function maxima) centered at temporal positions $\Psi_1, \Psi_2, \Psi_3, \dots$ etc. which are evenly distributed along the scanned frequency marker signal, so that the time intervals $\Delta\Psi_p = \Psi_p - \Psi_{p-1}$ would be constant and given by the constant dv/dt and the Etalon FSR, ΔF :

$$\Delta\Psi_p = \Delta F \cdot \left(\frac{dv}{dt} \right)^{-1} \quad (128)$$

In this case it would be possible to measure the constant time-to-wave-number transformation coefficient dv/dt with the measurement of the temporal positions of any pair of transmitted

frequency-marker maxima peaks Ψ_p and Ψ_{p-1} . Using the known Etalon FSR, ΔF , from the rearrangement of equation (128) as follows:

$$\frac{d\nu}{dt} = \frac{\Delta F}{\Delta\Psi_p} \quad (129)$$

For reasons becoming clear in the following, we define a variable Γ_p as the temporal center between the successive frequency marker maxima Ψ_p and Ψ_{p-1} :

$$\Gamma_p = \frac{\Psi_p + \Psi_{p-1}}{2} \quad (130)$$

We also define a variable ϑ_p as the Etalon FSR ΔF divided by the temporal separation of the frequency marker maxima $\Delta\Psi_p$ for the pair p :

$$\vartheta_p = \frac{\Delta F}{\Delta\Psi_p} \quad (131)$$

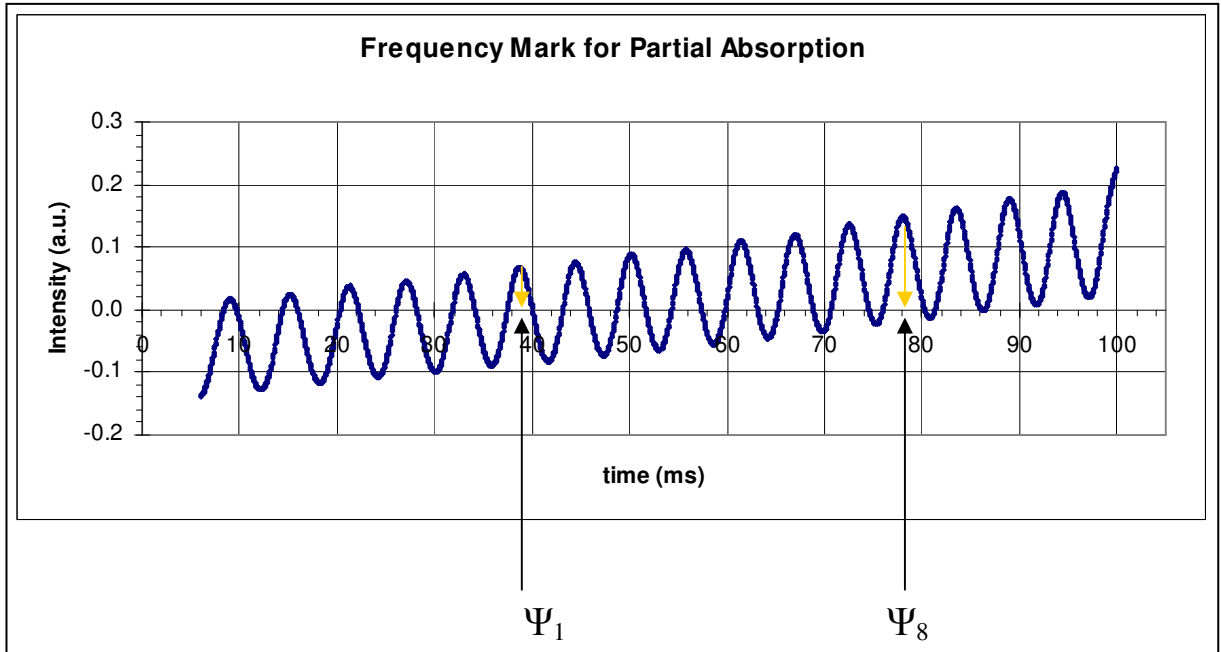


Figure 8. Transmission of the OCE from one of our measurements (example-measurement).

If equation (128) is true for any pair of maxima p , we will expect consequently no variation of ϑ_p for the different Γ_p , and a graphic representation of ϑ_p vs. Γ_p would be a horizontal line.

In Figure 9 we present a ϑ_p vs. Γ_p curve from our example-measurement, which presents the typical behavior of the measurements. The Etalon in this case was the OCE, from which we analyzed in detail 9 transmissions maxima around the center of the absorption peak. The corresponding absorption scan and reference predicted scan for the same measurement and time window are shown in Figure 10.

It is immediately evident that the assumption of constancy for dv/dt was not confirmed experimentally.

To linearize our wave-number axis with as much accuracy as possible, we used the fact that the distance from maxima to maxima in the wave-number axis must be exactly equal to the Free Spectral Range, ΔF , i.e. the dv/dt function must fulfill the integral equation (132) no matter how its local variation may be.

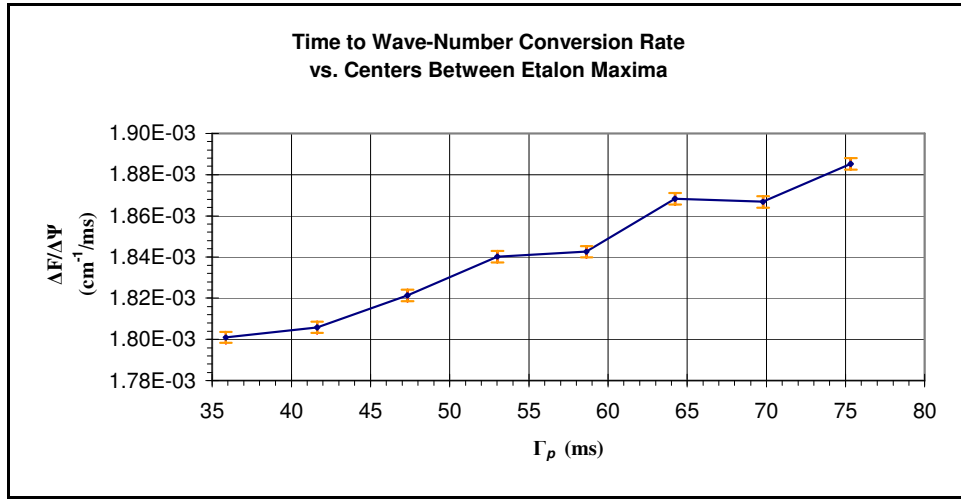


Figure 9: ϑ_p vs. Γ_p as example for a typical measurement.

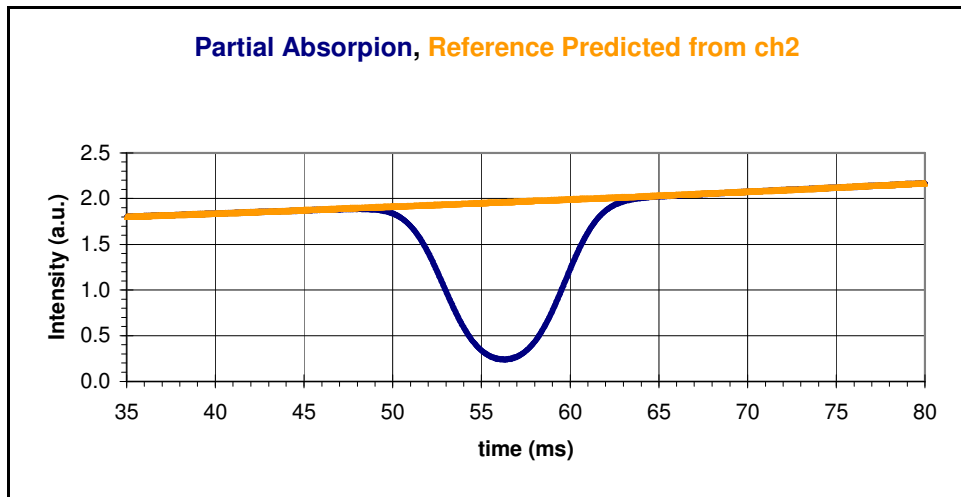


Figure 10: Detection Signal and Reference Predicted Signal of our example-measurement.

$$\Delta F = \int_{\Psi_{p-1}}^{\Psi_p} \left(\frac{d\nu}{dt} \right)_p dt \quad (132)$$

Since we had no additional information to find the local temporal dependency of the $d\nu/dt$ function we decided to use a linear approximation for each segment p (from Γ_{p-1} to Γ_p) as the first terms of a Taylor series:

$$\left(\frac{d\nu}{dt} \right)_p \cong a_p \cdot t + b_p . \quad (133)$$

Doing so, we obtain a set of 7 linear approximations which together achieve a similar accuracy as a polynomial expansion of grade 7.

The coefficients a_p and b_p are found immediately from the data used to generate the Figure 9, as each version p of the equation (133) has the two pairs $(\vartheta_{p-1}, \Gamma_{p-1})$ and (ϑ_p, Γ_p) as boundary conditions (to fulfill the requirement imposed by the equation (132)):

$$\begin{aligned} a_p &= \frac{\vartheta_p - \vartheta_{p-1}}{\Gamma_p - \Gamma_{p-1}} \\ b_p &= \vartheta_p - a_p \cdot \Gamma_p \\ b_p &= \vartheta_{p-1} - a_p \cdot \Gamma_{p-1} \end{aligned} \quad (134)$$

p goes from 1 to 9, $a_1 = a_9 = 0$, $b_1 = \vartheta_1$, $\Gamma_0 = 0$, $b_9 = \vartheta_8$, the segment 1 goes from $-\infty$ to Γ_1 and the segment 9 goes from Γ_8 to $+\infty$. Or in other words, we assume that in Figure 9 the function is a horizontal line from $-\infty$ to the first point Γ_1 and so is it also a horizontal line from the last point Γ_8 to $+\infty$. These assumptions are justified, as those segments are already positioned over the wings of the absorption line, quite far away from its center (see Figure 10), where the absorption can be neglected and therefore an accurate knowledge of the wave-number scale is no longer needed.

Integrating the equation (133) we find an approximation grad 2 for the direct temporal dependency of the wave-number function in each segment p :

$$\nu_p(t) = \frac{a_p}{2} \cdot (t^2 - \Gamma_{p-1}^2) + b_p \cdot (t - \Gamma_{p-1}) + c_p \quad (135)$$

$$\Gamma_{p-1} \leq t \leq \Gamma_p$$

So that from the 9 functions (135), those 7 with $a_p \neq 0$ working together achieve an accuracy similar to that of a polynomial approximation grad 14 for the overall function $v(t)$ over the corresponding 7 segments together (segment 2 to segment 8).

Since we are only interested in a relative wave-number scale in the sense that we only need to measure wave-number differences, we assign the ad-hoc value of zero to c_1 and then we calculate the following coefficients c_2 to c_8 requiring the continuity condition on the frontiers between successive segments:

$$\begin{aligned} c_1 &= 0 \\ c_2 &\equiv v_1(\Gamma_1) = v_1 \cdot \Gamma_1 \\ c_3 &\equiv v_2(\Gamma_2) = \frac{a_2}{2} \cdot (\Gamma_2^2 - \Gamma_1^2) + b_2 \cdot (\Gamma_2 - \Gamma_1) + c_2 \\ c_p &\equiv v_{p-1}(\Gamma_{p-1}) \end{aligned} \quad (136)$$

We will need not only the 24 coefficients, but also their variances and covariances in order to be able to calculate properly the uncertainty of each discretized wave-number. To explain these operations we need to present some information about the operative implementation of IPSIAM on this regard.

Our IPSIAM performs almost all the mentioned steps automatically, except for a few decisions that are taken by the operator after looking at the graphs generated by IPSIAM: IPSIAM performs an automatic recognition of all the peaks of Figure 8 and generates a table where these peaks are indexed and their corresponding approximate positions (cell of the maximum value) are presented. See Figure 11.

U	V	W	X	Y	Z	AA	AB	AC	AD	AE	AF
1	smoothed		slope zone	maximum	peaks	index	cell number	peak finder	summary		
2	curve			identifier	counter	peak					
3											
4											
5											
6	total number		second				index	line cell			
7	of smoothing		"semi"-numb								
8	cells		for smoothing								
9	25		6								
10											
11											
12											
13											
14											
15											
16											
17											
18											
19											
20											
21											
22											
23											
24											
25											
26											
27											
28											

Figure 11. Screen shot of IPSIAM: Table with recognized maxima of transmission of the OCE.

Looking at the graph of Figure 8, the operator decides which of the observed peaks will be chosen as the first peak (corresponding to Ψ_0 in our notation) of the group of 9 that are needed for our calculations, and gives this decision to the program through the indication of that index. For example in the Figure 8, IPSIAM found 16 peaks and the operator choose the peak index 5 as the first of the 9. See Figure 12.

The operator choose the index of the first selected OCE transmission maxima trying to leave the absorption peak as well centered as possible in the middle of the area defined by the segments 2 to 8 together.

1	ch3 offset adjusted	time ms1	time ms2	time ms3	time ms4	intensity parabolic predictions	cell n
2	grade 1	grade 2	grade 3	grade 4			
3							
4							
5	152	152	152	152	152		
6	2501	2501	2501	2501	2501		
7							Free
8							U(FS)
9							
10	start with peak index	5					
11	semi-range for fit q2	40					
12	observing the offset graph we decide to analyse the peaks using the next ranges:					which gives us the next	with this uncertainties:
13						time differences:	at this positions
14	Number of peak	from line	to line	aprox peak			
15	1	785	865	825	5.760475026	0.753887832	35.86859513
16	2	929	1009	969	5.744882989	0.89623905	41.62127414
17	3	1072	1152	1112	5.696048053	1.020463077	47.34173966
18	4	1215	1295	1255	5.637568193	1.166047743	53.00854778
19	5	1356	1436	1396	5.630366635	1.337595481	58.6425152
20	6	1497	1577	1537	5.553122189	1.426473968	64.23425961
21	7	1635	1715	1675	5.557532808	1.583825224	69.78958711
22	8	1774	1854	1814	5.503182399	1.6943426	75.31994471
23	9	1912	1992	1952			
24							
25	Cálculo del polinomio grado 2 para el pico 1: desde:					785 hasta:	865
26	D	E - F					
27		m2	m1	b	peaks position (pp):	32.98835762	
28	mn	-0.038017174	2.508248269	-41.31809674	Upp:	0.500844506	
29	Umn	0.000408297	0.026917109	0.443344124	Upp(rel)	0.015182463	
30	r2. Std Dev Y	0.99112389	0.002874135	#N/A			
31	F. df	4354.816781	78	#N/A			
32	ssreg. ssresid	0.071947233	0.000644331	#N/A			
33							
34							
35	Cálculo del polinomio grado 2 para el pico 2: desde:					929 hasta:	1009

Figure 12 Screen shot of IPSIAM: The operator indicates the index of the selected first peak on cell E10.

Once the selected index is given in the cell E10, the program performs automatically:

- the accurate measurement of the positions Ψ_p of all the 9 selected transmission maxima;
- the calculation of the 8 centers between maxima Γ_p , and
- the calculation of the 24 coefficients a_p , b_p and c_p .

In the Figure 13 we show a screen shot where part of the results of this automatic calculations are shown for the same data of the example-measurement.

Microsoft Excel - Onormalization-050217-HC-N14-stat-p55-centered-01-to-take-examples.xls

DE Deutsch (Deutschland) | Drawing Paid |

File Edit View Insert Format Tools Data Window Help

Type a question for help

Arial 10 B I U

M34

A	B	C	D	E	F	G	H
time (ms)	U(time)	Frequency scale (Nu)	U(Nu)		Ch1 oa normalized to	U(Ch1 oa / Ch1 pred oa)	Freq. Steps
	ms	cm-1	cm-1		Ch1pred oa	0	cm-1
					- r -	- U(r) -	
242		242	242		0	0	24
2501		2501	2501		242	242	250
					2501	2501	
U(TL)	transformation limits (TL)	time segments (CELLS! >(+1)!!)		transforming equation:	Nuk = (mk/2)*t**2 + bkt + Nuok		
				transforming parameters and their uncertainties for each segment:			
ms	ms			k	(m k)/2	U(m k)/2	b k
0.00461834	0	from	to		cm-1/ms2	cm-1/ms3	cm-1/ms
0.004406293	35.86859513	242	897	0	0	0	0.0018009
0.004491847	41.62127414	898	1041	1	4.2427E-07	3.32246E-07	0.00177054
0.00453796	47.34173966	1042	1184	2	1.34751E-06	3.35077E-07	0.00169373
0.004582015	53.00854778	1185	1326	3	1.65846E-06	3.41159E-07	0.0016643
0.004770236	58.6425152	1327	1467	4	2.08758E-07	3.46602E-07	0.00181811
0.004667896	64.23425961	1468	1606	5	2.27611E-06	3.4961E-07	0.00157573
0.004755664	69.78958711	1607	1745	6	-1.335E-07	3.56964E-07	0.00188537
0.004734812	75.31994471	1746	1883	7	1.65868E-06	3.58501E-07	0.00163527
		1884	2501	8	0	0	0.00188518
control of interception points:							
TL	U(TL)	Nu	U(Nu)	eq. Number			
35.86859513	0.004406293	0.064598621	9.72456E-05	eq0			
35.86859513	0.004406293	0.064598621	9.78911E-05	eq1			
41.62127414	0.004491847	0.07497314	0.000178563	eq1			
41.62127414	0.004491847	0.07497314	0.000178932	eq2			
47.34173966	0.00453796	0.085347829	0.000247913	eq2			
47.34173966	0.00453796	0.085347829	0.000248189	eq3			
53.00854778	0.004582015	0.095722605	0.000315599	eq3			
53.00854778	0.004582015	0.095722605	0.000315824	eq4			
58.6425152	0.004770236	0.106097109	0.000384252	eq4			
58.6425152	0.004770236	0.106097109	0.000384453	eq5			
64.23425961	0.004667896	0.116472104	0.000453729	eq5			

Go to actualize segments in columns C and D!!!
(Already Automatic!!!)

pressure-2 / Herriott cell length / graphs 2 / frequency scale and relat- / time to fre

Ready Calculate

Figure 13. Screen shot of IPSIAM: Part of the automatic calculated coefficients and time limits Γ_p .

The equations that IPSIAM applies in calculating the means of the 24 coefficients were already presented in the sets of equations (134) and (136). We also mentioned that IPSIAM makes an automatic detection of all the observable maxima of the frequency marker signal with approximate determination of their positions, but we have not said yet how IPSIAM performs the accurate measurement of the 9 selected maxima positions Ψ_p and their uncertainty. This explanation is as follows:

IPSIAM performs a fit of second grade around each approximate maximum so that the best parabola that covers and reproduces the form of the tip of each maximum is found. To perform this calculation IPSIAM uses a set of shifted reference systems, so that the parameters of each parabola have a diagonal covariance matrix, i.e. we choose to calculate the coefficients over the system of reference that eliminates the internal correlation among the parameters (see section 2.4 for more detail about the fact that the total uncertainty of a quantity is independent of the system of reference, but how that total uncertainty is distributed in terms of the variances and covariances of the input sub-quantities depends on the selection of the system of reference for those sub-quantities). Calling m_{FMp2} , m_{FMp1} , and m_{FMp0} the parameters of the best fir parabola for the maximum p , we have:

$$I_{FMp} = m_{FMp2} \cdot t^2 + m_{FMp1} \cdot t + m_{FMp0} \quad (137)$$

And because of the symmetry of the parabola, its center is located on its maximum (or minimum) and maximizing the equation (137) gives us the desired position Ψ_p for the maximum p :

$$\Psi_p = \frac{-m_{FMp1}}{2 \cdot m_{FMp2}} \quad (138)$$

Given that the parameters of the parabola are uncorrelated, the standard uncertainty of the position of the maxima, $u[\Psi_p]$ is easy calculated as:

$$u[\Psi_p] = \Psi_p \cdot \left(\frac{s^2[m_{FMp1}]}{m_{FMp1}^2} + \frac{s^2[m_{FMp2}]}{m_{FMp2}^2} \right)^{\frac{1}{2}} \quad (139)$$

As we will see, we will need also the covariances $u[\Psi_p, \Psi_q]$ so that we also determined experimentally the correlation coefficients r for these pairs for a group of measurements (because in general $u[X Y] = R[X Y] \cdot u[X] u[Y]$). The data and results are presented in the Table 13. The result is applicable for all the measurements.

Table 13: Data and results for the experimental determination of $r[\Psi_p, \Psi_q]$

k	Ψ_0	Ψ_1	Ψ_2	Ψ_3	Ψ_4	Ψ_5	Ψ_6	Ψ_7	Ψ_8
1	30.22	36.65	42.91	49.19	55.47	61.57	67.77	73.91	79.92
2	30.43	36.90	43.19	49.51	55.75	62.03	68.22	74.22	80.51
3	31.07	37.48	43.83	50.06	56.31	62.50	68.62	74.73	80.79
4	31.12	37.50	43.86	50.13	56.34	62.60	68.69	74.79	80.85
5	29.97	36.36	42.70	48.97	55.16	61.39	67.50	73.55	79.67
6	29.90	36.24	42.64	48.82	55.03	61.28	67.39	73.56	79.62
$s(\Psi_p, \Psi_p)$	0.4864	0.4956	0.4966	0.5055	0.5122	0.5196	0.5128	0.5022	0.5096
$r(\Psi_p, \Psi_{p+1})$	0.9967	0.9957	0.9963	0.9984	0.9934	0.9967	0.9941	0.9840	
$r(\Psi_p, \Psi_{p+2})$	0.9991	0.9985	0.9936	0.9968	0.9941	0.9933	0.9953		
$r(\Psi_p, \Psi_{p+3})$	0.9961	0.9997	0.9923	0.9936	0.9965	0.9897			
$r(\Psi_p, \Psi_{p+4})$	0.9946	0.9925	0.9846	0.9946	0.9796				
$r(\Psi_p, \Psi_{p+5})$	0.9892	0.9916	0.9928	0.9794					
$r(\Psi_p, \Psi_{p+6})$	0.9825	0.9960	0.9685						
$r(\Psi_p, \Psi_{p+7})$	0.9927	0.9755							
$r(\Psi_p, \Psi_{p+8})$	0.9633								

All the correlations coefficients $R[\Psi_p, \Psi_q]$ were found as almost 1 (from 0.9633 to 0.9997) so that we made the slightly simplifying generalization:

$$\begin{aligned} R[\Psi_p, \Psi_q] &= 1 \\ u[\Psi_p, \Psi_q] &= u[\Psi_p] \cdot u[\Psi_q] \end{aligned} \quad (140)$$

Now that we have the variances of the 9 Ψ_p and their covariances, we can use them to calculate the variances and covariances of the 8 Γ_p and of the 24 coefficients of the set of equations (135), so that we could at last calculate the variances and covariances of the discretized wave-number points. Nevertheless it will prove to be more efficient to calculate the variances and covariances of the segments of integrated absorbance directly, as we will see in section 3.9. In that

moment we will need to make use of all the variances and covariances that we have calculated up to now, plus two more that are the last to discuss as part of this section. The other two input quantities needed to calculate the wave-numbers, for which we have not said nothing yet about their variances and covariances are the FRS, ΔF , and the discretized sampling of times, t .

The uncertainty of the FSR is presented together with the description of the FSR measurement in the following sub-section.

Given that the discretization of the time sampling was done with a 500 MHz oscilloscope and that we used a sample size of 2500 points and a sampling frequency of 10 Hz, the discrete time step of 40 μ s was big enough compared with the uncertainty of the sampling of less than 2 ns, (i.e. relative uncertainty of less than 0.005%). We considered this uncertainty as negligible and regarded the t inputs as exact.

3.8.1. Free Spectral Range Measurements

We performed the FSR measurement through the application of one of the programs of IPSIAM, which was optimized to measure the wave-number difference of two absorption peaks copied on the same scan. With this program we measured and processed a wave-number window which included the R32 and R33 lines of CO₂. Then we varied in IPSIAM the FSR input, until we obtained the reference value for the wave-number difference for these two lines. As reference value we use the calculated difference using the center of peaks data reported in HITRAN. The Figure 14 shows some of the cells of the corresponding IPSIAM program. Is important to note that this program performs exactly all the same operations as does the program used to measure line intensities or the one used to measure the partial pressures. The linearization of the wave number scale is exactly as accurate as explained above.

The measured values of the FSR are:

- For the Ge Etalon at 28°C: $\Delta F = 0.0443964 \text{ cm}^{-1}$
- For the Open Confocal Etalon: $\Delta F = 0.0103745 \text{ cm}^{-1}$

HITRAN:		Measured R33-R32 Wave-Number Difference:		5.1068144E-02		cm-1
Line1 Name	R32	R33-R32 Wave-Number Difference from HITRAN:		5.1068000E-02		cm-1
line1 center f	4987.617549					
Line2 Name	R33					
line2 center f	4987.668617					

Figure 14. Part of the IPSIAM program used to measure the FSR.

The standard uncertainty of the FSR $u[\Delta F]$ was dominated by the experimental standard deviation of the repeated measurements and, for all the etalons, it was found to be:

$$u[\Delta F] = 0.0015 \cdot \Delta F \quad (141)$$

The approach of referring our FSR to the wave-number difference of two absorption line centers reported in HITRAN (CO₂ R32 and R33 in this case) is very practical, as in the future all our results may be easily corrected if the HITRAN data are changed.

Table 14. Equipment dedicated to the measurement of the frequency marker signal.

Part	Manufacturer	Model	Serial Number	Range / FSR/ Responsivity	Gain / Resolution / u[FSR]	Data Sheet Number	Short name
Freq. Marker Signal Detector	Grasseby Infrared	IS-1.0	GIL-553-S-IS	(2 - 5.5) μm	3.61 A/W	IRA - 330	Detector-3
Freq. Marker Signal Preamplifier		PPA-15-IS	GILP-079-S-IS	--	--		Preamp-3
Low Noise Preamplifier	Stanford Research	SR560	01303	0.03 Hz - 1 MHz / (0 - 1) V	(0 - 90) dB	--	LNP
Function Generator	Hewlett Packard	3245A	2831A 01953	(0 - 100) kHz	0.001 Hz	--	FG
Germanium Etalon	Laser Photonics	--	--	0.044396 cm^{-1}	0.000067 cm^{-1}	--	Ge Etalon
Open Confocal Etalon	TU- Berlin	--	--	0.010375 cm^{-1}	0.000016 cm^{-1}	--	OCE

3.9. Integrated Absorbance Measurements

IPSIAM calculates the integrated absorbance twice, each time using a different method which corresponds to a different stage in the development of the calculation of its uncertainty. It is important to remind at this point that the GUM-compliant estimation of the uncertainty is an unavoidable requirement in order to claim traceability for the respective measurement.

From all the uncertainty determinations, the one for the integrated absorbance measurement was the most challenging. As far as we know this is the first time that an Integrated Absorbance has been measured with a GUM-compliant uncertainty. Furthermore the resulting values represent the smallest relative uncertainties published so far for this type of quantities, although it is actually difficult (if not impossible) to compare measurements if their respective uncertainties are not calculated under the same criteria.

The two methods mentioned in the first paragraph of this section deliver the same result for the mean of the integrated absorbance. For the first one we have calculated two uncertainty limits (one under-estimated and one over-estimated), neither of them taking care of covariances and therefore neither of them having confidence levels known; so they are not GUM-compliant. For the second one we have made a fully GUM-compliant uncertainty determination. This GUM-compliant determination takes into account, on the one hand, all the possible correlations of each discretized wave-number point with all the other discretized wave-number points (they are correlated because the time-to-wave-number transformation functions were calculated using the same etalon, because they share some or all the parameters of their respective equations and because those parameters were calculated based on the etalon maxima position Ψ which are all 100% correlated with each other). On the other hand, it calculates two limiting cases for the correlations between the absorbance measurements (the absorbance measurements are correlated because they have the same form-function and the other input quantities of the Beer-Lambert law in common, therefore their relative sizes (and changes in sizes) are not independent, or in other words, they have some degree of correlation). The lower limit of the correlation between the absorbances is found assuming that the correlation matrix is the diagonal identity (i.e. correlations taken as zero for different absorbances). The upper limit is found assuming that each absorbance is fully positively correlated with all the others (i.e. the correlation matrix has a “1” in all its entries). In the last step we use the GUM-compliant lower-limit uncertainty and the GUM-compliant upper-limit uncertainty to combine them according to GUM criteria; so that we are able to calculate a final, unique, well-defined, GUM-compliant uncertainty. Of course, when several scans are combined to give an average scan, it is also possible to calculate rigorously the 2500x2500 experimental covariance matrix for the discretized absorbance points, but this approach is not applicable for measurements made with only one scan, and it would imply also the processing of less averaged scans, as for each averaged scan it would have been necessary to process also the individual scans that made up the averaged one, and

therefore the time required in processing the data would be so long that less data could have been processed during this research. Given that we wanted to combine our individual Line Intensity (or partial pressure) measurements in order to analyze them in the framework of linear analysis (for the reasons given in section 2.6), it was desirable to have as much measurements as possible so that the regressions or functional-structural analysis could be fed with as much data pairs as possible. That's why we did not implement the more rigorous approach to the determination of the absorbance's covariance.

Now let's see the formulae used by IPSIAM to calculate the two versions of the integrated absorbance and their respective uncertainties.

The first version to calculate the integrated absorbance, A_{abs} is

$$A_{abs} = \sum_{j=N_{ini}}^{N_{end}-1} \alpha_{kj} \cdot \Delta \nu_j ; \quad (142)$$

where

$$\Delta \nu_j = \nu_{j+1} - \nu_j . \quad (143)$$

N_{ini} and N_{end} are respectively the initial and final discretization-label numbers of the total wave-number segment to be integrated. This two numbers are chosen by the operator as part of the decisions that have to be made during the application of IPSIAM. A typical value for N_{ini} is 625 and for N_{end} is 2075. Furthermore, α_{kj} is given by the equation (121) in page 77. In that equation the label j was suppressed for simplicity, because we were talking about a unique wave-number ν_j without sweeping j , but now that we consider all the different values for j , we will write down the equations with j explicit in the variables that should carry it, as shown next:

$$\alpha_{kj} = -\ln\{t_{rkj}\} \quad (144)$$

$$t_{rkj} = \frac{I_{Dkj} - \xi}{I_{D\Theta kj} - \xi} \quad (145)$$

ν_j is given by the equation (135) in page 84. We write down that equation now also with the label j explicit, but without the label p because p takes successively all its values from 1 to 9 (each value only for its corresponding segment) as j is swept, therefore it passes through the 9 segments,

$$\nu_j(t_j) = \frac{a_p}{2} \cdot (t_j^2 - \Gamma_{p-1}^2) + b_p \cdot (t_j - \Gamma_{p-1}) + c_p , \quad (146)$$

where

$$1 \leq p \leq 9 ,$$

and the label p takes its following value when t_j enters the following segment,

$$\Gamma_{p-1} \leq t_j < \Gamma_p ,$$

as j is swept through its consecutive values:

$$N_{ini} \leq j \leq N_{end} - 1 .$$

The following figures illustrate the reasons for some of the other decisions made for the selection of the numerical integration method and its corresponding equations. The Figure 15 presents an absorbance vs. wave-number curve. The bars for the standard uncertainties at both axes are no visible since they are quite small compared with the size of the symbols. For this reason the standard uncertainty for each axis is presented in the following two figures (Figure 16 and Figure 17). Figure 18 presents the standard uncertainty of the wave-number difference Δv_j . Figure 19 presents a zoom where the rectangular areas implied by the equation (142) can be visualized. These rectangular areas are added up to give the total area under the curve. Figure 20 presents the same data pairs zoomed as before, but instead of showing the rectangles, now the standard uncertainties of the absorbance α_{kj} and of the wave-number difference Δv_j are also included, but the uncertainty of the wave-number difference is not observable at this scale.

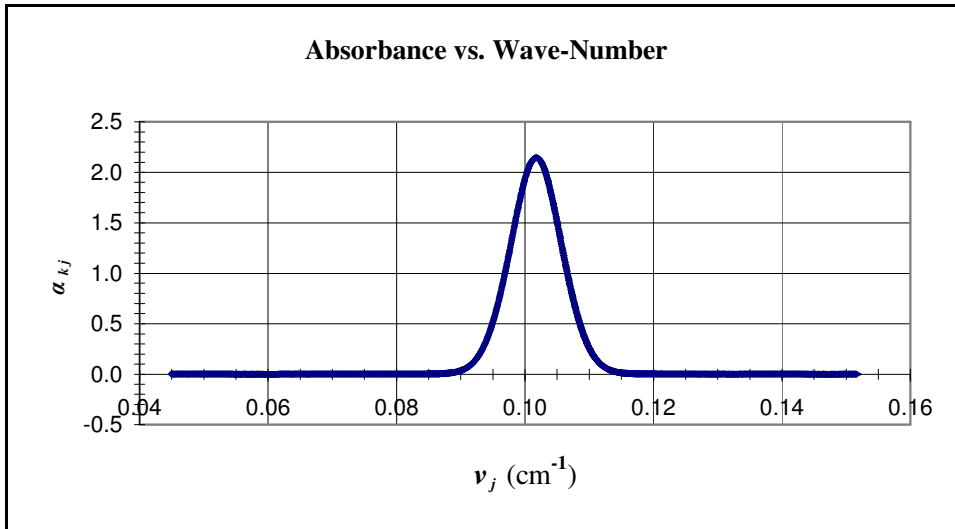


Figure 15. Example-measurement: Absorbance vs. wave-number.

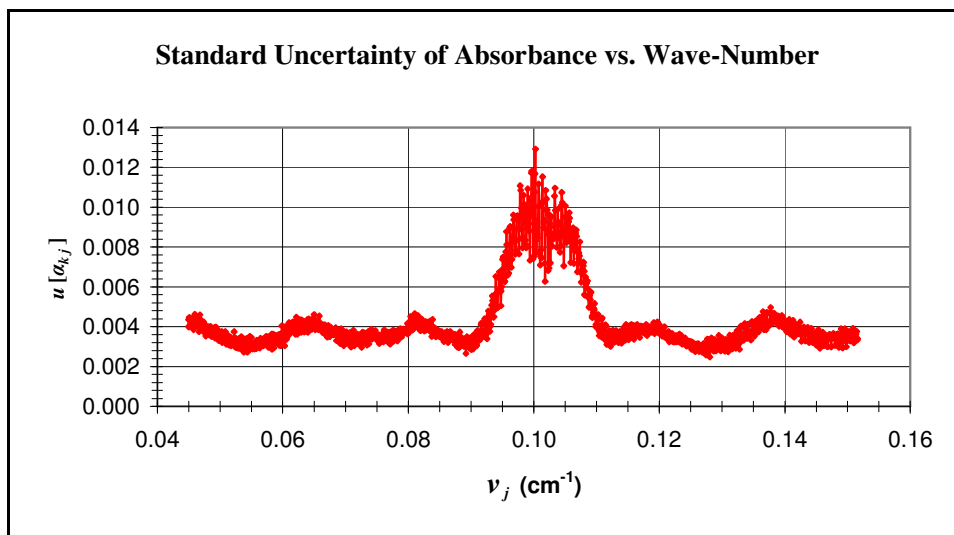


Figure 16. Example-measurement: Uncertainty of absorbance vs. wave number.

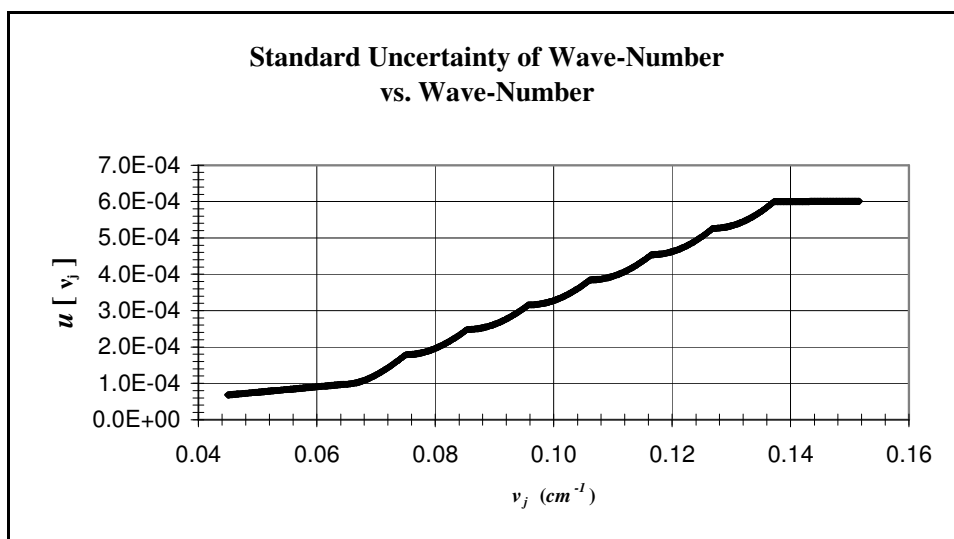


Figure 17. Example-measurement: Standard uncertainty of wave-number vs. wave number.

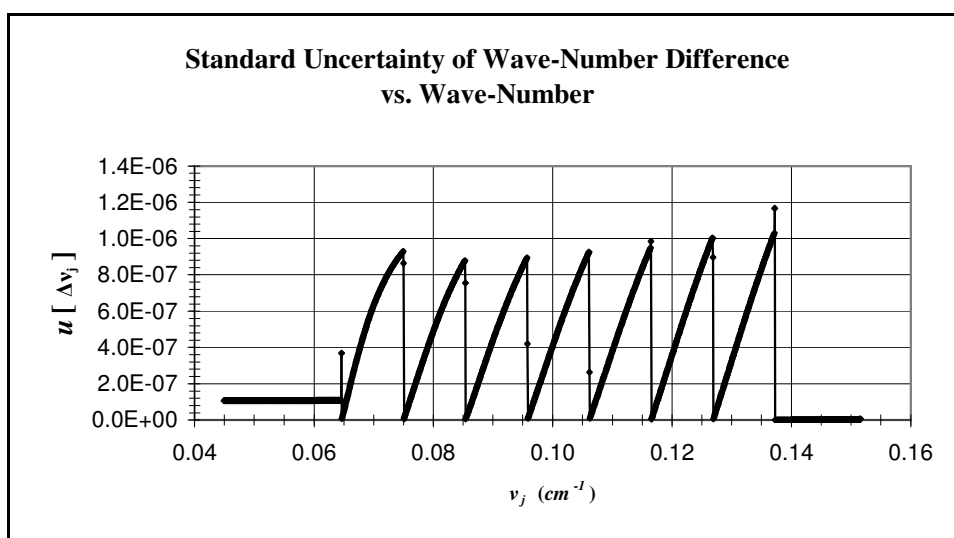


Figure 18. Example-measurement: Standard uncertainty of wave-number difference vs. wave-number.

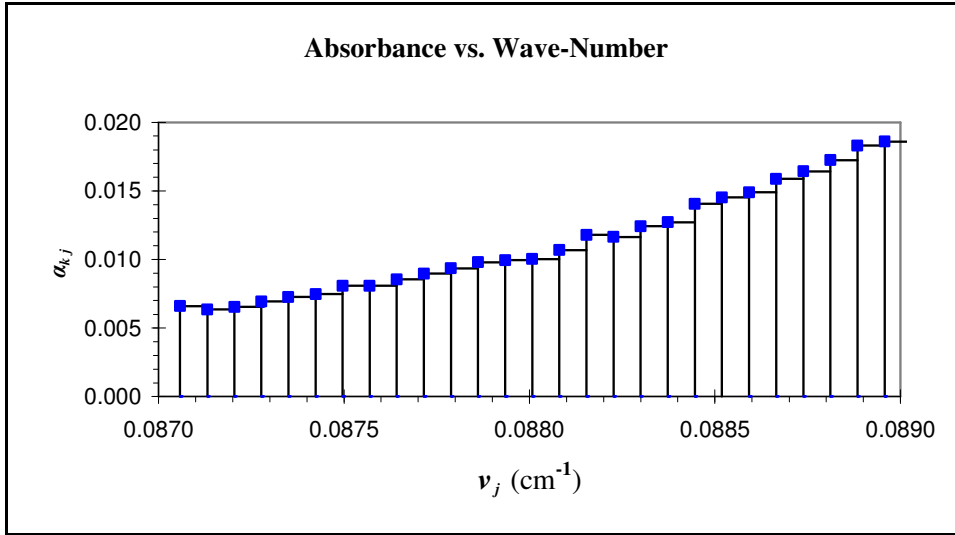


Figure 19. Example-measurement: Absorbance vs. wave-number. Zoom around 0.088 cm⁻¹ and integrating rectangles.

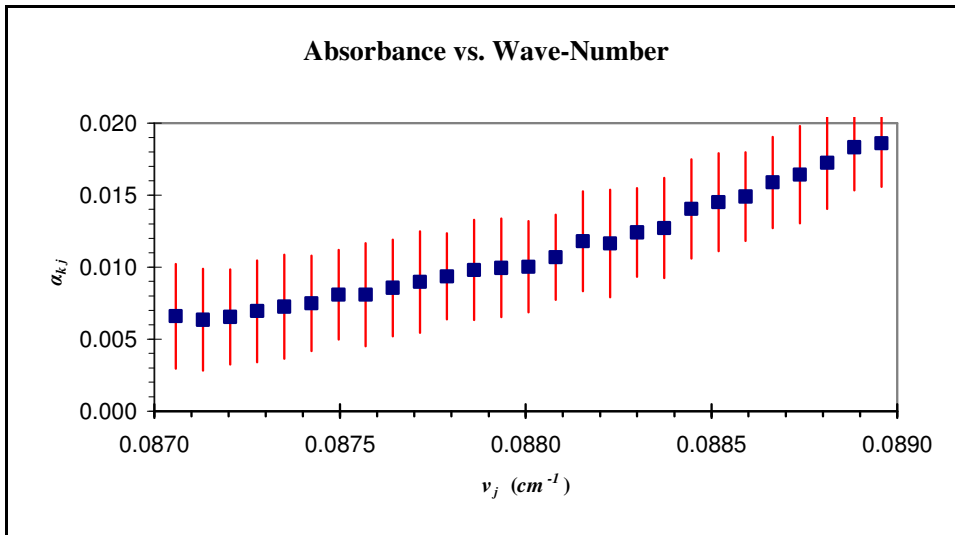


Figure 20. Example-measurement: Absorbance vs. wave-number. Zoom around 0.088 cm⁻¹ and standard uncertainty bars.

The Figure 19 and Figure 20 show clearly why we took only rectangular forms to cover the area from point to point: For the small-slope sectors of the curve the uncertainty of the absorbance is bigger than the change in absorbance from one point to the next, making it improper to follow the form of the curve by e.g. trapezoids. In addition, because of the symmetry of the curve, the small negative error produced by the rectangular steps in the positive-slope sector is compensated by the small positive error produced by the rectangular steps in the negative-slope sector of the curve.

Now let's present how we calculated the two non-GUM-conformal estimations of the uncertainty of the integrated absorbance A_{abs} .

The under-estimated limit was calculated assuming total independency of all the wave-number differences and absorbances, thus:

$$u[A_{abs}]_{under} = \left(\sum_{j=N_{ini}}^{N_{end}-1} \left((\alpha_j \cdot u[\Delta v_j])^2 + (\Delta v_j \cdot u[\alpha_j])^2 \right) \right)^{\frac{1}{2}} \quad (147)$$

The over-estimated limit was calculated using a formula derived from the analogy of the uncertainty of the area of a rectangle:

$$u[A_{abs}]_{over} = \left(\left(\sum_{j=N_{ini}}^{N_{end}-1} (\alpha_j \cdot u[\Delta v_j]) \right)^2 + \left(\sum_{j=N_{ini}}^{N_{end}-1} (\Delta v_j \cdot u[\alpha_j]) \right)^2 \right)^{\frac{1}{2}} \quad (148)$$

The hyphen across the u indicates that these uncertainties do not conform the GUM criteria.

For the example-measurement we found:

- $A_{abs} = 2.142 \cdot 10^{-2} \text{ cm}^{-1}$
- $u[A_{abs}]_{under} = 1.8 \cdot 10^{-5} \text{ cm}^{-1} \text{ (0.08\%)}$
- $u[A_{abs}]_{over} = 4.8 \cdot 10^{-4} \text{ cm}^{-1} \text{ (2.24\%)}$

We present next the second version of the calculation of the integrated absorbance and its (GUM-compliant) standard uncertainty. The majority of the algebraic calculations of this part of our work were done using Mathematica-4.0®.

For clarity let's recall the first version of the integrated absorbance equation:

$$A_{abs} = \sum_{j=N_{ini}}^{N_{end}-1} \alpha_{kj} \cdot \Delta v_j \quad (142)$$

We see that A_{abs} has $2 \cdot (N_{end} - N_{ini})$ input quantities: $(N_{end} - N_{ini})$ for α_k and $(N_{end} - N_{ini})$ for Δv . The easiest way to write down the GUM-compliant formula for its standard uncertainty is with help of an accessory vector $X(i)$, of length $2 \cdot N_{tot} = 2 \cdot (N_{end} - N_{ini})$, and the matrix $uXX(i,j)$, of size $2 \cdot N_{tot} \times 2 \cdot N_{tot}$. The first N_{tot} elements of the vector X are the α_k , the second N_{tot} elements of the vector X are the Δv , and the elements of the uXX matrix are the corresponding covariances among the elements of the vector X (i.e. the element $uXX(i,j)$ contains the covariance of the elements $X(i)$ and $X(j)$). Now the standard uncertainty of A_{abs} is found after solving the following equation:

$$u^2[A_{abs}] = \sum_{i=1}^{2 \cdot N_{tot}} \sum_{j=1}^{2 \cdot N_{tot}} \left(\frac{\partial A_{abs}}{\partial X(i)} \right) \cdot \left(\frac{\partial A_{abs}}{\partial X(j)} \right) \cdot uXX(i, j) \quad (149)$$

As we explained it in the third paragraph at the beginning of this section, the experimental determination of the elements of the uXX matrix would require too much effort and computational time for a practical implementation of the primary-standard. So, we decided to try an analytical-numerical implementation of the equation (149) that could be directly applied in our IPSIAM and also that could be equally valid for both: individual scans and averages of grouped scans.

The main difficulty with the analytical-numerical implementation of the equation (149) is of course the determination of the uXX matrix. This problem can be divided in three main problems:

- the determination of the $u(\alpha_i, \alpha_j)$ covariances,
- the determination of the $u(\alpha_i, \Delta v_j)$ covariances, and
- the determination of the $u(\Delta v_i, \Delta v_j)$ covariances.

Note that we have dropped the label k from the α_{kj} because we will not need it for the rest of this discussion. The analytical determination of the $u(\alpha_i, \alpha_j)$ covariances is not possible because it would require the exact knowledge of the absorption form-function F_f , among other things. However it is possible to make some general observations about the correlation matrix $R(\alpha_i, \alpha_j)$ on this regard, which is useful given that $u(\alpha_i, \alpha_j) = R(\alpha_i, \alpha_j) \cdot u(\alpha_i) \cdot u(\alpha_j)$. For instance the $R(\alpha_i, \alpha_j)$ terms are zero over the wings of the absorption curve, where no more absorption takes place (i.e. $u(\alpha_i, \alpha_j) = 0$ where $\alpha_i, \approx \alpha_j \approx 0$). Furthermore it is easy to see that the $R(\alpha_i, \alpha_j)$ terms are close to one for those absorbances which are located either very close together or symmetrically positioned, at equal distances of the center of the absorption peak (i.e. $u(\alpha_i, \alpha_j) = u(\alpha_i) \cdot u(\alpha_j)$ where $\alpha_i, \approx \alpha_j \neq 0$). And finally we can see that in any case the correlations are positive, i.e. $0 \leq R(\alpha_i, \alpha_j) \leq 1$, because the absorbance vs. wave number curve is always positive bell-shaped and the increase (decrease) of one absorbance point (e.g. through increasing (decreasing) number of absorbing molecules) implies the increase (decrease) of all the other points on the curve (at different rates of course, except for the symmetrical pairs). Based on these considerations we have developed two formulae: one for the case $R(\alpha_i, \alpha_j) = \delta(i, j)$, which give us the GUM-compliant lower limit of $u(\alpha_i, \alpha_j)$, and another for the case $R(\alpha_i, \alpha_j) = 1$, which give us the GUM-compliant upper limit of $u(\alpha_i, \alpha_j)$.

Although the absorbances α_i are clearly correlated with the wave-numbers v_j through the Lambert-Beer law, they are poorly correlated with the wave-number differences Δv_j so for this work we have assumed $u(\alpha_i, \Delta v_j) = 0$.

The $u(\Delta v_i, \Delta v_j)$ covariances have their origin in the common input quantities that those two differences may share. It is very difficult to write down a general formula for the covariance of two arbitrary wave-number differences, as the amount of shared input quantities depends on the relative “distance” in wave-numbers between the difference Δv_i and the difference Δv_j . For instance if both differences belong to the same segment p then they were calculated with exactly the same coefficients a_p, b_p , and c_p ; but if they belong to different segments then they were calculated using different sets of coefficients. In order to overcome this difficulty we decided to apply a hierarchical solution where the variation from segment to segment could be accounted for. To this end, we broke down the total area A_{abs} as the sum of the areas under different segments in the first place:

$$A_{abs} = \sum_{p=1}^9 A_p , \quad (150)$$

where the area of each segment is given by:

$$A_p = \sum_{j=N_{p-1}}^{N_p-1} \alpha_j \cdot \Delta v_j . \quad (151)$$

In this way we simplify the calculation of the uncertainty of the integrated absorbance through separation in different stages, where in the last stage the solution is found according to GUM with

$$u^2[A_{abs}] = \sum_{p=1}^9 \sum_{q=1}^9 \left(\frac{\partial A_{abs}}{\partial A_p} \right) \cdot \left(\frac{\partial A_{abs}}{\partial A_q} \right) \cdot u[A_p, A_q] , \quad (152)$$

which can be simplified to

$$u^2[A_{abs}] = \sum_{p=1}^9 u^2[A_p] + 2 \cdot \sum_{q=1}^8 \sum_{p=1}^{9-q} u[A_p, A_{p+q}] . \quad (153)$$

The elements of the right hand side of the equation (153) are the elements which must be calculated in the first stage: We substitute in the equation (151) the Δv_j recursively by their input quantities and their expressions; i.e. we substitute Δv_j by the right hand side (r.h.s.) of equation (143), then v_j and v_{j+1} with the corresponding r.h.s. of equation (146), then the coefficients a_p , b_p and c_p by the equations (134) and (136), then the Γ by the equation (130) and the ϑ by the equation (131). After these substitutions we have an expression which is written explicitly in terms of ΔF and the α , s , and Ψ input quantities, as follows:

$$A_p = \sum_{j=N_{p-1}}^{N_p-1} \alpha_j \cdot \Delta F \cdot \Delta t \cdot \left(\frac{\Psi_{p-2}^2 - 2 \cdot \Psi_{p-1}^2 + \Psi_p^2 + (2 \cdot \Psi_{p-1} - \Psi_p - \Psi_{p-2}) \cdot (t_j + t_{j+1})}{(\Psi_{p-2} - \Psi_{p-1}) \cdot (\Psi_{p-2} - \Psi_p) \cdot (\Psi_{p-1} - \Psi_p)} \right) \quad (154)$$

For simplification we define three functions of the Ψ :

$$\Omega_p = \Psi_{p-2}^2 - 2 \cdot \Psi_{p-1}^2 + \Psi_p^2 , \quad (155)$$

$$\Xi_p = 2 \cdot \Psi_{p-1} - \Psi_p - \Psi_{p-2} , \quad (156)$$

$$\Pi_p = (\Psi_{p-2} - \Psi_{p-1}) \cdot (\Psi_{p-2} - \Psi_p) \cdot (\Psi_{p-1} - \Psi_p) . \quad (157)$$

With these function, the equation (154) can be written as

$$A_p = \frac{\Delta F \cdot \Delta t}{\Pi_p} (\Omega_p \cdot Q_p + \Xi_p \cdot Z_p) , \quad (158)$$

where Q_p and Z_p include the terms with the sums

$$Q_p = \sum_{j=N_{p-1}}^{N_p-1} \alpha_j , \quad (159)$$

$$Z_p = \sum_{j=N_{p-1}}^{N_p-1} \alpha_j \cdot (t_j + t_{j+1}) . \quad (160)$$

The equations from (154) to (160) are well defined for $1 < p < 9$. In order to apply these formulae also to the segments $p = 1$ and $p = 9$, we define two extra Ψ as follows:

- $\Psi_{-1} = \Psi_0 - (\Psi_1 - \Psi_0) = 2 \cdot \Psi_0 - \Psi_1$,
- $u[\Psi_{-1}] = (u[\Psi_1] + u[\Psi_0])/2$,
- $\Psi_9 = \Psi_8 + (\Psi_8 - \Psi_7) = 2 \cdot \Psi_8 - \Psi_7$,
- $u[\Psi_9] = (u[\Psi_7] + u[\Psi_8])/2$.

Doing so, the formulae above give the correct results consistent with the equations (134) and the explanations given between the equations (134) and (135), on page 84.

Now we can use our accessory vector $X(i)$, of length 11 this time, charged with the input quantities of equation (158) as follows (as a remainder, we do not include Δt because for practical purposes this is an exactly known constant):

$$\begin{aligned}
 X(1) &= \Delta F \\
 X(2) &= \Omega_p \\
 X(3) &= \Xi_p \\
 X(4) &= \Pi_p \\
 X(5) &= Q_p \\
 X(6) &= Z_p \\
 X(7) &= \Omega_L \\
 X(8) &= \Xi_L \\
 X(9) &= \Pi_L \\
 X(10) &= Q_L \\
 X(11) &= Z_L
 \end{aligned} \tag{ 161 }$$

From these input quantities we know already that ΔF is completely independent from all the other quantities, the Ω , Ξ , and Π are correlated among them through the Ψ , but independent from the Q and the Z . In turn the Q and Z are correlated through the α . Taking all this in account we see that the corresponding 11×11 $uXX(i,j)$ matrix has the form:

$$uXX = \begin{pmatrix} u^2[\Delta F] & 0 & 0 & 0 & 0 & 0 & 0 & 0 & 0 & 0 & 0 \\ 0 & u^2[\Omega_p] & u[\Omega_p, \Xi_p] & u[\Omega_p, \Pi_p] & 0 & 0 & u[\Omega_p, \Omega_L] & u[\Omega_p, \Xi_L] & u[\Omega_p, \Pi_L] & 0 & 0 \\ 0 & u[\Omega_p, \Xi_p] & u^2[\Xi_p] & u[\Xi_p, \Pi_p] & 0 & 0 & u[\Xi_p, \Omega_L] & u^2[\Xi_p] & u[\Xi_p, \Pi_L] & 0 & 0 \\ 0 & u[\Omega_p, \Pi_p] & u[\Xi_p, \Pi_p] & u^2[\Pi_p] & 0 & 0 & u[\Pi_p, \Omega_L] & u[\Pi_p, \Xi_L] & u[\Pi_p, \Pi_L] & 0 & 0 \\ 0 & 0 & 0 & 0 & u^2[Q_p] & u[Q_p, Z_p] & 0 & 0 & 0 & u[Q_p, Q_L] & u[Q_p, Z_L] \\ 0 & 0 & 0 & 0 & u[Q_p, Z_p] & u^2[Z_p] & 0 & 0 & 0 & u[Q_p, Z_L] & u[Z_p, Z_L] \\ 0 & u[\Omega_p, \Omega_L] & u[\Xi_p, \Omega_L] & u[\Pi_p, \Omega_L] & 0 & 0 & u^2[\Omega_L] & u[\Omega_L, \Xi_L] & u[\Omega_L, \Pi_L] & 0 & 0 \\ 0 & u[\Omega_p, \Xi_L] & u^2[\Xi_L] & u[\Pi_p, \Xi_L] & 0 & 0 & u[\Omega_L, \Xi_L] & u^2[\Xi_L] & u[\Xi_L, \Pi_L] & 0 & 0 \\ 0 & u[\Omega_p, \Pi_L] & u[\Xi_p, \Pi_L] & u[\Pi_p, \Pi_L] & 0 & 0 & u[\Omega_L, \Pi_L] & u[\Xi_L, \Pi_L] & u^2[\Pi_L] & 0 & 0 \\ 0 & 0 & 0 & 0 & u[Q_p, Q_L] & u[Q_p, Z_L] & 0 & 0 & 0 & u^2[Q_L] & u[Q_L, Z_L] \\ 0 & 0 & 0 & 0 & u[Q_p, Z_L] & u[Z_p, Z_L] & 0 & 0 & 0 & u[Q_L, Z_L] & u^2[Z_L] \end{pmatrix} \tag{ 162 }$$

So, once the non-zero terms of the uXX matrix are known, we can calculate the variances and covariances of the equation (153) with the following equation:

$$u[A_p, A_L] = \sum_{i=1}^{11} \sum_{j=1}^{11} \left(\frac{\partial A_p}{\partial X(i)} \right) \cdot \left(\frac{\partial A_L}{\partial X(j)} \right) \cdot uXX(i, j) \tag{ 163 }$$

Now let's see how the elements of the uXX matrix were calculated. The $uXX(1,1)$ term was found as explained in section 3.8.1. The other terms of the uXX matrix (equation (162)) are calculated in 4 steps, as shown next. In the first and second steps we calculate the terms that depend on the Ω , Ξ or Π . In the third and fourth step we calculate the terms that depend on the Q and/or Z . Observe that now we are going to descend to the next level of the hierarchical approach, where the elements uXX are the targets (not the sources like in equation (163)). Therefore we need another accessory vector (W) and its covariance matrix (uWW). They will take the place of source in the equations type (163), which will be repeated several times because it is the general version of the formula of propagation of uncertainty (see section 2.4).

Step 1: The 9 terms of the square sub-matrix with diagonal $uXX(2,2)$ to $uXX(4,4)$ as well as the 9 terms of the square sub-matrix with diagonal $uXX(7,7)$ to $uXX(9,9)$ are calculated with the general formula of propagation of uncertainty. To this end we use another accessory vector $W(i)$ of length 3 and its corresponding 3x3 matrix $uWW(i,j)$. The elements of $W(i)$ are the input quantities of the Ω s, Ξ s and Π s. Observe that the Ω s, Ξ s and Π s belong all to the same label, either P (for the first sub-matrix) or L (for the second sub-matrix), so we will write down the formula using a general label M to denote any of the labels P or L . Observing the equations (155) to (157) we recall that Ω_M , Ξ_M and Π_M are all different functions of the same three input quantities, which we charge in the accessory vector $W(i)$:

$$\begin{aligned} W(1) &= \Psi_{M-2} \\ W(2) &= \Psi_{M-1} \\ W(3) &= \Psi_M \end{aligned} \quad (164)$$

To find the elements of the matrix $uWW(i,j)$, we recall that, based on the measurements summarized in the Table 13, we concluded that $r(\Psi_p, \Psi_q) \approx 1$ for all the labels p and q . Therefore:

$$uWW = \begin{pmatrix} u^2[\Psi_{M-2}] & u[\Psi_{M-2}]u[\Psi_{M-1}] & u[\Psi_{M-2}]u[\Psi_M] \\ u[\Psi_{M-2}]u[\Psi_{M-1}] & u^2[\Psi_{M-1}] & u[\Psi_{M-1}]u[\Psi_M] \\ u[\Psi_{M-2}]u[\Psi_M] & u[\Psi_{M-1}]u[\Psi_M] & u^2[\Psi_M] \end{pmatrix} \quad (165)$$

and the $u[\Psi_{M-j}]$ are given by the equation (139).

Now we can calculate the variances and covariances of the Ω , Ξ and Π with the general formula of propagation of uncertainty:

$$uXX(i, j) = \sum_{r=1}^3 \sum_{s=1}^3 \left(\frac{\partial X(i)}{\partial W(r)} \right) \cdot \left(\frac{\partial X(j)}{\partial W(s)} \right) \cdot uWW(r, s) \quad (166)$$

where the Ω , Ξ and Π are the elements of the vector X as defined by the equation (161) and the indexes i and j are restricted to the values 2 to 4 for the label P and 7 to 9 for the label L .

From the 18 elements calculated with the equation (166) (actually only 12 different elements were calculated because of the symmetry of the matrix) we will present next only the $uXX(2,2)$ and the $uXX(7,8)$ as example.

$$u_{XX}(2,2) = u^2[\Omega_P] = 4 \cdot (\Psi_P \cdot u[\Psi_P] - 2\Psi_{P-1} \cdot u[\Psi_{P-1}] + \Psi_{P-2} \cdot u[\Psi_{P-2}])^2 \quad (167)$$

$$u_{XX}(7,8) = u[\Omega_L, \Xi_L] = -2 \cdot \left(\frac{(u[\Psi_L] - 2 \cdot u[\Psi_{L-1}] + u[\Psi_{L-2}])}{(\Psi_L \cdot u[\Psi_L] - 2 \cdot \Psi_{L-1} \cdot u[\Psi_{L-1}] + \Psi_{L-2} \cdot u[\Psi_{L-2}])^{-1}} \right) \quad (168)$$

Step 2: The 9 terms of the square sub-matrix with diagonal $u_{XX}(2,7)$ to $u_{XX}(4,9)$ as well as the 9 terms of the square sub-matrix with diagonal $u_{XX}(7,2)$ to $u_{XX}(9,4)$ are calculated with the general formula of propagation of uncertainty. To this end we use an extended accessory vector $W(i)$ with elements given as explained next. For $i = 1$ to 3 we have an expression similar to equation (164), but the label is restricted only to P .

$$\begin{aligned} W(1) &= \Psi_{P-2} \\ W(2) &= \Psi_{P-1} \\ W(3) &= \Psi_P \end{aligned} \quad (169)$$

New elements are added as needed according to the following rules:

- $W(4) = \Psi_{P+1}$, if $L = P + 1$, plus
- $W(5) = \Psi_{P+2}$, if $L = P + 2$, plus
- $W(6) = \Psi_{P+3}$, if $L = P + 3$.

For $L = P + q$, with $q \leq 4 \leq 9$ the vector W has anyway only 6 elements, where the first three are steel given by the equation (169) and the last three are given by an equivalent equation as follows:

$$\begin{aligned} W(4) &= \Psi_{L-2} \\ W(5) &= \Psi_{L-1} \\ W(6) &= \Psi_L \end{aligned} \quad (170)$$

The corresponding matrix $u_{WW}(i,j)$ may be a 4x4, 5x5, or 6x6 matrix according to the length of $W(i)$. Observe that the Ω_P , Ξ_P and Π_P (i.e. the $X(i)$ for $2 \leq i \leq 4$) are all different functions of the same three input quantities Ψ_{P-2} , Ψ_{P-1} , and Ψ_P (i.e. the $W(i)$ for $1 \leq i \leq 3$). In turn, the Ω_L , Ξ_L and Π_L (i.e. the $X(i)$ for $7 \leq i \leq 9$) are all different functions of the same three input quantities Ψ_{L-2} , Ψ_{L-1} , and Ψ_L (i.e. the $W(i)$ for $4 \leq i \leq 6$). So the X_P may or may not have input quantities in common with the X_L but in any case all their input quantities are correlated with correlation coefficient $R = 1$ as found in the Table 13, so that according to equation (140) we have that $u_{WW}(i,j) = u[W(i)] \cdot u[W(j)]$. We call lw the length of the vector W (i.e. $4 \leq lw \leq 6$) and now we have all what we need to calculate the u_{XX} elements of this step with the general formula of propagation of uncertainty as follows:

$$u_{XX}(i,j) = \sum_{r=1}^{lw} \sum_{s=1}^{lw} \left(\frac{\partial X(i)}{\partial W(r)} \right) \cdot \left(\frac{\partial X(j)}{\partial W(s)} \right) \cdot u_{WW}(r,s) \quad (171)$$

Again we remind that only $2 \leq i \leq 4$ when $7 \leq j \leq 9$ and $7 \leq i \leq 9$ when $2 \leq j \leq 4$ are the cases covered in this step.

Given the high degree of correlation of the input quantities, all the results found for this step have the same form independently of the length of the vector W (i.e. independently of the sharing or not of input quantities) so we will present as example the terms $u_{XX}(2,7)$ and $u_{XX}(7,3)$ written in general with labels P and L , but some of the Ψ_P may be the same as the Ψ_L for the cases $L = P + 1$ and $L = P + 2$.

$$u_{XX}(2,7) = u[\Omega_P, \Omega_L] = 4 \cdot \left(\frac{(\Psi_P \cdot u[\Psi_P] - 2 \cdot \Psi_{P-1} \cdot u[\Psi_{P-1}] + \Psi_{P-2} \cdot u[\Psi_{P-2}])}{(\Psi_L \cdot u[\Psi_L] - 2 \cdot \Psi_{L-1} \cdot u[\Psi_{L-1}] + \Psi_{L-2} \cdot u[\Psi_{L-2}])^{-1}} \right) \quad (172)$$

$$u_{XX}(7,3) = u[\Omega_L, \Xi_P] = -2 \cdot \left(\frac{(u[\Psi_P] - 2 \cdot u[\Psi_{P-1}] + u[\Psi_{P-2}])}{(\Psi_L \cdot u[\Psi_L] - 2 \cdot \Psi_{L-1} \cdot u[\Psi_{L-1}] + \Psi_{L-2} \cdot u[\Psi_{L-2}])^{-1}} \right) \quad (173)$$

In the 3rd and 4th step we deal with the Q and Z , which have the α , and α and t , as input quantities. We do not include the $t_j + t_{j+1}$ input quantities in the vector W because, as already explained, these quantities are exactly known for our setup and practical purposes. The elements of the matrix u_{WW} are now the covariances among the absorbances α . For the reasons given above, in the paragraph dealing with absorbance covariances, in page 98, we have developed two formulae: one for the case $R(\alpha_i, \alpha_j) = \delta(i, j)$, which give us the GUM-compliant lower limit of $u(\alpha_i, \alpha_j)$, and another for the case $R(\alpha_i, \alpha_j) = 1$, which give us the GUM-compliant upper limit of $u(\alpha_i, \alpha_j)$, so for the two following steps or explanations we will have that:

- $u_{WW}(i,j)_{\min} = u[W(i)] \cdot u[W(j)] \cdot \delta(i, j)$
- $u_{WW}(i,j)_{\max} = u[W(i)] \cdot u[W(j)]$

We combine the results of both cases to calculate the final result, so both limits will be presented along for each part of the calculation.

Step 3: The 4 terms of the square sub-matrix with diagonal $u_{XX}(5,5)$ to $u_{XX}(6,6)$ as well as the 4 terms of the square sub-matrix with diagonal $u_{XX}(10,10)$ to $u_{XX}(11,11)$ are calculated with the general formula of propagation of uncertainty. To this end we use again the accessory vector $W(i)$, this time of length $(N_M - N_{M-1})$ and its corresponding $(N_M - N_{M-1}) \times (N_M - N_{M-1})$ matrix $u_{WW}(i,j)$. The elements of $W(i)$ are the absorbances α . Observe that the Q , and Z (i.e. the $X(i)$) belong all to the same label, either P (for the first sub-matrix, $5 \leq i \leq 6$) or L (for the second sub-matrix, $10 \leq i \leq 11$), so we will write down the formula using again a general label M to denote any of the labels P or L . The formula is then:

$$u_{XX}(i, j) = \sum_{r=1}^{N_M - N_{M-1}} \sum_{s=1}^{N_M - N_{M-1}} \left(\frac{\partial X(i)}{\partial W(r)} \right) \cdot \left(\frac{\partial X(j)}{\partial W(s)} \right) \cdot u_{WW}(r, s) \quad (174)$$

where i and j are restricted to take values from 5 to 6, for $M = P$; and from 10 to 11, for $M = L$. We have already all the information to solve the equation (174), and the results are presented next.

$$uXX(5,5)_{\min} = u^2 [Q_P]_{\min} = \sum_{i=1}^{N_P - N_{P-1}} u^2 [\alpha_{N_{P-1}+i-1}]$$

$$uXX(5,5)_{\max} = u^2 [Q_P]_{\max} = \left(\sum_{i=1}^{N_P - N_{P-1}} u [\alpha_{N_{P-1}+i-1}] \right)^2 \quad (175)$$

$$uXX(6,6)_{\min} = u^2 [Z_P]_{\min} = \sum_{i=1}^{N_P - N_{P-1}} (t_{N_{P-1}+i-1} + t_{N_{P-1}+i})^2 \cdot u^2 [\alpha_{N_{P-1}+i-1}]$$

$$uXX(6,6)_{\max} = u^2 [Z_P]_{\max} = \left(\sum_{i=1}^{N_P - N_{P-1}} (t_{N_{P-1}+i-1} + t_{N_{P-1}+i}) \cdot u [\alpha_{N_{P-1}+i-1}] \right)^2 \quad (176)$$

$$uXX(5,6)_{\min} = u [Q_P, Z_P]_{\min} = \sum_{i=1}^{N_P - N_{P-1}} (t_{N_{P-1}+i-1} + t_{N_{P-1}+i}) \cdot u^2 [\alpha_{N_{P-1}+i-1}]$$

$$uXX(5,6)_{\max} = u [Q_P, Z_P]_{\max} = \frac{\left(\sum_{i=1}^{N_P - N_{P-1}} u [\alpha_{N_{P-1}+i-1}] \right)}{\left(\sum_{j=1}^{N_P - N_{P-1}} (t_{N_{P-1}+j-1} + t_{N_{P-1}+j}) \cdot u [\alpha_{N_{P-1}+j-1}] \right)^{-1}} \quad (177)$$

The terms $uXX(10,10)$, $uXX(11,11)$ and $uXX(10,11)$ are given by the equivalent equations of sets (175), (176) and (177) respectively, but with label L instead of P .

Step 4: The 4 terms of the square sub-matrix with diagonal $uXX(5,10)$ to $uXX(6,11)$ as well as the 4 terms of the square sub-matrix with diagonal $uXX(10,5)$ to $uXX(11,6)$ are calculated with the general formula of propagation of uncertainty. To this end we use again the accessory vector $W(i)$, this time of length $\{(N_P - N_{P-1}) + (N_L - N_{L-1})\}$ and its corresponding $\{(N_P - N_{P-1}) + (N_L - N_{L-1})\} \times \{(N_P - N_{P-1}) + (N_L - N_{L-1})\}$ matrix $uWW(i,j)$. The elements of $W(i)$ are the absorbances α of the segment P , for the first $(N_P - N_{P-1})$ entries, and the absorbances α of the segment L , for the following $(N_L - N_{L-1})$ entries. Observe that for these elements of the matrix uXX the corresponding Q and Z (i.e. the $X(i)$) belong always to different labels, either P or L , so that they never have input quantities in common. Nevertheless all the groups of absorbances have some degree of correlation, from which we are calculating the two extreme cases. To simplify the notation we call again lw the length of the vector W . This time $lw = \{(N_P - N_{P-1}) + (N_L - N_{L-1})\}$. Now we can calculate these last elements of the uXX matrix, and the formula takes again the form:

$$uXX(i, j) = \sum_{r=1}^{lw} \sum_{s=1}^{lw} \left(\frac{\partial X(i)}{\partial W(r)} \right) \cdot \left(\frac{\partial X(j)}{\partial W(s)} \right) \cdot uWW(r, s) \quad (178)$$

where i and j must fulfill that only $5 \leq i \leq 6$ when $10 \leq j \leq 11$ and $10 \leq i \leq 11$ when $5 \leq j \leq 6$, so the solutions of equation (178) are as follows.

$$u_{XX}(5,10)_{\min} = u[Q_P, Q_L]_{\min} = 0 \quad (179)$$

$$u_{XX}(5,10)_{\max} = u[Q_P, Q_L]_{\max} = \left(\sum_{i=1}^{N_P - N_{P-1}} u[\alpha_{N_{P-1}+i-1}] \right) \cdot \left(\sum_{i=1}^{N_L - N_{L-1}} u[\alpha_{N_{L-1}+i-1}] \right)$$

$$u_{XX}(5,11)_{\min} = u[Q_P, Z_L]_{\min} = 0 \quad (180)$$

$$u_{XX}(5,11)_{\max} = u[Q_P, Z_L]_{\max} = \frac{\left(\sum_{i=1}^{N_P - N_{P-1}} u[\alpha_{N_{P-1}+i-1}] \right)}{\left(\sum_{i=1}^{N_L - N_{L-1}} (t_{N_{L-1}+i-1} + t_{N_{L-1}+i}) \cdot u[\alpha_{N_{L-1}+i-1}] \right)^{-1}}$$

$$u_{XX}(6,10)_{\min} = u[Z_P, Q_L]_{\min} = 0 \quad (181)$$

$$u_{XX}(6,10)_{\max} = u[Z_P, Q_L]_{\max} = \frac{\left(\sum_{i=1}^{N_L - N_{L-1}} u[\alpha_{N_{L-1}+i-1}] \right)}{\left(\sum_{i=1}^{N_P - N_{P-1}} (t_{N_{P-1}+i-1} + t_{N_{P-1}+i}) \cdot u[\alpha_{N_{P-1}+i-1}] \right)^{-1}}$$

$$u_{XX}(6,11)_{\min} = u[Z_P, Z_L]_{\min} = 0 \quad (182)$$

$$u_{XX}(6,11)_{\max} = u[Z_P, Z_L]_{\max} = \frac{\left(\sum_{i=1}^{N_P - N_{P-1}} (t_{N_{P-1}+i-1} + t_{N_{P-1}+i}) \cdot u[\alpha_{N_{P-1}+i-1}] \right)}{\left(\sum_{i=1}^{N_L - N_{L-1}} (t_{N_{L-1}+i-1} + t_{N_{L-1}+i}) \cdot u[\alpha_{N_{L-1}+i-1}] \right)^{-1}}$$

The other 4 terms have the same expressions because the symmetry of the covariance matrix, i.e. $u_{XX}(i,j) = u_{XX}(j,i)$.

At this point we have finished the description of the 4 steps to calculate the components of the u_{XX} matrix, so that now we are able to go up to the upper level of the hierarchical approach and

calculate the variances and covariances $u[A_p, A_q]$ as given by the equation (163), in page 100, but because we have two versions for some elements of the uXX matrix: $uXX(i,j)_{\min}$ and $uXX(i,j)_{\max}$, we have also the corresponding two versions of the segmented integrated area covariances: $u[A_p, A_q]_{\min}$ and $u[A_p, A_q]_{\max}$. With the known $u[A_p, A_q]_{\min}$ and $u[A_p, A_q]_{\max}$, we can calculate the two limits of the standard uncertainty of the integrated absorbance $u[A_{abs}]_{\min}$ and $u[A_{abs}]_{\max}$ using the equation (153).

According to the GUM, it is necessary to use all the information available in order to calculate properly the uncertainty of a given measurement. With this in mind, we recall from the statements made in the paragraph dealing with the absorbance covariances, on page 98, that $u(\alpha_i, \alpha_j) = u^2[\alpha_i] \cdot \delta_{ij}$ where $\alpha_i, \approx \alpha_j \approx 0$. Therefore only for the segments with appreciable absorbance it makes sense to consider the two limits of the variances and covariances, while for the segments clearly positioned over the wings it only makes sense to consider their minimal variances and covariances, because over the wings $\alpha_i, \approx \alpha_j \approx 0$, and therefore $u(\alpha_i, \alpha_j) = u^2[\alpha_i] \cdot \delta_{ij}$, which is the condition for the minimal version of the variances and covariances. Comparing the Figure 15 with the Figure 17 or Figure 18 we see that only the segments 4, 5 and 6 have appreciable absorbance, while the segments 1, 2 and 3 are mainly positioned over the left wing of the absorption peak and the segments 7, 8 and 9 are mainly positioned over the right wing of the absorption peak. For this reason it does not make sense to use the pure $u[A_{abs}]_{\max}$ calculated with full absorbance correlation over all the segments, but we need to define an upper limit for the integrated absorbance area which is calculated with full correlation only for the absorbances of segments 4, 5 and 6. Doing so, we found the next formulae for the lower and upper limit of the integrated absorbance area.

$$u[A_{abs}]_{lower} = u[A_{abs}]_{\min} \quad (183)$$

$$u[A_{abs}]_{upper} = \left(u^2[A_{abs}]_{\min} - \sum_{P=4}^6 u^2[A_P]_{\min} - \sum_{P=4}^5 u[A_P, A_{P+1}]_{\min} - u[A_4, A_6]_{\min} + \sum_{P=4}^6 u^2[A_P]_{\max} + \sum_{P=4}^5 u[A_P, A_{P+1}]_{\max} + u[A_4, A_6]_{\max} \right)^{\frac{1}{2}} \quad (184)$$

Finally we combine the results of the lower and upper limits to calculate the standard uncertainty of the integrated absorbance. We know that the final result lies somewhere between the lower and upper limit. Furthermore we know that the probability for the final result to be equal to the lower limit is zero, as we can not neglect the correlations among the appreciable absorbances in segments 4, 5 and 6 (and these correlations were neglected in the lower limit case). Similarly, we know that the probability for the final result to be equal to the upper limit is zero, as we know that not all the correlations among the appreciable absorbances can be exactly 1, but most of them have an intermediate value between 0 and 1. Using all this information we calculate a component of the uncertainty which covers the gap between the lower and upper limit using a symmetric trapezoidal

probability distribution (having equal sloping sides) and a top chosen ad-hoc to be 90% of the base.

So we resume the known facts, that:

- the probability to find the final result anywhere between the given limits is one,
- the probability to find the final result close to the limits (95% close in this case) is small,
- the probability to find the final result exactly on the given limits is zero, and
- we do not have more information about the probability distribution of the final result, so we assume a flat distribution for the 90% of the values between the limits.

According to GUM, the standard uncertainty $u[x]$ of a quantity x having estimated bounds a_- to a_+ and a symmetric trapezoidal distribution, a base of width $a_+ - a_- = 2 \cdot a$ and a top of width $2 \cdot a \cdot \beta$ is given by (see GUM section 4.3.9):

$$u[x] = \left(\frac{a^2 \cdot (1 + \beta^2)}{6} \right)^{\frac{1}{2}} \quad (185)$$

So in our case, we have $\beta = 0.9$ and $a = (u[A_{abs}]_{upper} - u[A_{abs}]_{lower})$. Furthermore we treat this component as fully correlated with the lower limit component, so the final result is:

$$u[A_{abs}] = u[A_{abs}]_{lower} + \left(\frac{(u[A_{abs}]_{upper} - u[A_{abs}]_{lower})^2 \cdot (1 + 0.9^2)}{6} \right)^{\frac{1}{2}}, \quad (186)$$

which can be simplified to

$$u[A_{abs}] = 0.45 \cdot u[A_{abs}]_{lower} + 0.55 \cdot u[A_{abs}]_{upper}. \quad (187)$$

With the equation (187) we have finally reached two of our goals:

- to calculate the standard uncertainty of the integrated absorbance in full agreement with GUM, and
- to optimize our result according to the computational resources and practical needs.

As example of the implementation, we present next the numerical results $u[A_{abs}]_{lower}$, $u[A_{abs}]_{upper}$, and $u[A_{abs}]$ for the example-measurement:

- $A_{abs} = 2.142 \cdot 10^{-2} \text{ cm}^{-1}$
- $u[A_{abs}]_{lower} = 3.47 \cdot 10^{-5} \text{ cm}^{-1}$ (0.16%)
- $u[A_{abs}]_{upper} = 1.87 \cdot 10^{-4} \text{ cm}^{-1}$ (0.88%)
- $u[A_{abs}] = 1.19 \cdot 10^{-4} \text{ cm}^{-1}$ (0.55%)

IPSIAM calculated these results using exactly the formulae presented above. In the following figures we present screen shots of some parts of IPSIAM where these calculations are implemented.

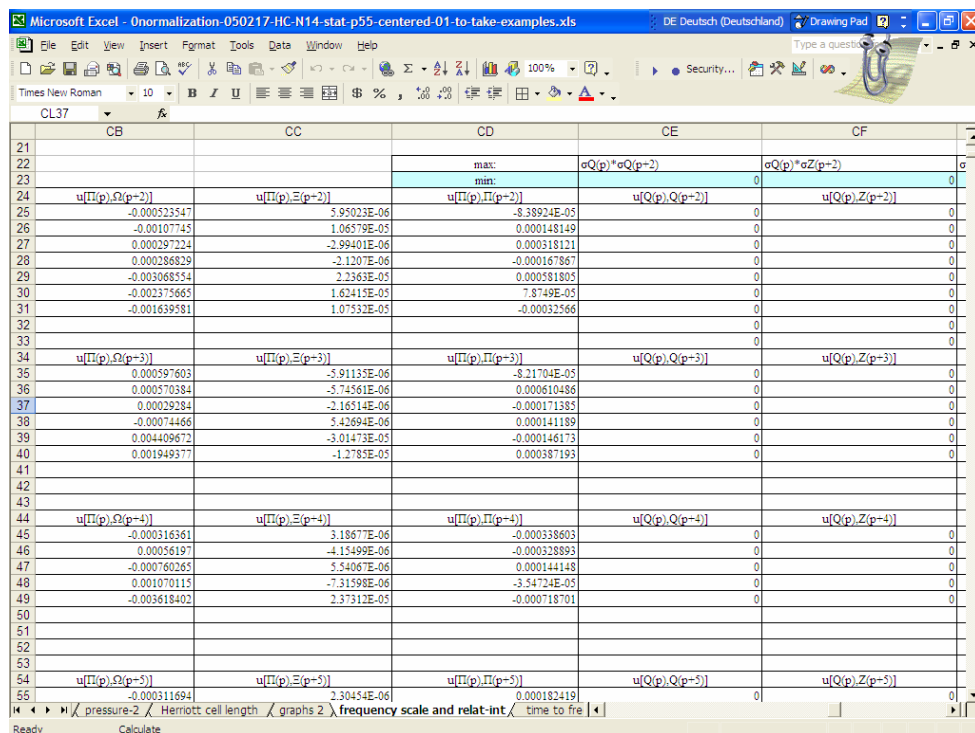


Figure 21. IPSIAM screen shot: Part of the calculation of $u[A_{abs}]$.

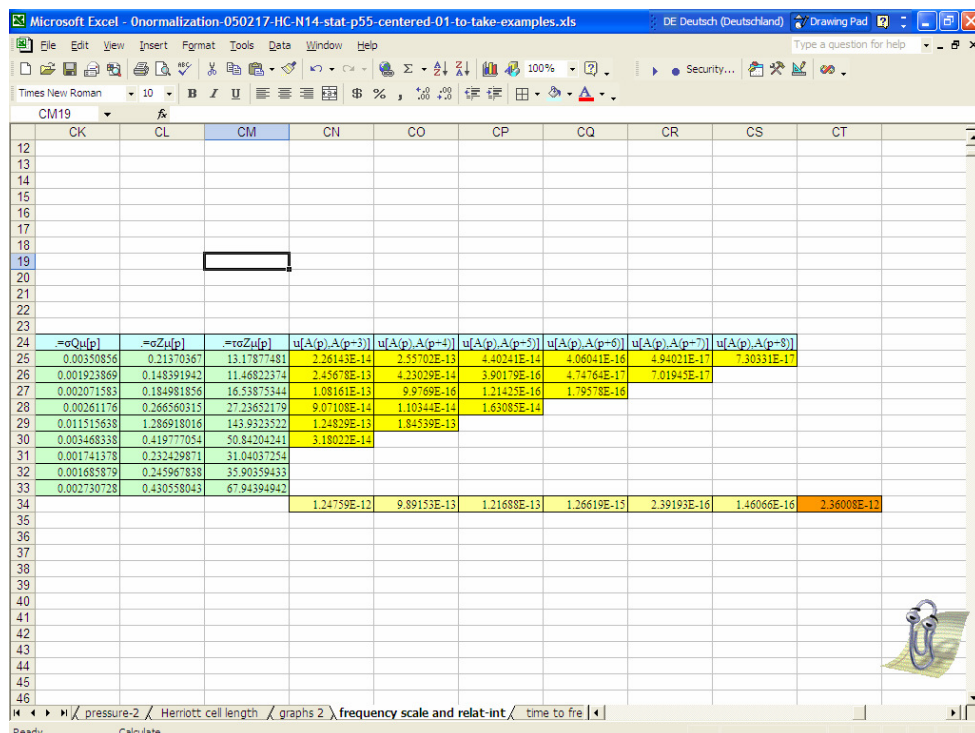


Figure 22. IPSIAM screen shot: Part of the calculation of $u[A_{abs}]$.

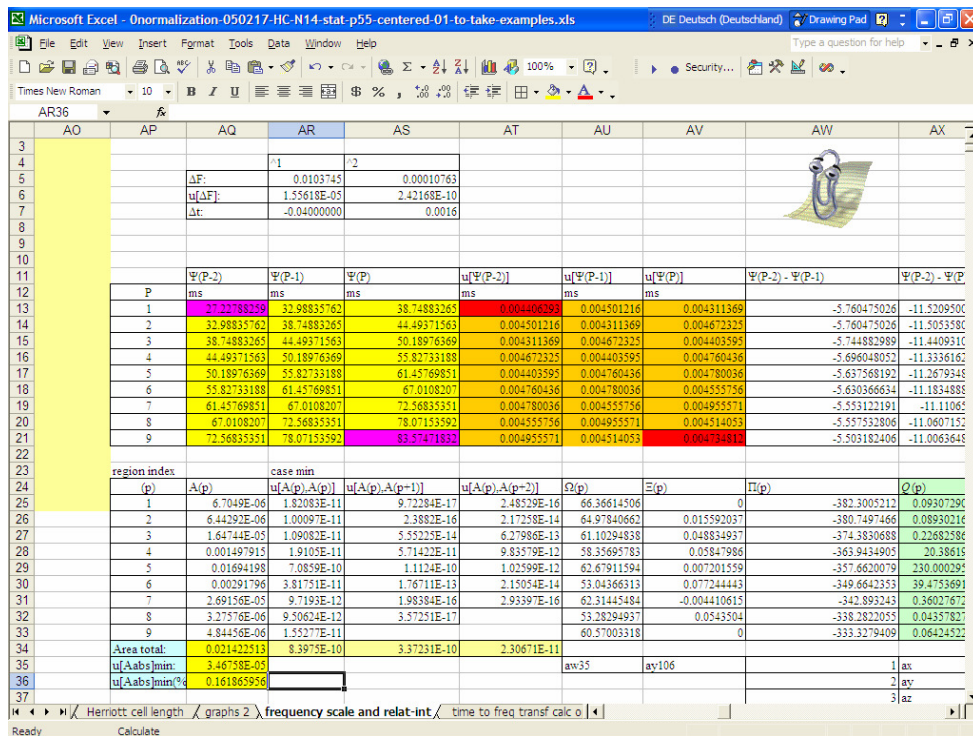


Figure 23. IPSIAM screen shot: Part of the calculation of $u[A_{abs}]$.

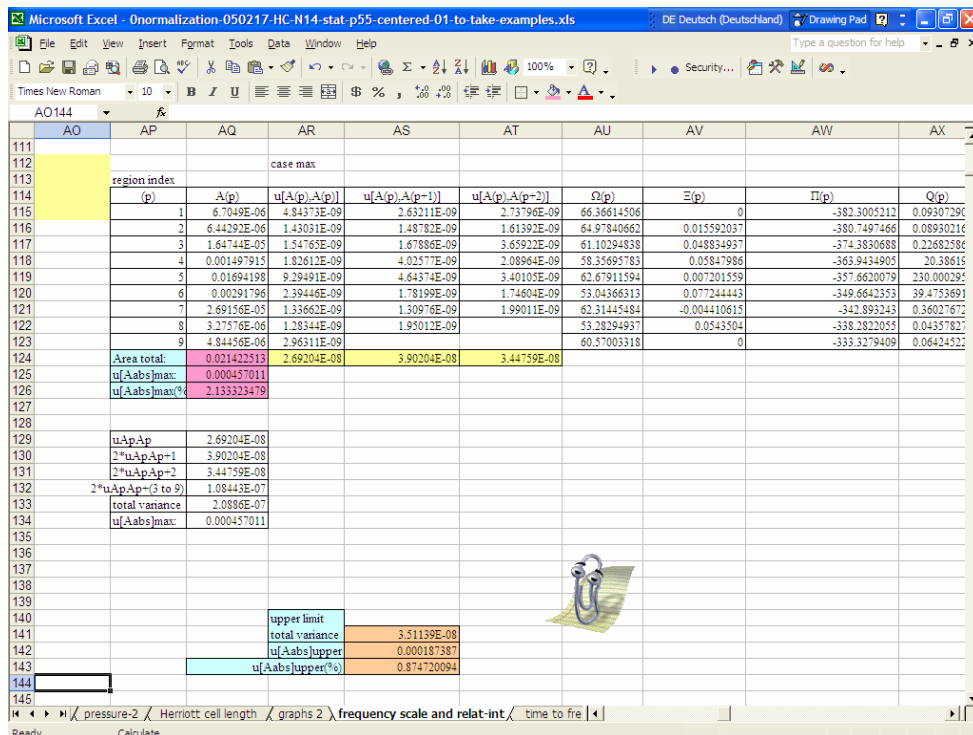


Figure 24. IPSIAM screen shot: Part of the calculation of $u[A_{abs}]$.

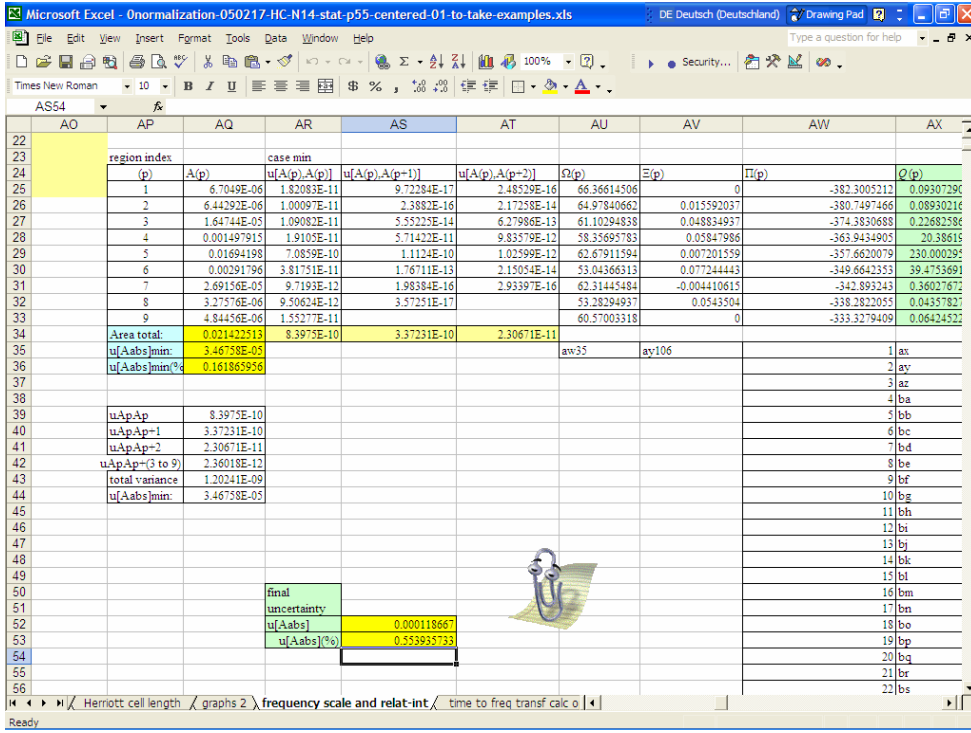


Figure 25. IPSIAM screen shot: Part of the calculation of $u[A_{abs}]$.

We remind now that the integrated absorbance was measured at some temperature T . So afterwards we use it to measure the corresponding line intensity or partial pressure, at that temperature T dictated by the experimental conditions. But we would like to combine the results of many measurements, which not necessarily were taken at the same temperature; we also would like to report the line intensities at some reference temperature T_0 , as it is customary. So in the last part of this section we will show how we calculated the integrated absorbance $A_{abs}(T_0)$ at some reference temperature T_0 , as well as its standard uncertainty.

As explained in page 63, we modeled the temperature dependency of the line intensity by means of a linear regression of the output values of the HITRAN data basis for the corresponding line intensity at different temperatures. These temperatures were selected to be similar to those measured during our experiments.

Substituting equation (100) in equation (101) and regrouping we have:

$$A_{abs}(T_0) = A_{abs}|_T + m_{ST} \cdot (T_0 - T) \cdot n \cdot L \quad (188)$$

We have use the symbol $A_{abs}|_T$ to emphasize that the integrated absorbance was measured at a given temperature T . We did not use $A_{abs}(T)$ in equation (188) in order to not cause confusion when the partial derivatives are applied to that equation, as the temperature dependency of A_{abs} is already explicitly written there. On this regard is also important to note that although we measured the gas density n indirectly by means of the ideal gas law, where also the temperature is an input quantity,

the temperature there is also correlated with the pressure in such a way that the gas density n actually does not have any correlation with the temperature. This can be seen more easily recalling that n is the number of molecules per cubic centimeter, which must be a conserved quantity in a closed environment independently of its temperature, as long as such processes as adsorption or desorption are not significantly affected by the temperature changes. The temperature dependency of L ($< 10^{-5}/\text{K}$) was neglected. So, in our case, we can consider all the input quantities of equation (188) as not correlated and the standard uncertainty of the integrated absorbance at reference temperature T_0 takes the form:

$$u[A_{abs}(T_0)] = \left(u^2[A_{abs}|_T] + \frac{\left(\frac{u^2[m_{ST}]}{m_{ST}^2} + \frac{u^2[n]}{n^2} + \frac{u^2[L]}{L^2} + \frac{u^2[T]}{(T_0 - T)^2} \right)}{(m_{ST} \cdot n \cdot L \cdot (T_0 - T))^{-2}} \right)^{\frac{1}{2}} \quad (189)$$

As in HITRAN we have chosen as reference temperature 296 K. In the measurement of the example the temperature was (295.5422 ± 0.0061) K, the temperature coefficient was $m_{ST} = (-4.122 \pm 0.045) \cdot 10^{-24} \text{ cm}^{-1}/\text{K}$, the molecular density was $(1.5279 \pm 0.0026) \cdot 10^{16} \text{ molec}/\text{cm}^3$ and the absorption length was $(1116.46 \pm 0.65) \text{ cm}$ (standard uncertainties). So that the integrated absorption at reference temperature was:

- $A_{abs}(T_0) = 2.139 \cdot 10^{-2} \text{ cm}^{-1}$
- $u[A_{abs}(T_0)] = 1.2 \cdot 10^{-4} \text{ cm}^{-1} \text{ (0.55\%)}$

3.10. Line Intensity Measurements

In the previous sections we explained how the IPSIAM workbooks calculate the gas density n (section 3.4), the total absorbing path-length L (section 3.3.2), and the integrated absorbance at reference temperature $A_{abs}(T_0)$ (section 3.9). With this input quantities the line intensity $S(T_0)$ at the reference temperature T_0 is also calculated in IPSIAM as

$$S(T_0) = \frac{A_{abs}(T_0)}{n \cdot L}. \quad (190)$$

The n and L are not correlated among each other, so that the standard uncertainty of the line intensity is easily calculated by

$$u[S(T_0)] = S(T_0) \cdot \left(\frac{u[A_{abs}(T_0)]}{A_{abs}(T_0)} + \left(\left(\frac{u[L]}{L} \right)^2 + \left(\frac{u[n]}{n} \right)^2 \right)^{\frac{1}{2}} \right). \quad (191)$$

The example-measurement corresponds to the R12 line of CO_2 and its resulting line intensity measurement is:

- $S(T_0) = 1.2549 \cdot 10^{-21} \text{ cm}^{-1}$
- $u[S(T_0)] = 8.2 \cdot 10^{-24} \text{ cm}^{-1}$ (0.65%)

The next figure present a screen shot of part of IPSIAM where these calculations take place.

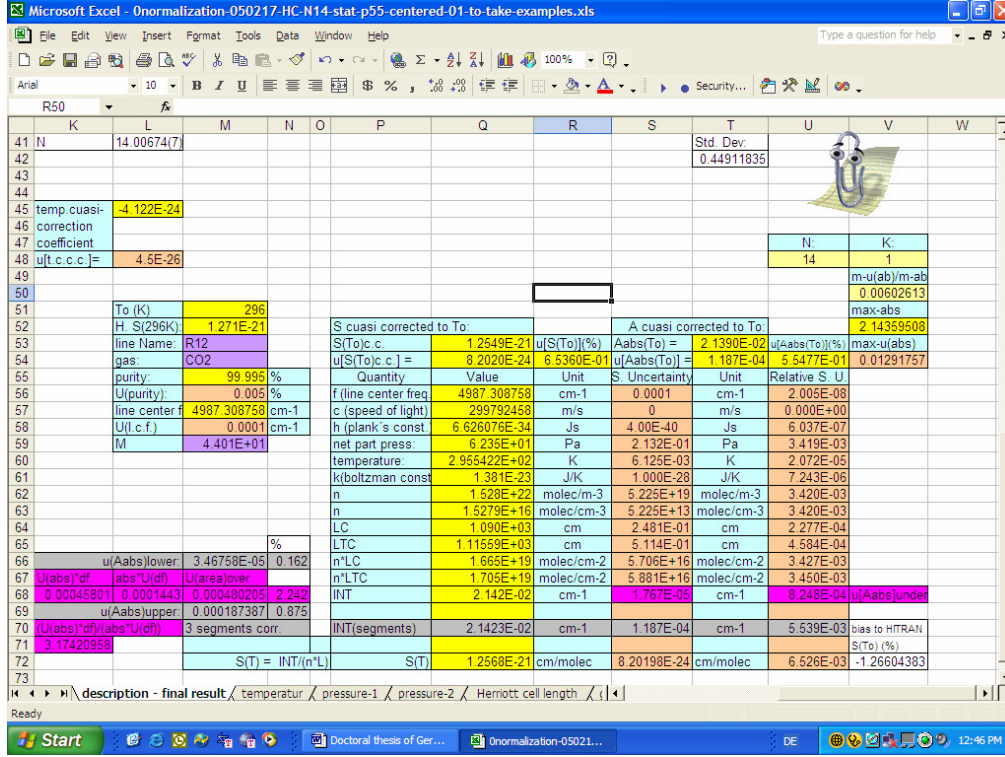


Figure 26. IPSIAM screen shot: Part of the calculation of $S(T_0)$, $u[S(T_0)]$ and other quantities.

3.11. Partial Pressure Measurements

The modified version of the “0-normalization-***.xls” workbook, called “0-pp-normalization-***.xls” performs the same tasks as the previous one, but, at the end, this IPSIAM program calculates the partial pressure p_i of the absorbing gas based on the known line intensity S and on the other input quantities of our model, i.e. absorbance-area A_{abs} , temperature T , absorbing length L and Planck’s constant k , according to the formula

$$P_i = \frac{A_{abs} \cdot k \cdot T}{S \cdot L} \quad (192)$$

The equation (192) is easily found using the equation (98), which we recall next,

$$n = \frac{A_{abs}}{S \cdot L}, \quad (98)$$

and the ideal gas law,

$$n_i = \frac{P_i}{k \cdot T} . \quad (92)$$

In these equations the line intensity must be given at the same measured temperature T at which the integrated absorbance $A_{abs}|_T$ was measured, so the explicit model is

$$P_i = \frac{A_{abs}|_T \cdot k \cdot T \cdot 10^6}{(S(T_0) + m_{ST} \cdot (T - T_0)) \cdot L} . \quad (193)$$

The 10^6 factor is necessary to change the gas density units from molec/m³ to mole/cm³, in order to make it compatible with the customary units of the line intensity (cm/molec). All the terms of equation (193) are uncorrelated. The standard uncertainty of the partial pressure is given then by

$$u[P_i] = P_i \cdot \left(\left(\frac{u[A_{abs}|_T]}{A_{abs}|_T} \right)^2 + \left(\frac{u[k]}{k} \right)^2 + \left(\frac{u[L]}{L} \right)^2 + \left(T^{-1} - \frac{m_{ST}}{S(T_0) + m_{ST} \cdot (T - T_0)} \right)^2 \cdot u^2[T] + \frac{u^2[S(T_0)] + (T - T_0)^2 \cdot u^2[m_{ST}]}{(S(T_0) + m_{ST} \cdot (T - T_0))^2} \right)^{\frac{1}{2}} \quad (194)$$

4. Experimental Results and Analysis

In this chapter we will present the results and analysis of the most important measurements and characterizations that we made in order to try to set up our spectrometer as a top-level instrument for line intensity measurements and as a primary standard for partial pressure measurements. To this end we will present first the general results of the measurements and their analysis of the most important input quantities individually, dedicating a subsection for each one of those. Then we will discuss the results and analysis of the line intensity and partial pressure measurements, where all the previous results are combined. All the uncertainty figures given in this chapter are standard uncertainties ($k = 1$).

In order to bring all the important experimental data, we will present tables with the results of the measurements for the most important input quantities used in the determination of the line intensities. To this end we will present the names of the IPSIAM-Results-Files where these results were calculated, in Appendix 7.3, while the tables with the corresponding results will be presented along the exposition in this chapter. The Table 25 shows the name of the IPSIAM-Results-Files used to calculate the CO₂ - R12 line intensity, and the Table 15 presents the first part of input quantities measured and calculated in those files.

4.1. Length Measurements

The length measurements were made as explained in the section 3.3.2. The Herriott Cell in our system can realize path lengths from (717.78 ± 0.47) cm to (6317.9 ± 1.5) cm (for the configurations $K = 1, N = 5$ and $K = 1, N = 33$, respectively).

For the measurement of the CO₂ R12 line intensity we used 6 different path lengths from the minimal value to (1613.29 ± 0.58) cm, as can be seen in the Table 15. Observe that the path length increase more rapidly than its uncertainty, so that with increasing path length the relative uncertainty decreases. In this case the path length relative uncertainty decreased from 0.07% to 0.04%.

Table 15. CO₂ R12 line intensity measurement input quantities - 1.

File	L	u[L]	u[L]	P	u[P]	u[P]	T	u[T]	u[T]	n	u[n]	u[n]
Consecutive	cm	cm	(%)	Pa	Pa	(%)	K	K	(%)	molec/cm ³	molec/cm ³	(%)
Number												
1	717.78	0.47	0.066	56.99	0.17	0.30	295.9571	0.0061	0.002	1.3945E+16	4.2E+13	0.30
2	717.78	0.47	0.066	54.40	0.16	0.30	296.7029	0.0077	0.003	1.3280E+16	4.0E+13	0.30
3	717.78	0.47	0.066	68.30	0.21	0.30	296.6836	0.0070	0.002	1.6674E+16	5.0E+13	0.30
4	717.78	0.47	0.066	86.49	0.26	0.30	296.6785	0.0067	0.002	2.1114E+16	6.3E+13	0.30
5	717.78	0.47	0.066	136.00	0.41	0.30	296.6651	0.0061	0.002	3.3203E+16	1.0E+14	0.30
6	717.78	0.47	0.066	58.75	0.18	0.30	296.6666	0.0061	0.002	1.4343E+16	4.3E+13	0.30
7	1014.96	0.50	0.049	87.13	0.26	0.30	295.5814	0.0061	0.002	2.1349E+16	6.4E+13	0.30
8	1014.96	0.50	0.049	95.85	0.29	0.30	295.6084	0.0061	0.002	2.3483E+16	7.0E+13	0.30
9	1014.96	0.50	0.049	95.83	0.29	0.30	295.6117	0.0062	0.002	2.3480E+16	7.0E+13	0.30
10	1014.96	0.50	0.049	107.12	0.32	0.30	295.5893	0.0061	0.002	2.6246E+16	7.9E+13	0.30
11	1014.96	0.50	0.049	107.11	0.32	0.30	295.5856	0.0064	0.002	2.6244E+16	7.9E+13	0.30
12	1115.61	0.51	0.046	62.35	0.21	0.34	295.5422	0.0061	0.002	1.5279E+16	5.2E+13	0.34
13	1115.61	0.51	0.046	47.59	0.15	0.31	295.4831	0.0065	0.002	1.1665E+16	3.6E+13	0.31
14	1115.61	0.51	0.046	36.43	0.11	0.31	295.4393	0.0061	0.002	8.9307E+15	2.8E+13	0.31
15	1115.61	0.51	0.046	80.53	0.24	0.30	295.8597	0.0061	0.002	1.9713E+16	5.9E+13	0.30
16	1115.61	0.51	0.046	106.53	0.32	0.30	295.9043	0.0061	0.002	2.6075E+16	7.8E+13	0.30
17	1313.79	0.54	0.041	54.07	0.16	0.30	295.5595	0.0061	0.002	1.3249E+16	4.0E+13	0.30
18	1313.79	0.54	0.041	66.09	0.20	0.30	295.5739	0.0061	0.002	1.6193E+16	4.9E+13	0.30
19	1313.79	0.54	0.041	87.70	0.26	0.30	295.5778	0.0061	0.002	2.1488E+16	6.4E+13	0.30
20	1313.79	0.54	0.041	80.70	0.24	0.30	295.5964	0.0061	0.002	1.9774E+16	5.9E+13	0.30
21	1514.92	0.56	0.037	66.31	0.20	0.30	295.7259	0.0061	0.002	1.6240E+16	4.9E+13	0.30
22	1514.92	0.56	0.037	80.22	0.24	0.30	295.6938	0.0061	0.002	1.9649E+16	5.9E+13	0.30
23	1514.92	0.56	0.037	53.97	0.16	0.30	295.6747	0.0061	0.002	1.3219E+16	4.0E+13	0.30
24	1613.29	0.58	0.036	51.36	0.15	0.30	297.7333	0.0069	0.002	1.2494E+16	3.7E+13	0.30
25	1613.29	0.58	0.036	62.97	0.19	0.30	297.6879	0.0062	0.002	1.5320E+16	4.6E+13	0.30
26	1613.29	0.58	0.036	55.37	0.17	0.30	297.7012	0.0135	0.005	1.3470E+16	4.0E+13	0.30
27	1613.29	0.58	0.036	71.38	0.21	0.30	297.6926	0.0063	0.002	1.7365E+16	5.2E+13	0.30
28	1613.29	0.58	0.036	76.45	0.23	0.30	297.7004	0.0063	0.002	1.8599E+16	5.6E+13	0.30

4.2. Pressure Measurements

The pressure measurements were made for a wide range of situations, from high-vacuum with dynamic flux to static measurements under moderated vacuum and low vacuum.

These pressure measurements of the CO₂ R12 Line Intensity Measurement were taken with the 10T-CDG. Their values varied from (36.43 ± 0.11) Pa to (136.00 ± 0.41) Pa. The relative

uncertainties of these pressure measurements varied from 0.30% to 0.34%. All the 28 pressure measurements are shown in the Table 15.

The dynamic measurements were made with the SRG1 and SRG2 simultaneously. They were located in opposite points of the VCMCH, so that we could control if there was a gradient of pressure during the measurements. We found no pressure gradient and the two measurements agreed always very well, so that we finally used the mean of both measurements.

4.3. Temperature Measurements

All our experiments were made at room temperature. As explained in section 3.6, we measured the temperature with two PT100 located inside the vacuum chamber (close to the opposite extremes of the chamber) and with seven PT100 in contact with the exterior walls of the chamber (evenly distributed around it). The two internal PT100 are not in contact with walls, but just fixed through their four contact legs. The sensor legs are soldered to four feed-through contacts that are about 10 cm long, so that the sensors are “hanging in space” inside the chamber.

We wish that we could measure the line intensities and partial pressures with the VCMHC kept at constant temperature at the milli-Kelvin level. Nevertheless we had no way to actively control the VCMCH temperature at that level, so that we had to take our measurements under temporal drifts (about 0.2°C per hour) and spatial gradients (about 0.5°C). We read the temperature sensors during all our measurements, including those when a high vacuum was made inside the chamber. This helped us to realize that the two internal sensors gave a better measurement of the gas temperature than the 7 outside sensors. These are too few to make a reliable map of the temperature distribution outside the chamber. In addition, we do not have information about the temperature of the surfaces inside the chamber, as from the mirrors, the rail system, the piezo-motor, etc.

At any given time point, there must be a well defined mean temperature for all the surfaces inside the chamber, despite the temperature gradients that may be present along the system, and despite the fact that this mean temperature may be changing with time. That mean is of course the integral of the temperature function over all the chamber internal surfaces divided by the whole internal surface area, as can be seen from the “extended first mean value theorem of the integral calculus [49]”. Given the high velocity of the gas molecules at ambient temperature and their uniform spatial distribution filling the whole volume inside the chamber, we conclude that the molecules undergo many collisions with practically all the segments of the internal surfaces in the chamber. After many collisions, the mean temperature of the gas must be equal to the mean temperature of the internal surfaces of the chamber.

We will present now as example the temperature measurements that we carried out on 2005-05-23. These temperature measurements are typical, and the conclusions that we make from them

are generally valid. Let's start with the measurements made with the seven external PT100 sensors (T1 to T7, see Figure 27 and Figure 28).

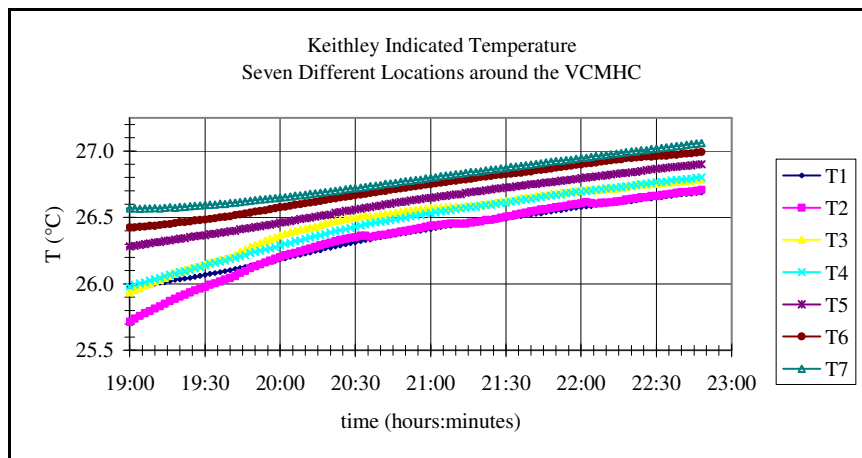


Figure 27. Temperature measurements on 20050523: Individual readings of the VCMHC external sensors.

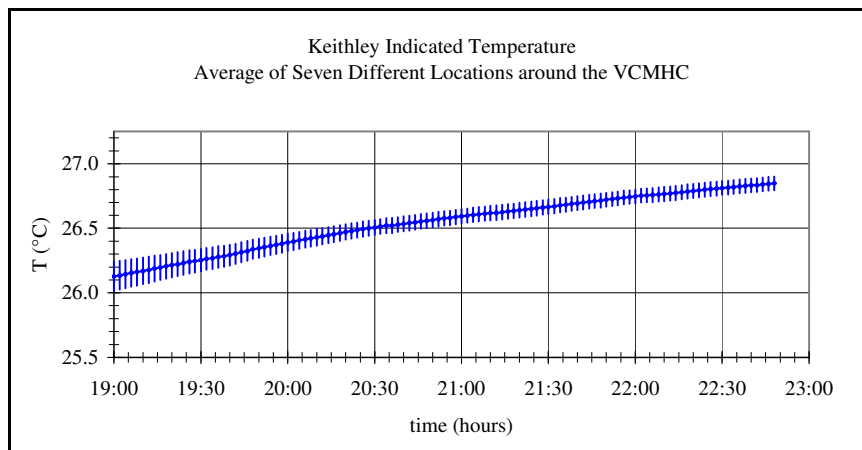


Figure 28. Temperature measurements on 20050523: Mean and standard deviation of the VCMHC external sensors.

It appears that, if we take the mean of the external sensors readings as an estimator of the gas temperature, its uncertainty would be at least 0.1°C , perhaps higher due to our lack of knowledge of the temperature of the internal surfaces. Let's take a look now to the measurements made with the two internal sensors simultaneously. Figure 29 to Figure 32 present their means and standard deviations.

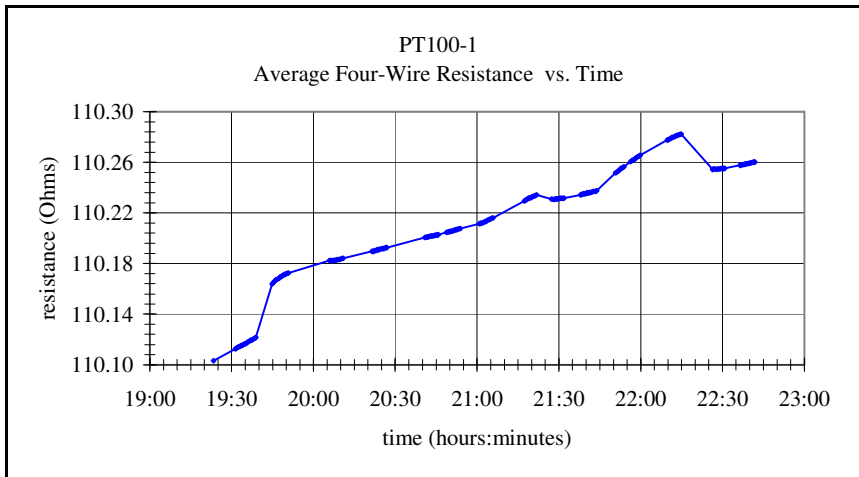


Figure 29. Temperature measurements on 20050523: Mean of the VCMHC internal sensor PT100-1.

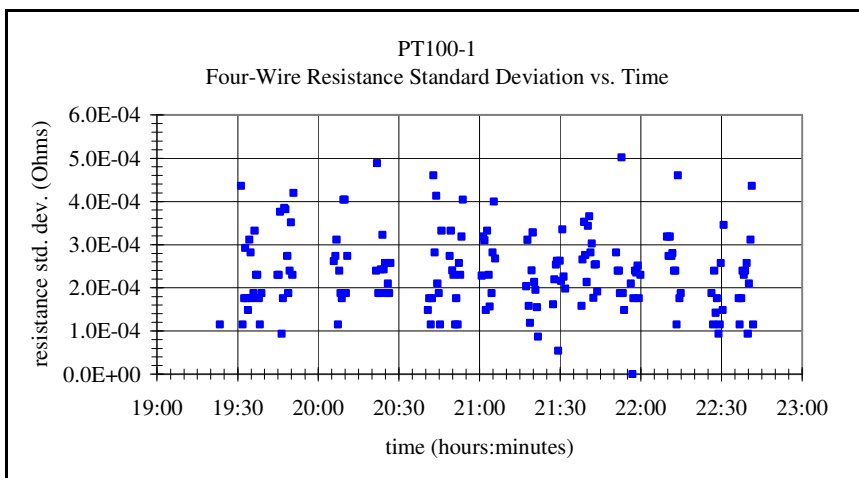


Figure 30. Temperature measurements on 20050523: Standard Deviation of the VCMHC internal sensor PT100-1

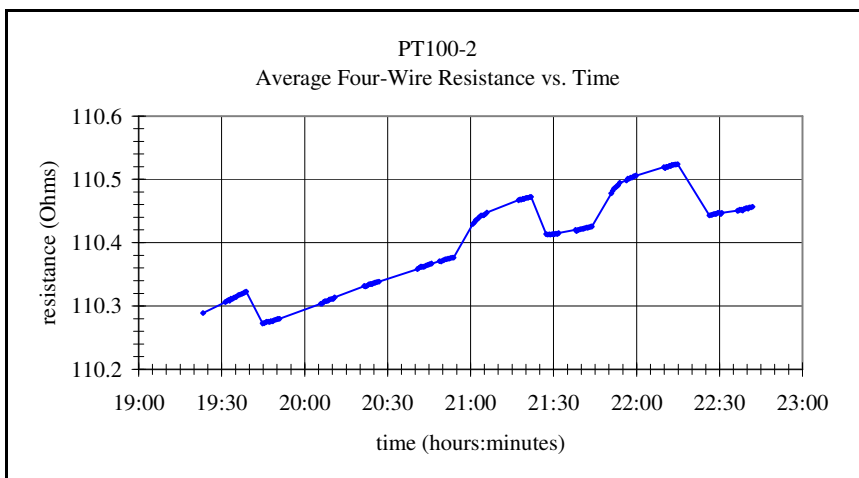


Figure 31. Temperature measurements on 20050523: Mean of the VCMHC internal sensor PT100-2.

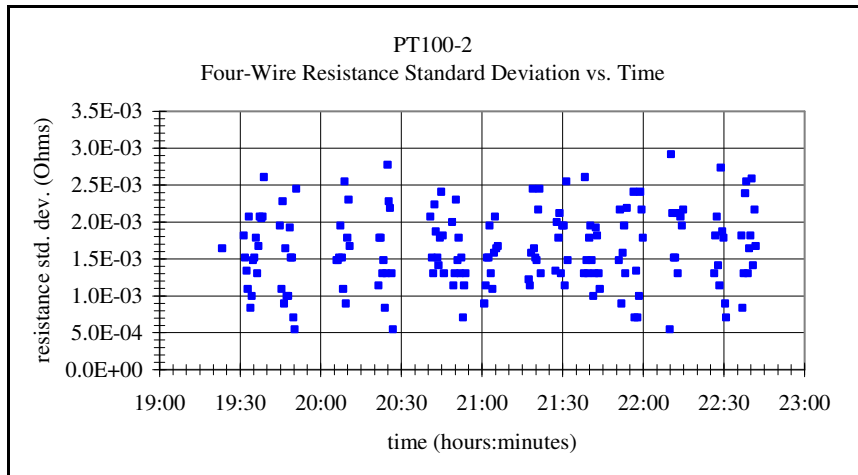


Figure 32. Temperature measurements on 20050523: Standard Deviation of the VCMHC internal sensor PT100-2.

As we can see in the Figure 29 and Figure 31, both sensors show a somewhat complicated structure. To clarify the significance of these structures let's present in the Figure 33 the pressures that we measured on that day.

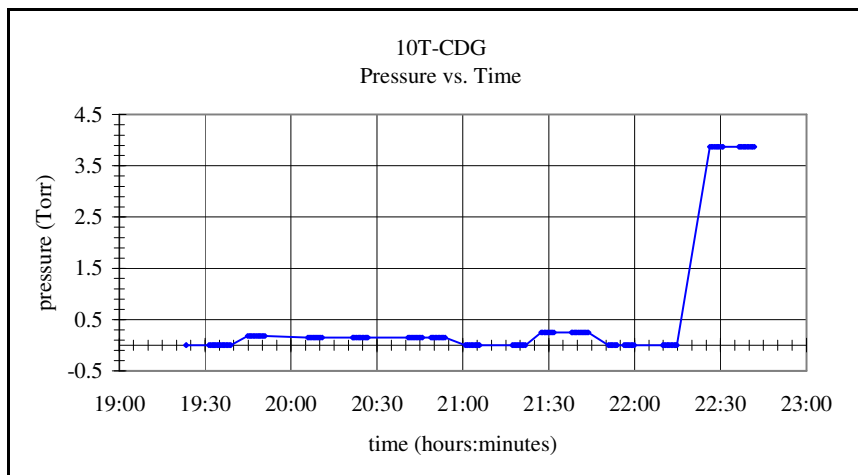


Figure 33. Pressure measurements on 20050523.

Comparing Figure 31 with Figure 33, it is clear that all the temperature “elevated” points were measured when there was high vacuum ($P = 0$ Torr) inside the VCMHC. PT100-2 is located inside the chamber in a region quite close to the external sensor T7. In Figure 27 we can see that, given the spatial gradient, the sensor T7 showed always the highest temperature of all the external measurements, i.e. in that region the chamber wall has a higher value than the mean temperature. It can be concluded, that when high vacuum was inside the chamber, the internal sensor started to measure the temperature of the conductors in contact with its legs. In contrast, when there was gas inside the chamber, the internal sensor signal was dominated by the gas temperature. The observed temperature structures are a superposition of two different curves: one for the temperature of the wall in that region (when there was high vacuum) and the second for the temperature of the gas (which is

equal to the mean temperature of the internal surfaces, as the chamber acts as a thermal-reservoir). In the following figures we present the internal measurements again, showing the approximate location of both curves and indicating explicitly which measurements belong to high vacuum and which to gas present. Furthermore we present the readings of the PT100-1 converted to temperature units according to its calibration certificate (Figure 35).

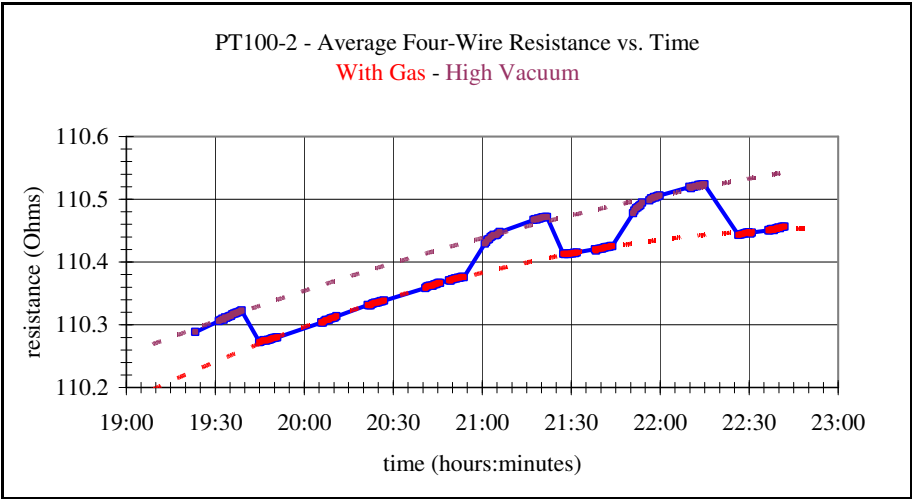


Figure 34. Temperature measurements on 20050523: Mean of the VCMHC internal sensor PT100-2. The plum curve shows the temporal variation of the chamber wall temperature in the region near the sensor, while the red curve shows the temporal variation of the mean temperature inside the chamber (which is equal to the gas temperature inside the chamber).

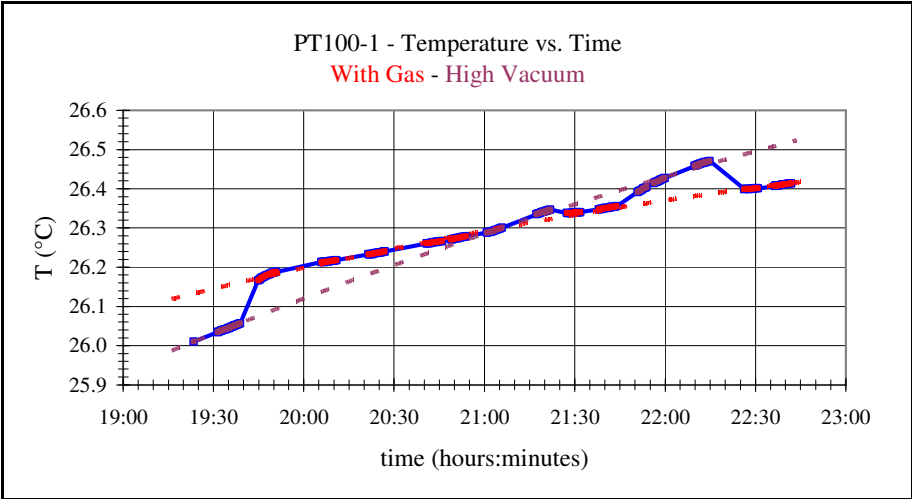


Figure 35. Temperature measurements on 20050523: Mean of the VCMHC internal sensor PT100-1. The plum curve shows the temporal variation of the chamber wall temperature in the region near the sensor, while the red curve shows the temporal variation of the mean temperature inside the chamber (which is equal to the gas temperature inside the chamber).

The PT100-1 is located quite close to the external sensor T3. Figure 27 shows that, at the beginning, the external sensor T3 measured a lower than the mean temperature; but then its reading increased until reaching the mean temperature. Correspondingly, the Figure 35 shows that the wall temperature close to PT100-1 presents a temporal variation which starts at lower than the mean values and grows intercepting the mean temperature curve (at about 21:00 hours) and grows beyond. This explains the structure of the PT100-1 temperature measurements. The red curves of both internal sensors (i.e. temperature measurements when there was gas inside the chamber) have the same form and correspond to the same temperature (the mean gas temperature), but we used only the readings of the PT100-1 because this one was calibrated while the PT100-2 not.

Through our method of measuring directly with PT100 inside the chamber (and avoiding its contact with the internal side of the chamber walls) we are able to perform a “direct” measurement of the gas temperature inside the VCMHC. Given the small uncertainty of the PT100-1 calibration (5 mK, $k = 1$), as well as the stability of the repeated measurements (compare the standard deviations in Figure 30 and Figure 32 with the means in Figure 29 and Figure 31), we were able to improve the accuracy of the gas temperature measurement in our experiment by two orders of magnitude compared with the earlier situation, when only the chamber wall temperatures were recorded; i.e. we dropped the temperature uncertainty from 0.2% to 0.002%.

Temperature Measurements for the CO₂ R12 Line Intensity Measurement

These temperature measurements varied from $(22.2893 \pm 0.0061) ^\circ\text{C}$ to $(24.5833 \pm 0.0069) ^\circ\text{C}$. The relative uncertainty of these measurements was mostly 0.002%. In two cases the relative uncertainties were 0.003% and 0.005%. All the 28 temperature measurements are shown in the Table 15 on page 115.

4.4. Gas Density Measurements

The density values for the CO₂ R12 line intensity measurement varied from $(8.9307 \pm 0.0069) \cdot 10^{15} \text{ molec/cm}^3$ to $(3.3203 \pm 0.0011) \cdot 10^{16} \text{ molec/cm}^3$. The relative uncertainties of these gas density measurements were typically 0.034% or less. Only 3 of the 28 density measurements presented bigger relative uncertainties (0.077%, 0.084% and 0.17%). See Table 15 on page 115.

4.5. Transmission Measurements for Linearization of the Absorbance Scale

The first version of the integrated absorbance and line intensity results are shown in Table 16.

Table 16. First version of the integrated absorbance and line intensity measurements for the R12 line.

File	$A_{\text{abs}}(\text{To})$	$u[A_{\text{abs}}(\text{To})]$	$u[A_{\text{abs}}(\text{To})]$	$S(\text{To})$	$u[S(\text{To})]$	$u[S(\text{To})]$
Consecutive	cm-1	cm-1	(%)	cm/molec	cm/molec	%
Number						
1	1.2338E-02	2.2E-05	0.18	1.2326E-21	4.4E-24	0.36
2	1.1956E-02	8.1E-05	0.68	1.2543E-21	9.4E-24	0.75
3	1.4984E-02	7.4E-05	0.49	1.2520E-21	7.3E-24	0.58
4	1.8830E-02	9.7E-05	0.52	1.2425E-21	7.5E-24	0.60
5	2.9463E-02	1.5E-04	0.51	1.2363E-21	7.3E-24	0.59
6	1.2892E-02	7.3E-05	0.57	1.2523E-21	8.1E-24	0.64
7	2.6764E-02	6.8E-05	0.26	1.2352E-21	4.9E-24	0.40
8	2.9337E-02	5.7E-05	0.19	1.2309E-21	4.4E-24	0.36
9	2.9057E-02	2.0E-04	0.69	1.2193E-21	9.2E-24	0.75
10	3.2598E-02	1.6E-04	0.48	1.2237E-21	6.9E-24	0.57
11	3.2576E-02	2.1E-04	0.64	1.2230E-21	8.7E-24	0.71
12	2.1130E-02	1.2E-04	0.55	1.2396E-21	8.1E-24	0.65
13	1.6487E-02	1.2E-04	0.72	1.2669E-21	9.9E-24	0.78
14	1.2509E-02	8.1E-05	0.65	1.2555E-21	9.0E-24	0.72
15	2.7788E-02	5.0E-05	0.18	1.2635E-21	4.5E-24	0.35
16	3.5442E-02	6.9E-05	0.19	1.2184E-21	4.4E-24	0.36
17	2.1454E-02	7.7E-05	0.36	1.2326E-21	5.8E-24	0.47
18	2.6292E-02	1.0E-04	0.39	1.2358E-21	6.1E-24	0.49
19	3.4715E-02	2.3E-04	0.66	1.2297E-21	9.0E-24	0.73
20	3.1643E-02	1.5E-04	0.47	1.2180E-21	6.8E-24	0.56
21	3.0178E-02	7.8E-05	0.26	1.2266E-21	4.9E-24	0.40
22	3.6087E-02	1.0E-04	0.28	1.2123E-21	5.0E-24	0.41
23	2.4752E-02	5.7E-05	0.23	1.2360E-21	4.7E-24	0.38
24	2.5025E-02	1.3E-04	0.53	1.2416E-21	7.6E-24	0.61
25	3.0502E-02	1.8E-04	0.59	1.2341E-21	8.2E-24	0.66
26	2.6914E-02	1.6E-04	0.59	1.2385E-21	8.2E-24	0.66
27	3.4532E-02	2.8E-04	0.80	1.2326E-21	1.1E-23	0.86
28	3.6983E-02	3.2E-04	0.85	1.2325E-21	1.1E-23	0.90

The Table 16 shows the first version of the results of our integrated absorbance and line intensity measurements for the CO₂ - R12 line, while the other input quantities for these measurements are shown on the Table 15. From that data we calculated the mean value and standard deviation of the line intensity:

- $S(T_0)_{\text{first-ver.}} = (1.236 \pm 0.014) \cdot 10^{-21} \text{ cm/molec.}$

This value is concordant with the corresponding HITRAN value given its uncertainty; i.e. our result is 2.75% smaller than the HITRAN value, but the uncertainty given in HITRAN of 2% to 5% ($k = 1$) would cover our value. Our smaller uncertainty of 1.1% ($k = 1$) would mean an improvement

in the accuracy of the R12 line intensity measurement. In order to improve our accuracy, we analyzed the data in the framework of linear analysis. By this way we could check that our results were compatible with the measurement model and we could find and correct for possible systematic errors, as was explained in section 2.6.

The individual line intensity measurements presented in the Table 16 were performed as explained in section 3.10, using the equation (190), which we rearrange now and write it down in the form:

$$A_{abs}(T_0) = S(T_0) \cdot n \cdot L . \quad (195)$$

Doing so we can consider the linear model: $y = m \cdot x + b$, with:

$$\begin{aligned} y &= A_{abs}(T_0) , & x &= n \cdot L , \\ m &= S(T_0) , & b &= 0 . \end{aligned} \quad (196)$$

This linear model should be analyzed using a functional-structural method, because our goal is to find the parameters of the model as physical quantities, and not to perform some regression or prediction of the variables. Nevertheless we will also show the results of the Ordinary Least Squares, or regression analysis. We remind at this point that Ordinary Least Squares gives two different sets of parameters for the same set of data (one for the regression of y on x and another for the regression of x on y) and therefore it is not suitable to assign physical interpretation to those parameters. The next figure presents the graphical representation of A_{abs} vs. $n \cdot L$ and its regression for the data of Table 15 and Table 16.

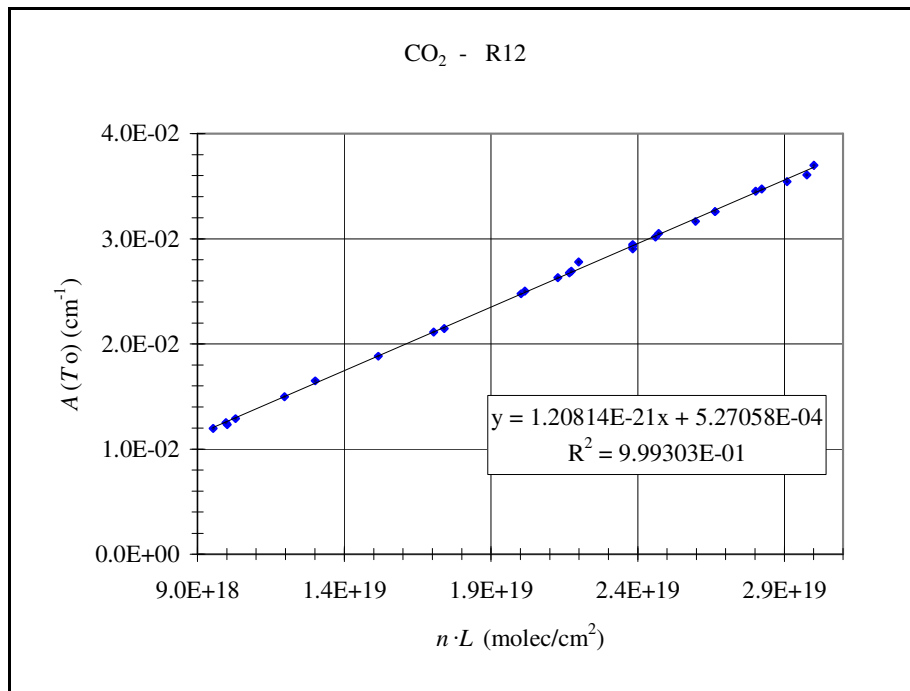


Figure 36. Results (first version) of the measurements for the R12 line intensity determination.

In this case the points show small scatter, so that the two cases of Ordinary Least Squares regression analysis deliver almost the same result, as shown in the next table.

Table 17. Ordinary Least Squares analysis of the $A(T_0)$ and $n \cdot L$ from the Table 15 and Table 16.

Ordinary Least Squares (OLS):	m	$u[m]$	b	$u[b]$
Regression of $A(T_0)$ on $n \cdot L$	1.2081E-21	6.3E-24	5.3E-04	1.4E-04
Regression of $n \cdot L$ on $A(T_0)$	1.2090E-21	6.3E-24	5.1E-04	1.4E-04

With the results of Table 17 we can see the first signal that something was wrong, because according to our model we expected “ $b = 0$ ”. More rigorously, we expected a b value comparable to the “zero control” integrated absorbance areas that we obtain for lack of absorbing gas. These measurements are performed and processed as ordinary measurements in order to check the performance of IPSIAM in several aspects, including the indirect measurement of the input laser intensity I_0 . During the measurement campaign for the R12 line intensity we took 20 “zero control” measurements, which are noted in Table 26 (Appendix 7.3, page 168).

Based on the measurements shown in Table 26, we expected a maximum value for b in the order of $5 \cdot 10^{-5} \text{ cm}^{-1}$. We also expected $u[b] > b$ so that we could regard b as statistically equivalent to zero. But the Ordinary Least Squares preliminary results presented an intercept which is about 4 times bigger than its standard uncertainty and therefore it can not be considered as equivalent to zero from a statistical point of view.

We confirmed our suspicions when we performed a functional-structural linear analysis, as we will explain next.

In order to apply the functional-structural methods presented in section 2.6, the variances of the errors distributions of “ y ” and “ x ” must be independent from “ x ” and independent from each other. This requirement can be roughly checked assuming that the standard uncertainties of the individual measurements are actually good estimators of the standard deviations of their distributions (this should be true if the standard uncertainty was calculated correctly according to GUM and the measurement model is complete enough) and then checking the correlations among the quantities mentioned. The correlations found were:

- $R(n \cdot L, u[n \cdot L]) = 0.43$,
- $R(n \cdot L, u[A_{abs}(T_0)]) = 0.58$, and
- $R(u[n \cdot L], u[A_{abs}(T_0)]) = 0.29$.

The correlation between $n \cdot L$ and $u[A_{abs}(T_0)]$ is not strong, but not negligible. Later on two tests will be applied in order to decide whether the model can be considered statistically suitable to describe the data.

Functional-Structural analysis for abscissa-data variance known

We applied this F-S analysis method to the $A_{abs}(T_0)$ vs. $n \cdot L$ data, and the results are:

$$\begin{aligned}\sigma_{exex} &= 4.09 \cdot 10^{33} , \\ \hat{m} &= 1.2083 \cdot 10^{-21} , \quad u[\hat{m}] = 6.3 \cdot 10^{-24} , \\ \hat{b} &= 5.2 \cdot 10^{-4} , \quad u[\hat{b}] = 1.4 \cdot 10^{-4} , \\ \hat{\mu}_{x'} &= 2.1 \cdot 10^{19} , \quad \hat{\sigma}_{x'x'} = 4.3 \cdot 10^{37} , \quad \hat{\sigma}_{eyey} = 3.8 \cdot 10^{-8} .\end{aligned}\tag{197}$$

Furthermore we found that

$$\chi^2 = \frac{\sum_{i=1}^N (x_i - \bar{x})^2}{\sigma_{exex}} = 2.9 \cdot 10^5 > 46.96\tag{198}$$

and

$$\frac{\sigma_{exex}^2}{(N-1) \cdot (uZZ[x, x] - \sigma_{exex})^2} = 3.3 \cdot 10^{-10} < 0.001 .\tag{199}$$

Both, the chi-test and the “rule of thumb”, gave positive response about the suitability of this F-S model to analyze the data. Also the graphical check presented a reasonable behavior, as we can see in the following figure, except for one point that perhaps may be considered as “outlier”.

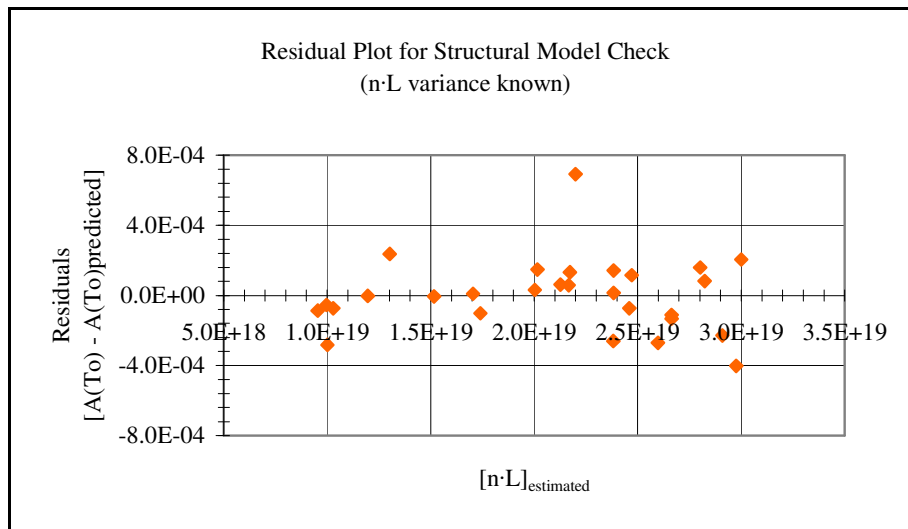


Figure 37. Graphical check of the structural model with abscissa-data known applied to the $A_{abs}(T_0)$ vs. $n \cdot L$ preliminary data.

After we verified the suitability of this Functional-Structural model for the analysis of the preliminary $A_{abs}(T_0)$ vs. $n \cdot L$ data, we realized that we could expect an intercept b slightly bigger than what we thought just considering the “zero control” measurements, i.e. we can expect actually something in the order of 10^{-4} cm^{-1} , but in any case we still expected $u[b] > b$. So we checked all our measurement procedures looking for some “offset” error. For instance if we had an error in the measurement of the absorbing path-length, that error would produce also a constant contribution that would reveal itself at the end as a significant intercept. We found no systematic errors in the measurements of any of the input quantities, until we checked the ratio of the laser intensity measurements in the detection channel.

We never tried to measure the laser optical intensity in absolute units because we only need the ratio of intensity measurements. The linearity of the detectors, however, was an assumption made in our evaluation so far.

Measurements and Analysis for the Linearization of the Transmission Measurements

Unfortunately we had no facilities to calibrate the IR detectors. In order to test the linearity, we used our Pellicle Beam Splitters to make a series of (correlated) intensity measurements; in which we could use our knowledge of the measurement relations to deduct a calibration function for the ratio of the intensity measurements.

Using two different PBS of 30% nominal transmission we took several measurements of the laser intensity as follows:

- without filter (100% transmission),
- through PBS1 (about 30% transmission),
- through PBS2 (about 30% transmission),
- through both PBS1 and PBS2 (about 9% transmission), and
- laser blocked (0% transmission).

The results of these measurements are shown in the next table.

Table 18. Measurements for the linearization of the transmission scale.

Filter	Electrical Transmission Signal average	Electrical Transmission Signal Std. Dev.	Optical Transmission Signal
"none"	1	0	1
PBS1	0.3425	0.0062	~ 0.3
PBS2	0.3242	0.0065	~ 0.3
PBS1·PBS2	0.1132	0.0023	~ 0.09
Total	0	0	0

If the transmission detection system was linear, the product of the transmission measurement for each of the PBS should be equal to the transmission measurement when both PBS were acting together. The mentioned product is 0.1110, in contradiction to the measured value for both PBS together (0.1132). Therefore the detection system produced a small positive error, at least close to the zone of 10% transmission.

For further analysis we assumed that the non-linearity of the transmission system should be minimal and represented by a smooth function. The positive error close to the 10% transmission region indicated that the error was also positive for all the other regions. A physical model to explain the possible non-linearity of the transmission detection system could be that the detector produces an avalanche effect right at the beginning of the detection threshold, but grows linearly when the detected optical signal increases. We described the avalanche-part of the curve with a small exponential term, which multiplies the linear term that describes the linear part of the curve. Figure 38 and Figure 39 illustrate the physical model with simulated data and reproduced quite well our measurements. The first curve shows that the detectors response is actually fairly linear, while the second curve permits the visualization of the small non-linearity.

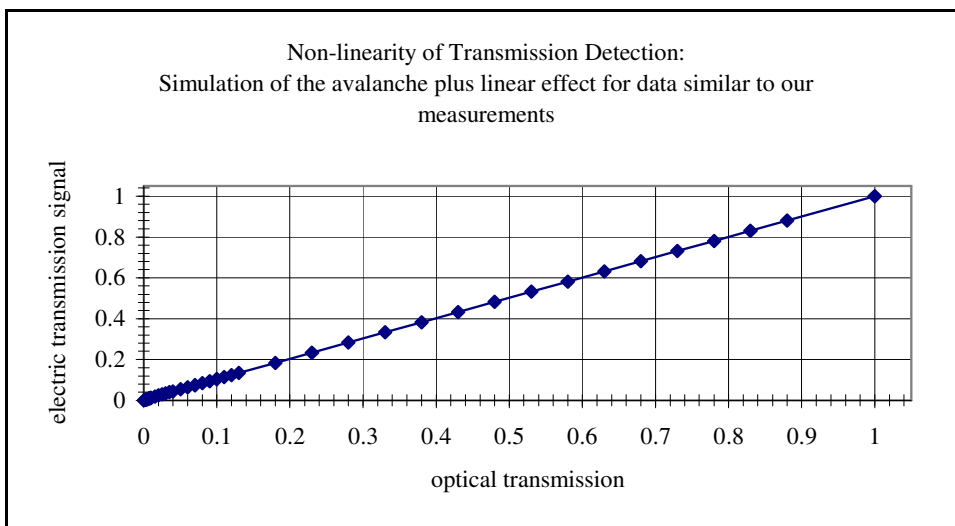


Figure 38. Simulated data of detectors' response similar to our measurements and showing the avalanche effect at the beginning of the curve: Electrical transmission signal versus optical transmission.

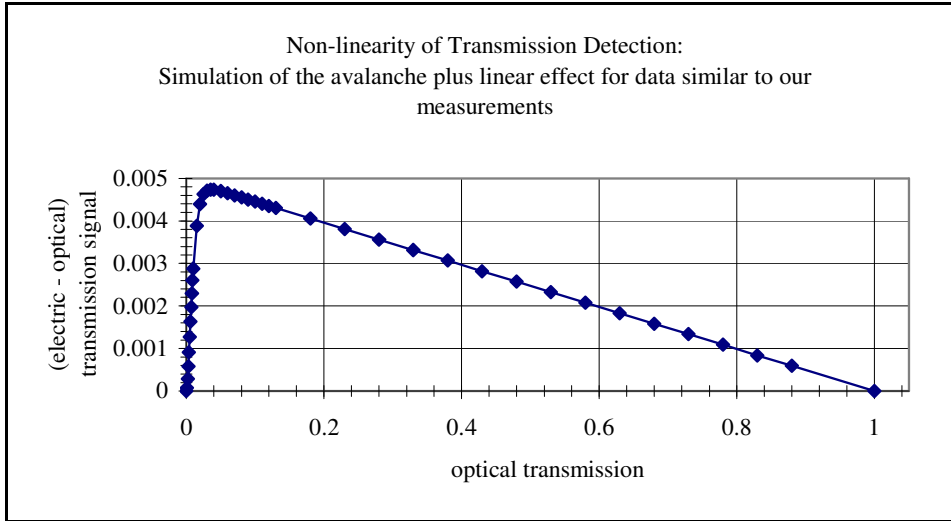


Figure 39. Simulated data of detectors' response similar to our measurements and showing the avalanche effect at the beginning of the curve: Residuals of the (electrical - optical) transmission signal versus optical transmission.

Observing the Figure 39 we realized that our physical model to explain the detectors minor non-linearity has a rapid growth of the exponential term for the avalanche effect and afterwards the behavior is dominated by the linear term. So we assumed that 4 of our 5 measurements, i.e. from $(I_{det.} = 1, I_{opt.} = 1)$ to $(I_{det.} = 0.1132, I_{opt.} \sim 0.09)$, were located well over the linear term and only the $(I_{det.} = 0, I_{opt.} = 0)$ measurement was part of the exponential behavior. This permitted us to find the optical transmission values through the application of two restrictions:

- that the four points must lie over a straight line, as said above, and
- that the product of the two transmissions close to 30% must be equal to the transmission close to 10%, which is a physical restriction independent of our model.

In this way we found enough information to solve the problem analytically and calculate both the real optical transmission values and the parameters of the linear part of the detectors' response curve. The results for the calculated optical transmissions are presented in the Table 19. The corresponding linearizing regression function to predict the optical transmission based on the measured electrical transmission signal is:

$$t_{opt} = 1.00497 \cdot t_{elect} - 0.00497 \quad (200)$$

Table 19. Measurements for the linearization of the transmission scale with the calculated values of the optical transmission.

Filter	Electrical Transmission Signal average	Optical Transmission
"none"	1	1
PBS1	0.3425	0.3392
PBS2	0.3242	0.3208
PBS1·PBS2	0.1132	0.1088

We corrected our transmission measurements using the equation (200) to linearize the transmission columns in the IPSIAM workbooks, and obtained in this way the final data with the corrected absorbances.

4.6. Line Intensity Measurements of CO₂

Once we corrected our first set of measurements of the CO₂ - R12 line intensity for the linearization of the transmission scale, we proceeded to analyze them in the framework of linear analysis again. The final integrated absorbance and line intensity results are shown in the Table 20. The mean and standard deviation of the R12 line intensity individual measurements is now:

- $S(T_0)_{ind.meas.} = (1.2582 \pm 0.0098) \cdot 10^{-21} \text{ cm/molec.}$

This is not that different from the result obtained from linear analysis, as can be seen after comparing it with the slope of the following figure, which presents the $A_{abs}(T_0)$ vs. $n \cdot L$ plot for the corrected data.

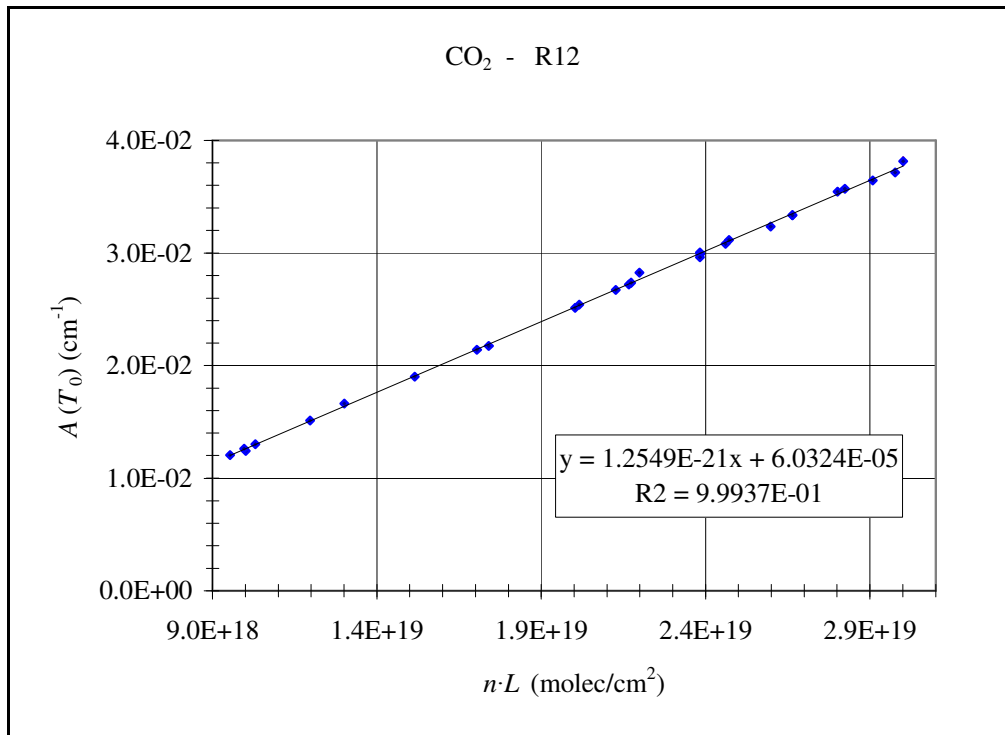


Figure 40. Final results of the measurements for the R12 line intensity determination.

Table 20. Corrected integrated absorbance and line intensity measurements for the R12 line.

File	$A_{\text{abs}}(\text{To})$	$u[A_{\text{abs}}(\text{To})]$	$u[A_{\text{abs}}(\text{To})]$	$S(\text{To})$	$u[S(\text{To})]$	$u[S(\text{To})]$
Consecutive	cm-1	cm-1	(%)	cm/molec	cm/molec	%
Number						
1	1.2439E-02	2.2E-05	0.18	1.2426E-21	4.4E-24	0.36
2	1.2050E-02	8.2E-05	0.68	1.2642E-21	9.4E-24	0.75
3	1.5120E-02	7.5E-05	0.49	1.2633E-21	7.3E-24	0.58
4	1.9035E-02	9.8E-05	0.52	1.2560E-21	7.5E-24	0.60
5	3.003E-02	1.6E-04	0.52	1.2600E-21	7.6E-24	0.60
6	1.2998E-02	7.4E-05	0.57	1.2626E-21	8.1E-24	0.64
7	2.7211E-02	7.0E-05	0.26	1.2558E-21	5.0E-24	0.40
8	2.9903E-02	5.8E-05	0.19	1.2546E-21	4.5E-24	0.36
9	2.961E-02	2.1E-04	0.70	1.2426E-21	9.5E-24	0.76
10	3.337E-02	1.6E-04	0.49	1.2527E-21	7.2E-24	0.58
11	3.334E-02	2.2E-04	0.66	1.2517E-21	9.2E-24	0.73
12	2.139E-02	1.2E-04	0.55	1.2549E-21	8.2E-24	0.65
13	1.665E-02	1.2E-04	0.72	1.2793E-21	1.0E-23	0.78
14	1.2611E-02	8.2E-05	0.65	1.2658E-21	9.1E-24	0.72
15	2.8265E-02	5.1E-05	0.18	1.2852E-21	4.5E-24	0.35
16	3.6453E-02	7.3E-05	0.20	1.2531E-21	4.6E-24	0.36
17	2.1726E-02	7.8E-05	0.36	1.2482E-21	5.9E-24	0.47
18	2.673E-02	1.1E-04	0.39	1.2562E-21	6.2E-24	0.50
19	3.569E-02	2.5E-04	0.69	1.2641E-21	9.6E-24	0.76
20	3.236E-02	1.6E-04	0.48	1.2457E-21	7.1E-24	0.57
21	3.0794E-02	8.1E-05	0.26	1.2516E-21	5.0E-24	0.40
22	3.717E-02	1.1E-04	0.30	1.2487E-21	5.3E-24	0.42
23	2.5123E-02	5.9E-05	0.23	1.2545E-21	4.8E-24	0.38
24	2.540E-02	1.4E-04	0.54	1.2603E-21	7.7E-24	0.61
25	3.113E-02	1.9E-04	0.60	1.2596E-21	8.5E-24	0.67
26	2.737E-02	1.6E-04	0.60	1.2592E-21	8.4E-24	0.67
27	3.546E-02	3.0E-04	0.84	1.2656E-21	1.1E-23	0.89
28	3.815E-02	3.4E-04	0.90	1.2715E-21	1.2E-23	0.95

Functional-Structural analysis for abscissa-data variance known

We applied this F-S analysis method to the corrected $A_{abs}(T_0)$ vs. $n \cdot L$ data, which assumes that the variance of the abscissa-data is known, and in this case it corresponds to the variance of the $n \cdot L$ data, which is: $\sigma_{exex} = 4.09 \cdot 10^{33}$. This Structural-Functional method is well suited for the analysis of our data, because we really know quite well the uncertainty of the individual measurements according to GUM and they present a fairly homogeneous set of values as can be seen in the Table 15. The mean and standard deviation of the uncertainty of the $n \cdot L$ data is:

$$u[n \cdot L] = (6.4 \pm 2.0) \cdot 10^{16}, \text{ and therefore } u^2[n \cdot L] \equiv \sigma_{exex} = 4.09 \cdot 10^{33}.$$

The estimators of the parameters calculated with this F-S model are:

$$\begin{aligned} \hat{m} &= 1.2550 \cdot 10^{-21}, \quad u[\hat{m}] = 6.2 \cdot 10^{-24} \\ \hat{b} &= 5.8 \cdot 10^{-5}, \quad u[\hat{b}] = 1.4 \cdot 10^{-4} \\ \hat{\mu}_{x'} &= 2.1 \cdot 10^{19}, \quad \hat{\sigma}_{x'x'} = 4.3 \cdot 10^{37}, \quad \hat{\sigma}_{eyey} = 3.7 \cdot 10^{-8} \end{aligned} \quad (201)$$

we remind that $x = n \cdot L$, $y = A_{abs}(T_0)$, and $y = m \cdot x + b$. Furthermore we found that

$$\chi^2 = \frac{\sum_{i=1}^N (x_i - \bar{x})^2}{\sigma_{exex}} = 2.9 \cdot 10^5 > 46.96 \quad (202)$$

and

$$\frac{\sigma_{exex}^2}{(N-1) \cdot (uZZ[x, x] - \sigma_{exex})^2} = 3.3 \cdot 10^{-10} < 0.001 \quad (203)$$

so that both, the chi-test and the “rule of thumb”, gave positive response about the suitability of this F-S model to analyze the data. Also the graphical check presented a reasonable behavior, as we can see in the following figure.

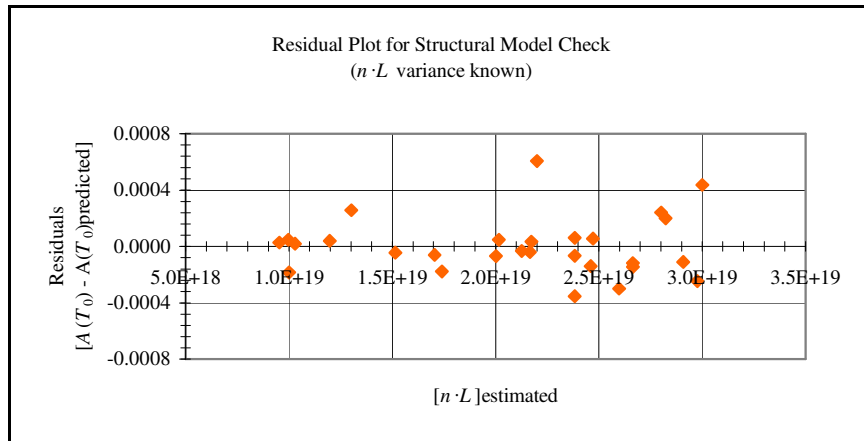


Figure 41. Graphical check of the structural model with abscissa-data known applied to the $A_{abs}(T_0)$ vs. $n \cdot L$ final data.

Now we obtained, as expected from the physical model, $u[b] = 1.4 \cdot 10^{-4} > 5.8 \cdot 10^{-5} = b$, an intercept smaller than its uncertainty and in the order of the “zero control” measurements ($\sim 5 \cdot 10^{-5}$ see Table 26), so that we can consider that the intercept is statistically equivalent to zero and the results are fully compatible with the physical model derived from the Beer-Lambert law.

The slope of the Functional-Structural model gives us the final result for our measurement of the CO₂ - R12 line intensity $S(T_0)$ at reference temperature $T_0 = 296$ K:

- R12: $S(T_0) = (1.2550 \pm 0.0062) \cdot 10^{-21}$ cm/molec ($k = 1$, 26 degrees of freedom).

The relative uncertainty of our measurement of the CO₂ - R12 (line center at $\nu = 4987.308758$) line intensity is therefore 0.49% ($k = 1$). Our measurement is 1.26% smaller than the corresponding HITRAN value, but in agreement with HITRAN given the bigger uncertainty of the HITRAN value.

Other transitions

We also measured the line intensities of three other CO₂ transitions in the same band: R10, R14 and R16. For lack of time we did not take enough repetitions to analyze these measurements in the framework of linear analysis. Next we present our results for these three transitions, which are respectively the mean value of a few measurements.

- R10: $S(T_0) = (1.171 \pm 0.010) \cdot 10^{-21}$ cm/molec ($k = 1$, 9 degrees of freedom).
- R14: $S(T_0) = (1.324 \pm 0.010) \cdot 10^{-21}$ cm/molec ($k = 1$, 5 degrees of freedom).
- R16: $S(T_0) = (1.327 \pm 0.010) \cdot 10^{-21}$ cm/molec ($k = 1$, 2 degrees of freedom).

The relative uncertainty of these measurements is about 0.77% ($k = 1$) and they are in agreement with the respective values given in HITRAN.

4.7. Partial Pressure Measurements of CO₂

Once we measured the line intensity of the CO₂ - R12 line we were prepared to use the spectrometer to measure partial pressures of CO₂ in gas mixtures using our improved value of the R12 line intensity. By this way we could compare our method with other methods of partial pressure measurement. We measured the partial pressure of CO₂ of two mixtures:

- A sample of the mixture code C49286 prepared by the BAM, which is a mixture of CO₂ and N₂ with reference relative amount of substance:
 - (0.10680 ± 0.00029) mol/mol % CO₂ ($k = 1$), and 99.8927 mol/mol % N₂.
- A sample of mixture prepared by Jorge Koelliker at the PTB-Braunschweig, which is also a mixture of CO₂ and N₂ with reference relative amount of substance of CO₂ of:
 - (5.1743 ± 0.0046) mol/mol % CO₂ ($k = 1$).

Partial Pressure Measurements of CO₂ in the Sample from BAM-Mixture C49286

We measured the partial pressure of CO₂ in this mixture two times. The main results of these measurements are shown in the following tables. The names of the corresponding IPSIAM-Results-files are given in the Table 27, on page 168.

Table 21. Results of partial pressure measurements of CO₂ in mixture C49286: Absorption path-length, total pressure, temperature and integrated absorbance.

File	L	$u[L]$	$u[L]$	P_{total}	$u[P_{total}]$	$u[P_{total}]$	T	$u[T]$	$u[T]$	$A_{abs}(T)$	$u[A_{abs}(T)]$	$u[A_{abs}(T)]$
Consecutive	cm	cm	(%)	Pa	Pa	(%)	K	K	(%)	cm-1	cm-1	(%)
Number												
1	4573.2	1.1	0.025	1314.5	3.9	0.30	301.0067	0.0062	0.0021	1.899E-03	3.7E-05	1.9
2	4573.2	1.1	0.025	7514	17	0.22	302.0011	0.0062	0.0021	9.79E-03	1.3E-04	1.3

Table 22. Results of partial pressure measurements of CO₂ in mixture C49286: R12 line intensity at measurement temperature, normalized integrated absorption and partial pressure of CO₂.

File	$S(T)$	$u[S(T)]$	$u[S(T)]$	$A_{abs} \cdot k \cdot T \cdot 10^6 / S(T)$	$u[A_{abs} \cdot k \cdot T \cdot 10^6 / S(T)]$	$u[A_{abs} \cdot k \cdot T \cdot 10^6 / S(T)]$	P_{part}	$u[P_{part}]$	$u[P_{part}] / P_{part}$
Consecutive	cm/molec	cm/molec	%	Pa·cm	Pa·cm	%	(%)	(%)	(%)
Number									
1	1.2344E-21	6.2E-24	0.50	6394	128	2.0	0.1064	0.0022	2.0
2	1.2303E-21	6.2E-24	0.50	33195	467	1.4	0.0966	0.0014	1.4

The measurement #1 was made with a total pressure of 13.1453 hPa, measured with the 10Torr-CDG. The measured relative partial pressure is concordant with the calibrated reference value of the BAM-mixture as we can see better comparing the two values as follows:

- 20050618 measurement: relative partial pressure = $(0.1064 \pm 0.0021) \%$ ($k = 1$)
- Certified value: relative partial pressure = $(0.10680 \pm 0.00029) \%$ ($k = 1$)

Our value is 0.37% smaller than the reference value, out of its 0.27% of relative uncertainty ($k = 1$), but it is covered by its extended relative uncertainty of 0.54% ($k = 2$). Nevertheless our relative uncertainty of 2% ($k = 1$) was quite big for our purposes and we wanted to reduce it. In order to reduce the relative uncertainty of the measured partial pressure it was necessary to increase the area of the integrated absorbance, and we increased the total pressure of the mixture in the chamber to 75.14 hPa (Measurement #2)

This measurement gave a result clearly smaller than the reference value:

- 20050620 measurement: relative partial pressure = $(0.0966 \pm 0.0014) \%$ ($k = 1$)
- Certified value: relative partial pressure = $(0.10680 \pm 0.00029) \%$ ($k = 1$)

We reduced the relative uncertainty of our measurement to 1.4%, but the result was now 9.55% smaller than the certified value. The reason for this error was that as we increased the pressure in the chamber, the absorption peak grew wider because of the pressure-widening effect. It appeared that our wave-number window was not wide enough to include the whole peak, as can be seen on figures for measurement #2 (Figure 45 to Figure 47) compared with the figures for measurement #1 (Figure 42 to Figure 44).

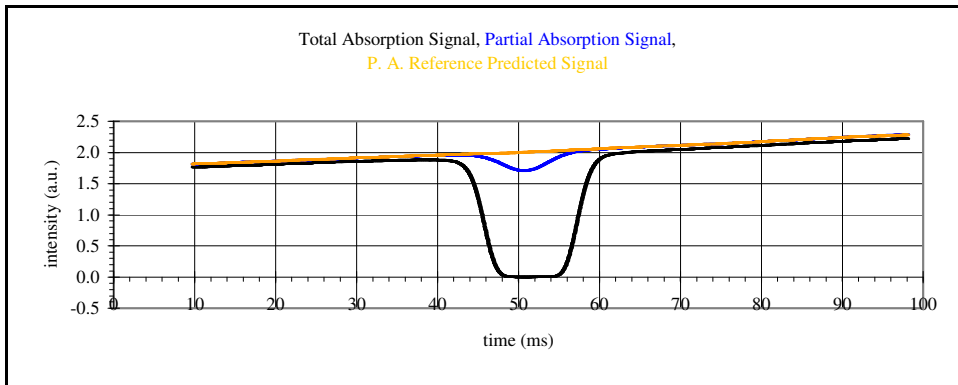


Figure 42. Partial pressure measurement on 20050618: Total absorption signal, partial absorption signal and reference signal predicted for the partial absorption signal.

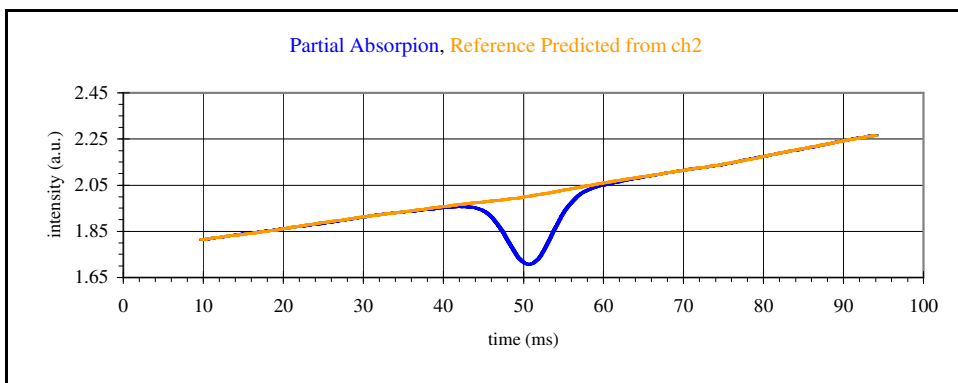


Figure 43. Partial pressure measurement on 20050618: Partial absorption signal and reference signal predicted for the partial absorption signal.

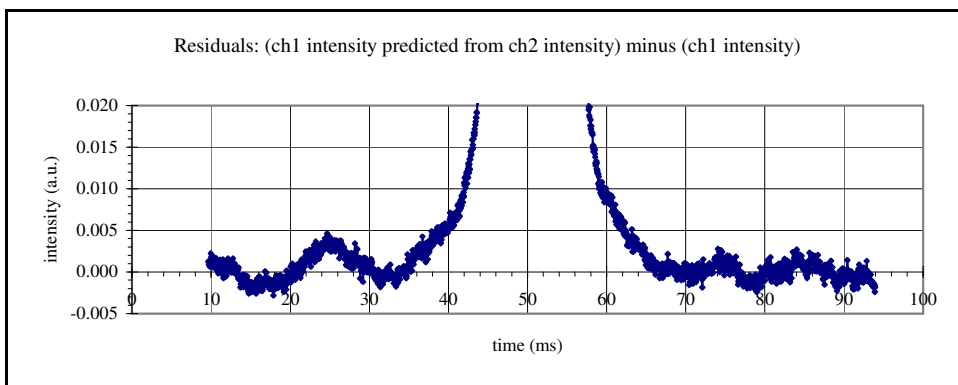


Figure 44. Partial pressure measurement on 20050618: Reference signal predicted for the partial absorption signal minus the partial absorption signal.

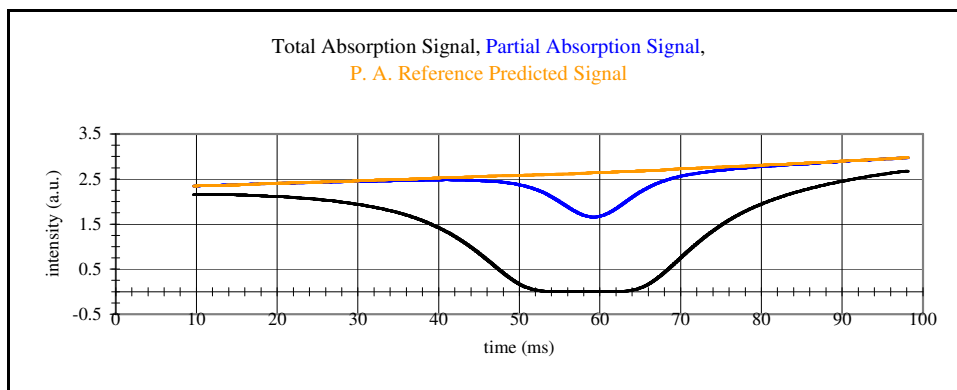


Figure 45. Partial pressure measurement on 20050620: Total absorption signal, partial absorption signal and reference signal predicted for the partial absorption signal.

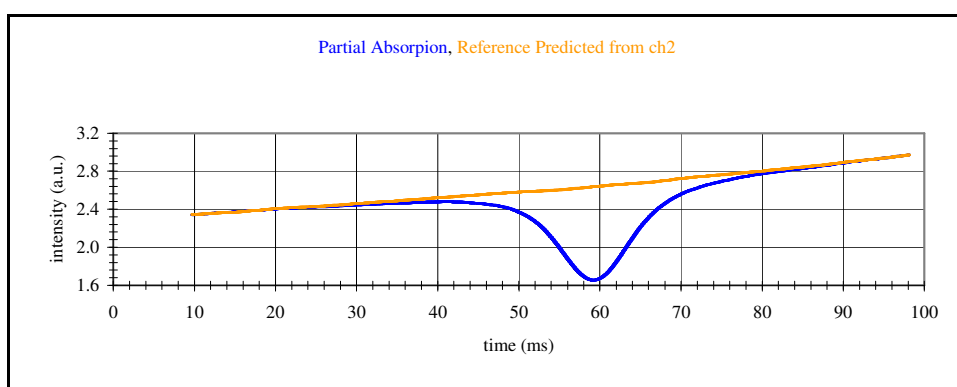


Figure 46. Partial pressure measurement on 20050620: Partial absorption signal and reference signal predicted for the partial absorption signal.

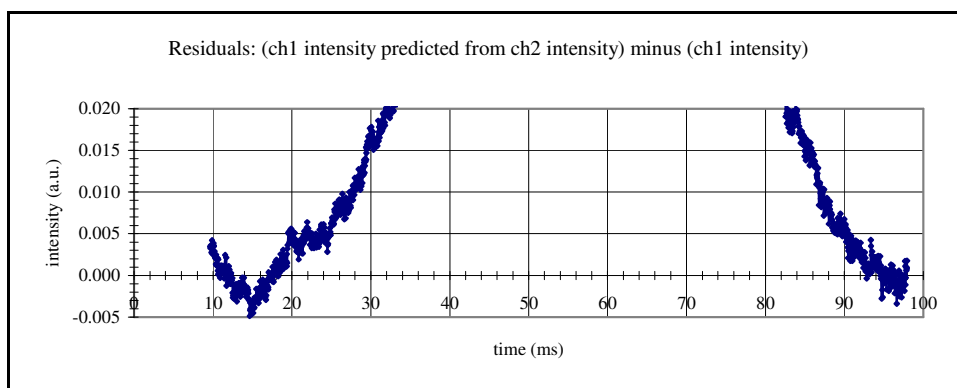


Figure 47. Partial pressure measurement on 20050620: Reference signal predicted for the partial absorption signal minus the partial absorption signal.

The Figure 45 and Figure 47 present the difference between the partial-absorption scan and its reference and they show that only the measurement made on 20050618 had a wave-number window wide enough compared to the width of the observed absorption peak. On 20050620 the pressure widening had caused that the same wave-number window was not enough any more to cover all the significant absorption region of the observed peak. This is especially evident for the right wing of

Figure 47, where the curve clearly has not reached yet the constant-level zone, but shows a slope until the end. This is the reason for the bias of the measurement taken on 20050620. Unfortunately, with these measurements we consumed the whole sample of C49286, so that we could not study the reproducibility of our measurements on this sample.

Partial Pressure Measurements of CO₂ in the Sample from PTB-mixture

We repeated the partial pressure measurement of CO₂ in this mixture 15 times. The main results of these measurements are shown in the Table 23 and Table 24. The corresponding IPSIAM-Results-Files names are presented in the Table 28, on page 169.

The 15 individual measurements of the CO₂ partial pressure were slightly biased towards smaller values, as we can see comparing the mean value of our results with the reference value:

- Our result of PTB-mixture as mean of individual measurements:
 - relative partial pressure = $(5.122 \pm 0.039) \%$ ($k = 1$)
- PTB-mixture reference value:
 - relative partial pressure = $(5.1743 \pm 0.0046) \%$ ($k = 1$)

The mean of the individual measurements is 1.0% smaller than the reference value, but it is still concordant with the reference value because our relative uncertainty of 1.5% at the 95% level of confidence ($k = 2$) includes clearly the reference value.

It is worth to emphasize the agreement between the mean of the standard uncertainties of the individual measurements of the partial pressure calculated in each IPSIAM-results file (0.0394%) and the standard deviation of the 15 individual measurements of the partial pressures (0.0392%). This agreement is a statistical confirmation that our system is actually calculating correctly the uncertainties according to GUM. This implies also that the assumptions made in trying to calculate correctly the rather difficult uncertainty of the integrated absorbance, were actually justified.

Finally for this section we would like to apply the F-S linear analysis to the partial pressure measurements. For this purpose we decided to analyze the “normalized integrated absorbance” vs. $P_i \cdot L$ (see Figure 48). We defined the “normalized integrated absorbance” as $A_{abs} \cdot k \cdot T \cdot 10^6 / S(T)$, in order to cancel out the variation of the area due to the temperature variation of the line intensity. The 10^6 factor is necessary because of the presence of spectroscopic units cm^{-1} (for the integrated absorbance) and molec/cm (for the line intensity) together with the SI unit J/K (for the Boltzmann constant).

Table 23. Results of partial pressure measurements of CO₂ in PTB-mixture: Absorption path-length, total pressure, temperature and integrated absorbance.

File Consecutive Number	L	$u[L]$	$u[L]$	P_t	$u[P_t]$	$u[P_t]$	T	$u[T]$	$u[T]$	$A_{abs}(T)$	$u[A_{abs}(T)]$	$u[A_{abs}(T)]$
	cm	cm	(%)	Pa	Pa	(%)	K	K	(%)	cm ⁻¹	cm ⁻¹	(%)
1	1115.61	0.51	0.046	656.1	2.0	0.30	299.9489	0.0064	0.0021	1.119E-02	1.0E-04	0.93
2	1115.61	0.51	0.046	972.6	2.9	0.30	302.6626	0.0061	0.0020	1.6248E-02	7.5E-05	0.46
3	1115.61	0.51	0.046	1143.3	3.4	0.30	302.6597	0.0061	0.0020	1.894E-02	1.1E-04	0.56
4	1806.74	0.60	0.033	656.1	2.0	0.30	299.9649	0.0062	0.0021	1.8084E-02	9.6E-05	0.53
5	1806.74	0.60	0.033	911.5	2.7	0.30	302.6696	0.0061	0.0020	2.457E-02	1.2E-04	0.49
6	1806.74	0.60	0.033	972.6	2.9	0.30	302.6660	0.0061	0.0020	2.627E-02	1.1E-04	0.42
7	2498.23	0.72	0.029	656.2	2.0	0.30	299.9780	0.0063	0.0021	2.505E-02	1.1E-04	0.42
8	2498.23	0.72	0.029	806.5	2.4	0.30	302.9500	0.0061	0.0020	3.020E-02	1.4E-04	0.47
9	2498.23	0.72	0.029	872.3	2.6	0.30	302.9523	0.0061	0.0020	3.266E-02	1.2E-04	0.38
10	3189.83	0.85	0.027	656.2	2.0	0.30	299.9912	0.0064	0.0021	3.248E-02	1.5E-04	0.47
11	3189.83	0.85	0.027	572.8	1.7	0.30	302.9227	0.0061	0.0020	2.746E-02	1.2E-04	0.42
12	3189.83	0.85	0.027	536.0	1.6	0.30	302.9243	0.0061	0.0020	2.570E-02	1.0E-04	0.40
13	3881.49	0.99	0.025	505.7	1.5	0.30	300.0133	0.0062	0.0021	3.033E-02	1.4E-04	0.47
14	4573.2	1.1	0.025	363.7	1.1	0.30	300.0245	0.0062	0.0021	2.574E-02	1.0E-04	0.40
15	4573.2	1.1	0.025	281.6	0.8	0.30	302.8915	0.0061	0.0020	1.9546E-02	9.5E-05	0.49

Table 24. Results of partial pressure measurements of CO₂ in PTB-mixture: R12 line intensity at measurement temperature, normalized integrated absorption and partial pressure of CO₂.

File	$S(T)$	$u[S(T)]$	$u[S(T)]$	$A_{abs} \cdot k \cdot T \cdot 10^6 / S(T)$	$u[A_{abs} \cdot k \cdot T \cdot 10^6 / S(T)]$	$u[A_{abs} \cdot k \cdot T \cdot 10^6 / S(T)]$	P_{part}	$u[P_{part}]$	$u[P_{part}] / P_{part}$
Consecutive Number	cm/molec	cm/molec	%	Pa·cm	Pa·cm	%	%	%	(%)
1	1.2387E-21	6.2E-24	0.50	37420	397	1.1	5.113	0.056	1.1
2	1.2275E-21	6.2E-24	0.51	55312	379	0.69	5.098	0.038	0.75
3	1.2275E-21	6.2E-24	0.51	64475	485	0.75	5.055	0.041	0.81
4	1.2386E-21	6.2E-24	0.50	60466	442	0.73	5.101	0.040	0.79
5	1.2275E-21	6.2E-24	0.51	83657	591	0.71	5.080	0.039	0.77
6	1.2275E-21	6.2E-24	0.51	89418	590	0.66	5.089	0.037	0.73
7	1.2386E-21	6.2E-24	0.50	83756	547	0.65	5.109	0.037	0.72
8	1.2263E-21	6.2E-24	0.51	102991	712	0.69	5.111	0.039	0.75
9	1.2263E-21	6.2E-24	0.51	111398	702	0.63	5.112	0.036	0.70
10	1.2385E-21	6.2E-24	0.50	108614	747	0.69	5.189	0.039	0.75
11	1.2265E-21	6.2E-24	0.51	93657	616	0.66	5.126	0.037	0.72
12	1.2264E-21	6.2E-24	0.51	87630	567	0.65	5.125	0.037	0.71
13	1.2384E-21	6.2E-24	0.50	101453	694	0.68	5.169	0.039	0.75
14	1.2384E-21	6.2E-24	0.50	86113	554	0.64	5.178	0.037	0.71
15	1.2266E-21	6.2E-24	0.51	66640	467	0.70	5.175	0.039	0.76
Mean:	1.2316E-21	6.2E-24	0.5034	82200	566	0.706	5.122	0.0394	0.77
Std. Dev.:	5.9E-24	2.5E-27	0.0026	21285	116	0.103	0.0392	0.0049	0.10

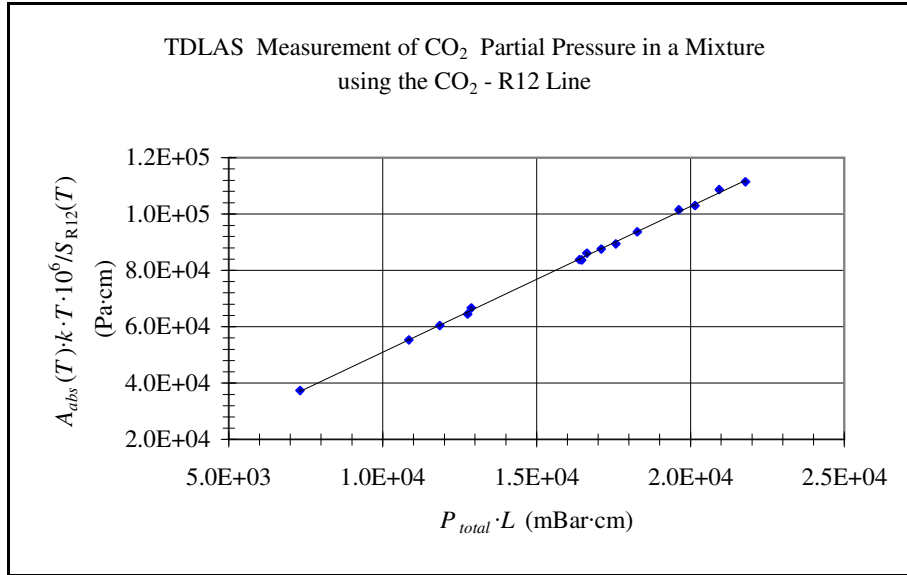


Figure 48. Plot of the data for the CO₂ partial pressure measurement in the PTB-mixture.

Functional-Structural analysis for abscissa-data variance known

We applied this F-S analysis method to the $A_{abs} \cdot k \cdot T \cdot 10^6 / S(T)$ vs. $P_t \cdot L$ data, which assumes that the variance of the abscissa-data is known, so that in this case the abscissa-data variance corresponds to the variance of the $P_t \cdot L$ data, which is: $\sigma_{exex} = 2340$. As before, this Structural-Functional method is well suited for the analysis of our data, because we really know quite well the uncertainty of the individual measurements according to GUM and they present a fairly homogeneous set of values as can be seen in Table 23. The mean and the standard deviation of the uncertainty of the $P_t \cdot L$ data is:

- $u[P_t \cdot L] = 48.4 \pm 12.4$, and therefore $u^2[P_t \cdot L] \equiv \sigma_{exex} = 2340$.

The estimators of the parameters calculated with this F-S model are:

$$\hat{m} = 5.170, \quad u[\hat{m}] = 0.042,$$

$$\hat{b} = -0.072, \quad u[\hat{b}] = 0.069, \quad (204)$$

$$\hat{\mu}_{x'} = 1.60 \cdot 10^4, \quad \hat{\sigma}_{x'x'} = 1.7 \cdot 10^7, \quad \hat{\sigma}_{eyey} = 3.2 \cdot 10^5,$$

where $x = P_t \cdot L$, $y = A_{abs} \cdot k \cdot T \cdot 10^6 / S(T)$, and $y = m \cdot x + b$. Furthermore we found that

$$\chi^2 = \frac{\sum_{i=1}^N (x_i - \bar{x})^2}{\sigma_{exex}} = 1.0 \cdot 10^5 > 29.14 \quad (205)$$

and

$$\frac{\sigma_{exex}^2}{(N-1) \cdot (uZZ[x, x] - \sigma_{exex})^2} = 1.4 \cdot 10^{-9} < 0.001 \quad (206)$$

so that both, the chi-test and the “rule of thumb”, gave positive response about the suitability of this F-S model to analyze the data.

We obtained an intercept statistically equivalent to zero at the 95% level of confidence.

Now our result for the CO₂ partial pressure in the PTB-mixture is not biased from the reference value, as we can see through their comparison:

- Our result on PTB-mixture as slope of the linear analysis:
 - relative partial pressure = $(5.170 \pm 0.042) \%$ ($k = 1$)
- PTB-mixture reference value:
 - relative partial pressure = $(5.1743 \pm 0.0046) \%$ ($k = 1$)

This result is only 0.08% smaller than the gravimetric reference value, i.e. it agrees fully with the reference value even for its relative small uncertainty of only 0.1%. Our relative uncertainty is larger (0.8%) but small enough to use our spectrometer as a primary standard to calibrate partial pressure measuring instruments (at least for CO₂ in the 0.1% to 5% relative partial pressure).

We interpret the improvement obtained in the partial pressure measurement result (when it was analyzed in the framework of linear analysis, as opposed to the mean of individual measurements) as the consequence of the coincidence of methodology in measuring both the line intensity and the partial pressure (the line intensity, which is an input quantity for the partial pressure measurement, was also measured using linear analysis).

4.8. Line Intensity Measurements of CO

When we obtained the first results of our line intensity measurements for the CO R4 line (line center at 2161.9682 cm⁻¹), we noticed that, as we varied the optical depth of the sample, our results presented a scatter in which the difference between the measurements were much bigger than the estimated uncertainty for the individual measurements. Furthermore the observed HWHM under Doppler conditions were always around three times bigger than the theoretical HWHM value.

After checking all the possible instrumental broadening effects, we concluded that the origin of this problem should lie in a too wide emission profile from our diode-laser. We developed a new algorithm to correct for this effect as explained in section 2.2.2, since we did not find a solution for this type of problem in the literature (the deconvolution algorithms published so far in the literature were designed to either separate partly overlapping peaks or reduce the amount of noise in the spectra, but always keeping a constant area for the absorbance vs. wave-number curve).

We implemented our algorithm in a sub-group of our IPSIAM LabVIEW programs. With these programs we were able to deconvolute our measurements as well as to generate and analyze synthetic data with different levels of noise. This was important in order to bring a statistical frame to interpret our (corrected) measurement results.

Figure 49 shows the measurement data of a transmission spectrum. The two shoulders at the base of the peak were quite intriguing, as well as the fact that the integration of the area under the corresponding absorbance curve gave a result for the line intensity of $2.50 \cdot 10^{-19}$ cm/molec, which is 36.5% smaller than the HITRAN value ($3.94 \cdot 10^{-19}$ cm/molec). The molecular density for this measurement was $1.990 \cdot 10^{13}$ molec/cm³ and the absorption path length was 1916 cm. With help of another measurement of weaker absorption (taken a few minutes earlier) we found the effective apparatus function for these measurements, which is graphically represented in the Figure 50.

After deconvoluting the strong absorption measurement we found the “corrected” extinction function as shown in Figure 51. Now the integration of the area under the corresponding absorbance curve gave a result for the line intensity of $3.65 \cdot 10^{-19}$ cm/molec, which is only 7.4% smaller than the HITRAN value.

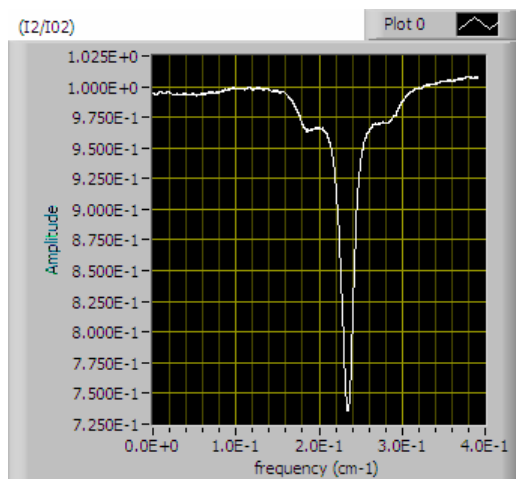


Figure 49. Graph from our IPSIAM program to deconvolute spectra affected by non-negligible apparatus function: Transmission of the strong absorption measurement.

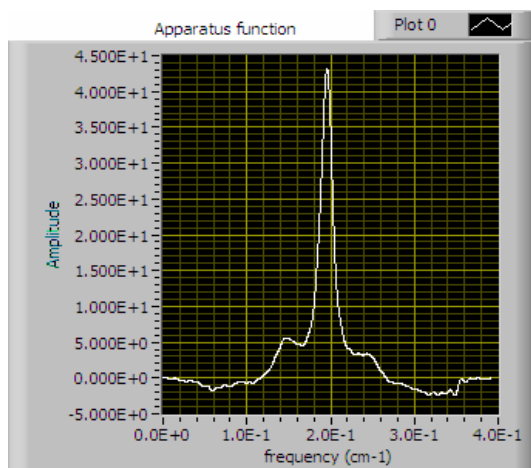


Figure 50. Graph from our IPSIAM program to deconvolute spectra affected by non-negligible apparatus function: Calculated apparatus function.

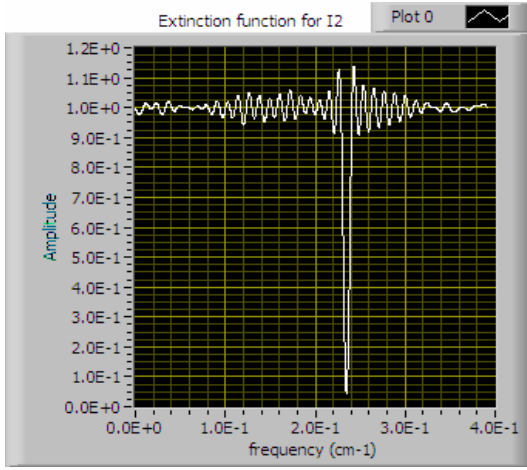


Figure 51. Graph from our IPSIAM program to deconvolute spectra affected by non-negligible apparatus function: Corrected extinction function of the strong absorption measurement.

The oscillations at the base of the corrected extinction function are a signal of the noise present in the spectra measurements. In order to study the effects of noise and other influences in our deconvolution process, we made several sets of simulations.

In the first set of simulations we studied the effect of the apparatus-function width (relative to the line absorption width) in the apparent line intensity of two “measurements” (one with 3% maximum absorption and the other with 10% maximum absorption) and in the corrected line intensity (calculated with our algorithm using the 3% max. absorption as the weak absorption signal and the 10% max. absorption as the strong absorption signal) and assuming zero-noise data. The results are shown in the next figure.

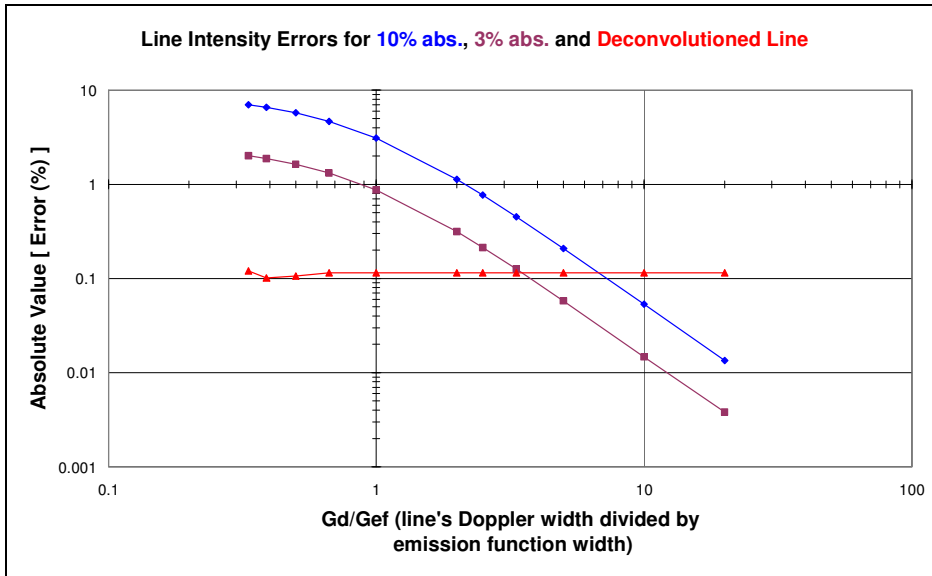


Figure 52. Simulated spectra affected by the apparatus-function: Apparatus-function width effect on the measurement of the line intensity based on apparent and corrected absorption lines.

The error of the apparent spectra was always negative (i.e. the apparatus-function broadening produce always an absorbance curve with smaller area than the “real” curve), but we plotted the absolute value of the error to use a logarithmical scale. As expected, the error grows with increasing apparatus function width (abscissa axis, left direction) and with increasing optical depth (curves are positioned at upper positions for increasing absorption).

The residual error of the corrected data is 0.1% and practically independent of the apparatus function’s width (although it does depend on the optical depth as we will see shortly). The result of the integration over an apparent line may be better than that of the corrected one (i.e. error smaller than 0.1%) if the apparatus-function width is narrow enough for a given optical thickness (from our example: if the apparatus-function width is 1/5 or less of the absorption line width for the 3% max. absorption spectrum; or 1/10 or less for the 10% max. absorption spectrum), or if the optical depth is thin enough for a given apparatus-function width (from our example: if the maximum absorbance is about 3% or less for an apparatus-function width which is 1/3 of the absorption line width).

In the second set of simulations we studied the effect of the optical depth in the apparent and corrected line intensity of spectra “measured” with an apparatus-function HWHM which is 2.57 times wider than the real Doppler HWHM (i.e. similar to our experimental conditions), still assuming zero-noise data and a fixed weak absorption spectrum of 3% maximum absorption (i.e. we varied only the optical depth of the strong absorption spectrum). The results of this second set of simulations are shown in the next figure.

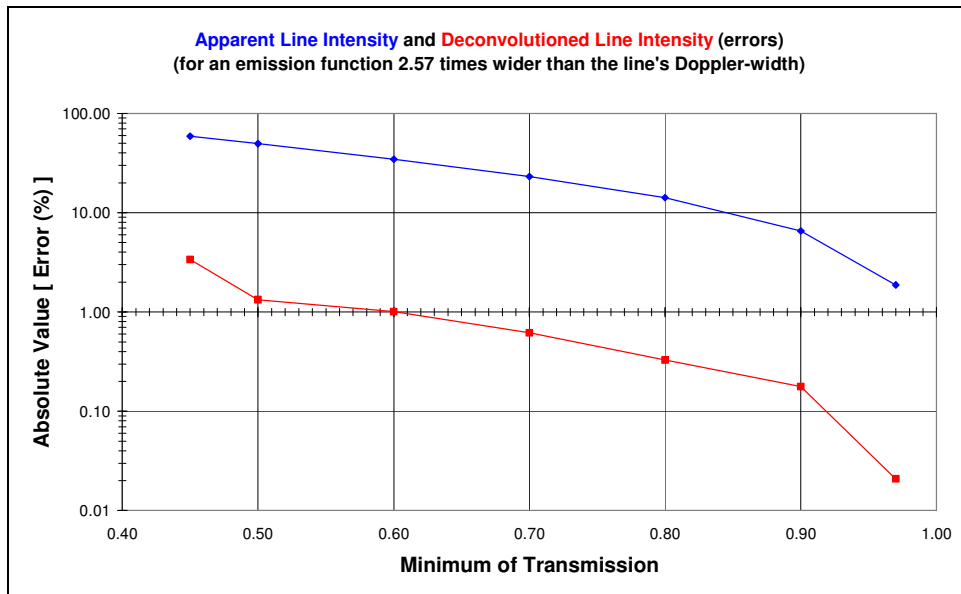


Figure 53. Simulated spectra affected by the apparatus-function: Optical depth effect on the measurement of the line intensity based on apparent and corrected absorption lines.

The improvement in accuracy reached with our method is about a factor of 40 in most cases. The apparent line errors begin at 2% for a line with 3% apparent maximum absorption and goes up 60% for an apparent maximum absorption of 55%. The corrected spectrum has a residual error of

only 0.02% for the 3% apparent maximum absorption and reaches 1% just when the apparent maximum absorption is 40%.

The measurement presented in the Figure 49 is in agreement with the simulation presented in the Figure 53: According to the simulation, a line with apparent minimum of transmission of 70% will produce an error in the (not-corrected) measurement of the line intensity of -30%. The error found in our measurement is about -36% (with an apparent minimum of transmission of 73%), but the simulation was noise-less and we expect some effects arising from the noise present in the data.

In the third set of simulations we studied the effect of the noise level in the result of the line intensity “measured” with the corrected spectrum (for an apparatus-function HWHM which is 2.57 times wider than the real Doppler HWHM, and original spectra with apparent maximum absorption of 3% for the weak absorption and 10% for the strong absorption). For each noise-level, 100 spectra were generated and processed. We calculated the mean and standard deviation for each group of 100 “measurements”. The results of this third set of simulations are shown in the next figure.

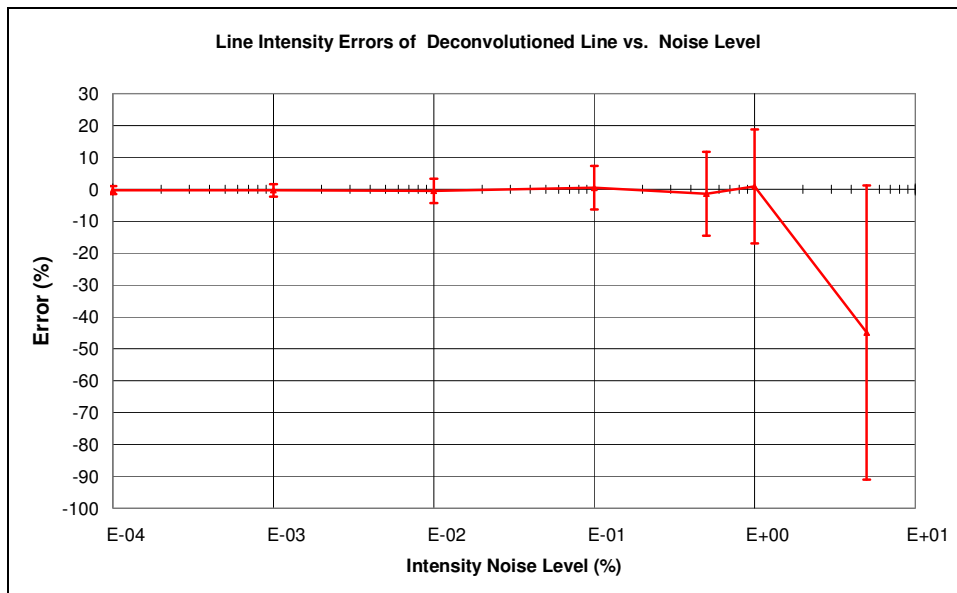


Figure 54. Simulated spectra affected by the apparatus-function: Noise level effect on the measurement of the line intensity based on corrected absorption lines.

The effect of a 5% of noise in the spectra is “catastrophic” for our algorithm, as it produces a spread of results which mean is biased with -45% error and a standard deviation of 45%. A noise level of 1% produced already an unbiased mean but the spread of data is still quite big (standard deviation of 20%). The mean is kept unbiased for noise levels of 1% or less. As the noise level is reduced so is the spread of results, but when the noise level reaches 1 ppm, the standard deviation of the results is still slightly over 1%.

The noise level of our measurements is in the order of 10^{-3} (i.e. 0.1%), so according to our simulation, if we perform many measurements (e.g. 100) the mean of our corrected measurements will give the correct value of the line intensity, but the measurements will show a spread of values

characterized by a standard deviation of about 8% (see Figure 54). Therefore the result of our corrected measurement (which presented a bias of -7.4%) is in good agreement with the predictions of our simulations.

In conclusion we could find the causes of the “strange” measurements successfully. The new algorithm is able to correct the effect of the apparatus-function in the integrated absorbance measurements (as far as we know this is the first time that such effect is corrected). Nevertheless our simulations demonstrated that the application of this algorithm would require an extremely high number of measurements in order to find the correct (unbiased) value of the line intensity (given the level of noise of our data). Therefore we decided not to proceed any further with this diode laser, but measure with lasers which have an emission profile narrow enough, so that we do not have to deconvolute the spectra.

Unfortunately we could not buy a new diode-laser on time to continue with the CO line intensity measurements (neither to measure CO partial pressures later), so that we had to leave the CO measurements like that and continued with the measurements on CO₂.

5. Discussion of TDLAS for Application as Primary Standard for Partial Pressure Measurements

Tunable Diode Laser Absorption Spectroscopy (TDLAS) is a well developed measuring principle which includes a variety of different techniques, like wavelength modulation spectroscopy, high frequency modulation spectroscopy, cavity enhanced absorption spectroscopy and others [50]⁴. Each of these techniques has its own advantages and disadvantages in dependency of different specific purposes and applications. Wavelength modulation integrated spectroscopy is not the most sensitive of the TDLAS techniques, but for our purposes it has the important advantage that, when applied to the complete integration over an isolated absorption line, it permits to eliminate the form-function of the Lambert-Beer law and leaves a simple equation ($A(T)_{abs} = S(T) \cdot n \cdot L$) which input quantities can be traceably measured. Furthermore, from that equation and the ideal gas law, it is possible to derive a simple measurement model for the partial pressure [$P_i = A_{abs} \cdot k \cdot T \cdot 10^6 / (S(T) \cdot L)$]. This model should permit the measurement of the gas partial pressure in absolute terms, i.e. without need of calibrating the spectrometer with some reference material of known partial pressure. Through the present research we have demonstrated the feasibility of that concept with the construction of a spectrometer (hardware), the development of IPSIAM (software) and its application to the absolute measurements of partial pressures of CO₂ in N₂ (using the R12 absorption line, which has its wave number center at 4987.308758 cm⁻¹, according to HITRAN).

Our method is based on the accurate measurement of a physical-chemical “constant” of the gas (a line intensity) and therefore it should be applicable to other gases that present “isolated” absorption lines, where the measurement of the corresponding line intensities can be done according to our procedure.

Other procedures (and software in general) may be implemented using the same 3-channels spectrometer set up that we constructed (or even simpler versions). An example on this regard is the pioneering work of E. Lanzinger and K. Jousten. They used the same VCMHC utilized in this work to set up a one-channel spectrometer and the program MARTA (from Dr. M. Martin) to measure line intensities and partial pressures of CO [8, 47]. Their approach included the fit of the absorbance vs. wave-number curve with a model form-function. At that time it was difficult to apply the GUM recommendations to that type of fits, but recently several methods including Monte-Carlo techniques [51] are being developed and some of them will be officially added to the GUM soon [52]. These techniques will facilitate the implementation of the GUM recommendations also to that type of

⁴ The mentioned techniques have been also implemented with quantum cascade lasers (QCL) and quantum cascade distributed feedback (QC-DFB) lasers by several groups. Quantum cascade lasers are not diode lasers so that perhaps a broader term like Tunable Semiconductor Laser Absorption Spectroscopy (TSLAS) could be useful to designate all these techniques and the different semiconductor devices that may be used to produce the laser beams.

measurement models. Another example is the development of a two-channel spectrometer by the Analytical Chemistry Group of the PTB in Braunschweig. That group and our group at PTB-Berlin worked collaboratively to the development of our goals, although the emphasis at the PTB-Braunschweig was the measurement of amount of substance using spectroscopic techniques⁵, and they use the fit-of-data-to-some-form-function method. They also demonstrated the feasibility of their TDLAS approach through their own measurements of CO₂ concentration in N₂ [10].

On the other hand, our IPSIAM programs could be used to control and process the results of other 3-channel spectrometers similar to our setup, i.e. our software is not limited to be used with our specific hardware, but can be implemented with similar versions of hardware (including of course other brand-names than those used in this research). As with any implementation of a measurement method, care must be taken that the inherent conditions of validity for the application are met. Two of those critical conditions for our method are:

- the apparatus-function's width must be negligible compared with the absorption line's width and,
- the transformation procedure that permit to convert the reference measurement (channel 2 signal) in predicted original intensity for the absorption spectrum (channel 1 intensity if no-absorption had taken place) must be kept working as accurate as possible. Quality controls like our "zero-control" measurements and the observation of the residuals of the "ch1 minus original ch1 prediction" graph at the wings of the absorption peak must be implemented to avoid an out-of-specification use of the measurement method.

In our experiments we found two cases of out-of-specification conditions for applying our method, which we will comment next.

The first out-of-specification- condition was the wide emission profile function of one of our diode-lasers, which emitted a laser signal about 2.5 wider than the CO absorption peak that we were trying to measure. It is interesting to note that although in the old days of pre-laser spectroscopy the people was very well aware of the limitations imposed by the apparatus-function of the old spectrometers, nowadays it seems that that awareness has declined given the (usually) extreme narrow emission profile of most diode lasers compared with the Doppler-widened absorption lines of all substances. Only in one [53] from many modern publications (including books and articles), we found caveats about the dependency of the line intensity measurement with real finite apparatus-function width of any spectrometer. Accordingly we did not find any deconvolution algorithm published which could be used to correcting data in order to eliminate the error introduced by the

⁵ It is worth noting that as part of our collaboration we, in Berlin, received the visit of Jorge Koelliker, from Braunschweig, who participated in a two weeks measurement campaign with us and used our IPSIAM programs to take some of the measurements used for the CO₂ R12 line intensity determination. He also made the selection of the 28 independent measurements out of a bigger number of measurements, where some of them could be considered as non-independent. Other collaborative works include our measurement of the free spectral range of the Si Etalon used by the Braunschweig group (with our two-lines R32-R33 method explained in section 3.8.1), as well as the gravimetric preparation of the PTB-mixture made by the group of Braunschweig and used by us to corroborate the accuracy of our measurements. We are working in the articles to publish the results of our collaborative work [9].

apparatus function in the line intensity measurements. On the contrary, all the deconvolution algorithms that we found (ref. from [18] to [23]) use the “constancy” of the area under the absorbance-vs.-wave-number-curve (i.e. the constancy of the line intensity) as part of their procedure to separate overlapped absorption peaks in measured spectra (even in those cases where the overlapping was caused by the finite apparatus-function width). Therefore we developed and proved our own algorithm to correct for the influence of the apparatus function in the measurement of the line intensity in those cases when the apparatus function width is not negligible small compared with the measured absorption line width. We applied this algorithm to the correction of CO spectra measured by us and we obtained results that are concordant with the values published by HITRAN, as we showed in section 4.8. With help of a simulation that we programmed to find the statistical properties of our algorithm under the conditions of our measurements, we find that the results after the deconvolution have a spread of about 10% around the mean (unbiased) value and therefore they are not good enough to be used as part of a primary standard. Nevertheless our algorithm may be useful even for primary standards under other conditions, e.g. when the apparatus function is about the same or smaller width than the absorption line. Furthermore our deconvolution algorithm may be useful for other measuring instruments which require less accuracy than a primary standard, and are also based on TDLAS techniques, like some recently commercially available instruments [54].

The second out-of-specification- condition was found when we increased the amount of C49286 sample in the measuring chamber (in order to increase the area of the absorption peak) and as a consequence we produced a pressure-broadening of the observed peak, so that our observed wave-number window was not wide enough to copy the whole absorption peak. In this case the main error was not introduced by the small area under the wings that we did not integrate, but by the erroneous localization of the predicted original intensity, which produced a reducing effect for the values of the absorption coefficients in the absorption peak (i.e. all the absorbance readings were erroneously smaller because of the systematic effect).

As shown in the “Results and analysis” chapter, when our system is used according to its specifications, it is capable of measuring line intensities with relative uncertainties of 0.50% ($k = 1$). This represents an improvement in the accuracy of this type of measurement of at least a factor of 4 (and probably a factor of 10) compared with the results published in HITRAN, which states uncertainties between 2% and 10% for the same lines measured by us. The improvement in accuracy reached in this work is not only quantitative, but also qualitative, as our measurements, as far as we know, are the first traceable measurements of integrated absorbances and line intensities of the studied transitions of CO₂. Their uncertainties were calculated in fully agreement with the GUM recommendations

The results of our line intensity measurements can be used in a wide spectrum of applications that have the line intensity as part of their input quantities. For instance we used our line intensity value as input quantity for partial pressure measurements. Our partial pressure measurements have relative uncertainties of 0.77% ($k = 1$) and, as far as we know, they are the first non-gravimetric traceable partial pressure measurements of a gas. The accuracy of our measurements was

experimentally confirmed through its application to the measurement of partial pressure of CO₂ on certified mixtures of known concentrations (mixture C49286 from BAM and PTB-mixture prepared at the PTB in Braunschweig). In both mixtures our measurement was in agreement with the reference gravimetric values for the CO₂ content (our bias: -0.37% for the C49286 mixture and -0.08% for the PTB-mixture) and the dispersion of repeated measurements of the same mixture (with a new sample of the PTB-mixture for each new measurement) shows the same standard deviation as predicted from our GUM-compliant uncertainty calculations (relative standard deviation = 0.77% = relative standard uncertainty).

The metrological level reached by our measuring installation permits to consider it as a primary standard for partial pressure measurements of CO₂.

6. Conclusions

Integrated absorbance spectroscopy is a measuring technique that can be used to make traceable measurements of line intensities and partial pressures. To this end several conditions must be met in several fields including the experimental setup, processing system and the implementation of a measurement assurance program capable to demonstrate the traceability of the measurement results.

We have demonstrated this possibility through the setting up of a 3 channel TDLAS spectrometer, the development of our IPSIAM software, and the implementation of the key elements of a measurement assurance program as part of our experiment. This measurement assurance program included:

- The selection of a measurement model that could deliver accurate results which uncertainties may be thoroughly calculated according to GUM. To this end we avoided the use of form-functions as part of the measurement model, which was the Lambert-Beer law. Instead we choose to perform a direct numerical integration of the absorbance curve.
- The traceable calibration of the measuring instruments that we used to measure the input quantities of our measurement model. These calibrations were performed by the respective laboratories of the PTB. Therefore our traceability chain is as short as possible and a high level of accuracy was achieved for all the measurements of our input quantities.
- The electronic and written documentation of all the information involved in making our measurements including the methods of measurement, the algorithms, the measurement procedures, the calibration of the measuring instruments and the processing of the measurement data. All the original files with raw data and their distinctive names were backed up. The names of those files were passed on along the analysis process and the whole workbook, where all the operations are made to obtain the results of our measurements were also backed up. In this way each one of our measurements was clearly connected to the source of information and processing that permitted its result, those sources being backed up. Our results are 100% auditable.
- Independent traceable realizations of the measured quantity to check our results. To this end we used a Certified Reference Material from BAM and a certified mixture from PTB-Braunschweig. Our results agreed with those measuring standards.
- The confirmation of the validity of our (GUM-compliant) uncertainty determination model through the study of the variability of repeated measurements. The confirmation was definitively positive.

With the confidence that brings the implementation of a measuring assurance program to support the results of a traceable measurement, our system was capable to measure several line intensities of CO₂ (R10, R12, R14, R16 of the first overtone of the fundamental band) with a relative expanded uncertainty of 1.0% ($k = 2$, about 95% level of confidence), (1.4% for individual measurements); which signifies an improvement in the level of accuracy of a factor of 4 (probably a factor of 10) in terms of the uncertainty figures given in HITRAN; but even more important, our measures represent an enormous qualitative improvement in these types of measurements because they are, as far as we know, the first measurements of these line intensities having the very important property of being traceable.

With the same confidence mentioned in the previous paragraph, our system was capable to measure partial pressures of CO₂ with a relative expanded uncertainty of 1.5% ($k = 2$, about 95% level of confidence). As far as we know these measurements (and the similar measurements made by the partner research group in PTB-Braunschweig) are the first traceable measurements of partial pressures of CO₂ (besides from gravimetric measurements, which of course can be traceable, but gravimetric techniques are used to prepare samples, not to measure the partial pressure of a gas in some unknown sample).

As part of our investigations we had to deal with laser emission functions that implied a non-negligible apparatus-function for our spectrometer. This led us to develop a new algorithm to correct for this effect on the measured spectra (as far as we know, this is the first time that such correction has been made for integrated absorbance measurements). We made several simulations based on an implementation of our deconvolution algorithm in LabVIEW, and compared the results of those simulations with the results of the application of our algorithm to measured spectra. There was agreement between the measured and the simulated results.

Whenever possible we analyzed the measured data in the framework of linear analysis because it permitted a thorough statistical interpretation of the data; plus other benefits, like eliminating the error introduced by a constant offset in the result of a measurement (if that measurement is evaluated as the slope of a linear relation) and permitting the corroboration of validity for an assumed (linear) physical model. To this end we reviewed the work done by statisticians on this regard. We found that Ordinary Least Squares (regression analysis) should be applied only to predict ordinate-data based on the measurement of abscissa-data. For applications seeking a physical interpretation of the slope and intercept (as measurable quantities), a Functional-Structural method should be applied. Therefore we applied either Ordinary Least Squares or a Functional-Structural method, as appropriate for the case at hand, along a variety of applications.

Several tasks lie ahead to continue with this line of research. Some of them are listed next:

- The spectrometer and its IPSIAM may be used to obtain high accuracy traceable measurements of line intensities for other transitions of CO₂ and for other gases as well.
- Our deconvolution algorithm may be improved using a Bayesian approach, which could be interesting to further investigate the effect of the apparatus-function (which never is the

ideal Dirac's delta) upon the line intensity measurements (especially if further improvement in the accuracy of this type of measurements is sought).

- Other, more sensible TDLAS techniques may be investigated in order to make traceable measurements with them. As part of this investigation we studied the theoretical aspects of the high frequency modulation technique on this regard and found that it was not suitable to set up a primary standard for line intensity and partial pressure measurements because the modulation factor represented a calibration factor that does not allow to realize the measurement in absolute terms, but further investigation is necessary to draw definitive conclusions about that issue.
- Our system may be used to complement line-shape studies in which different form-functions are investigated to find their suitability to describe the real form of some absorption line. Because the non-linearity of the form-functions, the optimization methods used to find their parameters produce results that are not independent from each other and there is always risk that the algorithm gets stucked in some local minimum instead of finding the "real" solution. Our system could be used to independently measure the area under the absorbance curve; this parameter is then used and kept fixed by the fit algorithm, which in turn can then find more accurately the rest of parameters, like the half width at half maximum, the Doppler-component-wide, the Lorentz-component-wide etc.
- Our IPSIAM may be used to process the data of a spectrometer having a temperature-controlled chamber. This would open a very good perspective to be able to measure the temperature dependency of line intensities and form-functions (in connection with the previous paragraph). On this regard it is worth to note the success achieved by us in the accurate measuring of the gas temperature (in spite of our lack of control of the chamber temperature). We achieved a gas temperature measurement relative uncertainty of only 0.004% ($k = 2$, about 95% level of confidence). Our strategy is worth to be recommended for all the applications which need accurate temperature measurements of the gas under study.

Finally we would like to comment that, given the successful construction of the spectrometer and the development of its IPSIAM software for its implementation as a primary standard for partial pressure measurements; the Vacuum Laboratory at the PTB may bring calibration services of partial pressure measuring instruments, at least for CO₂ for the moment, and probably also for CO and other gases in the future.

7. Appendix

7.1. Description of Data Manipulation for Line Intensity and Partial Pressure

Measurements

In order to be able to gather and process the amount of data needed to implement our method of measurement, a high degree of automatization for the collection and analysis of data was needed. To accomplish such automatization, we have written a group of programs including LabVIEW programs, Batch files with DOS-like commands, several EXCEL workbooks and several EXCEL macros; distributed in several folders of a special directory structure. All the programs and structures are part of an Integrated Processing System for Integrated Absorbance Measurements (IPSIAM).

The IPSIAM LabVIEW program stores the oscilloscope readings in files (named here o-files). Each o-file includes 5 columns of data: The first column is a time reading and corresponds to the time order of the data measured by the oscilloscope: Each time step is equal to the physical time span between two measured points of the oscilloscope scans. The other 4 columns are in order the readings from detectors one to three and from the ramp voltage. The digitizing oscilloscope is used in average mode, typically accumulating 75 scans per measurement. Each stored o-file corresponds to just one mean scan which is the result of 75 individual scans. The date and time (hh:mm:ss) is integrated in the o-file name, producing a new stored o-file for each scan. As part of the measurement procedure the o-file name must include a “wildcard” to indicate which type of measurement is being registered and to permit the corresponding automatic handling of the o-files by the IPSIAM analysis programs (to be described later). The wildcards are:

- -null- for null-absorption scan,
- -part- for partial-absorption scan and
- -tot- for total-absorption scan.

Other useful information is also included as part of the o-file names. The part of the o-file name including that useful information is called here the file base name. We operate the oscilloscope with a sample size of 2500 points; therefore each o-file contains 2500 measuring points per column, for a total of 12500 points per o-file.

If the operator chooses so, the IPSIAM LabVIEW programs can also read and/or store the readings of the PMD and TMD in files. The files containing the PMD and TMD data are called here m-files (from multimeter - files) and their names incorporate also some wildcards to permit the automatic handling of the data by the IPSIAM analysis programs. These wildcards are:

- -img- for pressure measurements made with the ionization gauge.

- -press-cdg- for pressure measurements made with the CDG.
- -press-srg1- for pressure measurements made with the SRG1.
- -press-srg2- for pressure measurements made with the SRG2.
- -resis1- for temperature measurements made with the internal PT100 #1
- -resis2- for temperature measurements made with the internal PT100 #2
- -keithley- for temperature measurements made with the 7 PT100 of the Keithley Scanner.

If these measurements are stored, the IPSIAM LabVIEW program automatically incorporates the date and hour as part of their m-file names, which are completed with their wildcards and the base name of the corresponding o-file which was written at the “same” time. If the base name is not changed by the operator, then the m-files accumulates successive readings under the same m-file name, until the hourly change gives a new hour figure, which being incorporated in the m-file name produces a new m-file for storing.

The IPSIAM analysis programs take the measured raw data stored by the IPSIAM LabVIEW program in the o-files and in the m-files and process them until the final result is found: either the line intensity or the partial-pressure. IPSIAM can handle any number of o-files from 3 (one null, one part, one tot) to 4500 (1500 of each null, part and tot) and their corresponding m-files. As part of the strategy of general applicability, we have devised a method in which the IPSIAM creates a series of name-files in which the original m-files and o-files names are stored so that the data files can be renamed to some standard numbered names which are used by the rest of the programs of IPSIAM. In this way clarity is kept about which data is being analyzed and the name of the files containing the raw data is passed along until the final result is obtained.

In order to document all the steps in using IPSIAM, we have written two sets of instructions for the operator: The general analysis protocol and the 0-normalization-protocol. They give the specific instructions that must be followed to complete the analysis procedure and contain the fields to document the decisions made by the operator.

The IPSIAM directory structure contains fifteen sub-folders, each capable to handle up to 300 o-files (100 null-files 100 partial-files and 100 total-files). The operator must copy the o-files distributed in those folders as needed, for instance using only one folder if there is less than 100 files of each type. In each sub-folder the “000rntxt.bat” must be called in order to copy the list of original file names and then rename the o-files with the generic names: null-xx.txt, part-yy.txt and tot-zz.txt, where “xx”, “yy” and “zz” stands for consecutive numbers which goes from 01 to the total number of null- partial- and total- files respectively. Then, macros in the workbook “000filenames.xls” read the text-format lists of names and create its equivalents in excel tables saved with excel format. Macros in the workbook “00txt2xls.xls” read the excel file name tables and count the total number of files for each type of scan (null-, part-, tot-) so that the next macro – “open txt and save xls” - can open each one of these files and save it with excel format (null-xx.xls, part-yy.xls and tot-zz.xls, respectively). Each one of the null-xx files are considered repetitions of the same null-measurement. The same

applies for the part-yy and tot-zz files. So the next step, accomplished by the macros in the workbook “actualizes.xls”, is to open and actualize the workbooks “asnull-v.xls”, “aspart-v.xls” and “astot-v.xls”, where “v” stands for a letter varying from a to d (fifteen workbooks in total), which have links to the null- part- and tot- files respectively. Each as***-v workbook calculates the mean and standard deviation of a column of the original files, or more explicitly:

- asnull-a.xls calculates two columns where each row is the mean (in the first column) and standard deviation (in the second column) of all the entries at that same row and first column of all the null-xx files (time measurement),
- asnull-b.xls calculates two columns where each row is the mean (in the first column) and standard deviation (in the second column) of all the entries at that same row and second column of all the null-xx files (signal from detection channel - detector #2 measurement),
- asnull-c.xls calculates two columns where each row is the mean (in the first column) and standard deviation (in the second column) of all the entries at that same row and third column of all the null-xx files (signal from reference channel - detector #1 measurement),
- asnull-d.xls calculates two columns where each row is the mean (in the first column) and standard deviation (in the second column) of all the entries at that same row and forth column of all the null-xx files (signal from frequency-marker channel - detector #3 measurement), and
- asnull-e.xls calculates two columns where each row is the mean (in the first column) and standard deviation (in the second column) of all the entries at that same row and fifth column of all the null-xx files (signal from function generator – ramp voltage measurement).

The equivalent explanation applies to the aspart-v.xls and astot-v.xls workbooks. Each of these fifteen “as***-v.xls” workbooks also reads and stores the list of names of the original files they are processing.

Once all the “as***-v.xls” workbooks have been actualized in all the sub-folders used, the operator goes to the parent folder and opens and actualize the workbooks “average-stddev-abs-null.xls”, “average-stddev-abs-part.xls” and “average-stddev-abs-tot.xls”. On opening these workbooks update their links to all the “as***-v.xls” files in all the sub-folders, so that the overall average and standard deviation of each row of the five columns are calculated for the null-, part-and tot- scans respectively.

In a similar way as described above, the m-files are read and processed to give their information to the last workbook of IPSIAM. This last workbook is called “0normalization-yymmdd-particular-name.xls”, where “yymmdd” stands for the year, month and day of the measurement date of the files being processed, and the “particular-name” contains the rest of information given by the operator to identify this final-result workbook properly. That information is given through a “save as” command so that the entire workbook is reproduced and the final result is saved in the workbook containing also all the information needed to evaluate the whole

measurement. When the “0-normalization-***” workbook is updated, its links to the “average-stddev-abs-null.xls”, “average-stddev-abs-part.xls”, “average-stddev-abs-tot.xls workbooks, as well as to the press-01.xls, resis-01.xls, srg-01.xls and srg-02.xls workbooks are actualized. Based on this information, and in some instructions and data given by the operator after looking to some control-graphs, this workbook performs automatically all the operations needed to find the “absorbance vs. wave-number” curve (see sections 3.7 and 3.8) and performs its numerical integration to give what we call the integrated absorbance or absorbance-area A_{abs} (see section 3.9).

This workbook calculates also the gas density n (see section 3.4) and the total absorbing path-length L (see section 3.3.2), so that the line intensity S at the measured temperature T is calculated also in this workbook as:

$$S(T) = \frac{A_{abs}}{n \cdot L} \quad (207)$$

Finally the transformation to reference temperature T_0 of both, the integrated absorbance $A_{abs}(T_0)$ and the line intensity $S(T_0)$ is made.

$$S(T_0) = \frac{A_{abs}(T_0)}{n \cdot L} \quad (208)$$

A modified version of the “0-normalization-***.xls” workbook, called “0 - pp -normalization - ***.xls” performs the same tasks as the previous one, but, at the end of IPSIAM, this program calculates the partial pressure of the absorbing gas P_i based on the known line intensity S of the absorption line observed, and on the other measurements including the absorbance-area A_{abs} and temperature T , according to the formula:

$$P_i = \frac{A_{abs} \cdot k \cdot T \cdot 10^6}{S \cdot L} \quad (209)$$

When the absorbing gas is a component of known concentration c of a certified mixture, the measurement of the partial pressure P_i is verified through the measurement of the total pressure P and the relation:

$$P_i = c \cdot P \quad (210)$$

7.2. Certificates of Calibration (mini-copies)

SRG 1
QS 1/05

Interne Kalibrierung
Laboratorium Vakuummetrologie der PTB in Berlin

Interne Nummer: QS 1/05
Gegenstand: Kugeltrotter aus Edelstahl für ein Gasreibungsvakuummeter, Kugel 4,7/195VAGG, Durchmesser 4,762 mm, an Eckventil CF16, Finger Nr. 12.

QS-Kartei Bez.: SRG-PTB-86-195
Prüfmittelnr.: keine
Hersteller: Im Labor vorbereitete Kugel.
Verwendung: Totaldruckmessung Herriottzelle
Datum: Die Kalibrierungen wurden am 11.11.04, 12.11.04 und am 7.1.05 durchgeführt.

1. Kalibrierung
Mit Hilfe der kontinuierlichen Expansion am Primärnormal CE2 des Labors wurde der effektive Energie- und Impulsaustauschkoefizient $\sigma(p)$ für Stickstoff, Kohlenmonoxid und Kohlendioxid im Bereich $1 \cdot 10^{-3}$ mbar bis $3 \cdot 10^{-3}$ durch Mittelwertbildung aus 5 Einzelwerten bestimmt. Die Kugel wurde vor der Kalibrierung ausgeheizt.
Die Raumtemperatur betrug $23,6^\circ\text{C} \pm 1,1^\circ\text{C}$. Diese relativ starke Temperaturschwankung wird durch eine unzureichende Klimatisierung verursacht, jedoch von der nur schwache Temperaturabhängigkeit von σ egalisiert.
Für σ ergab sich:

Werte von σ	
Stickstoff	1,101
CO	1,102 ¹
CO ₂	1,110

¹Zum Zeitpunkt der Kalibrierung lagen noch keine Werte für die Rückströmung R für CO und CO₂ vor. Es wurde deshalb unter der Maßgabe N₂ bzw. Ar kalibriert. Die kürzlich ermittelten Werte $R(\text{CO})$ bzw. $R(\text{CO}_2)$ zeigten, dass ein Faktor $f(\text{CO}) = 1$ bzw. $f(\text{CO}_2) = 0,90815$ multipliziert werden muß (die genannten Werte beinhalten diesen). Dieser ergibt sich vor allem durch die verschiedenen molaren Massen.

Seite 1

QS 1/05

Der Offset lag um $1,9 \cdot 10^{-7}$ l/s (DCR).
Die Auslese erfolgte in DCR. Bei den Berechnungen von σ wurden folgende Parameter benutzt:

Molekulargewichte:	
N ₂	28,013
CO	28,011
CO ₂	44,01 ^(SRG)
Kugeldurchmesser	4,762 mm
Dichte	7,715 g/cm ³
Viskosität	0
Akkommodation	1

Bei Druckmessungen sind diese Werte ebenfalls einzusetzen, für die Akkommodation jedoch die oben angegebenen Werte für σ . Die Kalibrierermethode erlaubt keine Aussage über die Druckabhängigkeit von σ (bei Viskosität = 0).²

Die verwendeten Originalmeldedaten befinden sich auf folgendem Datenträger:
CE2 Daten:
~\vakuum\Messplacetze\CE2\messprotokolle\2004\11121.txt (N₂)
~\vakuum\Messplacetze\CE2\messprotokolle\2004\11121.txt (CO)
~\vakuum\Messplacetze\CE2\messprotokolle\2005\0107.txt (CO₂)

SRG Daten:
hock04@c72324-~\data\Nov-04* (N₂) und (CO)

² Aus QS 3/02: „Wegen der Druckabhängigkeit von σ (bei Viskosität = 0) ist die Druckanzeige mit einem Korrekturfaktor $f(p)$ zu multiplizieren. Der tatsächliche Druck p ergibt sich dann aus dem angezeigten Druck p_a (mit dem einkalibrierten σ im Kontrollgerät) und dem Korrekturfaktor $f(p)$ aus der Gleichung

$$p_r = p_a \cdot f(p_a)$$

Wenn p_a in mbar angegeben wird, ergibt sich $f(p_a)$ bei diesem Rotor bis 0,01 mbar mit hinreichender Genauigkeit aus folgenden Gleichungen:

Stickstoff	$f(p_a) = 1 + 2,22 \cdot p_a$
Argon	$f(p_a) = 1 + 1,89 \cdot p_a$

Seite 2

QS 1/05

hock04@c72324-~\data\Jan-05* (CO₂)

2. Unsicherheiten
(a) Unsicherheit von σ für N₂ zum Zeitpunkt der Kalibrierung:
Diese setzt sich zusammen aus (für alle Angaben erweiterte relative Meßunsicherheit U , mit $k=2$):
Unsicherheit des Kalibriendrucks: $U_1(1) = 0,88 \%$
Unsicherheit durch Orientierungsabhängigkeit von σ : $U_1(2) = 0,10 \%$
Statistische Meßunsicherheit: $U_1(3) = 0,10 \%$
Systematische Unsicherheit der Untergrundmessung: $U_1(4) = 0,00 \%$
In der statistisch ermittelten Messunsicherheit ist die Unsicherheit bedingt durch die Frequenzabhängigkeit des Offsets sowie die Messunsicherheit des Offsets selbst mit berücksichtigt.
Dies ergibt, gerundet, eine totale erweiterte Unsicherheit (relativ) zum Zeitpunkt der Kalibrierung von

$$U_1(\sigma_0) = 0,90 \%$$

(b) Langzeitstabilität:
Langzeitversuche der PTB haben ergeben, dass relative Änderungen von σ innerhalb eines Jahres kaum über 1 % liegen, vorausgesetzt, die Kugel wurde sorgfältig behandelt.
Die Ergebnisse der bisherigen Kalibrierungen an dieser Kugel ergeben sich aus folgender Tabelle:

Kalibrierung	Datum	σ_0 für N ₂	Diff. z. letzten Kalibr.	σ_0 für Ar	Diff. z. letzten Kalibr.
an SE1	5'88			1,107	
QS 3/97	5'97	1,105		1,107	0,0%
QS 3/02	2'02	1,105	0,0%	1,107	0,0%
hier	1'05	1,076	-0,27%		

Die Langzeitstabilität wird mit 0,1 % pro Jahr (erweiterte Standardunsicherheit $k = 2$) abgeschätzt.
(c) Restabbremsung:

Seite 3

QS 1/05

Bei der Ermittlung der Gesamtunsicherheit von Druckmessungen ist noch der Einfluss der Schwankungen der Restabbremsung, sowie deren Drehzahlabhängigkeit, zu beachten. Bei der Messung stationärer Drücke kann der Einfluss der statistischen Schwankungen durch Mittelwertbildung aus einer größeren Zahl von Messungen verringert werden. Die Drehzahlabhängigkeit der Restabbremsung muss gesondert bestimmt werden. Stärkere Erschütterungen oder Stöße können die Restabbremsung erheblich erhöhen. Das Ausmaß derartiger Messwertbeeinflussungen ist von den örtlichen Verhältnissen abhängig und vom Benutzer abzuschätzen.

(d) Statistische Messunsicherheit.
Die Messunsicherheit zum Zeitpunkt der Nutzung als Sekundärnormal ist aus (a) bis (d) zusammenzusetzen.

3. Besondere Hinweise
(a) Der kalibrierte Rotor sollte nur mit dem zugehörigen, bei der Kalibrierung benutzten Meßrohr verwendet werden.
(b) Bei stabilen Temperaturverhältnissen am Messkopf wird die Restabbremsung am genauesten durch eine Langzeitmessung (12 h) bestimmt. Bei ungleicher Temperatur wird der so ermittelte Wert dann auch während der Messung verwendet. Liegen keine stabilen Temperaturverhältnisse vor, ist es ratsam, für Präzisionsmessungen eine Messung der Restabbremsung (über etwa 5 min.) vor und nach den Messungen vorzunehmen. Dieses Verfahren berücksichtigt auch eine mögliche Frequenzabhängigkeit des Offsets.
(c) Ein "Abstürzen" der Kugel (bei Unterbrechung der magnetischen Aufhängung ohne vorheriges Abbremsen der Umdrehungen) kann eine Veränderung von σ bewirken.
(d) Bei Nichtbenutzung sollte der Rotor im Vakuum oder wasserdampffreier Atmosphäre aufbewahrt werden. Der Rotor sollte nur mit einer Pinzette angefasst werden. Die maximale Ausheiztemperatur beträgt 300°C.

4. Rekalibrierung

Seite 4

SRG2

QS 2/05

Interne Kalibrierung

Laboratorium Vakuummetrologie der PTB in Berlin

Interne Nummer: QS 2/05

Gegenstand: Kugelrotor aus Edelstahl für ein Gasreibungsvakuummeter, Kugel Durchmesser 4,762 mm, an Eckventil CF16, Finger Nr. 21UM.

QS-Kartei Bez.: keine

Prüfmittelnr.: keine

Hersteller: Im Labor vorbereitete Kugel.

Verwendung: Totdruckmessung Herriottzelle

Datum: Die Kalibrierungen wurden am 11.11.04, 12.11.04 und am 7.1.05 durchgeführt.

1. Kalibrierung

Mit Hilfe der kontinuierlichen Expansion am Primärnormal CE2 des Labors wurde der effektive Energie- und Impulsaustauschkoeffizient $\sigma(p)$ für Stickstoff, Kohlenmonoxid und Kohlendioxid im Bereich $1 \cdot 10^{-4}$ mbar bis $3 \cdot 10^{-4}$ durch Mittelwertbildung aus 5 Einzelwerten bestimmt. Die Kugel wurde vor der Kalibrierung ausgeheizt.

Die Raumtemperatur betrug $23,6^{\circ}\text{C} \pm 1,1^{\circ}\text{C}$. Diese relativ starke Temperaturschwankung wird durch eine unzureichende Klimatisierung verursacht, jedoch von der nur schwache Temperaturabhängigkeit von σ egalisiert.

Für σ_0 ergab sich:

Werte von σ_0	
Stickstoff	1,154
CO	1,152 ^{*)}
CO ₂	1,158 ^{*)}

^{*)} Zum Zeitpunkt der Kalibrierung lagen noch keine Werte für die Rückströmung R für CO und CO₂ vor. Es wurde deshalb unter der Maßgabe N₂ bzw. Ar kalibriert. Die kürzlich ermittelten Werte $R(\text{CO})$ bzw. $R(\text{CO}_2)$ zeigten, dass ein Faktor $f(\text{CO}) = 1$ bzw. $f(\text{CO}_2) = 0,90815$ multipliziert werden muß (die genannten Werte beinhalten diesen).

Seite 1

QS 2/05

Der Offset lag um $1,9 \cdot 10^{-7}$ 1/s (DCR).

Die Auslese erfolgte in DCR. Bei den Berechnung von σ_0 wurden folgende Parameter benutzt:

Molekulargewichte:

N ₂	28,013
CO	28,011
CO ₂	44,01 ⁽²⁸⁷⁰⁾
Kugeldurchmesser	4,762 mm
Dichte	7,715 g/cm ³
Viskosität	0
Akkommodation	1.

Bei Druckmessungen sind diese Werte ebenfalls einzusetzen, für die Akkommodation jedoch die oben angegebenen Werte für σ_0 . Die Kalibriermethode erlaubt keine Aussage über die Druckabhängigkeit von σ (bei Viskosität = 0). ^{**)}

Die verwendeten Originalmeßdaten befinden sich auf folgendem Datenträger:

CE2 Daten:

~/vakuum/Messplaezte/CE2/messprotokolle/200411121.txt (N₂)

~/vakuum/Messplaezte/CE2/messprotokolle/200411121.txt (CO)

~/vakuum/Messplaezte/CE2/messprotokolle/20050107.txt (CO₂)

SRG Daten:

hock04@e72324-~/data/Nov-04/* (N₂) und (CO)

hock04@e72324-~/data/Jan-05/* (CO₂)

2. Unsicherheiten

(a) Unsicherheit von σ_0 für N₂ zum Zeitpunkt der Kalibrierung:

Diese setzt sich zusammen aus (für alle Angaben erweiterte relative Meßunsicherheit U , mit $k=2$):

^{**) Aus QS 3/02: Der tatsächliche Druck p_s ergibt sich dann aus dem angezeigten Druck p_i (mit dem einkalibrierten σ_0 im Kontrollgerät) und dem Korrekturfaktor $f(p)$ aus der Gleichung}

$$p_s = p_i \cdot f(p_i)$$

Wenn p_i in mbar angegeben wird, ergibt sich $f(p_i)$ bei diesem Rotor bis 0,01 mbar mit hinreichender Genauigkeit aus folgenden Gleichungen:

Stickstoff	$f(p) = 1 + 2,22 \cdot p_i$
Argon	$f(p) = 1 + 1,89 \cdot p_i$

Seite 2

QS 2/05

Unsicherheit des Kalibrierdrucks:

$U_i(1) = 0,38 \%$

Unsicherheit durch Orientierungsabhängigkeit von σ_0 :

$U_i(2) = 0,10 \%$

Statistische Meßunsicherheit:

$U_i(3) = 0,12 \%$

Systematische Unsicherheit der Untergrundmessung:

$U_i(4) = 0,00 \%$

In der statistisch ermittelten Messunsicherheit ist die Unsicherheit bedingt durch die Frequenzabhängigkeit des Offsets sowie die Messunsicherheit des Offsets selbst mit berücksichtigt.

Dies ergibt, gerundet, eine totale erweiterte Unsicherheit (relativ) zum Zeitpunkt der Kalibrierung von

$U_r(\sigma_0) = 0,90 \%$

(b) Langzeitstabilität:

Langzeitversuche der PTB haben ergeben, dass relative Änderungen von σ_0 innerhalb eines Jahres kaum über 1 % liegen, vorausgesetzt, die Kugel wurde sorgfältig behandelt.

Die Ergebnisse der bisherigen Kalibrierungen an dieser Kugel ergeben sich aus folgender Tabelle:

Kalibrierung	Datum	σ_0 für N ₂	Diff. z. letzten Kalibr.	σ_0 für Ar	Diff. z. letzten Kalibr.
	05/04	1,153			
hier	11/04	1,154	0,09%		

Die Langzeitstabilität wird mit 0,1 % pro Jahr (erweiterte Standardunsicherheit $k = 2$) abgeschätzt.

(c) Restabbremsung:

Bei der Ermittlung der Gesamtunsicherheit von Druckmessungen ist noch der Einfluss der Schwankungen der Restabbremsung, sowie deren Drehzahlabhängigkeit, zu beachten. Bei der Messung stationärer Drücke kann der Einfluss der statistischen Schwankungen durch Mittelwertbildung aus einer größeren Zahl von Messungen verringert werden. Die Drehzahlabhängigkeit der Restabbremsung muss gesondert bestimmt werden. Stärkere Erschütterungen oder Stöße können die Restabbremsung erheblich erhöhen. Das Ausmaß derartiger Messwertbeeinflussungen ist von den örtlichen Verhältnissen abhängig und vom Benutzer abzuschätzen.

Seite 3

QS 2/05

(d) Statistische Messunsicherheit.

Die Messunsicherheit zum Zeitpunkt der Nutzung als Sekundärnormal ist aus (a) bis (d) zusammenzusetzen.

3. Besondere Hinweise

(a) Der kalibrierte Rotor sollte nur mit dem zugehörigen, bei der Kalibrierung benutzten Meßrohr verwendet werden.

(b) Bei stabilen Temperaturverhältnissen am Messkopf wird die Restabbremsung am genauesten durch eine Langzeitmessung (12 h) bestimmt. Bei ungeländerter Temperatur wird der so ermittelte Wert dann auch während der Messung verwendet. Liegen keine stabilen Temperaturverhältnisse vor, ist es ratsam, für Präzisionsmessungen eine Messung der Restabbremsung (über etwa 5 min.) vor und nach den Messungen vorzunehmen. Dieses Verfahren berücksichtigt auch eine mögliche Frequenzabhängigkeit des Offsets.

(c) Ein "Abstürzen" der Kugel (bei Unterbrechung der magnetischen Aufhängung ohne vorheriges Abbremsen der Umdrehungen) kann eine Veränderung von σ_0 bewirken.

(d) Bei Nichtbenutzung sollte der Rotor im Vakuum oder wasserdampffreier Atmosphäre aufbewahrt werden. Der Rotor sollte nur mit einer Pinzette angefasst werden. Die maximale Ausheiztemperatur beträgt 300°C.

4. Rekalibrierung

Das Messgerät sollte abhängig von der je nach Verwendung tolerierbaren Langzeitstabilität rekalibriert werden.

Berlin, den 4. April 2005

Th. Bock

Laboratorium für Vakuummetrologie

Seite 4

158

Interne Kalibrierung

Laboratorium Vakuummetrologie der PTB in Berlin

Interne Nummer: QS 04/05
 Gegenstand: Kapazitives Membrandruckmessgerät, Messkopf MKS-Baratron Head, Type 690A13TRA, Messbereich bis 1000 Torr.
 Fabr.-Nr.: Serial 93106102A
 QS-Kartei Bez.: keine
 PN: keine
 Zubehör: Electr. 270C-5 SN: 93103202A und HP 345401A DMM SN 3146A31944
 Hersteller: MKS Instruments, Inc., Burlington, Mass., USA
 Verwendung: Das Gerät wird zur Messung des Totaldrucks an der Heriottzeile verwendet.
 Datum: Die Kalibrierung wurde am 13.07.2005 durchgeführt.

1. Kalibrierbeschreibung

Das Gerät wurde von 1 mbar bis 1300 mbar mit Stickstoff kalibriert. Der Spannungsausgang (Analogausgang 0-10V) des MKS-Gerätes wurde auf den Eingang des HP DMM gegeben und über die IEEE-Schnittstelle vom Messprogramm erfasst.

Schalterstellungen am Gerät bei der Kalibrierung:

Response: "Norm"
 Heater: "Reg"
 Range: "1" (1 mbar bis 13 mbar),
 „1" (20 mbar bis 1300 mbar)

Die Kalibrierung wurde durch statische Expansion und direkten Vergleich mit dem RUSKA 7010 (PN: 7.3-4012) an SE2 (letzte Kalibrierung 11/04, QS 08/0-4) gewonnen. Die relative Unsicherheit des Verfahrens ist in Abschnitt 4 behandelt.

Die Raumtemperatur betrug $(23,0 \pm 0,1)^\circ\text{C}$.

2. Hinweise

Zur Stabilisierung des Nullpunkts wird der Messkopf automatisch auf etwa 50°C temperiert. Zur Erreichung einer stabilen Temperaturverteilung wird empfohlen, die Elektronik und die Temperierung über Nacht vor Beginn der Messungen einlaufen zu lassen.

Es ist darauf zu achten, dass der Messkopf erschütterungsfrei angeschlossen wird.

3. Ergebnisse

Die folgende Tabelle gibt den Kalibrierdruck, die am DMM gemessene Spannung U und den Kalibrierfaktor p/U (p Kalibrierdruck) an.

p_{cal} in mbar	Anzeige in V	$p_{\text{cal}}/\text{Anzeige}$ in mbar/V
1,291E+00	9,689E-02	13,350
1,988E+00	1,499E-01	13,376
2,982E+00	2,234E-01	13,347
4,969E+00	3,719E-01	13,363
8,940E+00	6,694E-01	13,366
1,282E+01	9,586E-01	13,369
1,299E+01	9,730E-01	13,352
1,299E+02	9,733E+00	13,346
2,000E+02	1,499E+01	13,346
2,001E+02	1,499E+01	13,345
2,999E+02	2,248E+01	13,344
5,000E+02	3,748E+01	13,341
8,999E+02	6,748E+01	13,336
1,300E+03	9,755E+01	13,326
1,992E+01	1,492E+00	13,355
2,983E+01	2,242E+00	13,351
5,000E+01	3,748E+00	13,347
9,002E+01	6,744E+00	13,348
1,300E+02	9,742E+00	13,347
2,000E+02	1,499E+01	13,347
3,000E+02	2,248E+01	13,346
5,000E+02	3,747E+01	13,342
9,000E+02	6,748E+01	13,337
1,300E+03	9,755E+01	13,326

4. Unsicherheiten

Folgende Unsicherheiten sind bei der Benutzung als Referenznormal in Betracht zu

- (1) Relative Standardunsicherheit ($1-\sigma$) des Kalibrierdrucks: u_1 .

$$u_1 = 1,1 \cdot 10^{-3} \text{ (bis 10 mbar)}$$

$$u_1 = 1,3 \cdot 10^{-4} \text{ (ab 10 mbar)}$$

- (2) Digitalisierungsfehler ($4 \cdot 10^{-6}$) bei 5 angezeigten Stellen ist zu vernachlässigen: $u_2=0$.

- (3) Sofern das Gerät nicht mit dem zur Prüfung verwendeten Digitalanzeigergerät benutzt wird, ist die relative Unsicherheit u_3 des zur Anzeige gesetzten Gerätes (z.B. Digitalvoltmeters) zu berücksichtigen, die vom Betreiber zu ermitteln ist.

- (4) Geschätzte Langzeitinstabilität bis zur Rekalisierung u_4 : Langjährige Untersuchungen an ähnlichen Geräten haben gezeigt, dass die relative Langzeitinstabilität (Standardunsicherheit) etwa $1 \cdot 10^{-3}$ pro Jahr ist. Dies schließt die Langzeitinstabilität des verwendeten DMM ein.

Kalibrierung	Datum	p/U bei 1300 mbar in mbar/Volt	Veränderung gegen letzte Kalibrierung
hier	705	13,326	

Es wird eine Langzeitinstabilität/Jahr von

$$u_4 = 1 \cdot 10^{-3}$$

verwendet.

- (5) Durch Temperaturunterschiede zwischen Kalibrierung und bei Verwendung sind Empfindlichkeitsänderungen durch Temperaturänderungen zu berücksichtigen. Nach Herstellerangaben betragen diese:

$$u_5 < 4 \cdot 10^{-5} \text{ (von Anzeige)}$$

- (6) Die maximale Nichtreproduzierbarkeit des Gerätes wird mit $2 \cdot 10^{-3}$ vom Vollauschlag angegeben.

$$u_6 = 2 \cdot 10^{-3}$$

- (7) Die Nullpunktschwankungen bei konstantem Druck betragen in Einheiten des Drucks etwa $1 \cdot 10^{-2}$ mbar.

$$u_7 = 1 \cdot 10^{-2} \text{ (von Anzeige)}$$

- (8) Die relative Gesamtunsicherheit der Druckanzeige ist aus den Beiträgen u_1 bis u_7 zusammensetzen:

$$u_8 = \sqrt{u_1^2 + u_2^2 + u_3^2 + u_4^2 + u_5^2 + u_6^2 + u_7^2}$$

Üblicherweise wird für Kalibrierungen u_8 zur erweiterten Messunsicherheit U (Erweiterungsfaktor $k=2$) $U \sim 2u_8$ ergänzt. Die maximale Nichtreproduzierbarkeit dominiert bei diesem Gerät für den kalibrierten Bereich bei weitem.

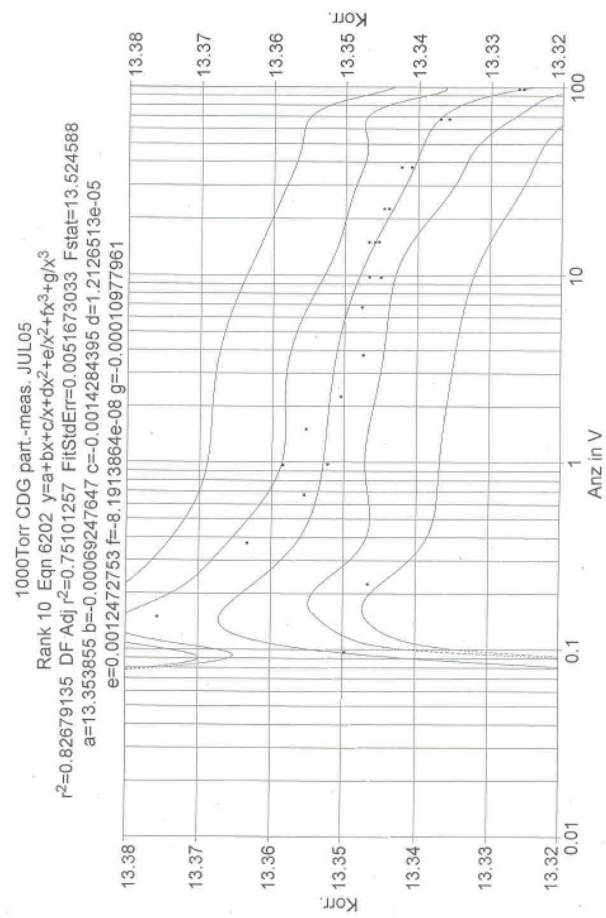
5. Rekalisierung

Abhängig von der je nach Verwendung tolerierbaren Langzeitstabilität sollte das Meßsystem rekaliert werden, hier spätestens nach 12 Monaten.

Berlin, den 18. Juli 2005

Thomas Bock

Laboratorium für Vakuummetrologie



Interne Kalibrierung

Laboratorium Vakuummetrologie der PTB in Berlin

Interne Nummer: QS 8/05
 Gegenstand: Kapazitives Membrandruckmessgerät, Messkopf MKS-Baratron Head, Modell 690A11TRB, Messbereich bis 10 Torr.
 Fabr.-Nr.: Serial 93109105A
 QS-Kartei Bez.: -
 PM-Nr.: -
 Zubehör: Signal Conditioner: 270 C-5, SN: 93103202A und HP 34401A, SN: 3146A31944, Inv.Nr. 94008862
 Hersteller: MKS Instruments, Inc., Burlington, Mass., USA
 Verwendung: Das Gerät wird zur Messung des Totdrucks an der Heriotzelle verwendet.
 Datum: Die Kalibrierung wurde am 01.04.2004 durchgeführt.

1. Kalibrierbeschreibung

Das Gerät wurde unter Berücksichtigung der Gebrauchsanleitung in Betrieb genommen und im Druckbereich 10^{-2} mbar bis 13 mbar mit dem Prüfgas Stickstoff kalibriert. Die Ausgangsspannung des Signal Conditioners wurde dabei auf den Eingang des Multimeters HP 34401A gegeben und über die GBIP Schnittstelle vom Messprogramm ausgelesen.

Zur Prüfdruckeinstellung wurde das Verfahren der stufenweisen Druckerniedrigung durch Expansion (statisches Verfahren) an der Apparatur SE2 des Labors angewandt. Die relative Unsicherheit der Prüfdruckeinstellung ist unter Abschnitt 5 angegeben.

Schalterstellungen am Gerät bei der Kalibrierung:

Response: "fast"
 Heater: "Reg"
 Sensor Range: 10
 Range select: 0,1 (10^{-2} mbar ... 1 mbar)
 1 (1 mbar ... 13 mbar)

Die Kalibrierungen wurden bei einer Raumtemperatur von ca. 23°C durchgeführt.

Seite 7/7

Nullpunkt Konstanz

Zur Stabilisierung des Nullpunkts wird der Messkopf automatisch auf etwa 45°C temperiert. Zur Erreichung einer stabilen Temperaturverteilung wird empfohlen, die Elektronik und die Temperierung über Nacht vor Beginn der Messungen einlaufen zu lassen. Zur Vermeidung nicht erfassbarer Nullpunktänderungen - insbesondere im unteren Messbereich sollte möglichst unmittelbar vor jeder Druckmessung der Nullpunkt bei einem Eingangsdruck von kleiner als $1 \cdot 10^{-4}$ mbar neu eingestellt werden.

Sofern das Betriebsgerät einschließlich des Messkopfes bereits eingelaufen ist, sollte nach dem Evakuieren mit dem Beginn der Messungen unter häufiger Nullpunktkontrolle mindestens 30 Minuten gewartet werden, um den Einfluss stärkerer Nullpunktänderungen zu vermeiden.

Es ist darauf zu achten, dass der Messkopf erschütterungsfrei angeschlossen wird, da die Nullpunktstabilität von auftretenden Stößen abhängig ist. Bei Belastung des Gerätes über den vorgesehenen maximalen Differenzdruck (13 mbar) hinaus muss bis zur nächsten Messung 6-12 Stunden gewartet werden, um auftretende Hysteresiseffekte vernachlässigen zu können (Erfahrungswert). Die Kalibrierwerte können durch solche eine Überbelastung ungültig werden (Kontrolle).

2. Definition des Anzeigefehlers

Die in Abschnitt 4 angegebenen Resultate geben den relativen Fehler F der Druckanzeige wieder. F ist definiert als

angezeigter Wert p_{an} minus richtiger Wert p , dividiert durch den richtigen Wert

$$F = \frac{p_{\text{an}} - p}{p}$$

so dass sich der wahre Druck ergibt aus

$$p = \frac{p_{\text{an}}}{F + 1}$$

3. Ergebnisse

Das Ergebnis ist in der nachstehenden Tabelle wiedergegeben. Sie gibt den Kalibrierdruck, den angezeigten Wert des Prüflings und den Fehler nach Abschnitt 3 wieder:

Seite 2

p_{cal} in mbar	p_{ind} in mbar	e in %
1,298E-02	1,334E-02	2,74
1,989E-02	2,039E-02	2,48
2,967E-02	3,047E-02	1,99
4,977E-02	5,050E-02	1,48
8,967E-02	9,035E-02	0,87
1,293E-01	1,301E-01	0,55
1,990E-01	1,995E-01	0,26
2,988E-01	2,993E-01	0,16
4,976E-01	4,977E-01	0,02
8,951E-01	8,947E-01	-0,04
1,293E+00	1,292E+00	-0,06
1,989E+00	1,988E+00	-0,07
4,971E+00	4,966E+00	-0,09
8,943E+00	8,932E+00	-0,12
1,291E+01	1,289E+01	-0,16
Mittelwert (1 mbar ... 10 mbar):		-0,09%
F_{av}		-0,08%

Die verwendeten Originalmessdaten befinden sich auf folgendem Datenträger:

F:\vakuum\Messplatz\SE2\daten\rohdaten\se2_xx mit xx= 78

Kopien und Auswertung der Datenfiles befinden sich unter:

F:\vakuum\Messplatz\SE2\daten\messprotokolle\se2_78_part_pres_meas.xls

4. Unsicherheiten

Folgende relative Standardunsicherheiten sind bei der Benutzung als Referenznormal in Betracht zu ziehen:

- (1) Relative Standardunsicherheit (1- σ) der PTB-Prüfdruckeinstellung u_1

$$u_1 < 1,4 \cdot 10^{-3}$$

Seite 3

- (2) Digitalisierungsfehler: Statistische relative Unsicherheit u_2 ist ± 1 Digit mal 0,29 gemäß ISO-Richtlinie dividiert durch den Anzeigewert.

$$u_2 = 0,29 \cdot 10^{-4} \text{ mbar}/p_{\text{an}}$$

- (3) Sofern das Gerät nicht mit der zur Prüfung verwendeten Messkette benutzt wird, ist die Unsicherheit u_3 der neuen Messkette zu berücksichtigen, die vom Betreiber zu ermitteln ist.

- (4) Geschätzte Langzeitstabilität bis zur Rekalibrierung u_4

Langjährige Untersuchungen an ähnlichen Geräten haben gezeigt, dass die relative Langzeitstabilität (Standardunsicherheit) im allgemeinen zwischen $1 \cdot 10^{-3}$ und $3 \cdot 10^{-3}$ pro Jahr liegt.

In der folgenden Tabelle ist der zwischen 1 mbar und 10 mbar gemittelte Anzeigefehler bei den bisherigen Kalibrierungen angegeben.

Kal.schein (Datum)	Mittelwert Fehler Stickstoff 1 ... 10 mbar	Differenz zur letzten Kalibrierung
QS 7/94 (7/94)	0,27%	
hier (QS8/05)	-0,09%	+0,36%

Es wird abgeschätzt ($k=1$): $u_4 = 2 \cdot 10^{-3}$ über 2 Jahre (0,1% pro Jahr).

- (5) Die vom Hersteller angegebene Nichtreproduzierbarkeit u_5 (einschl. Nichtlinearität und Hysterese) des Geräts wird mit $8 \cdot 10^{-4}$ von der Anzeige angegeben. Ein Vergleich der Fehlerwerte in der Nähe des Vollauschlags unter ähnlichen Temperaturbedingungen bei verschiedenen Gasen und unter Wiederholungsbedingungen bei einem ähnlichen Gerät (siehe QS 7/97) zeigte, dass die Nichtreproduzierbarkeit in aufsteigender Druckfolge (= Benutzungsart des Geräts) eher im Bereich von $3 \cdot 10^{-4}$ (67% Vertrauensintervall) liegt.

$$u_5 = 3 \cdot 10^{-4} \quad p \geq 1 \text{ mbar}$$

Für den Übergangsbereich der thermischen Transpiration erscheint jedoch die Herstellerangabe realistisch:

$$u_5 = 8 \cdot 10^{-4} \quad p < 1 \text{ mbar}$$

- (6) Die Temperaturverhältnisse beeinflussen neben der thermischen Transpiration vor allem das Verhalten des Messkopfes und Vorverstärkers und in wesentlich geringerem Maße auch die

Seite 4

weitere Messkette. Es sollte von einem relativen Einfluß von etwa $5 \cdot 10^{-4}/K$ ausgegangen werden, d.h. bei 1 K Unterschied zwischen Kalibrier- und späteren Betriebsbedingungen von

$$n_E = 5 \cdot 10^5$$

(7) Nullpunktschwankungen. Während der Messung nicht erfassbare Nullpunktschwankungen bewirken eine relative Standardunsicherheit von

$$w_7 = 5 \cdot 10^{-6} \text{ mbar/p}$$

(8) Abweichung durch Fikturve. Durch Anpassung einer Funktion an die Tabellenwerte und Benutzung der Anpassungsfunktion für spätere Messungen können Abweichungen sowohl im Interpolationsbereich zwischen Kalibrierpunkten als auch an den Kalibrierpunkten selbst auftreten. Diese sollten allerdings innerhalb der statistischen Schwankungen von Wiederholungsmessungen liegen (siehe oben Nr. 5) und es wird davon ausgegangen, dass dadurch keine wesentliche zusätzliche Unsicherheit zu berücksichtigen ist. Dies ist jedoch im Einzelfall vom Anwender der Anpassungskurve zu überprüfen.

(9) Trotz der identischen Molekülmassen von N_2 und CO muß ein zusätzlicher Unsicherheitsbeitrag durch unterschiedliches Adsorptionsverhalten einbezogen werden. Dieser wird mit ca. 0,1% abgeschätzt.

$$m_{\ell} = 1 \cdot 10^{-3}$$

(10) Die relative Gesamtunsicherheit der Druckanzeige ist aus den Anteilen u_1 bis u_5 zusammenzusetzen:

$$u_c = \sqrt{u_1^2 + u_2^2 + u_3^2 + u_4^2 + u_5^2 + u_6^2 + u_7^2 + u_8^2}$$

Üblicherweise wird für Kalibrierungen u_c die erweiterte relative Messunsicherheit $U_c = 2 u_c$ (Erweiterungsfaktor $k=2$) verwendet. Diese ist im vorliegenden Fall beispielsweise 0,55 % für 1 mbar.

5. Hinweise für den Nutzer

Die Kalibrierkurve $F(p)$ hängt von der Gastemperatur ab. Im molekularen Strömungsgebiet ist der Druck $p(T_2)$ im temperierten Messkopf gegeben durch

$$\frac{p(T_2)}{p(T_1)} = \sqrt{\frac{T_2}{T_1}}$$

wenn T_1 die Gastemperatur weit weg vom Messkopf (z.B. im Primärnormal) bezeichnet und die Temperaturen in Kelvin angegeben sind. Ändert sich T_1 beim Nutzer wesentlich gegenüber der bei der Kalibrierung (mehr als ein Grad) und ist Genauigkeit im 0,1% Bereich angestrebt, so ist F im molekularen Strömungsgebiet und im Übergangsgebiet gemäß dem obigen Wurzelverhältnis den tatsächlichen Temperaturverhältnissen anzupassen. Man erhält den richtigen Druck p_0 , wenn F durch F'

$$F' = F_{\text{var}} + (F - F_{\text{var}}) \left(\frac{\sqrt{\gamma_2/\gamma_1} - 1}{\sqrt{\gamma_2/\gamma_1} + 1} \right)$$

ersetzt wird. Dabei ist F der Fehler, der aus der Kalibrierung erhalten wurde, F_0 der mittlere Fehler im viskosen Bereich, T_j die Gastemperatur zum Zeitpunkt der Kalibrierung, T_i' zum Zeitpunkt der Nutzung, T_j die Temperatur im Messkopf (45°C oder 318,15 K) (alle Temperaturen in Kelvin!).

Beispiel: Bei der Kalibrierung sei $T_1 = 298,15 \text{ K}$, bei der Anwendung sei $T_2 = 296,15 \text{ K}$. Es ist $T_2 = 318,15 \text{ K}$. Gesucht wird der wahre Druck bei der Anzeige $0,01 \text{ mbar}$. Während der Kalibrierung betrug der Anzeigefehler bei $0,01 \text{ mbar}$ $5,2 \%$, im viskosen Bereich $2,0\%$, die Differenz somit $3,2\%$. Der relative Anzeigefehler in $\%$ ist somit

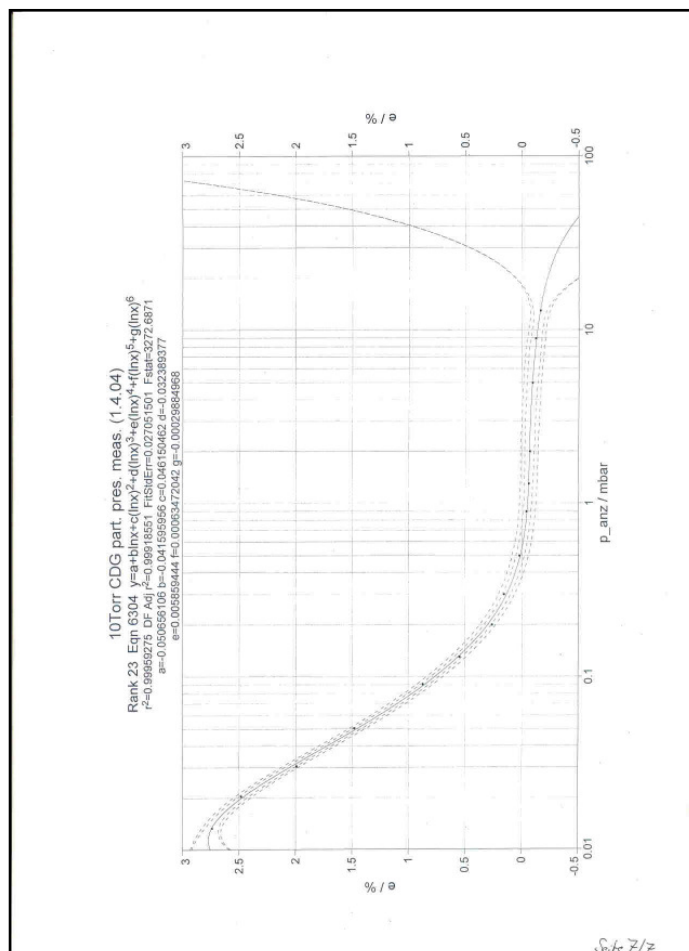
$$F^* = 2,0\% + 3,2\% \cdot 1,1055 = 5,5\% \text{ statt } F = 5,2\%.$$

6. Rekalibrierung

Um die Langzeitstabilität im oben erwähnten Rahmen zu halten, sollte das Meßsystem hier spätestens nach 24 Monaten, gerechnet ab Monat des Kalibrierscheins, rekaliibriert werden.

Berlin, den 7. Okt. 2005

Thomas Bock
Laboratorium für Vakuummetrologie





Kalibrierschein Calibration Certificate

Gegenstand:
Object: Pt 100 mit einem Multimeter

Hersteller:
Manufacturer: Multimeter: Hewlett Packard

Typ:
Type: Messfühler: Pt 100; Multimeter: HP 344 01A

Kennnummer:
Serial number: Messfühler: ohne; Multimeter: 3146A31942

Auftraggeber:
Applicant: PTB, Fachlab. 7.23

Anzahl der Seiten:
Number of pages: 4

Geschäftszeichen:
Reference No.: 7.31-1.5-03-15

Kalibrierzeichen:
Calibration mark: 165 PTB 03

Datum der Kalibrierung:
Date of calibration: 25. November 2003

Im Auftrag
By order: Berlin, 26.11.2003

Siegel
Seal:

Bearbeiter:
Examiner: A. Nisch
A. Aulich

Kalibrierscheine ohne Unterschrift und Siegel haben keine Gültigkeit. Dieser Kalibrierschein darf nur unverändert weiterverbreitet werden. Auszüge bedürfen der Genehmigung der Physikalisch-Technischen Bundesanstalt.
Calibration certificates without signature and seal are not valid. This calibration certificate may not be reproduced other than in full. Extracts may be taken only with the permission of the Physikalisch-Technische Bundesanstalt.

1. Gegenstand der Kalibrierung

Messgerät: Multimeter
Messfühler: Pt 100
Anschluss der Messleitungen: 4 Leiter

2. Kalibrierverfahren

Die Kalibrierung des Temperatursensordüfers in Verbindung mit dem Multimeter HP 344 01A wurde im Vergleichsverfahren mit zwei Normal-Widerstandsthermometern (Nr. 4421 und Nr. 4422 im Messbereich 15 °C bis 25 °C) durchgeführt. Die Kalibrierung ist auf die nationalen staatlichen Normale rückgeführt.

Die Kalibrierung erfolgte im gereinigten Flüssigkeitsbad. Die Eintauchtiefe betrug bei allen Messungen 270 mm. Das Temperatursensordüfer befand sich auf Raumtemperatur von (23 ± 0,5) °C. Es wurde keine Offsetkompensation durchgeführt.

Der Temperatursensordüfer befand sich während der Kalibrierung in einem Schutzrohr (Ø 20 mm) aus Glas.

3. Messergebnisse

In Tabelle 1 sind die Messergebnisse in der Reihenfolge der Kalibrierung angegeben.
Für die Widerstände $R(t_0)$ wurden folgende Werte ermittelt.

Tabelle 1

Temperatur t_0 in °C	$R(t_0)$ in Ω
15,009	105,843
17,000	106,618
19,000	107,397
20,001	107,786
21,005	108,176
23,001	108,951
24,997	109,726

Die Abhängigkeit des gemessenen Widerstandes von der Temperatur für den Bereich von 15 °C bis 25 °C wird durch folgende Gleichung charakterisiert:

$$R(t_0) = R_0 \cdot (1 + A \cdot t_0 + B \cdot t_0^2)$$

mit

$$R_0 = 99,98110 \, \Omega$$

$$A = 3,91701 \cdot 10^{-3} \, ^\circ\text{C}^{-1}$$

$$B = -7,12951 \cdot 10^{-7} \, ^\circ\text{C}^{-2}$$

4. Messunsicherheit

Die Gesamtmessunsicherheit der Kalibrierung beträgt 5 mΩ.

Die Messunsicherheit setzt sich zusammen aus den Unsicherheiten des Kalibrierverfahrens und denen des Digital-Temperatursensordüfers in Verbindung mit dem Temperatursensordüfer während der Kalibrierung zusammen. Ein Anteil für die Langzeitstabilität ist dabei nicht enthalten.

Angabe ist die erweiterte Messunsicherheit, die sich aus der Standardmessunsicherheit durch Multiplikation mit dem Erweiterungsfaktor $k = 2$ ergibt. Sie wurde gemäß dem "Guide to the Expression of Uncertainty in Measurement" (ISO, 1995) ermittelt. Der Wert der Messgröße liegt im Regelfall mit einer Wahrscheinlichkeit von annähernd 95 % im zugeordneten Wertebereich.

Die Physikalisch-Technische Bundesanstalt (PTB) in Braunschweig und Berlin ist das natur- und ingenieurwissenschaftliche Staatsinstitut und die technische Oberbehörde der Bundesrepublik Deutschland für das Messwesen und Teile der Sicherheitstechnik. Die PTB gehört zum Dienstbereich des Bundesministeriums für Wirtschaft. Sie erfüllt die Anforderungen an Kalibrier- und Prüflaboratorien auf der Grundlage der DIN EN ISO/IEC 17025.

Zentrale Aufgabe der PTB ist es, die gesetzlichen Einheiten in Übereinstimmung mit dem internationalen Einheitensystem (SI) darzustellen, zu bewahren und - insbesondere im Rahmen des gesetzlichen und industriellen Messwesens - weiterzugeben. Die PTB steht damit an oberster Stelle der metrologischen Hierarchie in Deutschland. Kalibrierscheine der PTB dokumentieren die Rückführung des Kalibriergegenstandes auf nationale Normale.

Zur Sicherstellung der weltweiten Einheitlichkeit der Maße arbeitet die PTB mit anderen nationalen metrologischen Instituten auf regionaler europäischer Ebene in EUROMET und auf internationaler Ebene im Rahmen der Metrokonvention zusammen. Das Ziel wird durch einen intensiven Austausch von Forschungsergebnissen und durch umfangreiche internationale Vergleichsmessungen erreicht.

The Physikalisch-Technische Bundesanstalt (PTB) in Braunschweig and Berlin is the national institute for science and technology and the highest technical authority of the Federal Republic of Germany for the field of metrology and certain sectors of safety engineering. The PTB comes under the auspices of the Federal Ministry of Economics. It meets the requirements for calibration and testing laboratories as defined in the EN ISO/IEC 17025.

It is the fundamental task of the PTB to realize and maintain the legal units in compliance with the International System of Units (SI) and to disseminate them, above all within the framework of legal and industrial metrology. The PTB thus is on top of the metrological hierarchy in Germany. Calibration certificates issued by it document that the object calibrated is traceable to national standards.

To ensure worldwide coherence of measures, the PTB cooperates with other national metrology institutes within EUROMET on the regional European level and on the international level within the framework of the Metro Convention. The aim is achieved by an intensive exchange of results of research work carried out and by comprehensive international comparison measurements.



Kalibrierschein
Calibration Certificate

Gegenstand:
Object: Temperatur- und Widerstandsmessgerät mit einem
Temperaturfühler

Hersteller:
Manufacturer: Automatic Systems Laboratories (ASL)

Typ:
Type: Temperatur- und Widerstandsmessgerät F 250
Temperaturfühler Pt 100

Kennnummer:
Serial number: Temperatur- und Widerstandsmessgerät 1249 027 214
Temperaturfühler (A) SV 1915/A V 2572 A

Auftraggeber:
Applicant: PTB Labor 7.23

Anzahl der Seiten:
Number of pages: 4

Geschäftszeichen:
Reference No.: 7.31-1.5-03-13

Kalibrationszeichen:
Calibration mark: 130 PTB 03

Datum der Kalibrierung:
Date of calibration: 18.09.2003

Im Auftrag
By order: Berlin, 2003-09-18
Dr. E. Tegeler

Bearbeiter:
Examiner: A. Aulich

Dr. E. Tegeler

Kalibrierscheine ohne Unterschrift und Siegel haben keine Gültigkeit. Dieser Kalibrierschein darf nur unverändert weitervertrieben werden. Auszüge bedürfen der Genehmigung der Physikalisch-Technischen Bundesanstalt.
Calibration certificates without signature and seal are not valid. This calibration certificate may not be reproduced other than in full. Extracts may be taken only with the permission of the Physikalisch-Technische Bundesanstalt.

1. Gegenstand der Kalibrierung

Messgerät: Temperatur- und Widerstandsmessgerät F 250
Messfühler: Pt 100
Außendurchmesser: 6 mm
Schutzrohrlänge: 350 mm
Material des Schutzrohres: Metall

2. Kalibrierverfahren

Die Kalibrierung des Prüflings wurde im Vergleichsverfahren mit 2 Normalwiderstandsthermometern (Nr. 4421 und Nr. 4422 im Messbereich 0 °C bis 50 °C) durchgeführt. Die Kalibrierung ist auf die nationalen staatlichen Normale rückgeführt.
Die Kalibrierung erfolgte im gerührten Flüssigkeitsbad und begann bei der tiefsten Messtemperatur. Die Eintauchtiefe betrug bei allen Messungen 300 mm. Das Temperatur- und Widerstandsmessgerät F 250 befand sich auf Raumtemperatur von 23 °C ($\pm 0,5^\circ\text{C}$).

3. Messergebnisse

In Tabelle 1 sind die Messergebnisse in der Reihenfolge der Kalibrierung angegeben.
Für die Widerstände $R(t_0)$ wurden folgende Werte ermittelt.

Tabelle 1

Temperatur t_{50} in °C	$R(t_0)$ in Ω
0,000	100,022
19,999	107,816
20,493	108,008
24,995	109,755
30,004	111,698
34,994	113,628
40,008	115,566
50,008	119,420
0,000	100,021

Die Abhängigkeit des gemessenen Widerstandes von der Temperatur für den Bereich von 0 °C bis 50 °C wird durch folgende Gleichung charakterisiert:

$$R(t_{50}) = R_0 + A \cdot t_{50} + B \cdot t_{50}^2$$

mit $R_0 = 100,021\,44\,\Omega$
 $A = 3,909\,71 \cdot 10^{-1}\,^\circ\text{C}^{-1}$
 $B = -6,113\,82 \cdot 10^{-6}\,^\circ\text{C}^{-2}$

4. Messunsicherheit

Die Gesamtmessunsicherheit der Kalibrierung beträgt 10 mK.
Sie setzt sich aus den Unsicherheiten der Normale, des Kalibrierverfahrens, der mathematischen Kennlinienapproximation und den Eigenschaften des kalibrierten Prüflings zusammen.
Ein Anteil der Langzeit-Instabilität des Prüflings ist dabei nicht berücksichtigt.

Angaben ist die erweiterte Messunsicherheit, die sich aus der Standardmessunsicherheit durch Multiplikation mit dem Erweiterungsfaktor $k = 2$ ergibt. Sie wurde gemäß dem "Guide to the Expression of Uncertainty in Measurement" (ISO, 1995) ermittelt. Der Wert der Messgröße liegt im Regelfall mit einer Wahrscheinlichkeit von annähernd 95 % im zugeordneten Werteintervall.

Die Physikalisch-Technische Bundesanstalt (PTB) in Braunschweig und Berlin ist das natur- und ingenieurwissenschaftliche Staatsinstitut und die technische Oberbehörde der Bundesrepublik Deutschland für das Messwesen und Teile der Sicherheitstechnik. Die PTB gehört zum Dienstbereich des Bundesministeriums für Wirtschaft. Sie erfüllt die Anforderungen an Kalibrier- und Prüflaboratorien auf der Grundlage der DIN EN ISO/IEC 17025.


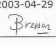
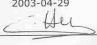
Zentrale Aufgabe der PTB ist es, die gesetzlichen Einheiten in Übereinstimmung mit dem internationalen Einheitensystem (SI) darzustellen, zu bewahren und - insbesondere im Rahmen des gesetzlichen und industriellen Messwesens - weiterzugeben. Die PTB steht damit an oberster Stelle der metrologischen Hierarchie in Deutschland. Kalibrierscheine der PTB dokumentieren die Rückführung des Kalibriergegenstandes auf nationale Normale.

Zur Sicherstellung der weltweiten Einheitlichkeit der Maße arbeitet die PTB mit anderen nationalen metrologischen Instituten auf regionaler europäischer Ebene in EUROMET und auf internationaler Ebene im Rahmen der Meterkonvention zusammen. Das Ziel wird durch einen intensiven Austausch von Forschungsergebnissen und durch umfangreiche internationale Vergleichsmessungen erreicht.

The Physikalisch-Technische Bundesanstalt (PTB) in Braunschweig and Berlin is the national institute for science and technology and the highest technical authority of the Federal Republic of Germany for the field of metrology and certain sectors of safety engineering. The PTB comes under the auspices of the Federal Ministry of Economics. It meets the requirements for calibration and testing laboratories as defined in the EN ISO/IEC 17025.

It is the fundamental task of the PTB to realize and maintain the legal units in compliance with the international System of Units (SI) and to disseminate them, above all within the framework of legal and industrial metrology. The PTB thus is on top of the metrological hierarchy in Germany. Calibration certificates issued by it document that the object calibrated is traceable to national standards.

To ensure worldwide coherence of measures, the PTB cooperates with other national metrology institutes within EUROMET on the regional European level and on the international level within the framework of the Metre Convention. The aim is achieved by an intensive exchange of results of research work carried out and by comprehensive international comparison measurements.

 HC 250 CALIBRATION CERTIFICATE	
Réf. : MB/03-5285/FC	Date : 29/04/2003
SAGEIS CSO 70, rue des Martyrs 38000 Grenoble Phone : 04 76 47 85 88 Telecopy : 04 76 46 84 56 E-mail : m.bresson@sageis-cso.fr	CUSTOMER Firm : Laser 2000 Allemagne Address : Argelsrieder Feld 14 D-62234 WESLING Contact name : Gabriela THUNIG
CALIBRATED SYSTEM	
Description Sensor Electronic unit	S/N #0108 9414 E
CALIBRATION CONDITIONS	
Temperature (°C) Pressure (hPa) Speed (mm/s)	Working distance (mm) Working range (mm) Number of measurements
20 1013.25 30	150 200 10
REFERENCE EQUIPMENT	
Description Hewlett Packard Laser source Hewlett Packard Electronic unit	Type 5518A S507A
S/N 3020 A03159 2944 A 00664	Calibration 24/09/01 24/09/01
Certificate nb B071036/1 B071036/1	
TESTS RESULTS	
Wavelength (nm) Standard deviation (ppm)	787.1912 0.1
Control : Comparison with the reference laser	
Displacement HP (fringes) 313661.22 313096.72 311495.64 312365.64 313315.44 313354.43 312998.94 311343.50 306990.17 309034.08	Displacement CSO (fringes) 252380.16 251765.42 250477.98 251177.54 251941.29 251972.64 251365.14 250355.63 246855.05 248498.60
Difference (ppm) -0.05 -0.04 0.02 -0.05 -0.03 -0.06 -0.05 -0.04 -0.05 -0.01	
Name: Function : Date : Visa :	M. BRESSON Product manager 2003-04-29 
	C. HENRION Product assurance 2003-04-29 

7.3. IPSIAM-Results-File names

Table 25. IPSIAM-Results-Files for the CO₂ R12 line intensity measurement.

File Name	File Consecutive Number
Onormalization-050330-HC-N10-K1-0p4torr-scan7from12.xls	1
Onormalization-050331-HC-N10-K1-01-0p4torr-centered-1.xls	2
Onormalization-050331-HC-N10-K1-02-0p5torr-centered.xls	3
Onormalization-050331-HC-N10-K1-03-0p65torr-centered.xls	4
Onormalization-050331-HC-N10-K1-04-1p02torr-centered.xls	5
Onormalization-050331-HC-N10-K1-0p44torr-centered-1.xls	6
Onormalization-050404-HC-N16-K2-part-175033-to-175103-centered-1.xls	7
Onormalization-050404-HC-N16-K2-part-180033-1.xls	8
Onormalization-050404-HC-N16-K2-part-180203-to-180333-centered-1.xls	9
Onormalization-050404-HC-N16-K2-part-181703-to-181733-centered-1.xls	10
Onormalization-050404-HC-N16-K2-part-181803-to-181903-centered-1.xls	11
Onormalization-050217-HC-N14-stat-p55-centered-01.xls	12
Onormalization-050217-HC-N14-stat-p55-centered-02.xls	13
Onormalization-050217-HC-N14-stat-p55-centered-03.xls	14
Onormalization-050403-HC-N14-K1-0p6torr-1scan18-38-33-centered-1.xls	15
Onormalization-050403-HC-N14-K1-0p8torr-1scan17-43-03-centered-1.xls	16
Onormalization-050404-HC-N22-K3-0p4torr-scan9a10de10-200003-200033-centered-fls30-1.xls	17
Onormalization-050404-HC-N22-K3-0p5torr-scan3a4de10-200503-200533-centered-fls30-1.xls	18
Onormalization-050404-HC-N22-K3-0p66torr-scan8a9de10-202333-202403-centered-fls30-1.xls	19
Onormalization-050404-HC-N22-K3-0p6torr-scan8a9de11-201503-201533-centered-fls30-1.xls	20
Onormalization-050404-HC-N18-K1-0p5torr-1scan-14-15-33-centered-1.xls	21
Onormalization-050404-HC-N18-K1-1scan-15-30-03-0p6torr-centered-1.xls	22
Onormalization-050404-HC-N18-K1-1scan-15-37-33-0p4torr-centered-1.xls	23
Onormalization-050405-HC-N28-K4-0p39torr-scan1a13de13-181033-181633-fls30-1.xls	24
Onormalization-050405-HC-N28-K4-0p45torr-scan1a12de12-173203-173733-fls30-1.xls	25
Onormalization-050405-HC-N28-K4-0p4torr-scan1a17de17-172003-172833-fls30-1.xls	26
Onormalization-050405-HC-N28-K4-0p54torr-scan1a12de12-174003-174533-fls30-1.xls	27
Onormalization-050405-HC-N28-K4-0p57torr-scan1a12de12-174903-175433-fls30-1.xls	28

Table 26. Zero control measurements that were taken “parallel” to the R12 line intensity measurements.

"Zero Control" File Name	$A_{abs}(T)$
Onormalization-050404-HC-N18-K1-zero-control.xls	-1.0108E-04
Onormalization-050331-HC-N10-K1-02-zero-control-non-centered.xls	-8.8098E-05
Onormalization-050331-HC-N10-K1-zero-control-01-non-centered.xls	9.2165E-05
Onormalization-050331-HC-N10-K1-zero-control-04-1p02torr-non-centered.xls	-6.8014E-05
Onormalization-050403-HC-N14-K1-final-zero-control-1.xls	4.9964E-05
Onormalization-050330-HC-N10-K1-zero-control-non-centered.xls	-6.1624E-05
Onormalization-050217-HC-N14-stat-p55-zero-control-01.xls	1.3153E-06
Onormalization-050217-HC-N14-stat-p55-zero-control-02.xls	6.1576E-06
Onormalization-050217-HC-N14-stat-p55-zero-control-03.xls	9.5759E-06
Onormalization-050404-HC-N22-K3-cero-control-scan10a12de14-211633-211733-fls30-1.xls	5.3006E-07
Onormalization-050404-HC-N22-K3-cero-control-scan13a14de14-211812-211833-fls30-1.xls	-2.0010E-05
Onormalization-050404-HC-N22-K3-cero-control-scan1a3de14-211203-211303-fls30-1.xls	-3.5591E-05
Onormalization-050404-HC-N22-K3-cero-control-scan4a6de14-211333-211433-fls30-1.xls	-5.4089E-05
Onormalization-050404-HC-N22-K3-cero-control-scan7a9de14-211503-211603-fls30-1.xls	-2.9805E-05
Onormalization-050405-HC-N28-K4-cero-control-scan10a11de13-183411-183433-fls30-1.xls	2.3101E-05
Onormalization-050405-HC-N28-K4-cero-control-scan12a13de13-183503-183533-fls30-1.xls	1.8487E-05
Onormalization-050405-HC-N28-K4-cero-control-scan1a13de13-182933-183533-fls30-1.xls	1.9260E-05
Onormalization-050405-HC-N28-K4-cero-control-scan1a3de13-182933-183033-fls30-1.xls	2.3347E-05
Onormalization-050405-HC-N28-K4-cero-control-scan4a6de13-183103-183203-fls30-1.xls	4.4615E-06
Onormalization-050405-HC-N28-K4-cero-control-scan7a9de13-183233-183333-fls30-1.xls	2.8091E-05
$Mean [A_{abs}(T)] =$	-9.093E-06
$Standard Deviation [A_{abs}(T)] =$	4.810E-05

Table 27. Results of partial pressure measurements of CO₂ in mixture C49286: IPSIAM-results file names and numbers.

File Name	File Consecutive Number
Onormalization-pp-050618-HC-CO2R12-K6-N64-194050-194550-mixture0p1perc-9p84torr.xls	1
Onormalization-pp-050620-HC-CO2R12-K6-N64-190120-190550-mixture0p1perc-1000TCDG-56p3torr.xls	2

Table 28. Results of partial pressure measurements of CO₂ in PTB-mixture: IPSIAM-results file names and numbers.

File Name	File Consecutive Number
Onormalization-pp-050525-HC-CO2R12-K1-N14-scan-1-to-11-of-11-235450-235950-mixture5perc-4p92torr-1.xls	1
Onormalization-pp-050601-HC-CO2R12-K1-N14-181550-182050-scan-1-to-11-of-11-mixture5perc-7p28torr-1.xls	2
Onormalization-pp-050601-HC-CO2R12-K1-N14-183120-183520-scan-1-to-10-of-10-mixture5perc-8p56torr-1.xls	3
Onormalization-pp-050525-HC-CO2R12-K2-N24-scan-1-to-9-of-9-234150-234550-mixture5perc-4p92torr-1.xls	4
Onormalization-pp-050601-HC-CO2R12-K2-N24-175120-175550-scan-1-to-10-of-10-mixture5perc-6p83torr-1.xls	5
Onormalization-pp-050601-HC-CO2R12-K2-N24-180250-180750-scan-1-to-11-of-11-mixture5perc-7p28torr-1.xls	6
Onormalization-pp-050525-HC-CO2R12-K3-N34-scan-1-to-11-of-11-232950-233450-mixture5perc-4p92torr-1.xls	7
Onormalization-pp-050531-HC-CO2R12-K3-N34-224420-224950-scan-1-to-12-of-12-mixture5perc-6p04torr-ncg-1.xls	8
Onormalization-pp-050531-HC-CO2R12-K3-N34-225620-225950-scan-1-to-8-of-8-mixture5perc-6p53torr-ncg-1.xls	9
Onormalization-pp-050525-HC-CO2R12-K4-N44-scan-1-to-12-of-12-231720-232250-mixture5perc-4p92torr-1.xls	10
Onormalization-pp-050531-HC-CO2R12-K4-N44-205020-205550-scan-1-to-12-of-12-mixture5perc-4p29torr-ncg-1.xls	11
Onormalization-pp-050531-HC-CO2R12-K4-N44-210120-210950-scan-1-to-5-and-11-to-15-of-15-mixture5perc-4p02torr-ncg-1.xls	12
Onormalization-pp-050525-HC-CO2R12-K5-N54-scan-1-to-12-of-12-225320-225850-mixture5perc-3p79torr-1.xls	13
Onormalization-pp-050525-HC-CO2R12-K6-N64-scan-1-to-12-of-12-223420-223950-mixture5perc-2p72torr-1.xls	14
Onormalization-pp-050531-HC-CO2R12-K6-N64-184450-184850-scan-1-to-9-of-9-mixture5perc-2p11torr-1.xls	15

7.4. Glossary

The terms included in this glossary are reproduced from the given sources.

Measurement (VIM 2.1)

Set of operations having the object of determining a value of a quantity

Note: The operations may be performed automatically.

Uncertainty (of the measurement) (VIM 3.9)

Parameter, associated with the result of a measurement, that characterizes the dispersion of the values that could reasonably be attributed to the measurand.

Notes:

1. The parameter may be, for example, a standard deviation (or a given multiple of it), or the half-width of an interval having a stated level of confidence.
2. Uncertainty of measurement comprises, in general, many components. Some of these components may be evaluated from the statistical distribution of the results of series of measurements and can be characterized by experimental standard deviations. The other components, which also can be characterized by standard deviations, are evaluated from assumed probability distributions based on experience or other information.
3. It is understood that the result of the measurement is the best estimate of the value of the measurand, and that all components of uncertainty, including those arising from systematic effects, such as components associated with corrections and reference standards, contribute to the dispersion.

Other notes and concepts from GUM about measurement and uncertainty:

“2.2.4 The definition of uncertainty of measurement given in 2.2.3 is an operational one that focuses on the measurement result and its evaluated uncertainty. However, it is not inconsistent with other concepts of uncertainty of measurement, such as

A measure of the possible error in the estimated value of the measurand as provided by the result of a measurement;

An estimate characterizing the range of values within which the true value of a measurand lies (VIM, first edition, 1984, entry 3.09).

Although these two traditional concepts are valid as ideals, they focus on unknowable quantities: the “error” of the result of a measurement and the “true value” of the measurand (in contrast to its estimated value), respectively. Nevertheless, whichever concept of uncertainty is adopted, an uncertainty component is always evaluated using the same data and related information. (See also E.5)”

“3.1 Measurement

3.1.1 The objective of a measurement (B.2.5) is to determine the value (B.2.2) of the measurand (B.2.9), that is, the value of the particular quantity (B.2.1, note 1) to be measured. A measurement therefore begins with an appropriate specification of the measurand, the method of measurement (B.2.7), and the measurement procedure. (B.2.8).

Note: The term “true value” (see annex D) is not used in this Guide for the reasons given in D.3.5, the terms “value of a measurand” (or a quantity) and “true value of a measurand” (or a quantity) are viewed as equivalent.

3.1.2 In general, the result of a measurement (B.2.11) is only an approximation or estimate (C.2.26) of the value of the measurand and thus is complete only when accompanied by a statement of the uncertainty (B.2.18) of that estimate.

3.1.3 In practice, the required specification or definition of the measurand is dictated by the required accuracy of measurement (B.2.14). The measurand should be defined with sufficient completeness with respect to the required accuracy so that for all practical purposes associated with the measurement its value is unique. It is in this sense that the expression “value of the measurand” is used in this Guide.

Example: If the length of a nominally one- metre long steel bar is to be determined to micrometer accuracy, its specification should include the temperature and pressure at which the length is defined. Thus the measurand should be specified as, for example, the length of the bar at 25,00°C and 101 325 Pa (plus any other defining parameters deemed necessary, such as the way the bar is to be supported). However, if the length is to be determined to only millimetre accuracy, its specification would not require a defining temperature or pressure or a value for any other defining parameter.

Note: Incomplete definition of the measurand can give rise to a component of uncertainty sufficiently large that it must be included in the evaluation of the uncertainty of the measurement result (see D.1.1, D.3.4, and D.6.2)

3.1.4 In many cases, the result of a measurement is determined on the basis of series of observations obtained under repeatability conditions (B.2.15, note 1)

3.1.5 Variations in repeated observations are assumed to arise because influence quantities (B.2.10) that can affect the measurement result are not held completely constant.

3.1.6 The mathematical model of the measurement that transforms the set of repeated observations into the measurement result is of critical importance because, in addition to the observations, it generally includes various influence quantities that are inexactly known. This lack of knowledge contributes to the uncertainty of the measurement result, as do the variations of the repeated observations and any uncertainty associated with the mathematical model itself.

3.1.7 This Guide treats the measurand as a scalar (a single quantity). Extension to a set of related measurands determined simultaneously in the same measurement requires replacing the scalar measurand and its variance (C.2.11, C.2.20, C.3.2) by a vector measurand and covariance matrix (C.3.5). Such a replacement is considered in this Guide only in the examples (see H.2, H.3 and H.4)

3.2 Errors, effects and corrections.

3.2.1 In general, a measurement has imperfections that give rise to an error (B.2.19) in the measurement result. Traditionally, an error is viewed as having two components, namely a random (B.2.21) component and a systemic (B.2.22) component.

Note: Error is an idealized concept and errors cannot be known exactly.

3.2.2 Random error presumably arises from unpredictable or stochastic temporal and spatial variations of influence quantities. The effects of such variations, hereafter termed random effects, give rise to variations in repeated observations of the measurand. Although it is not possible, to compensate for the random error of a measurement result, it can usually be reduced by increasing the number of observations, its expectation or expected value (C.2.9, C.3.1) is zero.

Notes:

1 The experimental standard deviation of the arithmetic mean or average of a series of observations (see 4.2.3) is not the random error of the mean, although it is so designated in some publications. It is instead a measure of the uncertainty of the mean due to random effects. The exact value of the error in the mean arising from these effects cannot be known.

2 In this Guide, great care is taken to distinguish between the terms “error” and “uncertainty”. They are not synonyms, but represent completely different concepts: they should not be confused with one another or misused.

3.2.3 Systematic error, like random error, cannot be eliminated but it too can often be reduced. If a systematic error arises from a recognized effect of an influence quantity on a measurement result, hereafter termed a systematic effect, the effect can be quantified and, if it is significant in size relative to the required accuracy of the measurement, a correction (B.2.23) or correction factor (B.2.24) can be applied to compensate for the effect. It is assumed that, after correction, the expectation or expected value of the error arising from a systematic effect is zero.

Note: The uncertainty of a correction applied to a measurement result to compensate for a systematic effect is not the systematic error, often termed bias, in the measurement result due to the effect as it is sometimes called. It is instead a measure of the uncertainty of the result due to the incomplete knowledge of the required value of the correction. The error arising from imperfect compensation of a systematic effect cannot be exactly known. The terms “error” and “uncertainty” should be used properly and care taken to distinguish between them.

3.2.4 It is assumed that the result of a measurement has been corrected for all recognized significant systematic effects and that every effort has been made to identify such effects.

EXAMPLE - A correction due to the finite impedance of a voltmeter used to determine the potential difference (the measurand) across a high-impedance resistor is applied to reduce the systematic effect on the result of the measurement arising from the loading effect of the voltmeter. However, the values of the impedances of the voltmeter and resistor, which are used to estimate the value of the correction and which are obtained from other measurements, are themselves uncertain. These uncertainties are used to evaluate the component of the uncertainty of the potential difference determination arising from the correction and thus from the systematic effect due to the finite impedance of the voltmeter.

Notes:

1 Often, measuring instruments and systems are adjusted or calibrated using measurement standards and reference materials to eliminate systematic effects; however, the uncertainties associated with these standards and materials must still be taken into account.

2 The case where a correction for a known significant systematic effect is not applied is discussed in the note 6.3.1 and in F.2.4.5.

3.3 Uncertainty

3.3.1 The uncertainty of the result of a measurement reflects the lack of exact knowledge of the value of the measurand (see 2.2) The result of a measurement after correction for recognized systematic effects is still only an estimate of the value of the measurand because of the uncertainty arising from random effects and from imperfect correction of the result for systematic effects.

Note: The result of a measurement (after correction) can unknowably be very close to the value of the measurand (and hence have a negligible error) even though it may have a large uncertainty. Thus the uncertainty of the result of a measurement should not be confused with the remaining unknown error.

3.3.2 In practice, there are many possible sources of uncertainty in a measurement, including:

- a) incomplete definition of the measurand;
- b) Imperfect realization of the definition of the measurand;
- c) Non representative sampling – the sample measured may not represent the defined measurand;
- d) Inadequate knowledge of the effects of environmental conditions on the measurement or imperfect measurement of environmental conditions;
- e) Personal bias in reading analogue instruments;
- f) Finite instrument resolution or discrimination threshold;
- g) Inexact values of measurement standards and reference materials;
- h) Inexact values of constants and other parameters obtained from external sources and used in the data-reduction algorithm;
- i) Approximations and assumptions incorporated in the measurement method and procedure;
- j) Variations in repeated observations of the measurand under apparently identical conditions.

These sources are not necessarily independent, and some of sources a) to i) may contribute to source j). Of course, an unrecognized systematic effect cannot be taken into account in the evaluation of the uncertainty of the result of a measurement but contributes to its error.

3.3.3 Recommendation INC-1 (1980) of the Working Group on the Statement of Uncertainties groups uncertainty components into two categories based on their method of evaluation, “A” and “B” (see 0.7, 2.3.2 and 2.3.3). These categories apply to uncertainty and are not substitutes for the words “random” and “systematic”. The uncertainty of a correction for a known systematic effect may in some cases be obtained by a Type A evaluation while in other cases by a Type B evaluation, as may the uncertainty characterizing a random effect.

Note: In some publications uncertainty components are categorized as “random” and “systematic” and are associated with errors arising from random effects and known systematic effects, respectively. Such categorization of components of uncertainty can be ambiguous when generally applied. For example, a “random” component of uncertainty in one measurement may become a “systematic” component uncertainty in another measurement in which the result of the first measurement is used as an input datum. Categorizing the methods of evaluating uncertainty components rather than the components themselves avoids such ambiguity. At the same time, it does not preclude collecting individual components that have been evaluated by the two different methods into designated groups to be used for a particular purpose (see 3.4.3).

3.3.4 The purpose of the Type A and Type B classification is to indicate the two different ways of evaluating uncertainty components and is for convenience of discussion only; the classification is not meant to indicate that there is any difference in the nature of the components resulting from the two types of evaluation. Both types of evaluation are based on probability distributions (C.2.3) and the uncertainty components resulting from either type are quantified by variances or standard deviations.

3.3.5 The estimated variance u^2 characterizing an uncertainty component obtained from Type A evaluation is calculated from series of repeated observations and is the familiar statistically estimated variance s^2 (see 4.2). The estimated standard deviation (C.2.12, C.2.21, C.3.3) u , the positive square root of u^2 , is thus $u = s$ and for convenience is sometimes called a Type A standard uncertainty. For an uncertainty component obtained from a Type B evaluation, the estimated variance u^2 is evaluated using available knowledge (see 4.3), and the estimated standard deviation u is sometimes called a Type B standard uncertainty.

Thus a Type A standard uncertainty is obtained from a probability density function (C.2.5) derived from an observed frequency distribution (C.2.18), while Type B standard uncertainty is obtained from an assumed probability density function based on the degree of belief that an event will occur (often called subjective probability (C.2.1)). Both approaches employ recognized interpretations of probability.

Note: A Type B evaluation of an uncertainty component is usually based on a pool of comparatively reliable information (see 4.3.1)

3.3.6 The standard uncertainty of the result of a measurement, when that result is obtained from the value of a number of other quantities, is termed combined standard uncertainty and denoted by u_c . It is the estimated standard deviation associated with the result and is equal to the positive square root of the combined variance obtained from all variance and covariance (C.3.4) components, however evaluated, using what is termed in this Guide the law of propagation of uncertainty (see clause 5).

3.3.7 To meet the needs of some industrial and commercial applications, as well as requirements in the areas of health and safety, and expanded uncertainty U is obtained by multiplying the combined standard uncertainty u_c by a coverage factor k . The intended purpose of U is to provide an interval about the result of a measurement that may be expected to encompass a large fraction of the distribution of values that could reasonably be attributed to the measurand. The choice of the factor k , which is usually in the range 2 to 3, is based on the coverage probability or level of confidence required of the interval (see clause 6).

Note: The coverage factor k is always to be stated, so that the standard uncertainty of the measurand quantity can be recovered for use in calculating the combined standard uncertainty of other measurement results that may depend on that quantity.

...

3.4.3 In order to decide if measurement system is functioning properly, the experimentally observed variability of its output values, as measured by their observed standard deviation, is often compared with the predicted standard deviation obtained by combining the various uncertainty components that characterize the measurement. In such cases, only those components (whether obtained from Type A or Type B evaluations) that could contribute to the experimentally observed variability of these output values should be considered.

Note: Such an analysis may be facilitated by gathering those components that contribute to the variability and those that not into two separate and appropriately labelled groups.

...

3.4.8 Although this Guide provides a framework for assessing uncertainty, it cannot substitute for critical thinking, intellectual honesty, and professional skill. The evaluation of uncertainty is neither a routine task not a purely mathematical one; it depends on detailed knowledge of the nature of the measurand and of the measurement. The quality and utility of the uncertainty quoted for the result of measurement therefore ultimately depend on the understanding, critical analysis, and integrity of those who contribute to the assignment of its value.”

Standard uncertainty (GUM 2.3.1)

Uncertainty of the result of a measurement expressed as a standard deviation.

Type A evaluation (of uncertainty) (GUM 2.3.2)

Method of evaluation of uncertainty by the statistical analysis if series of observations.

Type B evaluation (of uncertainty) (GUM 2.3.3)

Method of evaluation of uncertainty by means other than the statistical analysis if series of observations.

Combined standard uncertainty (GUM 2.3.4)

Standard uncertainty of the results of a measurement when that result is obtained from the values of a number of other quantities, equal to the positive square root of a sum of terms, the terms being the variances or covariances of these other quantities weighted according to how the measurement result varies with changes in these quantities.

Expanded uncertainty (GUM 2.3.5)

Quantity defining an interval about the result of a measurement that may be expected to encompass a large fraction of the distribution of values that could reasonably be attributed to the measurand.

Notes:

1. The fraction may be viewed as the coverage probability or level of confidence of the interval.
2. To associate specific level of confidence with the interval defined by the expanded uncertainty requires explicit or implicit assumptions reading the probability distribution characterized by the measurement result and its combined standard uncertainty. The level of confidence that may be attributed to this interval can be known only to the extent to which such assumptions may be justified.
3. Expanded uncertainty is termed overall uncertainty in paragraph 5 of Recommendation INC- 1 (1980).

Coverage factor (GUM 2.3.6)

Numerical factor used as a multiplier of the combined standard uncertainty in order to obtain an expanded uncertainty.

Note: a coverage factor k , is typically in the range 2 to 3.

(Measurable) Quantity (VIM 1.1)

Attribute of a phenomenon, body or substance that may be distinguished qualitatively and determined quantitatively.

Notes:

1 The term quantity may refer to a quantity in a general sense [see example a)] or to a particular quantity' [see example b)].

EXAMPLES

- a) quantities In a general sense: length, time, mass, temperature, electrical resistance, amount-of substance concentration;
- b) particular quantities:
 - length of a given rod
 - electrical resistance of a given specimen of wire
 - amount-of-substance concentration of ethanol in a given sample of wine.
- 2 Quantities that can be placed in order of magnitude relative to one another are called quantities of the same kind.
- 3 Quantities of the same kind may be grouped together into categories of quantities, for example:
 - work, heat, energy
 - thickness, circumference, wavelength.
- 4 Symbols for quantities are given in ISO 31.

System of quantities (VIM 1.2)

Set of quantities, in the general sense, among which defined relationships exist.

Base quantity (VIM 1.3)

One of the quantities that, in a system of quantities, are conventionally accepted as functionally independent of one another.

EXAMPLE: the quantities length, mass and time are generally taken to be base quantities in the field of mechanics.

Note: The base quantities corresponding to the base units of the International System of Units (SI) are given in the Note to 1.12.

Derived quantity (VIM 1.4)

Quantity defined, in a system of quantities, as a function of base quantities of that system.

EXAMPLE: in a system having base quantities length, mass and time, velocity is a derived quantity defined as: length divided by time.

Value (of a quantity) (VIM 1.18)

Magnitude of a particular quantity generally expressed as a unit of measurement multiplied by a number.

EXAMPLES

- a) length of a rod: 5,34 m or 534 cm;
- b) mass of a body: 0,152kg or 152g;
- c) amount of substance of a sample of water (H_2O) 0,012 mol or 12 mmol.

Notes:

- 1 The value of a quantity may be positive, negative or zero.
- 2 The value of a quantity may be expressed in more than one way.

- 3 The values of quantities of dimension one are generally expressed as pure numbers.
- 4 A quantity that cannot be expressed as a unit of measurement multiplied by a number may be expressed by reference to a conventional reference scale or to a measurement procedure or to both.

True value (of a quantity) (VIM 1.19)

Value consistent with the definition of a given particular quantity.

Notes:

- 1 This is a value that would be obtained by a perfect measurement.
- 2 True values are by nature indeterminate.
- 3 The indefinite article "a", rather than the definite article "the", is used in conjunction with "true value" because there may be many values consistent with the definition of a given particular quantity.

Conventional true value (of a quantity) (VIM 1.20)

Value attributed to a particular quantity and accepted, sometimes by convention, as having an uncertainty appropriate for a given purpose.

EXAMPLES

- a) at a given location, the value assigned to the quantity, realized by a reference standard may be taken as conventional true value;
- b) the CODATA (1986) recommended value for the Avogadro constant, N_A : $6,0221367 \times 10^{23} \text{ mol}^{-1}$.

Notes:

- 1 "Conventional true value" is sometimes called assigned value, best estimate of the value, conventional value or reference value. "Reference value", in this sense, should not be confused with "reference value" in the sense used in the Note to 5.7.
- 2 Frequently, a number of results of measurements of a quantity is used to establish a conventional true value.

Numerical value (of a quantity) (VIM 1.21)

Quotient of the value of a quantity and the unit used in its expression.

EXAMPLES

in the examples in 1.18, the numbers:

- a) 5,34 , 534;
- b) 0,152 , 152;
- c) 0,012 , 12.

Metrology (VIM 2.2)

Science of measurement.

Note: Metrology includes all aspects both theoretical and practical with reference to measurements, whatever their uncertainty, and in whatever fields of science or technology they occur.

Principle of measurement (VIM 2.3)

Scientific basis of a measurement.

EXAMPLES

- a) the thermoelectric effect applied to the measurement of temperature;
- b) the Josephson effect applied to the measurement of electric potential difference;
- c) the Doppler effect applied to the measurement of velocity;
- d) the Raman effect applied to the measurement of the wave number of molecular vibrations.

Method of measurement (VIM 2.4)

Logical sequence of operations, described generically, used in the performance of measurements.

Note: Methods of measurement may be qualified in various ways such as:

- substitution method
- differential method

-null method

Measurement procedure (VIM 2.5)

Set of operations, described specifically, used in the performance of particular measurements according to a given method.

Note: A measurement procedure is usually recorded in a document that is sometimes itself called a "measurement procedure" (or a measurement method) and is usually in sufficient detail to enable an operator to carry out a measurement without additional information.

Measurand (VIM 2.6)

Particular quantity subject to measurement.

EXAMPLE vapour pressure of a given sample of water at 20°C.

Note: The specification of a measurand may require statements about quantities such as time, temperature and pressure.

Influence quantity (VIM 2.7)

Quantity that is not the measurand but that affects the result of the measurement.

EXAMPLES

- a) temperature of a micrometer used to measure length;
- b) frequency in the measurement of the amplitude of an alternating electric potential difference;
- c) bilirubin concentration in the measurement of haemoglobin concentration in a sample of human blood plasma.

Measurement signal (VIM 2.8)

Quantity that represents the measurand and which is functionally related to it.

EXAMPLES

- a) the electrical output signal of a pressure transducer;
- b) the frequency from a voltage-to-frequency converter;
- c) the electromotive force of an electrochemical concentration cell used to measure a difference in concentration.

Note: The input signal to a measuring system may be called the stimulus; the output signal may be called the response.

Result of a measurement (VIM 3.1)

Value attributed to a measurand, obtained by measurement.

Notes:

- 1 When a result is given, it should be made clear whether it refers to:
 - the indication
 - the uncorrected result
 - the corrected resultand whether several values are averaged.
- 2 A complete statement of the result of a measurement includes information about the uncertainty of measurement.

Indication (of a measuring instrument) (VIM 3.2)

Value of a quantity provided by a measuring instrument.

Notes:

- 1 The value read from the displaying device may be called the direct indication; it is multiplied by the instrument constant to give the indication.
- 2 The quantity may be the measurand, a measurement signal, or another quantity to be used in calculating the value of the measurand.
- 3 For a material measure, the indication is the value assigned to it.

Uncorrected result (VIM 3.3)

Result of a measurement before correction for a systematic error.

Corrected result (VIM3.4)

Result of a measurement after correction for systematic error.

Accuracy of measurement (VIM 3.5)

Closeness of the agreement between the result of a measurement and a true value of the measurand.

Notes:

- 1 “Accuracy” is a qualitative concept.
- 2 The term precision should not be used for “accuracy”.

Repeatability (of results of measurements) (VIM 3.6)

Closeness of the agreement between the results of successive measurements of the same measurand carried out under the same conditions of measurement.

Notes:

- 1 These conditions are called repeatability conditions.
- 2 Repeatability conditions include:
 - The same measurement procedure
 - The same observer
 - The same measuring instrument, used under the same conditions.
 - The same location
 - Repetition over a short period of time.
- 3 Repeatability may be expressed quantitatively in terms of the dispersion characteristics of the results.

Reproducibility (of results of measurements) (VIM 3.7)

Closeness of the agreement between the results of measurements of the same measurand carried out under changed conditions of measurement.

Notes:

- 1 A valid statement of reproducibility requires specification of the conditions changed.
- 2 The changed conditions may include:
 - principle of measurement
 - method of measurement
 - observer
 - measuring instrument
 - reference standard
 - location
 - conditions of use
 - time
- 2 Reproducibility may be expressed quantitatively in terms of the dispersion characteristics of the results.
- 4 Results are here usually understood to be corrected results.

Experimental standard deviation (VIM 3.8)

For a series of n measurements of the same measurand, the quantity s characterizing the dispersion of the results and given by the formula:

$$s = \sqrt{\frac{\sum_{i=1}^n (X_i - \bar{X})^2}{n-1}}$$

X_i being the result of the i th measurement and \bar{X} being the arithmetic mean of the n results considered.

Notes:

- 1 Considering the series of n values as a sample of a distribution, \bar{X} is an unbiased estimate of the mean μ , and s^2 is an unbiased estimate of the variance σ^2 of that distribution.
- 2 The expression s/\sqrt{n} is an estimate of the standard deviation of the distribution of \bar{X} and is called the experimental standard deviation of the mean.
3. "Experimental standard deviation of the mean" is sometimes incorrectly called standard error of the mean.

Error (of measurement) (VIM 3.10)

Result of a measurement minus a true value of the measurand.

NOTES

- 1 Since a true value cannot be determined, in practice a conventional true value is used (see 1.19 and 1.20).
- 2 When it is necessary to distinguish "error" from "relative error", the former is sometimes called absolute error of measurement. This should not be confused with absolute value of error, which is the modulus of the error.

Deviation (VIM 3.11)

Value minus its reference value.

Relative error (VIM 3.12)

Error of measurement divided by a true value of the measurand.

Note: Since a true value cannot be determined, in practice a conventional true value is used (see 1.19 and 1.20).

Random error (VIM 3.13)

Result of a measurement minus the mean that would result from an infinite number of measurements of the same measurand carried out under repeatability conditions.

Notes:

- 1 Random error is equal to error minus systematic error.
- 2 Because only a finite number of measurements can be made, it is possible to determine only an estimate of random error.

Systematic error (VIM 3.14)

Mean that would result from an infinite number of measurements of the same measurand carried out under repeatability conditions minus a true value of the measurand.

Notes:

- 1 Systematic error is equal to error minus random error.
- 2 Like true value, systematic error and its causes cannot be completely known.
- 3 For a measuring instrument see "bias" (5.25).

Correction (VIM 3.15)

Value added algebraically to the uncorrected result of a measurement to compensate for systematic error.

Notes:

- 1 The correction is equal to the negative of the estimated systematic error.
- 2 Since the systematic error cannot be known perfectly, the compensation cannot be complete.

Correction factor (VIM 3.16)

Numerical factor by which the uncorrected result of a measurement is multiplied to compensate for systematic error.

Note: Since the systematic error cannot be known perfectly, the compensation cannot be complete.

Measuring instrument (VIM 4.1)

Device intended to be used to make measurements, alone or in conjunction with supplementary devices(s).

Material measure (VIM 4.2)

Device intended to reproduce or supply, in a permanent manner during its use, one or more known values of a given quantity.

EXAMPLES

- a) a weight;
- b) a measure of volume (of one or several values, with or without a scale)
- c) a standard electric resistor
- d) a gauge block
- e) a standard signal generator
- f) a reference material.

Note: The quantity concerned may be called the **supplied quantity**.

Measuring chain (VIM 4.4)

Series of elements of a measuring instrument or system that constitutes the path of the measurement signal from the input to the output.

EXAMPLE: an electro-acoustic measuring chain comprising a microphone, attenuator, filter, amplifier and voltmeter.

Measuring system (VIM 4.5)

Complete set of measuring instruments and other equipment assembled to carry out specified measurements.

EXAMPLES

- a) apparatus for measuring the conductivity of semiconductor materials;
- b) apparatus for the calibration of clinical thermometers.

Notes:

- 1 The system may include material measures and chemical reagents.
- 2 A measuring system that is permanently installed is called a **measuring installation**.

Sensor (VIM 4.14)

Element of a measuring instrument or a measuring chain that is directly affected by the measurand.

EXAMPLES

- a) measuring junction of a thermoelectric thermometer;
- b) rotor of a turbine flow meter;
- c) Bourdon tube of a pressure gauge;
- d) float of a level-measuring instrument;
- e) photocell of a spectrometer.

Note: In some fields the term “detector” is used for this concept.

Detector (VIM 4.15)

Device or substance that indicates the presence of a phenomenon without necessarily providing a value of an associated quantity.

EXAMPLES

- a) halogen leak detector;
- b) litmus paper.

Notes:

- 1 An indication may be produced only when the value of the quantity reaches a threshold, sometimes called the **detection limit** of the detector.
- 2 In some fields the term “detector” is used for the concept of “sensor”.

Note to VIM chapter 6:

“In science and technology, the English word "standard" is used with two different meanings: as a widely adopted written technical standard, specification, technical recommendation or similar document (in French "norme") and also as a measurement standard (in French "etalon"). This Vocabulary is concerned solely with the second meaning and the qualifier "measurement" is generally omitted for brevity.”

(Measurement) standard (VIM 6.1)

Material measure, measuring instrument, reference material or measuring system intended to define, realize, conserve or reproduce a unit or one or more values of a quantity to serve as a reference.

EXAMPLES

- a) 1 kg mass standard;
- b) 100.Ω standard resistor;
- c) standard ammeter;
- d) caesium frequency standard;
- e) standard hydrogen electrode;
- f) reference solution of cortisol in human serum having a certified concentration.

Notes:

- 1 A set of similar material measures or measuring instruments that, through their combined use constitutes a standard is called a **collective standard**.
- 2 A set of standards of chosen values that, individually or in combination, provides a series of values of quantities of the same kind is called a **group standard**.

International (measurement) standard (VIM 6.2)

Standard recognized by an international agreement to serve internationally as the basis for assigning values to other standards of the quantity concerned.

National (measurement) standard (VIM 6.3)

Standard recognized by a national decision to serve, in a country, as the basis for assigning values to other standards of the quantity concerned.

Primary standard (VIM 6.4)

Standard that is designated or widely acknowledged as having the highest metrological qualities and whose value is accepted without reference to other standards of the same quantity.

Note: The concept of primary standard is equally valid for base quantities and derived quantities.

Secondary standard (VIM 6.5)

Standard whose value is assigned by comparison with a primary standard of the same quantity.

Reference standard (VIM 6.6)

Standard, generally having the highest metrological quality available at a given location or in a given organization, from which measurements made there are derived.

Working standard (VIM 6.7)

Standard that is used routinely to calibrate or check material measures, measuring instruments or reference materials.

Notes:

- 1 A working standard is usually calibrated against a reference standard.
- 2 A working standard used routinely to ensure that measurements are being carried out correctly is called a check standard.

Transfer standard (VIM 6.8)

Standard used as an intermediary to compare standards.

Note: The term transfer device should be used when the intermediary is not a standard.

Travelling standard (VIM 6.9)

Standard, sometimes of special construction, intended for transport between different locations.

EXAMPLE: a portable battery-operated caesium frequency standard.

Traceability (VIM 6.10)

Property of the result of a measurement or the value of a standard whereby it can be related to stated references, usually national or international standards, through an unbroken chain of comparisons all having stated uncertainties.

Notes:

- 1 The concept is often expressed by the adjective traceable.
- 2 The unbroken chain of comparisons is called a traceability chain.

Calibration (VIM 6.11)

Set of operations that establish, under specified conditions, the relationship between values of quantities indicated by a measuring instrument or measuring system, or values represented by a material measure or a reference material, and the corresponding values realized by standards.

Notes:

- 1 The result of a calibration permits either the assignment of values of measurands to the indications or the determination of corrections with respect to indications.
- 2 A calibration may also determine other metrological properties such as the effect of influence quantities.
- 3 The result of a calibration may be recorded in a document, sometimes called a calibration certificate or a calibration report.

Conservation of a (measurement) standard (VIM 6.12)

Set of operations necessary to preserve the metrological characteristics of a measurement standard within appropriate limits.

Note: The operations commonly include periodical calibration, storage under suitable conditions and care in use.

Reference material (RM) (VIM 6.13)

Material or substance one or more of whose property values are sufficiently homogeneous and well established to be used for the calibration of an apparatus, the assessment of a measurement method, or for assigning values to materials.

Note: A reference material may be in the form of a pure or mixed gas, liquid or solid. Examples are water for the calibration of viscometers, sapphire as a heat-capacity calibrant in calorimetry, and solutions used for calibration in chemical analysis.

This definition, including the Note, is taken from ISO Guide 30:1992.

Certified reference material (CRM) (VIM 6.14)

Reference material, accompanied by a certificate, one or more of whose property values are certified by a procedure which establishes traceability to an accurate realization of the unit in which the property values are expressed, and for which each certified value is accompanied by an uncertainty at stated level of confidence.

Notes:

2 CRMs are generally prepared in batches for which the property values are determined within stated uncertainty limits by measurements on samples representative of the whole batch.

3 The certified properties of certified reference materials are sometimes conveniently and reliably realized when the material is incorporated into a specially fabricated device, e.g. a substance of known triple-point into a triple-point cell, a glass of known optical density into a transmission filter, spheres of uniform particle size mounted on a microscope slide. Such devices may also be considered as CRMs.

4 All CRMs lie within the definition of "measurement standards" or "etalons" given in the "international Vocabulary of basic and general terms in metrology (VIM)".

5 Some RMs and CRMs have properties which, because they cannot be correlated with an established chemical structure or for other reasons, cannot be determined by exactly defined physical and chemical measurement methods. Such materials include certain biological materials such as vaccines to which an International unit has been assigned by the World Health Organization.

This definition, including the Notes, is taken from ISO Guide 30:1992.

8. References

-
- ¹ R. J. Francey, and L. P. Steele, "Measuring atmospheric carbon dioxide - the calibration challenge", *Accreditation and Quality Assurance* **8**, 200 (2003).
- ² J. C. Mouanda, D. Courtois, and C. Thiébeaux, "Laboratory and Atmospheric Ozone Measurements by Infrared-Laser Heterodyne Detection", *Applied Physics B*, **57**, 119 (1993).
- ³ V. Hopfe, D. W. Sheel, W. Graehlert, D. Raisbeck, J. M. Rivero, and O. Throl, "Prozessüberwachung industrieller CVD-Beschichtungsanlagen mittels NDIR-DLS und FTIR-Sensorik (NIR Diode Laser and FTIR Based Process Control for Industrial CVD Reactors)", *VDI-Berichte Nr. 1667*, 111 (2002).
- ⁴ V. E. Bean, W. J. Bowers Jr., W. S. Hurst and G. J. Rosasco, "Development of a Primary Standard for the Measurement of Dynamic Pressure and Temperature", *Metrologia*, **30**, 747, (1993/94).
- ⁵ H. M. Heise, "Clinical Applications of Near- and Mid- Infrared Spectroscopy", in: *Infrared and Raman Spectroscopy of Biological Materials*, H.-U. Gremlich and B. Yan (Eds.), Marcel Dekker, New York, Chap. 8, 259, 2001.
- ⁶ H. Albrecht, G. Müller, M. Schaldach, "Entwicklung eines Raman-spektroskopisches Gasanalyse-systems", *Biomed. Tech.* **22**, 361 (1977).
- ⁷ ISO, "Gas analysis -- Preparation of calibration gas mixtures -- Gravimetric method" ISO 6142:2001.
- ⁸ E. Lanzinger, K. Jousten, and M. Kühne, "Partial pressure measurement by means of infrared laser absorption spectroscopy", *Vacuum*, **51**(1), 47-51, (1998).
- ⁹ G. Padilla, J. Koelliker-Delgado, K. Jousten, O. Werhahn, and D. Schiel. „Precise and Traceable CO₂ - R(12) Line Strength for Laser-Spectroscopy-based Gas Analysis near 2 μ m", to be published soon.
- ¹⁰ J. Koelliker, "Uncertainty estimation of direct traceable amount of carbon dioxide fraction measurement results by means of TDLAS", Dissertation, Technische Universität Carolo Wilhelmina zu Braunschweig, (expected for 2006).
- ¹¹ G. J. Padilla Viquez, "Functional Linear Analysis Applied to Metrology", in *Proceedings of the International Conference in Metrology: Trends and Applications in Calibration and Testing Laboratories*, Jerusalem 2000.
- ¹² BIPM, IEC, IFCC, ISO, IUPAC, IUPAP, OIML, "International Vocabulary of Basic and General Terms in Metrology", ISO, Switzerland, 1993.
- ¹³ C. Gerthsen, (Bearbeitet von H. Vogel), „Gerthsen Physik“, 20. Auflage, Springer-Verlag, 1999.
- ¹⁴ H. J. Eichler, H.-D. Kronfeldt and J. Sahm, „Das Neue Physikalische Grundpraktikum“, Springer-Verlag, 2001.
- ¹⁵ W. Demtröder, „Laser Spectroscopy: Basic Concepts and Instrumentations“, 2nd. Enlarged Edition, Springer-Verlag, 1995.
- ¹⁶ G. Herzberg, "Molecular Spectra and Molecular Structure Vol. II: Infrared and Raman Spectra of Polyatomic Molecules", Krieger Publishing Company, 1991.

-
- ¹⁷ H. M. Heise, „IR-Gasanalytik“ (in H. Günzler, A.M. Bahadir, R. Borsdof, K. Danzer, W. Fresenius, R. Galensa, W. Huber, I. Lüderwald, G. Schwegdt, G. Tölg and H. Wisser [Editors], „Infrarotspektroskopie: Highlights aus dem Analytiker-Taschenbuch“, Springer Verlag, 1996).
- ¹⁸ W. E. Blass and G. W. Halsey, “Deconvolution of Absorption Spectra”, Academic Press, 1981.
- ¹⁹ P. A. Janson (Editor), „Deconvolution With Applications in Spectroscopy“, Academic Press, 1984.
- ²⁰ R. N. Jones and K. Shimokoshi, “Some Observations on the Resolution Enhancement of Spectral Data by the Method of Self-Deconvolution”, *Applied Spectroscopy* **37**, No.1, 59 (1983).
- ²¹ R. D. May, “Response Function of a Tunable Diode Laser Spectrometer from an Iterative Deconvolution Procedure”, *J. Quant. Spectrosc. Radiat. Transfer* **39**, No. 3, 247 (1988).
- ²² J. Pliva, A. S. Pine, and P. D. Willson, “Deconvolution of infrared spectra beyond the Doppler limit”, *Applied Optics* **19**, No. 11, 1833 (1980).
- ²³ R. D. May, “Computer Processing of Tunable Diode Laser Spectra”, *Applied Spectroscopy* **43**, No. 5, 834 (1989).
- ²⁴ J. R. Nielsen, “The Absorption Laws for Gases in the Infra-Red”, *Reviews of Modern Physics* **16**, No. 3, 307 (1944).
- ²⁵ R. J. Anderson and P. R. Griffiths, “Errors in Absorbance Measurements in Infrared Fourier Transform Spectrometry because of Limited Instrument Resolution”, *Analytical Chemistry*, **47**, No. 14, 2339 (1975).
- ²⁶ S. S. Penner, “Quantitative Molecular Spectroscopy and Gas Emissivities”, Addison-Wesley, 1959.
- ²⁷ A. Thorne, U. Litzén and S. Johansson, “Spectrophysics: Principles and Applications”, Springer-Verlag, 1999.
- ²⁸ D. R. Herriott, H. Kogelnik, and R. Kompfner, *Appl. Opt.* **3**, 523 (1964).
- ²⁹ J. Altmann and P. Pokrowsky, *Appl. Opt.* **19**, 3449 (1980).
- ³⁰ J. Brochard and P. Cahuzac, *J. Opt. (Paris)* **8**, 207 (1977).
- ³¹ D. R. Herriott and H. J. Schulte, *Appl. Opt.* **4**, 883 (1965).
- ³² J. Altmann, R. Baumgart, and C. Weitkamp, *Appl. Opt.* **20**, 995 (1981).
- ³³ E. L. Antonsen, R. L. Burton, G. G. Spanjers, and S. F. Engelman *Rev. Sci. Instrum.* **74**, 88 (2003).
- ³⁴ H. Weber, „Angewandte Optik - Sommer-Semester 2002“, Notes for the Applied Optics Course, summer 2002, Technical University Berlin.
- ³⁵ J.-Ph. Pérez, „Optik“, Spektrum Akademischer Verlag, 1996.
- ³⁶ J. McManus and P. Kebabjan, „Narrow optical interference fringes for certain setup conditions in multipass absorption cells of the Herriott type“, *Appl. Opt.* **29**, 898 (1990).
- ³⁷ BIPM, IEC, IFCC, ISO, IUPAC, IUPAP, OIML, “Guide to the Expression of Uncertainty in Measurement”, corrected edition, ISO, Switzerland, 1995.
- ³⁸ A. Madansky, "The fitting of straight lines when both variables are subject to error", *Journal of the American Statistical Association*, **54**, 173 (1959).

-
- ³⁹ M. Kendall and A. Stuart "The Advanced Theory of Statistics" vol.2 -Inference and relationship, Fourth edition, Butler and Tanner, London, 1979.
- ⁴⁰ Plackett, R. L. "A historical note on the method of least squares" *Biometrika*, **36** 458 (1949).
- ⁴¹ D. V. Lindley "Regression Lines and the Linear Functional Relationship" *Journal of the Royal Statistical Society (Suppl.)*, **9**, 218 (1947).
- ⁴² R. A. Ganse, Y. Amemiya and W. A. Fuller "Prediction When Both Variables Are Subject to Error, With Application to Earthquake Magnitudes" *Journal of the American Statistical Association*, December, 761 (1983).
- ⁴³ B. M Troutman and G. P. Williams. "Fitting Straight Lines in the Earth Sciences": chapter 7th of the book: *Use and Abuse of Statistical Methods in the Earth Sciences* 1.19 (1984).
- ⁴⁴ W. A. Fuller, "Measurement Error Models", John Wiley & Sons, 1987.
- ⁴⁵ L. S. Rothman, D. Jacquemat, et al., The HITRAN 2004 molecular spectroscopy database, *Journal of Quantitative Spectroscopy and Radiative Transfer* (2005, in press).
- ⁴⁶ K. Jousten (co-Author and Editor) et al. „Wutz Handbuch Vakuumtechnik - Theorie und Praxis“, 8. Auflage, Vieweg Verlag, 2004.
- ⁴⁷ E. Lanzinger, "Partialdruckmestimmung von Kohlenmonoxid im Hochvakuum mittels Infrarot-Absorptionsspektroskopie unter Verwendung einer Vielfachreflexionszelle nach Herriott", Dissertation, Universität Hannover, 1997.
- ⁴⁸ V. Pustogow, „Untersuchung der Quantenzahlabhängigkeit der Druckverbreiterungskoeffizienten in der ν_3 -Bande von NO_2 Mittels Diodenlaserspektrometrie“, Dissertation, Technische Universität Berlin, 1995.
- ⁴⁹ H.-J. Bartsch, „Taschenbuch mathematischer Formeln“ 18. verb. Auflage, Fachbuchverlag Leipzig, 1998.
- ⁵⁰ A. A. Kosterev and F. K. Tittel, "Chemical Sensors Based on Quantum Cascade Lasers", *IEEE Journal of Quantum Electronics* **38**, No. 6, 582, 2002.
- ⁵¹ B. R. L. Siebert and K.-D. Sommer, „Weiterentwicklung der GUM und Monte-Carlo-Techniken“, *Technisches Messen* **71**, 68 (2004).
- ⁵² „Guide to the Expression of Uncertainty in Measurement Supplement 1: Numerical Methods for the Propagation of Distributions” (Supplement 1. 20040316: 2004) (This version is intended for circulation to the member organizations of the JCGN and National Measurement Institutes for review).
- ⁵³ A. Thorne, U. Litzén and S. Johansson, "Spectrophysics: Principles and Applications", Springer-Verlag, 1999.
- ⁵⁴ A. Mahr, „Gasanalyse mittels Infrarot Spektroskopie im Vakuum“, Vortrag gehalten in der 69. Jahrestagung der Deutschen Physikalischen Gesellschaft, 4. - 9. März 2005, Berlin.

Acknowledgements

I would like to thank in the first place my Lord Jesus Christ, for everything (“Am Anfang, bevor die Welt geschaffen wurde, war Er, der “das Wort” ist. Er war bei Gott und in allem Gott gleich. Von Anfang an war er bei Gott. Durch ihn wurde alles geschaffen; nichts ist entstanden ohne ihn. In allem Geschaffenen war er das Leben, und für die Menschen war er das Licht”).

I am deeply obligated to Dr. Karl Jousten for giving me the opportunity to work on this project under his leadership at the Vacuum Group of the PTB, for his encouraging support in realizing my ideas, and for his great guidance through the development of this research. I am also grateful to all the other members of the Vacuum Group of the PTB: Thomas Bock, Ute Becker, Christian Buchmann, Rolf Niepraschk, Olaf Jahn, Dr. Hans-Jörg Kos; who contributed in many different ways to the success of this project. I am also deeply obligated to the members of the “Spektrometrie an Gasen und Plasmen” group, especially to Dr. Joachim Seidel and Dr. Andreas Steiger, for the numerous fruitful discussions and continued support to this project. Furthermore I want to thank our collaboration partners from the PTB-Braunschweig: Jorge Koelliker, Dr. Olav Werhahn and Dr. Detlef Schiel, for all the fruitful collaboration.

Many thanks also to Dipl.-Ing. Hans-Joachim Heine for facilitating us the sample from the BAM-mixture C49286 (which was very useful for our research) and for the interesting and fruitful discussions.

It has been a pleasure to work also with the members of the Optical Institute of the TU Berlin. I am especially obligated to Dr. Heinz-Detlef Kronfeldt and Prof. Dr. Hans J. Eichler for their support and all the fruitful discussions. I am very grateful also to Dr. Bernd Sumpf and Dr. Heiner Schmidt for their help and always useful advice.

I owe special thanks to Dr. Roswitha Paul-Walz and all the team of support to foreigner students at the TU Berlin. Their support helped to make a wonderful experience of these years of work. In this way I am very grateful to all our friends in Berlin and abroad in Germany. Some of them were already mentioned, some other are: Evelyn and Georg Rupschus, Barbara and Reiner Schroerschwartz, Walter Mayer, Anabel and Felix, Tere and Toti, Isabel and Ralf, Anita and Hassan, Orlando and Family, Jerry and family, Hans and Chata, Esteban and Family, Frau Munck, Frau Kamm and Herr Rosenfelder. Their friendship has been an indirect but powerful support to this work. Also in this way I am very grateful to all our friends, coworkers and Family in Costa Rica and other countries, whose friendship and love has been an invaluable support for our stay in Germany and the successful development of this work. I will not give their names here, because the list is too long, but we are not less indebted to each one of them.

Last, but not least in any way, I am deeply and lovely grateful to my wife, Tati. Mi Osita has been my main source of support and inspiration during these years. She has managed to keep building a wonderful home, while she continued developing herself personally, professionally, and as

a wonderful wife and an excellent aid, who even has helped me with some tasks at the Lab and in the typing of some parts of this thesis. This work is dedicated to her.

This study was developed at the Vacuum Laboratory of the National Metrology Institute of Germany (Physikalisch-Technische Bundesanstalt - PTB) and sponsored by the PTB and by the German Academic Exchange Service (Deutscher Akademischer Austausch Dienst - DAAD). I also received support and partial sponsorship from the Government of Costa Rica through the Ministry of Science and Technology (Ministerio de Ciencia y Tecnología de Costa Rica - MICIT), the Ministry of Economy Industry and Commerce (Ministerio de Economía Industria y Comercio de Costa Rica - MEIC), the National Council of Scientific and Technological Research (Consejo Nacional de Investigaciones Científicas y Tecnológicas de Costa Rica - CONICIT), and the National Metrology Institute of Costa Rica (Laboratorio Costarricense de Metrología - LACOMET). I am very grateful to all these institutions and especially indebted to all those persons who on behalf of their institutions decided to support this work.

Curriculum Vitae

25.06.1969	Born in San José, Costa Rica
1975 - 1980	Primary school
1981 - 1985	Secondary school
1986 - 1989	Study of physics at the Costa Rica University: Bachelor in Physics (1990).
1989 - 1991	Technical and research assistant at the physical laboratories, Costa Rica University.
1992 - 1993	Physics teacher and researcher at the National University in Perez Zeledón, San José.
1993	Design and construction of an automated system of solar energy heating for the hydrotherapy swimming pool of the Elementary School for Special Children of Perez Zeledón (as part of my applied research activities at the National University).
Since 1994	Permanent position as researcher and metrologist at the National Metrology Institute of Costa Rica - LACOMET (Laboratorio Costarricense de Metrología).
1994 - 2001	Head of the Pressure and Vacuum Laboratory at LACOMET.
1995	Guest researcher at the National Metrology Institute of the United States of America - NIST (National Institute of Standards and Technology): “Evaluation of Pressure Transducers for their Utilization as Transfer Standards”.
1996 - 1997	General coordinator of the Physical Metrology Laboratories at LACOMET.
1997 - 1999	Graduate study at the Costa Rica University: Magister Scientiae in Physics (1999). Thesis: The Complex Inflaton.
2000	Coordinator of the first Central American and Caribbean Course of Physical Metrology, as part of the XXVI CURCCAF (Central American and Caribbean Course of Physics, sponsored by the Organization of American States).
2001	Coordinator and teacher of two regional courses on pressure metrology (attendants from Bolivia, Peru and Costa Rica).
2000 - 2001	Teacher of Physics and Metrology at the Costa Rica University (part time)
2001 - 2005	Doctoral research at the National Metrology Institute of Germany - PTB (Physikalisch- Technische Bundesanstalt) and the Technical University Berlin. Thesis: Investigation of TDLAS for its Application as Primary Standard for Partial Pressure Measurements.